Institut National de la Recherche Scientifique
INRS-ETE, Université du Québec

CHARACTERIZATION AND ESTIMATION OF RAINFALL IN BANGLADESH BASED ON GROUND RADAR AND SATELLITE OBSERVATIONS

Par

Shah Alamgir

Thèse présentée pour l'obtention du grade de *Philosophiae Doctor* (**Ph.D**.)
en sciences de l'eau

Spécialité : Télédétection et hydro-météorologie

Jury d'évaluation

Examinateur externe	Godelieve Deblonde, Ph.D. Environment Canada
Examinateur externe	Ramata Magagi, Ph.D. CARTEL, Université de Sherbrooke
Examinateur interne	André St-Hilaire, Ph.D. INRS-ETE, Université du Québec
Codirecteur de thèse	Irene Rubinstein, Ph.D. Université de York, Canada
Codirecteur de thèse	Emmanouil Anagnostou, Ph.D. Université de Connecticut, USA
Directeur de thèse	Monique Bernier, Ph.D. INRS-ETE, Université du Québec

May 2009

ACKNOWLEDGEMENT

Ground radar data and different satellite data products were collected from Bangladesh Meteorological Department (BMD), Ministry of Defense, Bangladesh and Distributed Active Archive Centre (DAAC), NASA, USA respectively. The data collection was one of the most critical and challenging tasks in this research due to time constraint, limitation of research funds and departmental policies with different public agencies. Firstly, the author would like to express his unlimited thanks to BMD and NASA for their timely fashion unrestricted supports and providing data for free. The automatic rain gauge data and BMD's three hourly rain data were provided by the Institute of Flood Management formerly IFCRD and Water Resources Planning Organization in Bangladesh respectively. The author gratefully acknowledges Mr. Shahnewaz, Institute of Water Modeling for his continuous assistance in data collection from different organizations in Bangladesh. The author extends his gratefulness to Professor Nazul Islam from Bangladesh University of Engineering and Technology for his indefinite supports and providing additional clarification on gound obserbation data collected from Bangladesh.

This thesis was made possible by the scientific input from several professors in this field. Firstly, I would like to express my unlimited thanks to Professor Monique Bernier, INRS-ETE, who has been providing research directions, constructive advices, academic and moral supports as a research director since 2000. Special thanks are extended to Professor Emmanouil Anagnoustoe, University of Connecticut, for his invaluable help in satellite data collection, data processing, research co-directions, and computer facilities. I could not have finished this study without research directions from Professor Anagnoustoe. I learned advance techniques related to satellite data processing and rainfall algorithms etc. directly from Professor Anagnoustou. The algorithms developed by the TRMM Science Team and Professor Anagnoustou were also used in this research. Therefore, I would like to acknowledge all his supports without any reservation.

Thanks also to all the people who were willing to extend their constant support to this research work. In particular, Professor Bernard Long, Yves Gauthier, Suzanne Dussault, from INRS-ETE and Dr. Faisal Hossain from University of Connecticut, USA, were pivotal in providing computer facilities, data processing, and administrative supports for this study. Thanks to Professor Alain Rousseau, INRS-ETE, for providing constructive advices during the development of this thesis.

My wife Bilkis, daughter Tiana and son Sowad are equally acknowledged for their support. Without their supports, the author could not have completed this thesis. Finally, the author would like to thank all internal and external members in the jury of thesis evaluation for their valuable comments and suggestions in the thesis.

This study was supported by the World Bank which funded the National Water Management Plan Project in Bangladesh, and research funds from Professor Monique Bernier, INRS-ETE, Canada as well as graduate research assistance from Professor Emmanouil Anagnoustoe, Department of Civil and Environmental Engineering, University of Connecticut, USA.

Finally, the author would like to dedicate this research work to the people of Bangladesh who have been suffering from flooding.

RÉSUMÉ

Le Bangladesh est un pays de l'Asie du Sud-Est qui fait face à des inondations à chaque année couvrant jusqu'au deux tiers de son territoire. La topographie du pays est caractérisée par un relief très plat (10 m d'altitude). Le plateau de Shillong, le long de la frontière nord du pays, agit comme une barrière topographique par rapport aux vents dominants (de direction sud) lors de la mousson de sorte que la quantité de précipitation est très élevée sur le versant sud du plateau. La topographie jumelée à la circulation des vents générés par les orages produisent localement des précipitations importantes dues au rehaussement des masses d'air. La connaissance de leur répartition et leur quantification précise est donc essentielle pour la prévention des inondations ainsi que pour la gestion de l'eau au Bangladesh.

Toutefois, le système de mesures pluviométriques au Bangladesh n'est pas adéquat. Le nombre de pluviomètres est insuffisant car les précipitations varient dans le temps et l'espace en fonction de la topographie et des conditions climatiques. De plus, les radars météo au sol au Bangladesh ne sont pas bien étalonnés et le champ radar le plus important, la réflectivité radar, n'est pas toujours sauvegardé à cause de l'absence de système de contrôle radar et de la capacité réduite des systèmes d'archivage des données. Ainsi, les radars météo ne peuvent être utilisés quantitativement dû à l'absence d'étalonnage absolu de l'algorithme des précipitations. Donc, il est essentiel, d'étalonner les systèmes radar et de développer une procédure d'estimation des précipitations en temps quasi réel au Bangladesh afin d'améliorer l'étalonnage des modèles pour la simulation du ruissellement dans le contexte de la prévision des crues. Les produits du satellite Tropical Rain Measuring Mission (TRMM) ont donc été validés à cette fin.

Dans ce contexte, six objectifs de recherche avaient été définis pour cette thèse et ils ont été atteints: 1) D'abord, les caractéristiques des systèmes pluvieux du Bangladesh ont été analysées à partir des données radar, TRMM et GMS-5. Ils se développent dans le Nord du pays. Leur durée moyenne est de 5.7 heures et ils se déplacent à 5m/s. La période optimum des précipitations maximales est entre 00-06 LST dans les régions du Nord, 06 LST dans les régions du Sud ainsi que 06 LST et 15-18 LST dans le Centre. Ce maximum de précipitations la nuit est assez particulier mais s'expliquerait par le caractère océanique du pays. Une autre particularité est que l'intensité des précipitations orageuses de la période de pré-mousson est supérieure à celle des

précipitations de la mousson; 2) La performance des estimations du radar météo de Dhaka a été évaluée à l'aide des données de pluviomètres et le radar sous-estime de 25 % les valeurs des pluviomètres à cause des paramètres utilisés dans la relation Z-R et de la couverture limitée (100 km); 3) La performance des produits pluviométriques de TRMM (1998-2002) a également été évaluée à l'aide des données de 31 stations. Le produit 3B42 détecte tous les jours de pluie et peut déterminer 98 % des précipitations. 4) L'analyse du produit TRMM 2A25 (2000-2003) a montré que les précipitations pré-mousson sont fortes comparées à celles pendant et après la mousson. La structure verticale varie dans le temps. Durant la période pré-mousson, les échos en altitude sont plus forts qu'à la base et c'est l'inverse après la mousson. Cette différence dans la structure des précipitations serait la cause de la surestimation des précipitations par TRMM 3B42RT durant la période pré-mousson et la sous-estimation durant la mousson. Le produit 3B42RT a aussi confirmé les précipitations maximales à 06 LT. 5) Des paramètres spécifiques pour le radar de Dhaka de l'algorithme de précipitation radar ont été déterminés à l'aide de la technique du filtre de Kalman et des données de 3 stations voisines. La corrélation entre les données des pluviomètres et du radar est passée de 43 % à 58 % en utilisant les nouveaux paramètres, à 90 % en incluant un facteur d'ajustement d'erreur et à 96 % avec le filtre de Kalman. 6) Enfin, les produits radar 2A25 (intensité) et 2A23 (type de pluie) ont été utilisés pour étalonner des données micro-ondes passives (TM1) de plus faible résolution spatiale. Une approche basée sur les réseaux de neurones, développée par Grecu et Anagnostou (2001), a été comparée à celle de Kummerow *et al.* (2001) utilisée pour le produit TM1-2A12. L'approche RN donne de meilleurs résultats parce qu'elle utilise plusieurs bandes et les différentes caractéristiques du système nuageux (stratiformes / convectifs). Qu'importe l'algorithme, les estimés sont meilleurs pour les précipitations stratiformes que convectives. En conclusion, l'utilisation de radar au sol calibrés et de données satellitaires micro-ondes actives et passives (TRMM, AMSR-E) pourrait faciliter le suivi en temps réel des précipitations au Bangladesh.

STUDY SUMMARY

The heavy rainfall often causes flood disasters, which is a serious problem for Bangladesh. In addition, localized heavy rainfall within the country often causes short-term flash floods and worsens flood disasters. The most severe floods occurred in 1998, when about 9 million ha (63 %) of the country was inundated (Saleh *et al.* 1998). Severe floods also occurred in 1987 and 1988, with the flood-affected area reaching about 43 % and 52 % of the country, respectively. Flood forecasting and warning systems in Bangladesh are not technically well operational due to lack of near real-time rainfall data. The rainfall measurement system in Bangladesh is not adequate. Several traditional and a few auto recording rain gauges are available but their spatial and temporal resolutions are very poor. The rainfall in nature has high variability in time and space for different topography, weather and climate condition. In addition, In addition, there are four ground radars in Bangladesh operating with limited technical assistance. These radars are not well calibrated and the most important radar field i.e. radar reflectivity is not saved in radar operating system due to lack of radar controlling system and limitation of data archiving system. As a result, the radars are not quantitatively utilized due to lack of absolute calibration of rainfall algorithm. Therefore, calibration of radar system and development of a near real-time rainfall estimation scheme in Bangladesh are fundamental requirement to improve model calibration in run-off simulation for flood forecasting.

In this study, techniques, limitations and issues related to radar and satellite based rainfall estimation are outlined from previous studies for different regions and climate conditions. It is also noted that there have been very few attempts to use radar and satellite based rainfall estimation in Bangladesh. Therefore, characterization of rainfall system, its variability and diurnal cycle in and around Bangladesh is the first things to understand before proceeding with development of any rainfall algorithm for South East Asia. Using remote sensing data for hydro-meteorological application has become an important issue since 1988 flood in Bangladesh. Consequently, a research work on satellite based rainfall estimation over Bangladesh has been done using Infra-red (IR) satellite data. It is well documented that IR based algorithm for rainfall estimation has a lot of uncertainty and biases in the result due to the lack of direct physical relationship between precipitation and cloud top temperature. Thus, a methodology has to be

developed to estimate near real-time rainfall in Bangladesh using satellite data. Few techniques are already developed for specific region and climate condition of the world with different time and space domain.

At present, the rain-gauges over Bangladesh are the only tool by which to measure rainfall, so there is no way of understanding the properties of the precipitation systems occurring there. However, the rain gauge network is not well covered over whole Bangladesh. To obtain precise rainfall distributions and to clarify the characteristics of precipitation systems, radar data from the Bangladesh Meteorological Department (BMD) are used for the first time in a research context. The data utilize are the BMD radar from Dhaka for 135 days consecutive from 16 April 2000 to 30 August 2000. The Dhaka radar collects only rain status data in six pre-defined ranges instead of radar reflectivity. It is also understood that there is no radar data available between 03-06 LST of radar operations. Therefore, a methodology has been developed in this study in order to retrieve the precipitation rate from the rain status. A correlation between three-days-running averaged rainfall estimated by radar and rain-gauges was calculated and it ranged from 0.63-0.89 over the months of radar operations in 2000. It is found that the radar data were systematically underestimated by about one-fourth the rain-gauge value. It is noted that small size (~80 km2) echoes contribute greatly to the total precipitation, but there were few large size echoes.

The BMD radar data coverage is divided into 3-regions: Northern, Central, and Southern. The distribution of precipitation over Bangladesh obtained from radar data shows heavy precipitation in the northeast and southeast of the country, which is consistent with the rain-gauge rainfall data. Using the radar data characteristics of 185 analyzed convective systems, the development location, lifetime, shape, size, propagation speed, and direction were investigated. In general, precipitation systems develop in the Northern region and tend to move eastward. It is also found that the precipitation system development in the central and Southern regions is significant during the peak-monsoon months (June-August). Analysis of the radar data also shows that the average time of maximum precipitation in the Northern region is 00-06 LST, in the Central region 06 LST and 15-18 LST, and in the Southern region 06-09 LST. It is noted that the average lifetime and movement speed of these systems are ~5.7 hours and ~5 m/sec respectively.

Three-hourly rain data from BMD at 33 gauge locations are also utilized to analyze the radar results. It is found that the distributions of rainfall obtained by both the radar and the rain gauges

are similar in pattern, but the time of the maximum rainfall determined by the radar is a few hours earlier than that determined by the rain gauges. The distribution of rainfall over the whole radar domain suggests that the most likely time for rainfall to occur in Bangladesh is between 21 to 09 local standard time (LST), while 06 LST is the most likely time for maximum rainfall to occur over the entire country. The occurrence of 21 to 09 LST rainfall is possibly linked to the local effects such as complex terrain and sea and land breeze circulations. The morning maximum rainfall at 06 LST in Bangladesh is different from that of the Indian subcontinent or of the mountain area where, generally, maximum rainfall occurs in the afternoon. The northern border of Bangladesh, close to the Shillong hill of India, is the region with the highest rainfall, while the second highest volume of rainfall occurs on the eastern border. Furthermore, the radar data over Bangladesh are also utilized to obtain the diurnal variations and characteristics of precipitation in relation to cloud activity. The nature of the diurnal cycle of precipitation in Bangladesh is that there is a morning peak at 0600 LST with minimum at noon. The frequency of the echoes exhibits two peaks-one in the afternoon (~ 1500 LST) and the other in the morning (0600 LST) hours. The smaller echoes dominate in the afternoon while larger echoes develop in the early morning.

The Japanese Geostationary Meteorological Satellite (GMS-5) high resolution (10 km mesh) hourly data were also used in this study. The GMS-5 hourly data are sampled in 1°×1° grid boxes in the domain of 600 km × 600 km over Bangladesh (land) and the north part of the Bay of Bengal (ocean) to obtain diurnal cycle of cloud activity. The cloud embedded area (CEA) shows afternoon (~1700 LST) and morning (~0300 LST) peaks over land typically composed of relatively small deep (<214K) and large shallow (<243K) convective cloud systems. In contrast, only afternoon (1400-1600 LST) peak is observed over ocean typically composed of small shallow and large deep convective cloud systems. Meanwhile the frequency of the cloud systems exhibits the clear afternoon (~ 1600 LST) peak over the land and the ocean that indicates that afternoon is the initiation times of land-based clusters over Bangladesh and water-based clusters in the analyzed ocean (87.44°-93.33°E; 15.7°-21.08°N). The northwestern part of Bangladesh was largely affected by pre-monsoon clouds, while the whole country was affected by the peak monsoon activities.

An attempt was made to compare TRMM 3B42 products rainfalls with surface-based rain-gauge (RNG) rainfall obtained at 31 stations over Bangladesh for the years 1998-2002. Day-by-day rainfall amounts determined by TRMM and RNG are compared for continued 274 days (from 1 March to 30 November) in each year and at every station. Out of 274 days, averaged for 5 years rainfall over 31 stations, 97.08 % and 98.91 % days are detected as rainy day by TRMM and RNG respectively. Rainy days detected by TRMM matched 95.99 % of the days detected by RNG. On an average, TRMM can determine about 98.24 % of the RNG rainfall. The TRMM overestimates rainfall during pre-monsoon and underestimates during monsoon while alike during post monsoon period. Overall, TRMM underestimates rainfall in the heavy-rainfall regions of Bangladesh.

This study also presents the vertical structure using TRMM-2A25 data and diurnal variation using TRMM- 3B42RT data of precipitation from pre-monsoon to post-monsoon periods in and around Bangladesh. TRMM-2A25 data analysis reveals that pre-monsoon, monsoon and post-monsoon precipitations are strong, moderate and less intensified, respectively. Strong rain rates are found at higher altitudes for pre-monsoon and relatively at lower altitudes for later periods. From averages of 4 years of data, it is found that maximum rain rate in April, July and October is 114.19, 73.88 and 49.28 mm/h, respectively. In general, pre-monsoon echoes are high compared to monsoon and post-monsoon periods. However, the maximum echo top height of about 18.25, 18.8 and 18.25 km is found during the pre-monsoon, monsoon and post-monsoon periods, respectively. Analyzing TRMM-3B42RT data, it is found that the maximum rainfall over Bangladesh and northeast of the Bay of Bengal are appearing at 06 LST (local time) during monsoon period. In the same period the maximum rainfall over India is found at 18 LST. For the entire rainy season (March-November) the maximum rainfall over Bangladesh is occurred at 06 LST with a secondary maximum peak at 15 LST. The morning maximum rainfall at 06 LST over Bangladesh is confirmed after compared with the same obtained from ground-based rain gauge data. This analysis reveals that in Bangladesh the overestimation and underestimation of rainfall by TRMM in pre-monsoon and monsoon respectively depends on different vertical structures of precipitation fields in corresponding periods.

With the understanding of rainfall characteristics in Bangladesh, this research work also extends development of a statistical procedure of quantitative estimation of rainfall in Bangladesh from combination of radar observations and rain gauge measurements. The uncertainty bounds associated with those estimates are also evaluated at a given space and time resolution. It is identified that there are six parameters controlling the various processing stages in radar rain algorithm. Sensitivity analysis showed that there is a host of parameter values coming from different gauge clusters in the parameter space that are equally acceptable as predictors of rainfall. Consequently, a methodology is devised to assess the uncertainty arising from errors in algorithm structure and parameter selection. Within this methodology, the algorithm calibration problem is formulated into the estimation of posterior probabilities of acceptable algorithm responses, thereby avoiding the concept of determining a likelihood values associated with errors between observed and estimated precipitation amounts derived through repetitive sampling of parameter space on the basis of Monte Carlo technique. The rainfall estimation from the method of Z-R relationship yielded the largest mean relative error of 43.8 % among the selected algorithms. The Kalman filtering technique was also applied in order to adjust radar rain estimation errors. The mean relative error with average calibration, radar-gauge adjustment and Kalman filter approache is respectively 14.5 %, 10.2 % and 7.9 %. The correlations between radar and gauge rainfall for different approaches are 0.584 (not corrected i.e. before error adjustment), 0.902 (with error adjustment but without filtering), and 0.963 (corrected with Kalman filtering). It is found that there is very little error adjustment made by the Kalman filter.

Finally, this study also presents development of satellite based overland rainfall estimation from Space-borne Precipitation Radar and Passive Microwave data. The Tropical Rainfall Measuring Mission (TRMM) satellite carries two sensors that are very useful to precipitation: the precipitation radar (PR) and Microwave Imager (TMI). In this study PR's standard products, that is rain profile and rain type, are used to calibrate overland rain retrievals from the TMI channels. PR-TMI calibration is done for two different regions (GBM and Southern US), and results are compared to examine the significance of differences. Coincident PR and TMI data from six summer months is used for the overland microwave (MW) algorithm calibration. The calibration scheme developed by Grece and Anagnoustoe (2001) consists of (i) rain area delineation, (ii) convective/stratiform rain classification, and (iii) a multiple linear regression model for rain rate estimation. The current algorithm is also compared with the latest [version 6 (V6)] TRMM 2A12

product in terms of rain detection, and rain-rate retrieval error statistics on the basis of PR reference rainfall. The performance of the algorithm is different for the two regions. For instance, the reduction in random error (relative to 2A12 V6) is about 26 % for USA and 135 % for GBM. However, a significant difference is observed between two regions. USA region has shown better results than the GBM region.

Using CFAD plots of 3D PR reflectivities, for stratiform and convective rains, it has shown the Bangladesh region is dominated by medium stratiform clouds. The USA region is also dominated by convection during the summer season, but it seems there is also a significance of medium stratiform clouds. It has been argued that over-land microwave rainfall estimation algorithms perform better for deep convection rain systems. It is also found that the region with higher detection failure is the region where stratiform rain is dominant and convective does not penetrate above zero isotherms.

TMI-2A12 rain algorithm developed by Kummerow *et al.*, 2001 and the NN scheme developed by Grecu *et al.,* 2001 were applied over US and GBM (i.e. Bangladesh) regions in order to understand the performance of both schemes. TRMM PR rain estimate were used to improve the calibration of passive microwave (i.e. TMI) algorithm for precipitation estimation at the radiometer footprint scale over Bangladesh. In this study, a passive microwave (PM) calibration scheme developed by Grecu and Anagnostou (2001) has been investigated. This algorithm is known as neural network based scheme which identifies rain/no-rain area and delineates the convectic and stratiform rain types. Finally, multiple linear regressions are used to relate PR rain and TMI brightness temperatures. The NN scheme performs better than that of 2A12, particularly over Bangladesh, because the neural network approach for rain area delineation makes use of many channels and different features of the cloud system. Rain retrieval over GBM region with US parameter provides higher correlation and efficiency than 2A12 scheme. Stratiform type rain shows higher coorelation and efficency than convective type of rain.

It is not enough to investigate any hydrological scenarios due to temporal limitation of TRMM satellite data but TRMM rain product is found very useful to calibrate other satellite products. Therefore, it is recommended to calibrate SSM/I (and/or AMSR, AMSU-B data) passive microwave data using current calibrated TRMM TMI data over Bangladesh. The Global IR data (½-hourly interval) can also be calibrated using multi-sensor microwave based rain product.

A Bayesian formulation could be prepared to optimally determine this combination, as well as the uncertainty associated with the merged products, while coincident rainfall estimates from dense rain gauge network available in Bangladesh would be used to determine the covariance matrices associated with this formulation. It is expected that the passive microwave (PM) retrievals would be unbiased with respect to PR rainfall, but the random error would be probably vary from sensor to sensor. The different PM sensor error statistics would be assessed using the rain gauge rainfall measurements. Finally, the end rain product can be used in hydrological model (e.g. HYDROTEL, HSP-F, Mike SHE) to investigate error propagation in modeling for hydrologic variables over different time and space scales.

An upgrade of the BMD radar system is highly recommended. Then, in the near future it will be possible to obtain quantitative amounts of rainfall from BMD radar. The TRMM PR and calibrated PM rain products can be used to calibrate BMD radar in order to estimate real-time rainfall for flood forecasting model (currently used Mike 11) development in Bangladesh.

TABLE OF CONTENTS

LIST OF TABLES

LIST OF FIGURES

LIST OF ACRONYMS

1DD	:	1 Degree Daily technique
4-D Var	:	Four-dimensional variational assimilation
AGPI	:	Adjusted GOES Precipitation Index (GPI + GSCAT)
AIP	:	Algorithm Intercomparison Project
AMSR	:	Advanced Microwave Scanning Radiometer
AMSR-E	:	Advanced Microwave Scanning Radiometer - EOS
AMSU	:	Advanced Microwave Sounding Unit
ANN	:	Artificial Neural Network
AP	:	Anomalous Propagation
ATI	:	Area Time Integral
ATSR	:	Along Track Scanning Radiometer
AVHRR	:	Advanced Very High Resolution Radiometer
BG	:	Bangladesh Raingauge
BMD	:	Bangladesh Meteorological Department
BTD	:	Brightness Temperature Difference
BWDB	:	Bangladesh Water Development Board
CCD	:	Cloud Cold Duration
CDF	:	Cumulative Distribution Frequency
CEA	:	Cloud Embedded Area
CFAD	:	Contoured Frequency Verses Altitude Plots
CGPM	:	Canadian GPM Program
COARE	:	Coupled Ocean-Atmosphere Response Experiment
CSA	:	Canadian Space Agency
CSI	:	Cumulative Success Index
CST	:	Convective-Stratiform Technique
DAAC	:	Distributed Active Archive Center
DPR	:	Dual Frequency Precipitation Radar
DMSP	:	Defense Meteorological Satellite Program (USA)
DSD	:	Drop Size Distribution

ECMWF	:	European Centre for Medium-Range Weather Forecasts
ECST	:	Enhanced Convective-Stratiform Technique
EEA	:	Echo Embedded Area
EGPM	:	European GPM Program
EOS	:	NASA Earth Observing System
ERS	:	European Remote sensing Satellite
ESA	:	European Space Agency
EUMETSAT	:	European Organization for the Exploitation of Meteorological Satellites
FAR	:	False Alarm Ratio
FAP	:	Flood Action Plan
FFWC	:	Flood Forecasting and Warning Centre
FO	:	Frequency of Occurrence
FOV	:	Field of View
GARP	:	Global Atmosphere Research Programme
GATE	:	GARP (Global Atmosphere Research Programme) Atlantic Tropical Experiment
GBM	:	Ganges, Brahmaputra and Meghna Basin
GEO	:	Geostationary
GEWEX	:	Global Energy and Water cycle Experiment
GHRC	:	Global Hydrological Research Centre
GMS	:	Geostationary Meteorological Satellite (Japan)
GOES	:	Geostationary Operational Environmental Satellite (USA)
GPCP	:	Global Precipitation Climatology Project (GPCP)
GPI	:	GOES Precipitation Index
GPM	:	Global Precipitation Measuring Mission
GPROF	:	Goddard Profiling Algorithm
GSCAT	:	Goddard Scattering Algorithm
GSFC	:	Goddard Space Flight Center
HIRLAM	:	High Resolution Limited Area Model
IFCDR	:	Institute of Flood Control and Drainage Research
IFOV	:	Instantaneous Field of View

IR	:	Infrared
ITCZ	:	Inter Tropical Convergence Zone
JICA	:	Japanese International Cooperation Agency
LAM	:	Limited Area Model
LEO	:	Low Earth Orbit
LIS	:	Lightning Imaging Sensor
LST	:	Local Standard Time
MCC	:	Mesoscale Convective Complex
MCS	:	Monte Carlo Simulation
Meteosat	:	Geostationary Meteorological Satellites of EUMETSAT (Europe)
MIRA	:	MW IR Rainfall Algorithm
MIRRA	:	Microwave/Infrared Rain Rate Algorithm
MLR	:	Multiple Linear Regressions
MODIS	:	MODerate resolution Imaging Spectroradiometer
MOMT	:	Multi-sensor Optimal Merging Technique
MSG	:	METEOSAT Second Generation
MW	:	Microwave
NASA	:	National Aeronautics and Space Administration
NASDA	:	National Space Development Agency
NCAR	:	National Center for Atmospheric Research
NCEP	:	National Centers for Environmental Prediction (NOAA)
NESDIS	:	National Environmental Satellite Data and Information Service
NEXRAD	:	Next Generation Weather Radar
NIR	:	Near IR
NOAA	:	National Oceanic and Atmospheric Administration
NPR	:	Nadir Pointing Radar
NWP	:	Numerical Weather Prediction
OSF	:	Operational Support Facility
PCT	:	Polarization Corrected Temperature
PDF	:	Probability Density Function

PERSIANN	:	Precipitation Estimation from Remotely Sensed Information using Artificial Neural Networks
PIA	:	Path-Integrated Attenuation
PIP	:	Precipitation Intercomparison Project
PM	:	Passive Microwave
POD	:	Probability of Detection
PPI	:	Plain Position Indicator
PPS	:	Precipitation Processing System\Subsystem
PR	:	Precipitation Radar
QPF	:	Quantitative Precipitation Forecast
RACC	:	Rain and Cloud Classification
RMSE	:	Root Mean Square Error
RMS	:	Root Mean Square
RNG/RG	:	Rain Gauge
RNR	:	Rain/No-rain
SAR	:	Synthetic Aperture Radar
SEM	:	Satellite Error Model
SEVIRI	:	Spinning Enhanced Visible and Infrared Imager
SPARRSO	:	Space Research and Remote Sensing Organization
SI	:	Scattering Index
SSE	:	Sum of Squared Error
SSM/I	:	Special Sensor Microwave Imager
SSMI/S	:	Special Sensor Microwave Imager/Sounder
SST	:	Sea Surface Temperature
TB	:	Brightness temperature
TMI	:	TRMM Microwave Imager
TMPI	:	Threshold-Matched Precipitation Index
TOGA	:	Tropical Ocean and Global Atmosphere
TOGA COARE:		TOGA Coupled Ocean-Atmosphere Response Experiment
TRMM	:	Tropical Rainfall Measuring Mission
UAGPI	:	Universal Adjusted GPI

VRP	:	Vertical Reflectivity Profile
VI	:	Variability Index
VIHC	:	Vertically Integrated Hydrometeor Content
VIRS	:	Visible and InfraRed Scanner
VIS	:	Visible
WARPO	:	Water Resources Planning Organization
WMO	:	World Meteorological Organization
WSR-88D	:	Weather Surveillance Radar – 1988 Doppler
WV	:	Water Vapour

SYNTHÈSE

INTRODUCTION

Contexte

Les précipitations constituent l'un des principaux processus du cycle hydrologique et leur suivi pose un défi de taille. Les précipitations et leur variabilité, en plus d'être des composantes importantes du cycle hydrologique à l'échelle du globe, influencent le développement de tous les organismes vivant à la surface de la planète. Dans le cas des régions tropicales en particulier, compte tenu des conditions socio-économiques qui prévalent dans plusieurs pays, les populations dépendent en grande partie des précipitations et de leur variabilité dans le temps et l'espace pour leurs besoins en eau pour l'agriculture et les activités quotidiennes ainsi que pour le suivi des inondations et des sécheresses.

Le Bangladesh (avec une superficie de 144 000 km^2) est un pays de l'Asie du Sud-Est qui fait face à des inondations à chaque année couvrant jusqu'à deux tiers de son territoire. La topographie du pays est caractérisée par un relief très plat dont l'élévation ne dépasse jamais 10 m au-dessus du niveau moyen de la mer. La station indienne de Cherrapunji a enregistré la plus forte précipitation annuelle, soit 26 461,2 mm, d'août 1860 à juillet 1861, celle-ci étant généralement en moyenne supérieure à 8 000 mm/an (Pant *et al.*, 1997). Cette station est située sur le versant sud du plateau de Shillong, à environ 10 km de la frontière du Bangladesh. Le plateau de Shillong agit comme une barrière topographique par rapport aux vents dominants de la mousson de direction sud de sorte que la quantité de précipitation est très élevée sur le versant sud du plateau. La topographie jumelée à la circulation des vents générée par les orages produisent localement des quantités de précipitation plus importantes dû au rehaussement des masses d'air.

Les pluies fortes causent souvent des inondations catastrophiques, une situation qui constitue un grave problème au Bangladesh. De plus, les pluies fortes qui se manifestent localement à l'intérieur du pays causent souvent des crues soudaines qui amplifient les désastres causés par les inondations. Matsumoto (1998) a traité du phénomène des inondations au Bangladesh et il a montré que les pluies fortes, conjointement avec d'autres phénomènes, représentaient une des

causes d'inondation. Au cours des dernières années, les inondations les plus graves sont survenues en 1998 alors que 9 millions d'hectares (63 % du territoire) ont été inondés (Saleh *et al.*, 1998). Des inondations majeures sont également survenues en 1987 et 1988, l'étendue de la zone inondée atteignant respectivement environ 43 % et 52 % du pays. L'estimation précise des précipitations est essentielle à cause des conséquences majeures que représentent les inondations et les sécheresses, qui constituent des désastres naturels fréquents au Bangladesh. La connaissance de la répartition et la quantification précise des précipitations peuvent s'avérer aussi utiles pour la prévention des désastres ainsi que pour la gestion de l'eau au Bangladesh.

Toutefois, le système de mesures pluviométriques au Bangladesh n'est pas adéquat. On trouve des pluviomètres non enregistreurs traditionnels ainsi que des pluviomètres enregistreurs automatiques, mais les précipitations sont de par leur nature caractérisées par une très grande variabilité dans le temps et l'espace en fonction de la topographie, de la température et des conditions climatiques. De plus, les radars météo au sol au Bengladesh ne sont pas bien étalonnés et le champ radar le plus important, la réflectivité radar, n'est pas toujours sauvegardée dans les systèmes radar à cause de l'absence de système de contrôle radar et de la capacité réduite des systèmes d'archivage des données. Ainsi, les radars météo ne peuvent être utilisés quantitativement dû à l'absence d'étalonnage absolu de l'algorithme des précipitations. Donc, il est essentiel, d'une part, d'étalonner les systèmes radar et, d'autre part, de développer une procédure d'estimation des précipitations en temps quasi réel au Bangladesh afin d'améliorer l'étalonnage des modèles pour la simulation du ruissellement dans le contexte de la prévision des crues.

Questions scientifiques et hypothèses de recherche

Cette recherche s'intéresse aux questions suivantes et vise à y répondre à titre de contribution à la science :

Comment peut-on utiliser les caractéristiques, la variabilité ainsi que le cycle diurne des précipitations pour améliorer l'estimation des précipitations au Bangladesh ?

Comment une procédure statistique peut-elle être appliquée pour améliorer l'estimation des précipitations au-dessus d'une région caractérisée par des précipitations importantes en Asie du Sud-Est ?

Le travail repose sur les quatre hypothèses suivantes (sans s'y limiter) :

- *La caractérisation du système de précipitations à l'intérieur et autour du Bangladesh peut améliorer le développement des algorithmes d'estimation des précipitations basés sur les données radar et satellitaires au Bangladesh.*
- *Les approches statistiques peuvent améliorer l'estimation des précipitations au-dessus des régions caractérisées par de fortes précipitations en Asie du Sud-Est.*
- *Les données radar terrestres corrigées peuvent améliorer l'estimation des précipitations en temps quasi-réel de même que la simulation du ruissellement au Bangladesh.*
- *L'estimation des précipitations à partir des données satellitaires peut être utile pour améliorer l'estimation des précipitations en temps quasi-réel au Bangladesh.*

Objectifs de recherche

1. Caractériser le système de précipitations au-dessus du Bangladesh à l'aide des données radar et du réseau de pluviomètres.
2. Évaluer la performance de l'extraction des précipitations par radar à l'aide des mesures des pluviomètres au Bangladesh.
3. Caractériser et évaluer les produits pluviométriques dérivés des données de TRMM au-dessus du Bangladesh.
4. Étudier le cycle diurne et les variations intra-saisonnières des précipitations à l'intérieur et autour du Bangladesh.
5. Développer une procédure statistique pour l'estimation quantitative des précipitations au Bangladesh à partir des observations radar au sol.

6. Mise au point d'une procédure d'étalonnage pour l'extraction des précipitations à partir des données satellitaires radar au-dessus du Bangladesh.

ORGANISATION DE LA THÈSE

Le chapitre 1 introduit la problématique et les objectifs de la thèse. Le chapitre 2 présente les aspects théoriques de la formation des nuages et du système de la mousson en Asie du Sud-Est ainsi que la problématique des mesures de précipitation dérivées des données radar et satellitaires. Le chapitre 3 résume l'état de l'art dans le domaine de l'estimation des précipitations à l'aide des données radar et satellitaires. Les avantages, les limites et l'applicabilité de plusieurs algorithmes d'extraction des précipitations par télédétection sont présentés dans ce chapitre. La climatologie du Bangladesh est également décrite. Au chapitre 4, une description sommaire de la zone d'étude ainsi que des données utilisées est présentée. Les méthodes mises de l'avant pour atteindre les différents objectifs proposés sont présentées au chapitre 5, alors que les résultats sont discutés en relation avec les objectifs visés au chapitre 6. Enfin, les conclusions et les recommandations sont présentées successivement dans les chapitres 7 et 8.

Afin d'éviter les répétitions dans le texte, une liste des acronymes est proposée en début de thèse (p. ex. BG, CEA, FO, PPI, PM, TRMM, TMI etc.). Également, pour faciliter la compréhension du texte, un glossaire des termes techniques utilisés dans cette étude a été inclus à la fin de la thèse.

ÉTAT DE L'ART

Le chapitre 3 présente les limites et les problématiques de l'estimation des précipitations à l'aide des données radar et satellitaires à partir d'études antérieures réalisées dans différentes régions et conditions climatiques. Il est à noter qu'il y a eu très peu d'expériences effectuées dans le domaine de la prévision des précipitations à l'aide des données radar et satellitaires au Bangladesh. Ainsi, la caractérisation du système pluvieux, de sa variabilité et de son cycle diurne tant à l'intérieur qu'à l'extérieur du Bangladesh constitue un élément essentiel à maîtriser avant de pouvoir procéder à la mise au point d'un algorithme des précipitations. L'utilisation des données de télédétection pour les applications hydro-météorologiques est devenue un sujet d'intérêt au Bangladesh depuis l'inondation de 1988 et, par conséquent, des travaux de recherche

sur la prévision des précipitations basés sur les données satellitaires infrarouge ont été réalisés (Islam *et al.*, 2004; Islam et Wabid, 2003). Des données infrarouge ont été utilisées bien qu'il soit démontré que les algorithmes basés sur l'infrarouge pour l'estimation des précipitations comportent beaucoup d'incertitude et de biais au niveau des résultats dû au fait qu'il n'existe pas de relation physique directe entre les précipitations et la température au sommet des nuages. De plus, les estimés de précipitations dérivés des données du satellite TRMM n'ont pas encore été validés pour le Bangladesh. Ainsi, une nouvelle méthodologie, décrite au chapitre 5, a été développée pour l'estimation des précipitations en temps quasi réel au-dessus du Bangladesh. Peu de techniques ont été développées jusqu'à maintenant pour des régions et des conditions spécifiques dans le monde en fonction d'échelles temporelles et spatiales différentes.

ZONE D'ÉTUDE ET DESCRIPTION DES DONNÉES

Le chapitre 4 présente une description générale de la zone d'étude, aborde la question de la disponibilité des données et décrit les différents ensembles de données. Les différents capteurs satellitaires et produits y sont décrits. Leur application dans le contexte des produits pluviométriques est discutée.

Description générale de la zone d'étude

Le Bangladesh (Figure 4.1), pays de l'Asie du Sud-Est, a une superficie totale d'environ 144 000 km^2. Le pays est situé dans la portion nord-est de l'Asie du Sud, entre 20° 34" et 26° 38" de latitude nord et 88° 01" et 92° 41" de longitude est. Le Bangladesh est l'un des pays les plus densément peuplés de la planète, avec une densité de 1 000 habitants par km^2. Environ 80 % du Bangladesh est situé dans les plaines inondables de trois grands fleuves : le Gange, le Brahmapoutre et le Meghna ainsi que leurs tributaires. Le bassin du Meghna enregistre l'intensité la plus forte de précipitation au monde.

Dans le sud, se trouve la baie du Bengale, la source de la vapeur d'eau, tandis qu'au nord, se trouvent les zones de haute altitude que sont l'Himalaya et le plateau tibétain. L'organisation et les phases diurnes des systèmes pluviométriques durant la mousson d'été, tant à l'intérieur qu'à l'extérieur du Bangladesh, sont affectées par ces éléments d'origine orographique dont les vents

de direction sud-ouest, les anomalies dans les températures terre-océan et la circulation de la brise océanique (Liu and Yanai, 2001).

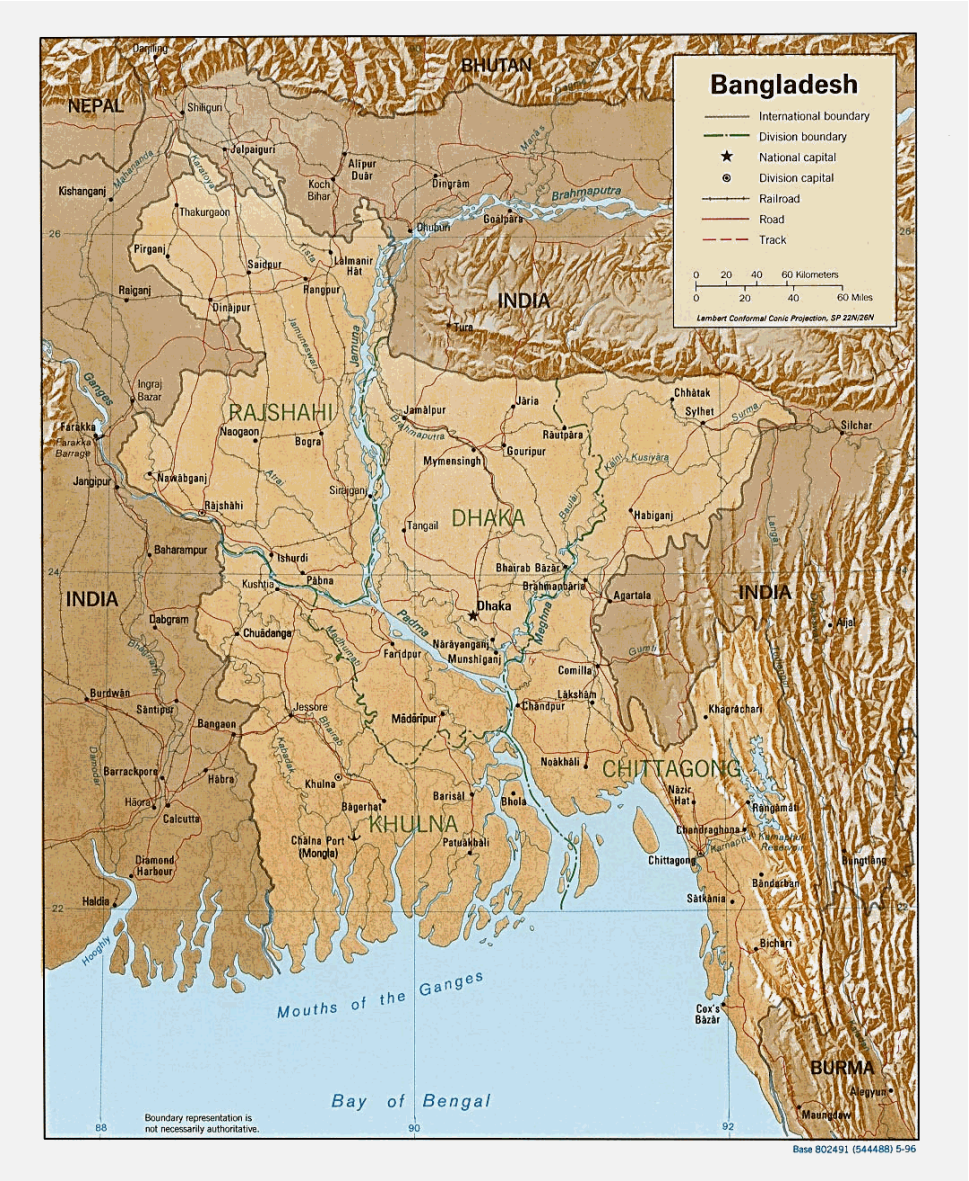

Figure 4.1. Carte des principales régions du Bangladesh

Le relief du Bangladesh est très plat : l'élévation est d'environ 1-10 m au-dessus du niveau de la mer excepté pour certaines portions réduites dans le sud-est (élévation de ~200 m), à la frontière du Myanmar, et dans le nord-est (élévation de ~100 m), à la frontière de l'Inde, près de la montagne de Shillong. Il y a peu de montagnes atteignant plus de 1 000 m dans le pays. Le

plateau de Shillong et la montagne de Chittagong, situés respectivement près des frontières nord-est et sud-est de l'Inde, ont des effets considérables sur la quantité de précipitation enregistrée dans les zones limitrophes.

Le climat de la région est caractérisé par des températures élevées ainsi qu'un taux d'humidité considérable. Les précipitations annuelles sont supérieures à 5 000 mm près du plateau de Shillong (Ohsawa *et al.*, 1997a), le plateau de Shillong agissant comme une barrière topographique par rapport aux vents de direction sud de la mousson. La quantité de précipitation est extrêmement élevée sur le versant sud du plateau de Shillong.

Les précipitations de la mousson comptent pour approximativement 80 % des précipitations annuelles totales de juin à septembre au Bangladesh (McGregor and Nieuwolt, 1998). La mousson en direction nord de la baie du Bengale s'étend à travers le pays jusqu'au piedmont de la chaîne de l'Himalaya dans le nord. La pluie tombe généralement sous forme d'averses à partir d'un important couvert nuageux durant la mousson, mais celle-ci peut être également associée à des orages forts et des cyclones tropicaux (McGregor and Nieuwolt, 1998). La fraction des précipitations provenant des systèmes de convection est d'environ 70 % (Mohr *et al.*, 1999). On rapporte qu'approximativement 50 % des nuages précipitent durant la mousson (Islam and Wahid, 1999). Dans les portions nord et sud-est du Bangladesh, le rehaussement orographique par des barrières topographiques contribue également à la quantité annuelle de précipitation. Il n'y a pas de tendance directionnelle précise dans les précipitations dans la région étudiée et les précipitations annuelles varient de 1 000 à 3 000 mm, avec un pic dans les régions qui sont propices aux précipitations orographiques. Au Bangladesh, une fraction plus faible des précipitations provient des cellules de convection. Durant la période de juin à septembre, le Bangladesh est influencé par la mousson humide de direction nord, résultant en des conditions climatiques relativement homogènes.

Sur la base de la moyenne statistique des cinquante dernières années, le taux de précipitation annuelle au-dessus au Bangladesh est de 2 360 mm et varie de 1 650-2 930 mm. En un endroit en particulier, il varie même de 1 200-5 600 mm. La température au Bangladesh varie de moins de 5° C à plus de 43° C. Le pic se produit en avril-mai, mais ce dernier dépasse 43° C dans les portions ouest de la région du nord-ouest. Les minima de températures sont observés durant la

période de janvier-février, avec 1,7° C à Srimongal, dans la région du nord-est du Bangladesh. Le tableau 4.1 donne un aperçu de la climatologie du Bangladesh.

Table 4.1 Monthly Average Temperature and Precipitation in Bangladesh, Source: BMD

	Jan.	Fév.	Mar.	Avr.	Mai	Juin	Juil.	Août	Sept.	Oct.	Nov.	Déc.
Temp. Max. (°C)	25,4	28,1	32,3	34,2	33,4	31,7	31,1	31,3	31,6	31,0	28,9	26,1
Temp. Min. (°C)	12,3	14,0	19,0	23,1	24,5	25,5	25,7	25,8	25,5	23,5	18,5	13,7
Précip. (mm)	07,0	19,8	40,7	110,7	257,5	460,9	517,6	431,9	289,9	184,2	35,0	09,4

DISPONIBILITÉ DES DONNÉES

Données radar au sol

Les données utilisées dans cette étude proviennent de l'expérience IFCDR/JICA Rainfall Experiment, réalisée entre 1999 et 2003, dans la région nord-est du Bangladesh. L'expérience reposait sur l'utilisation d'un radar Doppler en bande S à Dacca (Figure 4.3) et d'environ quinze pluviomètres à auget basculeur dans la région de Dacca et de Sylhet. Le BMD dispose également d'un réseau de pluviomètres répartis sur 33 sites où l'on fait l'acquisition de mesures de précipitation à intervalle de 3 heures sur l'ensemble du pays.

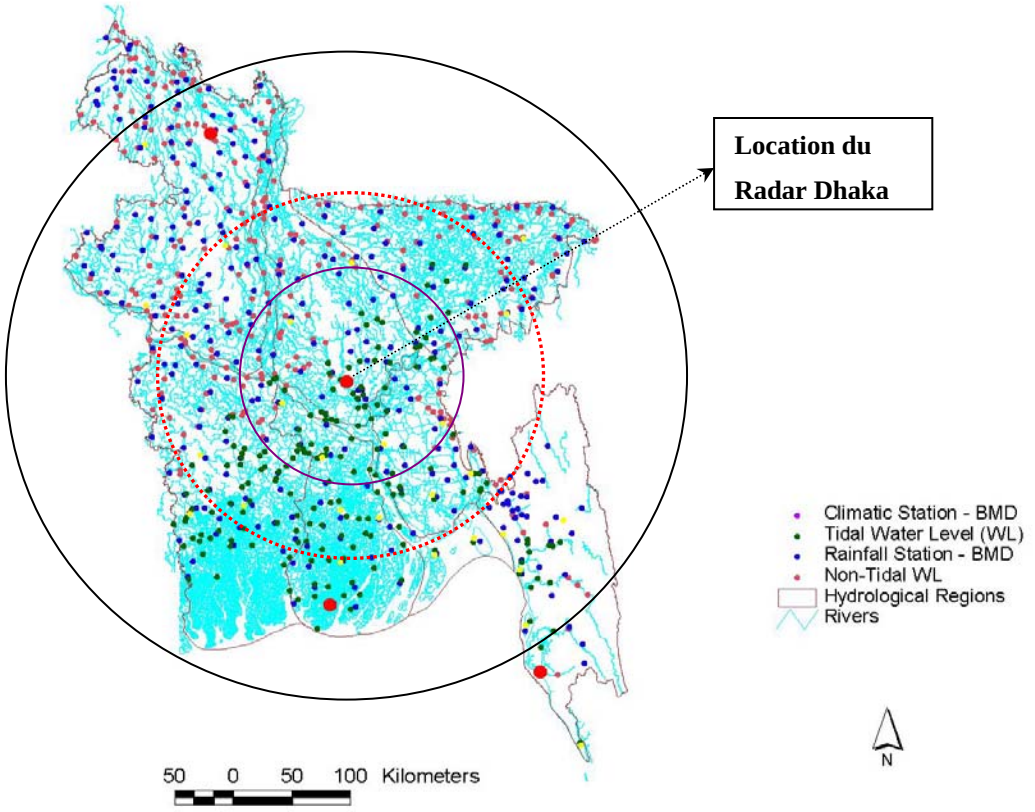

Figure 4.3. Les points bleus représentent les sites des pluviomètres au Bangladesh, alors que les quatre points rouges représentent la localisation des radars (Source : Les données viennent du Ministère de la météorologie du Bangladesh)

Le BMD a installé un radar météorologique en bande S (longueur d'onde : ~10 cm) à Dacca (90.4° N, 23.7° E), sur le toit d'un bâtiment d'une hauteur de 60 m qui fournit une couverture de 600 km par 600 km. L'altitude du site radar est de 8 m au-dessus du niveau de la mer. Le rayon maximum du radar de Dacca a été conçu au départ pour couvrir 400 km, mais son rayon d'action effectif n'est à l'heure actuelle que d'environ 250 km. Ce dernier opère à la fréquence de 2 700-2 900 MHz, avec une largeur de faisceau de 1,7°. Le radar de Dacca ne fonctionne qu'à des angles d'élévation de zéro et acquiert des données de balayage PPI (dimension de pixel : grille de 2,5 km) à des intervalles de 2-3 minutes de façon continue pendant une heure, avec une pause de 2 heures en cours d'opération. Il n'y a pas de bâtiments en hauteur autour du site du radar. Le radar n'est pas en opération à partir de 03 LST quotidiennement. Les données radar de Dacca sont archivées du 16 avril au 30 août 2000. Le radar (Figure 4.3.) couvre presque entièrement le Bangladesh incluant des portions limitrophes de l'Inde et du Myanmar.

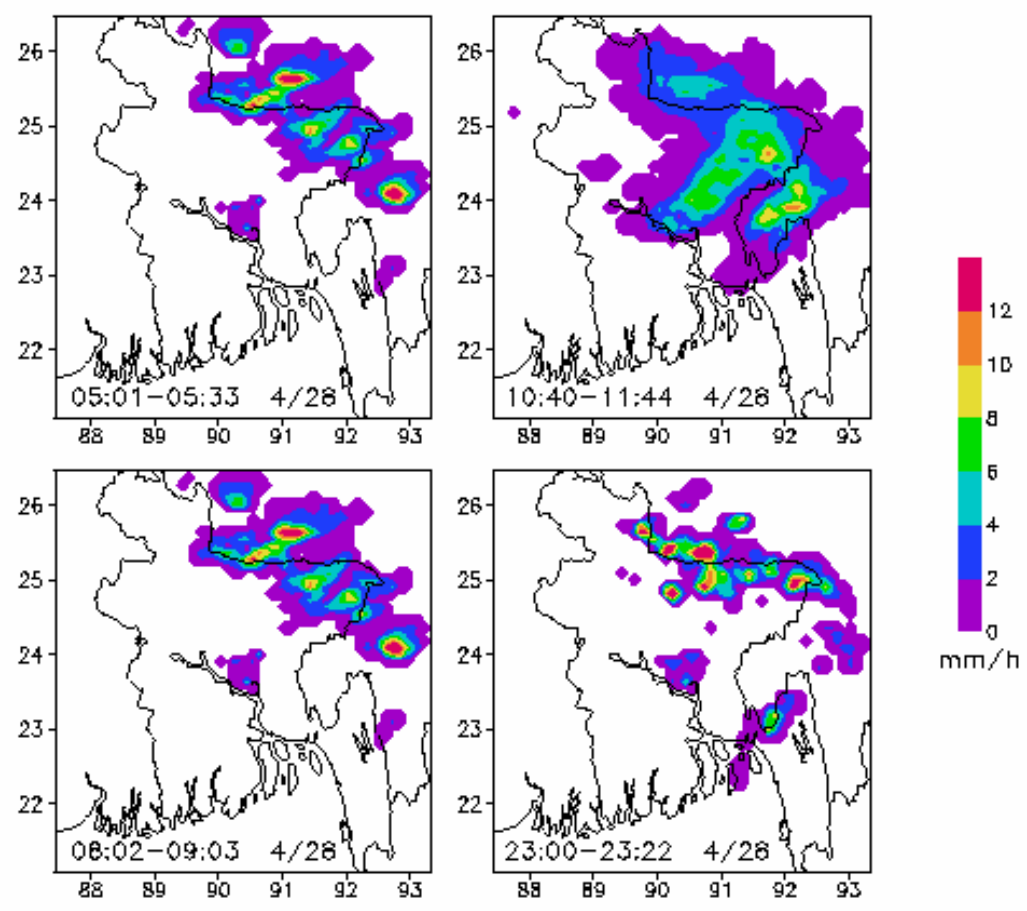

Figure 4.4. Précipitations radar enregistrées le 28 avril 2000, le taux de précipitation (mm/hr) étant calculé par unité de surface dans une grille de 10 km

Données satellitaires

Les données satellitaires proviennent du GHRC (Global Hydrological Research Centre), de la NASA (National Aeronautics and Space Administration) et du DAAC (Distributed Active Archive Center). Les données de la NASA couvrent la période de 1998-2004. Les données satellitaires couvrent principalement le Bangladesh (région GBM) et le sud des États-Unis. Les données satellitaires de TRMM comprennent à la fois des passages en mode ascendant et descendant au-dessus de la région GBM et des États-Unis. Les données satellitaires suivantes sont utilisées dans cette recherche (Figure 4.4a):

- Données radar de TRMM - Profils d'atténuation de la réflectivité, atténuation intégrée sur le parcours (PIA), profils de taux de précipitation, hauteur de la bande de brillance et classification des précipitations à partir des produits 2A25 et 2A23.

- Les données TMI de TRMM – Multifréquences et température de brillance de 1B11;

- Le produit 2A12 de TRMM;

- Les produits 3B42 et 3B43 (V5 et V6) de TRMM;

- Données infrarouge à l'échelle du globe (Global IR) d'août 2000 à août 2002 (c.-à-d**.** les données IR de GMS-5).

SIG et données hydrométéorologiques

- Données hydrométéorologiques disponibles pour le Bangladesh (Annexe : A).

- Couvertures SIG disponibles pour l'ensemble du Bangladesh (Annexe : B).

- Données de précipitations enregistrées par pluviomètre au Bangladesh (ainsi qu'une partie de la région indienne) pour la période de 1998 à 2002, disponibles dans différents intervalles de 5 min, 30 min, 1 heure, 3 heures quotidiennement, etc. (Annexe: C).

- Données de précipitation du site Mesonet (Oklahoma), aux États-Unis, pour la période de 2000-2002, à intervalle de 5 min.

Description des capteurs satellitaires et des produits

Le tableau suivant énumère les systèmes orbitaux et les capteurs satellitaires utilisés pour fins météorologiques :

Géosynchrone	Orbite polaire
GOES-12 à partir d'avril 2003	3 satellites DMSP : SSM/I – 11, 13, 14
GOES-10 à 135° ouest	3 satellites POES : NOAA-14, 15 et 17
Meteosat-7 à 0°	3 satellites de la NASA : TRMM, TERRA, AQUA
GMS-5 à 140° est	Satellites NOAA 15 et 16 : AMSU & AMSU-B
Meteosat-5 à 63° est	Satellite EOS- AQUA : AMSR-E
GOES-9 qui remplace GMS-5 en mi-2003	Satellite ADEOS-II : AMSR

Le satellite météorologique géostationnaire GMS-5

Les données horaires de température équivalente de corps noir (T_{BB}) de la bande infrarouge 1 (IR1) du satellite météorologique géostationnaire japonais GMS-5 sont utilisées pour la zone située entre 10°-30° N et 80°-100° E. Pour quantifier la fréquence d'occurrence et la zone recouverte de nuages (couverture de pixels de nuages dans une grille de 10 km dans une image) à partir des données satellitaires, on effectue une analyse objective sur les données de T_{BB} de GMS-5 dans deux zones différentes ayant chacune une couverture de 600 km x 600 km : l'une est située au-dessus du Bangladesh (terre) et l'autre, au-dessus de la baie du Bengale (océan). Les données de GMS-5 sont échantillonnées pour une grille de 0,1° × 0,1°, d'avril à septembre 2002, c.-à-d. l'année pour laquelle des données radar sont disponibles.

Pour obtenir des valeurs mensuelles moyennes, environ 720 images IR de GMS sont utilisées pour le calcul des moyennes. En fonction de l'objectif visé dans leur recherche, les chercheurs ont utilisé plusieurs seuils de température différents (Spencer *et al.*, 1989; Goldenberg *et al.*, 1990; Mapes and Houze, 1993; Machado *et al.*, 1998; Islam *et al.*, 1998; Negri and Adler, 1987). On obtient aussi la fréquence d'occurrence pour la plus grande zone à partir des données de GMS-5 en utilisant des seuils de température de <263K et <220K. Le seuil de <263K de T_{BB} est utilisé pour obtenir de l'information sur la convection de haut niveau. On détermine également l'amplitude et la phase des premières composantes de Fourier de la région <263 K.

Capteurs et produits de TRMM

Le satellite TRMM a été lancé en novembre 1997 (Kummerow *et al.*, 1998). Il acquiert des données à partir d'une orbite non héliosynchrone à faible inclinaison et le temps d'acquisition local varie au cours du mois. Ce satellite est conçu pour prendre des mesures dans les tropiques et la zone sous-tropicale (35° N – 35° S) mais, depuis qu'on a augmenté l'altitude de l'orbite à 403 km en août 2001, les fauchées de l'imageur à hyperfréquences (TMI) de TRMM couvrent désormais le sud de la Méditerranée jusqu'à 39° N. TRMM possède le premier radar satellitaire de détection des précipitations (13,8 GHz) soit le capteur de précipitations (PR). Sa sensibilité est inférieure à 0,7 mm/hr (Kummerow, 1998) et il est le seul instrument à bord de la plateforme de TRMM (Tableau 4.3) fournissant directement la distribution verticale des profils de précipitation. Ce capteur radar sera particulièrement utile pour la détermination des précipitations orographiques peu profondes difficiles à détecter à l'aide des techniques passives à hyperfréquences.

Le satellite est également doté du radiomètre TMI semblable à celui de SSM/I, excepté qu'il possède deux bandes spectrales additionnelles (polarisations verticale et horizontale), à 10,7 GHz. Le capteur TMI propose une amélioration par rapport au capteur SSM/I, avec l'ajout d'une bande polarisée à 10,7 GHz et une résolution spatiale améliorée par un facteur d'environ 2,5 (Kummerow *et al.*, 1998). La polarisation horizontale est jugée préférable à cause de l'effet d'émissivité de la surface qui lui donne une portée dynamique plus large au-dessus des terres et de l'océan comparativement aux données en polarisation verticale. De plus, en raison de l'altitude plus basse du satellite TRMM, la résolution spatiale du radiomètre TMI est d'environ deux fois plus fine que celle de SSM/I et elle offre l'avantage de pouvoir distinguer entre les précipitations convectives et les précipitations stratiformes.

La Figure 4.4a liste les produits dérivés des données des trois capteurs du satellite TRMM. Dans cette étude, deux produits standards (niveau 2) du PR, c'est-à-dire le profil des précipitations (2A25) et le type de précipitation (2A23), seront utilisés pour étalonner les extractions de précipitation au sol à partir des bandes de TMI.

Imageur à hyperfréquences TMI de TRMM

Le capteur TMI (successeur de SSM/I sur DMSP) est un radiomètre passif multibandes à hyperfréquences opérant dans cinq fréquences : 10,65, 19,35, 37,0 et 85,5 GHz en polarisation double et 22,235 GHz en polarisation unique. Le TMI fournit des informations sur le contenu des précipitations intégré sur la colonne, le contenu en eau des nuages, la glace de nuage, l'intensité des précipitations et les types de précipitation (c.-à-d. stratiforme ou convective).

Tableau 4.3 Caractéristiques des instruments du satellite TRMM

	Balayeur infrarouge visible	**Imageur à hyperfréquences TRMM**	**Radar de précipitations**
Fréquence/ Longueur d'onde	0,63, 1,6, 3,75, 10,8, 12 µm	10,65, 19,35, 37,0, 85,5 GHz en polarisation double, 22,235 GHz en polarisation verticale	13,8 GHz en polarisation horizontale
Mode de balayage	Transversal	Conique	Transversal
Résolution au sol	2,1 km	Portée de 5 km à 85,5 GHz à 45 km à 10,65 GHz	4,3 km au nadir
Largeur de la fauchée	720 km	760 km	220 km

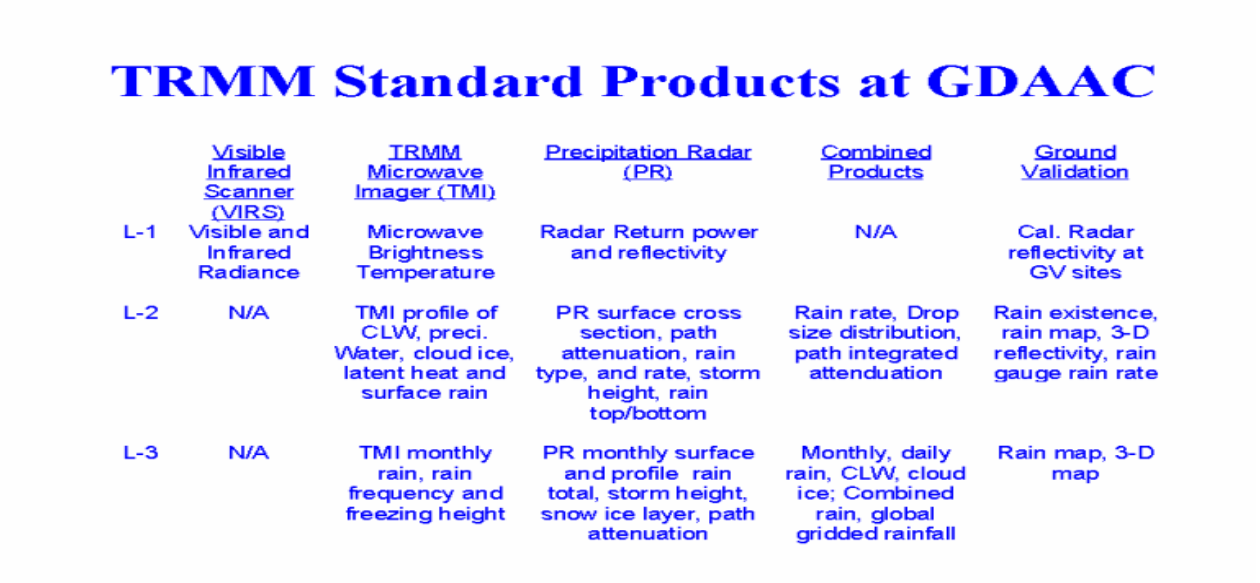

Figure 4.4 a. Produits dérivés des données du satellite TRMM.
Source :trmm.nasa.gsfc.gov

Radar de détection des précipitations - PR

Le capteur PR, le premier capteur de ce type dans l'espace, est un radar à balayage électronique qui mesure la distribution des précipitations en 3-D au-dessus de la terre et des océans permettant ainsi de définir l'épaisseur de la couche de précipitation. Le capteur a une fréquence atténuée de 13,8 GHz (longueur d'onde de 2,2 cm) en polarisation horizontale, une largeur de fauchée de 220 km, une résolution spatiale de 4,3 km près du nadir et une résolution verticale de 250 m. L'agence spatiale du Japon, la NASDA, a démontré qu'un seuil normal de sensibilité d'environ 17 dBz présente une stabilité cohérente à l'intérieur de 0,8 dB.

Données infrarouge à l'échelle du globe et produits de précipitation IR étalonnés de TRMM

Les données IR utilisées dans cette étude proviennent principalement de la constellation internationale de satellites météorologiques en orbite géosynchrone, les satellites GOES (Geosynchronous Operational Environmental Satellites, État-Unis), GMS (Geosynchronous Meteorological Satellite, Japon) et Meteosat (Meteorological Satellite, Communauté européenne). Il y a généralement deux plateformes GOES en activité, GOES-EST et GOES-OUEST, qui couvrent respectivement l'est et l'ouest des États-Unis. Les vides dans la couverture géosynchrone (notamment au-dessus de l'Océan Indien avant juin 1998) doivent être comblés par des données IR provenant des satellites météorologiques en orbite polaire de la série NOAA. Les estimations de précipitation de TRMM sont fournies sur une grille à l'échelle du globe de 0.25° x 0.25° au-dessus de la zone de 50° N-S de latitude, en dedans de six heures du temps d'observation.

Trois produits sont disponibles : un produit de fusion de toutes les estimations de précipitation disponibles de TMI et de SSM/I étalonnées par TRMM (accumulations aux trois heures); une estimation infrarouge géosynchrone étalonnée à l'aide des données hyperfréquences fusionnées (estimations aux heures); et une combinaison des deux premiers champs (accumulations aux trois heures).

Le produit 3B40RT (haute qualité ou HQ) : c'est un produit de fusion combinant toutes les estimations de précipitation hyperfréquences de SSM/I et de TMI disponibles en un seul produit de précipitation de haute qualité. Les estimations de SSM/I sont calculées à l'aide de l'algorithme GPROF 5.0-SSMI tandis que les estimations de TMI sont calculées avec l'algorithme GPROF

5.0-TMI (le produit A212 de TRMM en temps réel). Avant la fusion, les données de SSM/I sont étalonnées par rapport aux données de TMI en utilisant des histogrammes jumelés séparés de surface terrestre et océanique à l'échelle du globe.

Le produit 3B41RT (taux de précipitation variable infrarouge ou VAR) : ce sont des estimations de précipitation réalisées à partir des observations infrarouge géostationnaires à l'aide d'un étalonnage spatialement et temporellement variable du produit HQ. L'algorithme utilise une approche basée sur un seuil de probabilité adapté qui assure que l'histogramme des taux de précipitation infrarouge moyennés par rapport à la grille correspond localement à l'histogramme des taux de précipitation HQ moyennés par rapport à la grille. Dans ce cas, on parle de l'algorithme du taux de précipitation variable infrarouge (VAR).

Le produit 3B42RT (fusion des produits HQ et VAR) : c'est le produit de la fusion des produits 3B40RT (HQ) et de 3B41RT (VAR). La procédure actuelle en est une de simple remplacement : pour chaque maille de la grille, la valeur de HQ est utilisée lorsque disponible, sinon la valeur de VAR est utilisée. Adler *et al.* (2000) utilisent présentement une combinaison des données de TRMM et infrarouge géosynchrone (geo-IR) pour fournir des estimations de précipitation aux trois heures au-dessus de la zone située entre 50° N et 50° S à l'aide d'une approche basée sur l'algorithme 3B42 post-temps-réel multicapteurs de TRMM. Ce produit utilise au départ une combinaison d'estimations de TRMM et d'estimations de SSM/I étalonnées par TRMM.

MÉTHODOLOGIE

Le chapitre 5 de la thèse décrit les approches utilisées pour réaliser chacun des six objectifs de la recherche.

À l'heure actuelle, le seul outil dont on dispose pour mesurer les précipitations au Bangladesh est un réseau de pluviomètres à faible densité de sorte qu'il n'existe pas vraiment de façon d'acquérir une connaissance des propriétés des systèmes pluvieux existants. Dans un premier temps, les données radar du Bangladesh Meteorological Department (BMD) ont été utilisées pour obtenir des répartitions précises de précipitations et pour déterminer les caractéristiques des systèmes pluvieux (objectif 1). C'est la première fois que ces données radar sont utilisées dans un contexte de recherche. Les précipitations radar ont été analysées pour 135 jours consécutifs, à partir du

16 avril 2000, et comparées aux précipitations mesurées par les pluviomètres (objectif 2). Les radars du BMD acquièrent des données de précipitation dans six domaines. Le statut des précipitations est converti en taux de précipitation et la méthodologie (Anagnostou and Karajewski, 1999) est décrite à la section 5.2 (Équations 5.1 à 5.4). Nous avons ainsi obtenu les variations diurnes ainsi que les caractéristiques des précipitations en fonction de l'activité nuageuse.

Par ailleurs, la performance des données radar et des produits pluviométriques de TRMM est évaluée à l'aide des données de précipitation acquises par pluviomètre (objectif 3). Les précipitations dérivées du produit 3B42 de TRMM (résolution de 1° x 1°) sont comparés aux précipitations de 33 pluviomètres au sol pour les années 1998-2002. Les quantités de précipitations journalières déterminées à l'aide des données de TRMM et des pluviomètres sont comparées pour 274 journées consécutives (du 1er mars au 30 novembre), pour chaque année et pour chaque station.

Le cycle diurne des précipitations au Bangladesh est également analysé à l'aide des produits pluviométriques de GMS-5, du radar au sol et de TRMM (objectif 4). Les précipitations journalières de 2002 à 2004 pour 33 pluviomètres du BMD (Figure 4.2.) sont moyennées pour déterminer les variations intra-saisonnières des précipitations au Bangladesh. Les données horaire de température équivalente de corps noir ou température de brillance (T_{BB}) IR1 du GMS-5 sont traitées pour une grille de 10 km dans la zone située entre 80-100° E et 10-30° N, d'avril à septembre 2000, afin de voir l'activité des nuages à grande échelle et de pouvoir comparer avec les observations radar.

Une approche statistique est testée afin d'améliorer les estimations pluviométriques radar au sol au Bangladesh (objectif 5). En effet, il y a en deux problèmes dans l'utilisation des données radar du BMD. D'une part, les données sont limitées au statut des précipitations en fonction de six portées différentes (1-4 mm/h; 5-16 mm/h; 17-32 mm/h; 33-64 mm/h; 65-128 mm/h; et >129 mm/h). D'autre part, une relation précise de Z (réflectivité) - R (taux de précipitation) est nécessaire pour la région. Dans cette étude, nous avons tenté d'obtenir le taux de précipitation à partir des données de statut de précipitation dérivées des données radar du BMD. Les données de statut de précipitation ont été converties en taux de précipitation horaire (R) selon la méthodologie décrite dans la section 5.2. La quantité de précipitation estimée par le radar de

Dacca est comparée avec celle des pluviomètres et celle-ci s'avère beaucoup plus faible que celle mesurée par chaque pluviomètre individuel. Les coefficients de corrélation entre les taux de précipitation radar et ceux des pluviomètres pour les différents mois (0,63-0,89) sont présentés à la section 6.2.2. Les différences entre les deux taux peuvent provenir d'incohérences dans le calcul des moyennes temporelles et spatiales des données radar et des données de pluviomètres. Ces différences peuvent également provenir du calcul des précipitations à partir des données de statut de précipitation basé sur la relation Z-R simple. Enfin, la relation Z-R standard ($Z=200R^{1,6}$) est utilisée pour convertir le taux de précipitation en sa réflectivité. Les données de réflectivité sont utilisées pour estimer les valeurs des paramètres de l'algorithme de précipitation radar dans l'équation 5.5. Le radar de Dacca acquiert des données de balayage de PPI avec un azimut de zéro.

Enfin, nous présentons le développement d'une procédure d'estimation des précipitations au sol basée sur l'utilisation des données satellitaires de précipitation radar et de radiomètre passif à hyperfréquences (objective 6). Le satellite de la mission TRMM (Tropical Rainfall Measuring Mission) est équipé de deux capteurs utiles pour l'analyse des précipitations : un capteur radar de détection des précipitations (PR) et un imageur à hyperfréquences (TMI). Dans cette étude, deux produits standards du PR, c'est-à-dire le profil des précipitations (2A25) et le type de précipitation (2A23), sont utilisés pour étalonner les extractions de précipitation au sol à partir des bandes de TMI. L'étalonnage de PR-TMI est réalisé pour deux zones différentes (la région des fleuves Gange-Brahmapoutre-Meghna, ou GBM, et le sud des États-Unis) et les résultats sont comparés pour évaluer l'importance des différences. Des données simultanées du PR et de TMI, couvrant quatre mois d'été (juin-septembre) de l'année 2000, sont utilisées pour l'étalonnage de l'algorithme hyperfréquences de surface (MW). La procédure d'étalonnage développée par Grecu and Anagnostou (2001) consiste en (i) la délimitation de la zone de précipitation, (ii) la classification convective/stratiforme des précipitations et (iii) l'utilisation d'un modèle de régression multiple linéaire pour l'estimation du taux de précipitation (Figure 5.4).

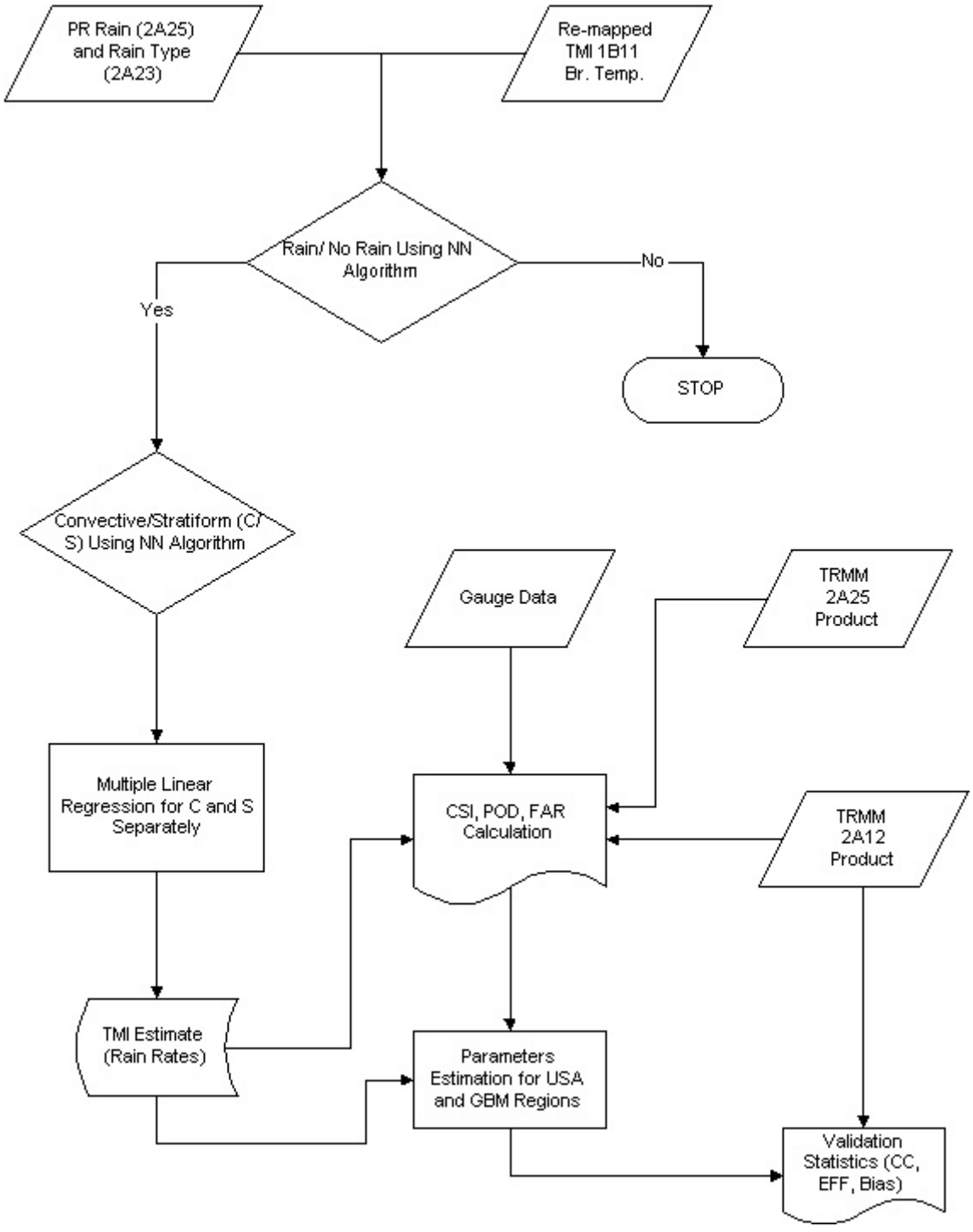

Figure 5.4. Organigramme de l'algorithme de précipitation basé sur les données du capteur passif à hyperfréquences

RÉSULTATS ET DISCUSSION

Caractérisation des précipitations au Bangladesh

Le taux de précipitation a été extrait du statut des précipitations dérivé des données radar du BMD. La corrélation entre les précipitations estimées par le biais d'une moyenne mobile de trois jours à partir des données radar et des pluviomètres variait mensuellement de 0,63-0,89, en 2000. Les données radar ont été systématiquement sous-estimées du quart par rapport à la valeur des pluviomètres. Des échos de faible dimension (~80 km^2) contribuent grandement à la quantité totale de précipitation, mais on a observé peu d'échos de grande dimension. La répartition des précipitations au-dessus du Bangladesh dérivée des données radar montre des précipitations importantes dans le nord-est et le sud-est du pays, ce qui est cohérent avec les données de précipitation des pluviomètres. À l'aide des caractéristiques des données radar de 185 systèmes convectifs analysés, il a été possible d'identifier la localisation, la durée de vie, la forme, la dimension, la vitesse de propagation et la direction des précipitations. La couverture des données radar du BMD est divisée en trois régions : le nord, le centre et le sud. En général, les systèmes pluvieux se développent dans la région nord et tendent à se déplacer vers l'est. Le développement des systèmes pluvieux dans les régions du centre et du sud est significatif durant les mois de la mousson (juin à août). La durée de vie moyenne de ces systèmes est de ~5,7 heures. La vitesse de mouvement est de ~5 m/sec.

Distribution horaire et journalière des précipitations

L'analyse des données radar montre que l'heure moyenne de précipitation maximale est de 00-06 LST dans la région nord, de 06 LST et de 15-18 LST dans le centre et 06-09 LST dans le sud. Le cycle diurne des précipitations au Bangladesh est caractérisé par un pic matinal à 0600 LST avec un minimum à midi. La fréquence des échos montre deux pics, un en après-midi (~1500 LST) et l'autre durant la matinée (0600 LST). Les plus petits échos dominent durant l'après-midi tandis que les échos plus importants sont observés tôt en matinée.

Les données des pluviomètres du BMD sur 33 sites sont utilisées pour vérifier les résultats radar. Les répartitions de précipitations obtenues à l'aide du radar et des pluviomètres affichent un patron similaire, mais l'heure de la précipitation maximale déterminée par le radar est plus hâtive que celle des pluviomètres. La répartition des précipitations à travers tout le domaine du radar

suggère que le temps le plus probable pour enregistrer une précipitation au Bangladesh se situe entre 21 et 09 LST (heure locale), alors que 06 LST est l'heure la plus probable pour enregistrer la précipitation maximale sur l'ensemble du pays. On doit mentionner qu'aucune donnée n'est disponible pour la période entre 03-06 LST. L'occurrence de précipitations entre 21 et 09 LST est possiblement associée aux effets locaux tels qu'un terrain complexe et la circulation des vents océaniques et terrestres. La précipitation maximale du matin à 06 LST au Bangladesh est différente de celle du sous-continent indien ou de la zone montagneuse où, généralement, la précipitation maximale se produit en après-midi. La frontière nord du Bangladesh, près de la montagne de Shillong en Inde, est la région qui enregistre le taux de précipitation le plus élevé, tandis que la zone frontalière vient en deuxième quant au volume de précipitation le plus élevé.

Comparaison TRMM et pluviomètres

Des 274 journées moyennées sur 5 années de précipitations pour les 31 stations, 97,08 et 98,91 % de ces journées sont détectées respectivement comme des journées avec précipitation par TRMM et les pluviomètres (Figure 6.18). Les journées avec précipitation détectées par TRMM étaient corrélées à 95,99 % avec les journées détectées par les pluviomètres. En moyenne, TRMM peut détecter environ 98,24 % des précipitations des pluviomètres. TRMM surestime les précipitations au cours de la période de la pré-mousson et sous-estime celles-ci durant la mousson, alors que pour la période post-mousson, elles sont semblables. Globalement, TRMM sous-estime les précipitations dans les zones de fortes précipitations au Bangladesh (Figure 6.18).

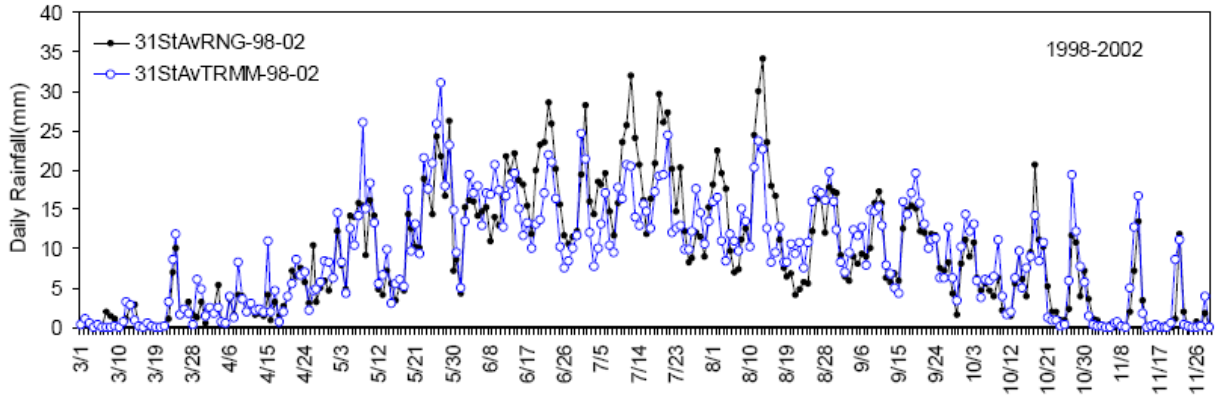

Figure 6.18. Séquences temporelles des moyennes de précipitation (mm) sur 5 ans (1998-2002) déterminées à partir des données de TRMM et de 31 stations à travers le pays.

Cycle diurne des précipitations GMS-5

Les données horaires du satellite japonais à haute résolution GMS-5 (Japanese Geostationary Meteorological Satellite) (grille de 10 km) sont échantillonnées en fonction d'une grille de 1° × 1° sur une zone de 600 km × 600 km au-dessus du Bangladesh (portion terrestre) et de la partie nord de la baie du Bengale (portion océanique) pour obtenir le cycle diurne de l'activité nuageuse. La région recouverte de nuages montre des pics en après-midi (~1700 LST) et en matinée (~0003 LST) au-dessus des portions terrestres qui sont généralement constitués de systèmes de nuages convectifs relativement profonds et de petite dimension (<214K) et plus grands mais superficiels (<243K). Au contraire, on observe uniquement un pic en après-midi (1400-1600 LST) au-dessus des portions océaniques composé généralement de systèmes de petits nuages convectifs superficiels et de gros nuages profonds. Au même moment, la fréquence des systèmes de nuages affiche un pic de temps clair (~1600 LST) au-dessus des portions terrestres et océaniques indiquant que l'après-midi est la période de formation des cellules d'origine terrestre au-dessus du Bangladesh et des cellules d'origine océanique dans la zone océanique étudiée (87,44°-93,33° E; 15,7°-21,08° N). La partie nord-ouest du Bangladesh est affectée surtout par des nuages pré-mousson alors que le pays dans son ensemble est soumis aux activités maximales de la mousson.

Structure verticale et variation diurne des précipitations d'après les données TRMM

La structure verticale des précipitations a été analysée à l'aide des données 2A25 de TRMM et la variation diurne des précipitations à l'aide des données 3B42RT de TRMM et cela à partir de la période de la pré-mousson jusqu'à celle de la post-mousson, à l'intérieur et autour du Bangladesh. L'analyse des données 2A25 de TRMM révèle que les précipitations durant la période de la pré-mousson, de la mousson et de la post-mousson sont respectivement fortes, modérées et moins intenses. Des taux élevés de précipitation sont observés aux altitudes plus hautes durant la pré-mousson et relativement plus faibles aux altitudes plus basses au cours des périodes plus tardives. Quant aux moyennes pour les données de 4 ans, on observe que les taux de précipitation maximum en avril, juillet et octobre sont respectivement de 114,19, 73,88 et 49,28 mm/h. En général, les échos de la période de la pré-mousson sont plus marqués comparativement aux périodes de la mousson et de la post-mousson. Cependant, on observe la

hauteur maximale du sommet des échos d'environ 18,25, 18,8 et 18,25 km respectivement durant la période de la pré-mousson, de la mousson et de la post-mousson. L'analyse des données 3B42RT de TRMM révèle que les précipitations maximales au-dessus du Bangladesh et de la baie du Bengale ont été enregistrées à 06 LST durant la période de la mousson. Au cours de la même période, le maximum de précipitation est enregistré à 18 LST en Inde. Pour l'ensemble de la période des pluies (mars à novembre), le maximum de précipitation au-dessus du Bangladesh a été enregistré à 06 LST, avec un pic maximum secondaire à 15 LST. Le maximum de précipitation du matin à 06 LST au-dessus du Bangladesh est confirmé après comparaison avec les données correspondantes obtenues des pluviomètres au sol. Cette analyse révèle, qu'au Bangladesh, la surestimation et la sous-estimation des précipitations par TRMM durant la pré-mousson et la mousson dépendent respectivement des différentes structures verticales des champs de précipitation au cours des périodes correspondantes.

Estimation quantitative des précipitations au Bangladesh à partir d'une combinaison d'observations radar et de mesures de pluviomètres

Une procédure statistique pour l'estimation quantitative des précipitations au Bangladesh a été développée à partir d'une combinaison d'observations radar et de mesures de pluviomètre. Les limites d'incertitude associées à ces estimations sont également évaluées à une résolution spatiale et temporelle donnée. Il y a six paramètres qui contrôlent les diverses étapes de traitement. L'analyse de sensibilité a montré qu'il existe une multitude de valeurs de paramètres provenant des différentes régions dans l'espace du paramètre qui sont également acceptables comme prédicteurs de précipitations. En conséquence, une méthodologie est conçue pour évaluer l'incertitude émanant des erreurs dans la structure de l'algorithme et le choix des paramètres. Dans le contexte de cette méthodologie, le problème de l'étalonnage de l'algorithme est formulé dans l'estimation des probabilités a posteriori du niveau de réponse acceptable de l'algorithme, évitant ainsi le concept de la détermination des valeurs de vraisemblance associées aux erreurs entre les quantités de précipitation observées et estimées obtenues par le biais de l'échantillonnage répétitif de l'espace des paramètres en utilisant la technique de Monte Carlo. Ces valeurs de vraisemblance, conjointement avec la distribution a priori assumée de l'ensemble des paramètres, sont utilisées pour construire la distribution a posteriori reflétant ainsi la performance de l'algorithme. Un des avantages de cette approche est que la distribution a

posteriori est systématiquement mise à jour dans le cadre bayésien permettant ainsi l'incorporation de nouvelles informations à partir d'observations réalisées durant des périodes différentes (ou sur différents sites radar).

Estimation des précipitations au sol basée sur l'utilisation des données satellitaires de précipitation radar et de radiomètre passif à hyperfréquences

L'algorithme développé par Grecu et Anagnostou (2001) est également comparé à la version la plus récente [version 6 (V6)] du produit 2A12 de TRMM en termes de détection des précipitations et des statistiques d'erreur d'extraction du taux de précipitation sur la base des précipitations de référence du PR. Il s'avère que le produit 2A12 n'est pas performant au dessus du Bangladesh car son taux de détection des précipitations est très faible. Toutefois, la performance de l'algorithme diffère pour les deux régions. Par exemple, la réduction de l'erreur aléatoire (relative à la version 6 de 2A12) est d'environ 26 % et 135 % respectivement pour les États-Unis et la région GBM. La région des États-Unis affiche de meilleurs résultats que la région GBM (Figure 6.40).

À l'aide de graphiques CFAD (C*ontoured Frequency versus Altitude Plots* ou statistiques de contours de fréquence par rapport à l'altitude) de la réflectivité du PR en 3D (Figure 6.41), pour les précipitations stratiformes et convectives, on montre que le Bangladesh est dominé par des précipitations stratiformes. D'ailleurs, les régions qui montrent un taux de détection erronée plus élevé sont celles où les précipitations stratiformes dominent. Les États-Unis sont dominés par la convection durant la saison estivale, mais il semble qu'il y ait aussi une présence importante de nuages stratiformes moyens. Il est démontré que les algorithmes d'estimation des précipitations au sol basés sur les hyperfréquences performent mieux dans le cas des systèmes pluvieux à convection profonde. L'algorithme de Grecu et Anognostou (2001) performe mieux que celui de 2A12, particulièrement au-dessus du Bangladesh, parce que l'approche basée sur les réseaux de neurones pour la délimitation des zones de précipitation utilise plusieurs bandes et différentes caractéristiques du système nuageux.

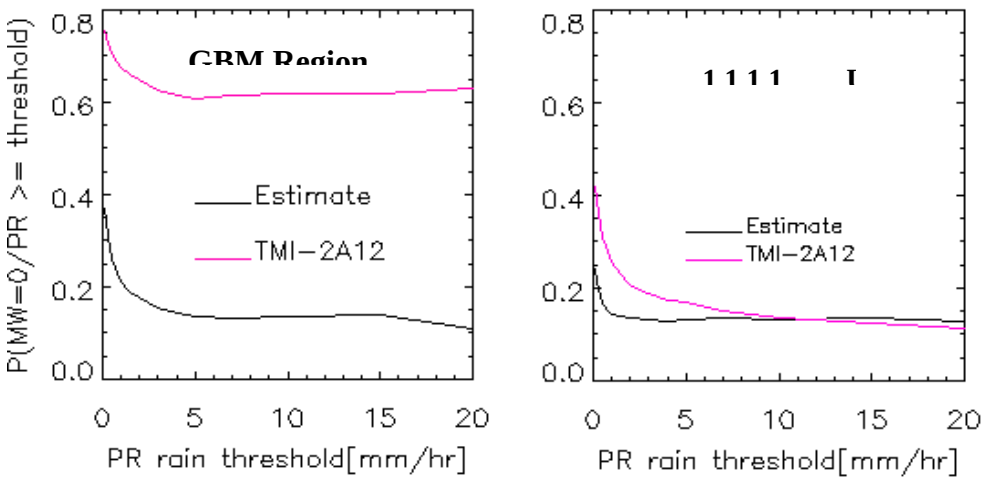

Figure 6.40 Erreurs de détection de précipitation de TMI en fonction du seuil de précipitation PR. 'Estimate' est une valeur estimée et 'TMI-2A12' correspond à la précipitation de surface dérivée du produit 2A12 Ver5.0 de TRMM.

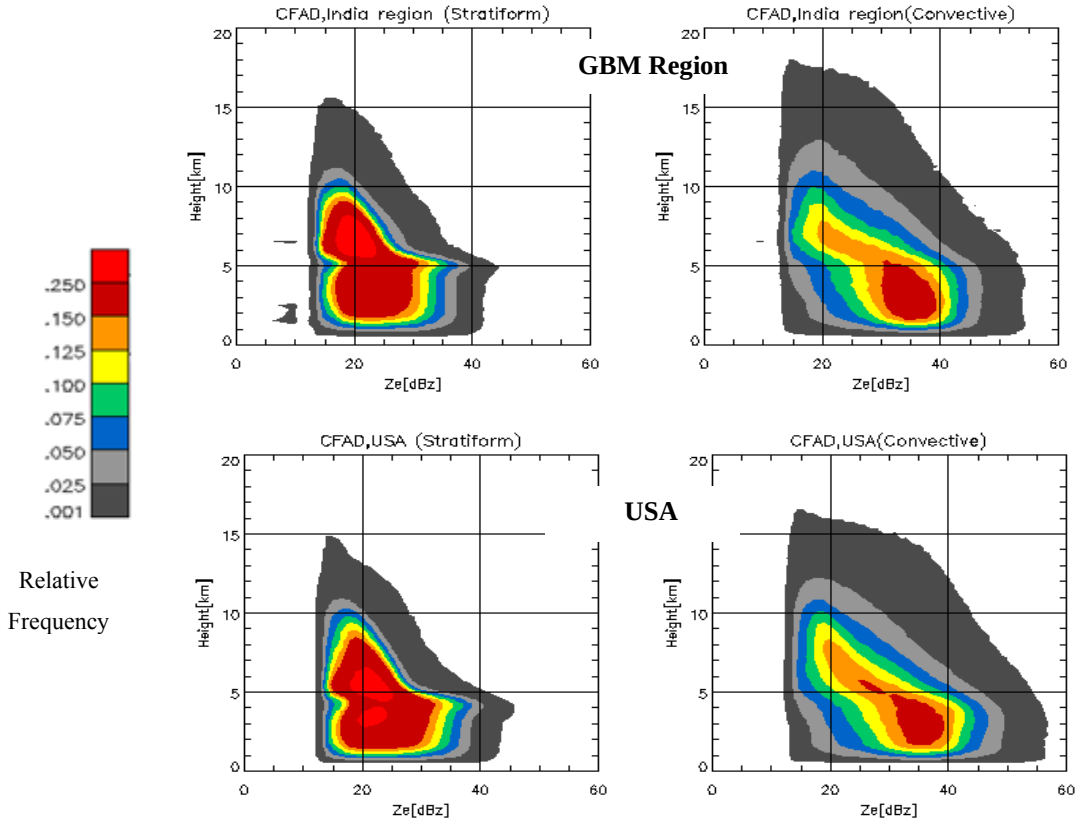

Figure 6.41 Comparaison du profil de réflectivité de PR au-dessus de deux régions à l'aide de graphiques CFAD (Contoured Frequency versus Altitude Plots ou statistiques de contours de fréquence par rapport à l'altitude).

CONCLUSIONS

Les six objectifs de recherche définis au départ pour cette thèse ont été atteints : 1) D'abord, les caractéristiques des systèmes pluvieux du Bangladesh ont été analysées à partir des données radar, TRMM et GMS-5. Les systèmes généralement constitués de systèmes de nuages convectifs se développent dans le Nord du pays. Leur durée moyenne est de 5.7 heures et ils se déplacent à 5m/s. La période optimum des précipitations maximales est entre 00-06 LST dans les régions du Nord, 06 LST dans les régions du Sud ainsi que 06 LST et 15-18 LST dans le Centre. Ce maximum de précipitations la nuit est assez particulier mais s'expliquerait par le caractère océanique du pays. Une autre particularité est que l'intensité des précipitations orageuses de la période de pré-mousson est supérieure à celle des précipitations de la mousson; 2) La performance des estimations du radar météo de Dacca a été évaluée à l'aide des données de pluviomètres et le radar sous-estime de 25 % les valeurs des pluviomètres à cause des paramètres utilisés dans la relation Z-R et de la couverture limitée (100 km); 3) La performance des produits pluviométriques de TRMM (1998-2002) a également été évaluée à l'aide des données de 31 stations. Le produit 3B42 détecte tous les jours de pluie et peut déterminer 98 % des précipitations. 4) L'analyse du produit TRMM 2A25 (2000-2003) a montré que les précipitations pré-mousson sont fortes comparées à celles pendant et après la mousson. La structure verticale varie dans le temps. Durant la période pré-mousson, les échos en altitude sont plus forts qu'à la base et c'est l'inverse après la mousson. Cette différence dans la structure des précipitations serait la cause de la surestimation des précipitations par TRMM 3B42RT durant la période pré-mousson et la sous-estimation durant la mousson. Le produit 3B42RT a aussi confirmé les précipitations maximales à 06 LT. 5) Des paramètres spécifiques pour le radar de Dacca de l'algorithme de précipitation radar ont été déterminés à l'aide de la technique du filtre de Kalman et des données de 3 stations voisines. La corrélation entre les données des pluviomètres et du radar est passée de 43 % à 58 % en utilisant les nouveaux paramètres, à 90 % en incluant un facteur d'ajustement d'erreur et à 96 % avec le filtre de Kalman. 6) Enfin, les produits radar 2A25 (intensité) et 2A23 (type de pluie) ont été utilisés pour étalonner des données micro-ondes passives (TM1) de plus faible résolution spatiale. Une approche basée sur les réseaux de neurones, développée par Grecu et Anagnostou (2001), a été comparée à celle de Kummerow et al (2001) utilisée pour le produit TM1-2A12. L'approche RN donne de meilleurs résultats parce qu'elle utilise les différentes

caractéristiques du système nuageux (stratiformes / convectifs). Qu'importe l'algorithme, les estimés sont meilleurs pour les précipitations stratiformes que convectives.

Il n'a pas été possible d'étudier un quelconque scénario hydrologique en raison des limites temporelles des données satellitaires de TRMM, mais le produit pluviométrique de TRMM s'est avéré très utile pour étalonner les autres produits satellitaires ce qui pourrait faciliter le suivi en temps réel des précipitations au Bangladesh. Ainsi, il est recommandé d'étalonner les données de l'imageur passif à hyperfréquences de SSM/1 (et/ou les données de AMSR et AMSU-B) à l'aide des données étalonnées actuelles de TM1 de TRMM au-dessus du Bangladesh. Les données infrarouges à l'échelle du globe (Global IR à intervalle de ½-heure) peuvent également être étalonnées à l'aide du produit pluviométrique basé sur les multicapteurs hyperfréquences.

RECOMMANDATIONS

Les caractéristiques des précipitations, leur variabilité ainsi que leur cycle diurne ont été examinés à l'aide des données pluviométriques dérivées des radars terrestres, de GMS-5 et de TRMM. Les paramètres de l'algorithme de précipitation radar ont été calculés basé sur les six catégories de statut des précipitations radar. Les données de TMI ont été étalonnées à l'aide des données PR de TRMM d'estimation des précipitations radar au-dessus du Bangladesh. On recommande une mise à niveau (enregistrement de la réflectivité et des balayages pour le volume) du réseau de radars du BMD et, dans un futur prochain, il sera possible d'obtenir des valeurs pluviométriques quantitatives à partir des données radar du BMD. Il est nécessaire d'avoir des données pluviométriques radar à long terme pour trouver la relation Z-R avec un meilleur ajustement et pour étalonner les résultats radar avec les valeurs des pluviomètres.

Les effets orographiques locaux n'ont pas été étudiés dans cette étude. Ainsi, les effets orogéniques locaux par rapport aux précipitations de la mousson au Bangladesh devraient être examinés de façon plus détaillée à l'aide des observations radar et des extractions de précipitation par capteur passif à hyperfréquences. Dans notre analyse, nous n'avons pas trouvé de fort contraste entre les amplitudes des variations diurnes au niveau des activités des nuages au-dessus des portions terrestres et océaniques. Ce résultat diffère par rapport au cycle diurne rapporté au-dessus des continents tropicaux et, aussi des autres continents durant l'été (Meisner and Arkin, 1987). Ainsi, nous favorisons à l'avenir une analyse plus poussée utilisant des données à long

terme et à grande échelle pour vérifier le résultat présent et pour documenter la forme réelle du cycle diurne de l'activité nuageuse à l'intérieur et autour du Bangladesh.

Au sud du Bangladesh, le maximum de précipitation est enregistré le matin alors que, dans la partie nord du pays, ce maximum est plutôt observé du milieu de la nuit au petit matin (Ohsawa *et al.*, 2001; Prasad, 1974). Toutefois, l'information sur le noyautage des orages et la longévité des noyaux dérivée des données à haute résolution temporelle et spatiale, de même que les mécanismes responsables du développement de la convection, font toujours l'objet de discussion. À cause de l'absence de données d'observation à long terme, la simulation de modèles, comme le modèle MM5, utilisé par Warner *et al.* (2003) et Mapes *et al.* (2003b) pour l'étude du patron diurne des précipitations dans le nord-ouest de l'Amérique du Sud, pourrait être utilisée dans un futur prochain pour élargir la présente étude.

Il n'a pas été possible d'étudier un quelconque scénario hydrologique à cause des contraintes temporelles des données satellitaires de TRMM, mais nous avons trouvé par contre que le produit pluviométrique de TRMM est très utile pour étalonner les autres produits satellitaires. Ainsi, il est recommandé d'étalonner les données du capteur passif à hyperfréquences de SSM/I (et/ou AMSR et AMSU-B) à l'aide des données étalonnées de TMI de TRMM au-dessus du Bangladesh. Il existe également des données infrarouges à l'échelle du globe à intervalle de ½-heure et il est également recommandé d'étalonner ces données IR à l'aide du produit pluviométrique multicapteurs à hyperfréquences. Enfin, ce produit peut être utilisé dans la modélisation hydrologique pour étudier la propagation des erreurs dans les différents flux hydrologiques par le biais de la simulation de modèles et des données d'observation.

À l'heure actuelle, les satellites F-13, F-14 et F-15 sont opérationnels. Le SSM/I est un système radiométrique passif à hyperfréquences à sept bandes, à quatre fréquences et à polarisation linéaire qui mesure les températures de brillance atmosphérique, océanique et terrestre dans les hyperfréquences de 19,35, 22,235, 37,0 et 85,5 GHz. Chaque satellite DMSP possède une orbite héliosynchrone quasi-polaire de 101 minutes, à une altitude de 830 km au-dessus de la Terre, avec une inclinaison de 98,9° et une largeur de fauchée de 1 400 km permettant une couverture à l'échelle du globe deux fois par jour. La combinaison des satellites avec couverture jour/nuit et aurore/crépuscule permet le suivi d'information à l'échelle du globe, notamment sur les nuages, à toutes les six heures. L'orbite polaire fournit une couverture nominale au-dessus des latitudes de

85° N-S, bien que des contraintes dans les techniques d'extraction limitent les estimations utiles de précipitation dans le cas des terres froides (diffusion), des terres (émissions) ou de la glace de mer (diffusion et émission). Le satellite SSM/I est un capteur opérationnel et les données enregistrées souffrent des lacunes habituelles associées à ce type de données dû aux erreurs de traitement, des périodes de temps mort reliées aux récepteurs, etc. Avec le temps, la couverture s'est améliorée au fur et à mesure des améliorations apportées au système.

De façon optimale, les différences entre les estimations des divers satellites devraient être aléatoires à des échelles spatiales réduites et temporelles courtes et négligeables pour des échelles spatiales plus grandes et des échelles temporelles plus longues. Malheureusement, ceci n'est pas le cas présentement pour la plupart des estimations terrestres des capteurs à hyperfréquences. Dans cette optique, il est nécessaire de formuler une méthodologie efficace pour étudier et éliminer les différences systématiques entre les estimations pluviométriques hyperfréquences et, ainsi, construire une base de données unifiée de produits pluviométriques à partir d'une combinaison d'estimations de divers instruments passifs à hyperfréquences. La base de données du capteur passif à hyperfréquences sera utilisée pour entraîner de façon cohérente l'extraction des précipitations haute fréquence de l'infrarouge satellitaire, ce qui permettrait de produire conjointement avec les estimations hyperfréquences moins fréquentes des estimations de précipitation optimale à diverses échelles spatiales (0,1-0,5°) et temporelles (de 1 heure à 6 heures) au-dessus de l'Asie du Sud-Est.

Nous proposons une approche "du bas vers le haut" dans laquelle l'effort est concentré sur une façon d'associer (ou de transférer en partie) l'information dérivée de l'estimation des précipitations haute résolution en temps réel aux échelles temporelles plus longues et à des échelles spatiales plus grandes. En particulier, les estimations pluviométriques de PR de TRMM seraient utilisées pour améliorer l'étalonnage d'un certain nombre d'algorithmes de capteur passif à hyperfréquences (TMI, SSM/I, AMSR et AMSU-B) pour l'estimation des précipitations à l'échelle de l'empreinte au sol du radiomètre. Une formulation bayésienne pourrait être proposée pour déterminer de façon optimale cette combinaison, de même que l'incertitude associée aux produits de fusion. Les estimations pluviométriques simultanées du réseau dense de pluviomètres disponible au Bangladesh seraient utilisées pour déterminer les matrices de covariance associées à cette formulation. Il est supposé que les extractions de PM seraient non biaisées par rapport aux

précipitations de PR, mais l'erreur aléatoire varierait probablement d'un capteur à l'autre. Les différentes erreurs statistiques des capteurs PM seraient évaluées à l'aide des mesures de précipitation des pluviomètres. Enfin, le produit pluviométrique final pourrait être utilisé dans les modèles hydrologiques (p. ex. HYDROTEL, HSP-F, Mike SHE) pour étudier la propagation des erreurs dans la modélisation des variables hydrologiques à des échelles temporelles et spatiales différentes.

Une mise à niveau du réseau de radars du BMD est fortement recommandée et, dans le proche futur, il serait alors possible d'obtenir des valeurs quantitatives de précipitation à partir des radars du BMD. Les produits pluviométriques de PR de TRMM et les produits étalonnés de PM pourraient être utilisés pour étalonner les radars du BMD afin de pouvoir estimer les précipitations en temps réel dans le contexte du développement des modèles de prévision d'inondations (Mike 11 est le modèle en cours d'utilisation) au Bangladesh.

CHAPTER 1

1. INTRODUCTION

1.1 Statement of the Problem

Rainfall is one of the most important processes in the hydrological cycle, but also one of the most difficult to monitor. Rainfall and its variability are not only important constituents of the global hydrological cycle, but also influence the course of development of all living organisms on our planet. Particularly over tropical regions, given the socioeconomic condition of many countries, people critically depend on the precipitation and its variability in time and space because of water use in agricultural and everyday life, flood and drought monitoring. Precise estimation of precipitation is essential because of such important consequences as flooding and drought, which are particularly common natural disasters in Bangladesh. Thunderstorms in Bangladesh cause death and huge damage due to flash floods every year. Matsumoto (1998) discussed the flood situation in Bangladesh and pointed out that heavy rainfall there together with other phenomena is one of the causes of floods. Knowledge of the precise distribution and quantification of precipitation therefore may prove helpful for disaster prevention and water management in Bangladesh.

Bangladesh (area 144,000 km^2) is a country in South East Asia experiences flooding in every year on up to two-thirds of its territory. The topography of Bangladesh is characterized by very flat plains except few areas to south-east and north-east rise to more than 100 m above mean sea level. Cherrapunji, an Indian station that is world's heaviest annual rainfall (26,461.2 mm, August 1860 to July 1861) and is on average greater than 8000 mm (Pant *et al.* 1997). It is located on the southern slope of the Shillong Plateau and is about 10 km away from the border with Bangladesh. The Shillong Plateau works as a topographic barrier to the prevailing southerly monsoon wind, the amount of rainfall is extremely high on the southern slope of the Shillong Plateau. The topography and wind circulation generated from the storm produce locally higher rainfall amounts due to uplifting.

Rainfall, unlike any other hydrological parameters, is highly discontinuous both spatially and temporally. The variations of rainfall intensity with duration can be large from one rainfall event to another as well as from region to region. Moreover the coverage of the precipitation measurements by ground conventional means (rain gauge networks or weather radars) is much less than adequate. Because of its long service and widespread use, the rain gauge has become the standard for measuring surface rainfall and is often assumed to be "ground truth" in studies using other measurement technologies, such as radar. But there are random and systematic errors are associated with different type of point rainfall measurement. Since these are well known, only brief mention will be made here, it includes wind/turbulence, wetting, evaporation losses (Sevruk, 1982). Systematic mechanical errors due to the rainwater lost during the tipping movement of the bucket are also well-known and relative measurement errors range from limited overestimation at the lower intensities to underestimation of as much as 10 to 15 % at the highest rain rates (La Barbera, P *et al.* 2002). The wind/turbulence errors are usually around 5 % but can be as large as 40 % in high winds, such as with thunderstorm outflows. From previous study, it is observed that most often, instrument errors, observer errors, errors due to differences in observation time and low-intensity rains etc. are found at point measurement type of device.

In general, gauge accuracy is high but the primary problem is that the gauge measurement is for a point, whereas, the radar yields a rainfall estimate for a much larger area. Estimating or interpolating precipitation events from these scattered gauge observations can misrepresent the event, especially convective showers and even large-scale stratiform precipitation events. The ground radar certainly has an advantage in providing a surface precipitation estimate because of the high spatial and temporal resolution from a single point and in real-time but they suffer from calibration error, topographic blocking, beam broadening, beam overshoot, and non-unique reflectivity rain rate relationships. Satellite estimates can have also high resolution and its accuracy depends on the technique and calibration used. The most widely used data so far have been visible and infrared observations from geostationary meteorological satellites. The main advantage of these data is the wide spatial coverage and the relatively high frequency of observations. However, there is no direct physical relationship between these observations and precipitation. Active and passive microwave data from polar orbiting satellites provide observations strongly connected to precipitation. Yet, their temporal resolution (once or twice a day) and spatial coverage, limits considerably their utility in many applications.

In order to minimize the gauge density problem, remote sensed (radar and satellite) based measurements and numerical models have been widely used in recent years. The rainfall estimates provided by the assimilation of the results of numerical weather prediction models present several problems, including low resolution and undulations associated with the spectral representation of topography in such models (Costa and Foley, 1998). Due to the subtle differences in numerical model simulations and observational datasets both in situ and remotely-sensed, the question as to which of the mechanism dominates the physics behind the diurnal cycle in a particular location or meteorological regime remains an open one (Nesbitt and Zipser, 2003) to discuss. The relationships between the actually measured quantities and rainfall amounts on the ground are poorly understood. The concave shape of land-sea in the south, Myanmar hills in the southeast, Shillong hill in the northeast, Tibetan Plateau in the north and large Indian landmass in the west of Bangladesh make it interesting region to study.

Government of Bangladesh has taken many measures from structural to non-structural measurement like flood forecasting using 1-dimensional fully hydrodynamic model MIKE 11 (developed by Danish Hydraulic Institute, Denmark) incorporating all major rivers and floodplains. This is linked to a lumped conceptual rainfall-runoff model (MIKE 11 RR) which generates inflows from catchments within the country. But such model needs real-time rainfall data within and outside of Bangladesh to forecast lead-time flood in Bangladesh. There are four ground weather radars in Bangladesh to monitor real-time rainfall but they are lacked of proper calibration and controlling system for rainfall estimate. The lighting network was extended from Europe, America to African region in order to improvement of IR based rainfall estimation for convective system (Moroles *et al.* 2003) but Asian region is not yet covered by ground based lighting network and thus an improvement of IR based algorithm for monsoon convective rainfall estimation in this region is an another issue.

There have been few detailed studies on the distribution of precipitation that have not been based on radar data for the entire country. A few investigations have used rain gauge data, Karmaker and Khatun (1995), Islam and Wahid (2000). The information obtained from rain-gauges is not always sufficient for the quantification of the exact amount of precipitation, in particular, precipitation from small clouds that cannot be collected by the low density network of rain-gauges. A dense rain-gauge network is required to produce accurate estimates of precipitation,

but this is impossible in remote areas and is very expensive for extensive coverage. Moreover, characteristics of precipitation such as growth location, lifetime, shape, size, propagation speed and the direction of precipitation systems are not obtainable from rain-gauge data, but they are very important for determining the mechanism of a monsoon system as well as model parameterization.

Ground radar and satellite rainfall estimation issues, its limitations and possibilities are explained further detail in section 2.4 and 2.5 respectively.

1.2 Science Questions and Hypothesises

This research is focused on the following questions to be answered towards science contribution:

How characteristics of rainfall, its variability and the diurnal cycle in and around Bangladesh can be helped to improve rainfall estimation over Bangladesh?

How statistical procedure can be applied to improve near real-time rainfall estimation over highly precipitated region in South East Asia?

There are four hypothesises outlined below (not limited to):

- *Characterization of rainfall system in and around Bangladesh can improve radar and satellite based rainfall algorithm development in Bangladesh.*
- *Statistical approaches can improve rainfall estimation over highly precipitations areas in South East Asia.*
- *Corrected ground radar data can improve nearly real time rainfall estimation as well as run-off simulation in Bangladesh.*
- *Satellite based rainfall estimation can help to investigate improvements of near real time rainfall estimation in Bangladesh.*

1.3 Research Objectives

i. To characterize rainfall system over Bangladesh using radar data and rain gauge network.
ii. To evaluate performance of radar rainfall using rain gauge measurement in Bangladesh
iii. To evaluate performance of TRMM satellite based rain products over Bangladesh.
iv. To study diurnal cycle and seasonal variations of rainfall in and around Bangladesh.

v. To develop a statistical procedure of ground based radar rain algorithm parameter estimation in Bangladesh.
vi. To investigate and establish a calibration procedure of TRMM satellite based rain retrieval over Bangladesh.

1.4 Thesis Outline

Theoretical background related to cloud formation and monsoon system in south-east Asia, radar and satellite based rainfall measurement issues are described in chapter 2. Chapter 3 gives a brief overview of state of the art about radar and satellite based rainfall estimation. Advantages, limitations and scope of a numerous remotely sensed rainfall retrieval algorithms are also described in this chapter. A brief description of the study area and data description are outlined in chapter 4, methodology to achieve each objective are included in chapter 5, results and discussions related to each objective are described in chapter 6. Finally, study conclusions and recommendations are summarized in chapter 7 and 8 respectively.

A list of acronym (e.g. BG, CEA, FO, PPI, PM, TRMM, TMI etc.) is illustrated in the beginning of this thesis (see page xxi) in order to reduce repetitive uses of its description. A glossary (e.g. Attenuation, Backscatter, Emissivity, Monsoon, Scattering etc.) is also included at the end of this thesis to provide further clarification on different terminology used in this study. As stated, the appendixes are also attached.

CHAPTER 2

2. THEORETICAL BACKGROUND

2.1 Introduction

In this chapter, the theoretical considerations related to the proposed methodologies are described. Therefore, cloud formation, monsoon climatology, rainfall sources, rainfall measurement issues, statistical approaches are briefly described to the following subsections.

2.2 Cloud Formation and Main Types

Clouds are formed when air containing water vapour is cooled below a critical temperature called the dew point and the resulting moisture condenses into droplets on microscopic dust particles (condensation nuclei) in the atmosphere. The air is normally cooled by expansion during its upward movement. Upward flow of air in the atmosphere may be caused by convection resulting from intense solar heating of the ground; by a cold wedge of air (cold front) near the ground causing a mass of warm air to be forced aloft; or by a mountain range at an angle to the wind. Clouds are occasionally produced by a reduction of pressure aloft or by the mixing of warmer and cooler air currents.

Convective precipitation is often characterized by high horizontal reflectivity gradients, strong vertical motions, and high rain rates. Stratiform precipitation, which usually is present during the mature and dissipating stages of a convective system, is characterized by lower horizontal reflectivity gradients, weaker vertical motions, and lower rain rates. Convective and stratiform rain regions have different mean vertical motion distributions which result in different precipitation growth mechanisms (Houghton 1968). The differences in the microphysics may affect the drop size distribution and lead to different reflectivity-rain rate (Ze-R) relationships for convective and stratiform cloud (Tokay and Short 1996). Therefore, knowledge of the convective-stratiform distribution is very important. More importantly, though, Houze (1982, 1989) and Johnson and Young (1983) have indicated that convective and stratiform rain regions

have different diabatic heating profiles. Therefore, it is crucial that the total rainfall estimated from the satellite retrievals be correctly partitioned into convective or stratiform components.

Stratiform clouds are, by definition, stably stratified and stratiform precipitation results from such clouds. Hydrometeors (snow or rain) in stratiform clouds grow primarily by ascent through a widespread updraft whose magnitude is less than 1 m/s. The growth occurs primarily by continued condensation/deposition (i.e. the diffusion of water vapour onto droplets or ice crystals, respectively). Purely stratiform rain results from mid-latitude frontal systems, convergence into lows, or upslope flow, all situations in which the lower troposphere is stably stratified.

Convective clouds, on the other hand, result from buoyant ascent, whose magnitude (by definition at least 1 m/s) is 1 to 2 orders of magnitude larger than the widespread, forced ascent that produces stratiform rain. Convective rainfall, then, results from convective clouds. Hydrometeors are lifted in the updraft, where they grow primarily by accretion (i.e. collection by raindrops or riming by graupel).

2.3 South East Asian Monsoon Climatology

The monsoon climate of South Asia including Bangladesh is due to the unique geographical layout of the region. The Himalayas lie to the north while the warm Indian Ocean and Bay of Bengal lie to the south. These two features drive the atmosphere to produce the conditions that form the monsoon. During the South Asian winter, global circulation patterns drive the upper level of the atmosphere to flow from north to south. This brings south the cold Siberian air mass that, unmodified, would bring harsh, frigid winters into South Asia, but the Himalayan Mountains prevent that from occurring. This allows a very warm air mass to form over the Indo-Gangetic Plane during the months of April and May (Gunnel 1997). At this time temperatures in the region commonly reach 40 degrees centigrade or more. Temperatures are able reach these extremes due to the blocking effect of the Himalayan Mountains which prevents the cold Siberian air masses from reaching the Indo Gangetic Plane intact. The air that does come from the north will adiabatically descend down the south slope of the mountains which warms that air significantly and reduces its moisture content to nil. This air eventually sinks back to the surface over Bangladesh causing the intense heat. Since the density of the air is directly related to the pressure by the Equation of State, the pressure decreases. However, as one looks into the higher levels of

the Troposphere, the pressure will be higher than its surroundings due the Hypsometric relationship. This causes a large upper level high pressure system to from which acts as a giant lid over the Indo-Gangetic plane.

The heat low will spin as required by the balance of forces in a counter clockwise direction. This draws warm-moist air from the Indian Ocean and the Bay of Bengal into the low levels of the atmosphere. Since the temperatures over the region are very high and temperature is directly related to the moisture content of the air, the air mass in place over the Indo-Gangetic plane can hold tremendous amounts of moisture. The warm-moist air wedges itself under the existing dry air mass (Gunnel 1997). This results in a thermodynamically unstable situation since the moist air is less dense than the warm air. It allows significant rising motion in the lower levels of the Troposphere which leads to clouds and eventually rain. While the atmosphere may be thermodynamically unstable, forced lift is usually needed to initiate convective rain. This is provided by the Himalayan Mountains which force the moisture laden air upward where it condenses and falls as rain.

The classic and most prominent form of the monsoon climate is to be found on the Indian subcontinent. At the beginning of winter, the subcontinent cools rapidly, while the Indian Ocean is still warm because the temperature of water takes longer to change than does the temperature of land. The warm water heats the air over the oceans, forcing the air to rise. This movement draws cool air from the Himalayas and northern India to the Indian Ocean. These northeast winter monsoon winds bring cool, sunny, and dry weather to India during the winter.

The monsoon season ends in South Asia when cooler air from the North filters into the Tibetan highlands during the month of October. The heat source for the heat engine that powers the monsoon low pressure system is gone, and thus the monsoon low fades away as well. This cut off the moisture flow from the Bay of Bengal, and thus cuts off the rain. The circulation then reverses as a High pressure system which forms over Tibet. This brings heavily modified, dry Siberian air into the Bangladesh region and the Winter Monsoon to south-eastern India (Gunnel 1997).

As summer returns, the pattern reverses. The temperature in southern Asia rises faster than that of the Indian Ocean. Some areas of northern and central India reach temperatures of more than 40°C. Hot air rises over the land, drawing masses of cool, damp air from the ocean towards the

land. These southwest winds mark the return of the summer monsoon rains. Moisture blown in by these winds condenses, resulting in sustained, heavy rains, which normally begin in June and last until September.

The Himalayas form a barrier that forces the warm air to drop its moisture over southern Asia. The southern flanks of the Himalayas receive large amounts of precipitation, while the northern slopes receive small amounts. This orographic effect also occurs along the south-western coast of India as a result of the Western Range. Thus, certain areas of India receive tremendous amounts of rain during the summer monsoon season. In South Asia the onset of the summer monsoon generally progresses north-westward, and the withdrawal advances south-eastward (Mooley *et al.* 1987). In Bangladesh the onset of the summer monsoon starts in the south-eastern tip of the country at the beginning of June, progresses toward the northwest and reaches the north-western part by the middle of June. The withdrawal occurs in the opposite direction, starting in the north-western part at the end of September and retreating from the entire country by mid-October (Ahmed *et al.*. 1993), on average more than 70 % of Bangladesh's annual rainfall is concentrated in the 4 months from June to September. The mean rainfall during the monsoon season from June to September ranges roughly from 1000 to 3000 mm in the country, with maxima near the Shillong Plateau in the north-eastern part and along the coast line in the southern part and with a minimum of west central part (Matsumoto, 1988, Hussain *et al.* 1996).

The rainfall over Bangladesh is basically dominated by the north-south oscillation of the monsoon trough. The rainfall increases when the monsoon trough is located at the foot of the Himalayas, because synoptic-scale convective activity is much more vigorous to the south of the monsoon trough axis than to the north of it. In addition, the strong south-westerly wind to the south of the monsoon trough intensifies local convective activity owing to the effects of the orography to the north and east of the country (Ohsawa *et al.* 2000).

2.4 Sources of Rainfall over Bangladesh

There are three main sources of rainfall in Bangladesh: (i) the western depressions of winter; (ii) the early summer thunderstorms known as the nor'westers and (iii) the summer rains from south-western trades known as monsoon.

a. Western Depressions of Winter

The westerly depressions (anticyclones) form in the region of the Elburz Mountains, or even further west, in the Mediterranean region. They generally intensify as they move eastward and precipitate considerable amounts of snow on the western Himalayas. Continuing eastward they bring rain to the lower slopes of the eastern Himalayas, and as they are 'trapped' in the sea of the Assam Hills, to all parts of Bangladesh also. The main period of these rains is from 20th January to 25th February. In these 35 days, it rains from 10 mm (Cox's Bazar) to 40 mm (Srimangal) and more. Any rainfall during this period is very useful for dry season agriculture.

b. Nor'westers

There is a slight break, of about fifteen days, before the second rainy period begins on about the 10th of March. The Nor'westers are due to a varity of reasons, of which the main ones are the steady flow of cool dry air above 1800 metres altitudes from the north-west (anti-trades), and a warm moist current below 1800 meters from the south, intense evaporatranspiration in the Bengal Basin and Assam, and the katabatic winds from surrounding mountains. The Nor'westers is usually of a short duration, but is intense, with a wind speed of 100 km/hr, and heavy rainfall. Hailstorms occur during this period and hail of up to 50 mm in diameter is not uncommon. The main period of the Nor'westers lasts within the first week of May. The rainfall varies in the period from 88 mm (Dinajpur) to 418 mm (Srimangal). There are however showers due to local instability of air-masses through the month of May.

c. Monsoon

The main rainy period begins with the coming of the moisture-laden south-west-trades popularly known as the monsoons, which are drawn to the Indian Sub-continent by the intense heat, and consequent low pressure over the Punjab and upper Ganges valley, which gives rise to a "tropical cell" with convection currents of massive proportions. These winds blow across the North Indian Ocean and reach the Malabar Coast of Indian two weeks before they come up the Bay of Bengal to Bangladesh. One arm of these vast trades moves up the Ganges valley, while another one brings copious rains to the west coasts of Myanmar and quickly moves north into Assam. It is the orogenic rains caused by the striking of this east-flowing air mass against the Arakan Yomas, Meghalaya Plateau and the Himalayas that forms the major part of the rainfall of Bangladesh.

The trade winds, the rains they bring ad also the period of the year which they effect are called Monsoons.

Since the monsoon current travels from the south and east to the north and west, the rains begin in places like Cox's Bazar and Noakhali on about the 20th of May, and spread to Kushtia and Rajshahi in about ten days. The monsoons bring heavy rainfall for five months, from the end of May to Mid-October. The mean cloudiness then is from eight to nine-tenths. The total rainfall in these months varies from 1220 mm at Rajshahi to 3380 mm at Cox's Bazar and over 5500 mm near Sylhet. Cherapunji, one of the rainiest places in the world, lie just to the border of north Sylhet.

After the 14th of October, the monsoon rainfall peters out rapidly. In the western half of the country and in Central Bengal, the rains are normally over between the 29th and 25th of October, whereas in the east and south-east they do not end till about the 10th of November. Very little little rain falls from this time till the middle of January. Mean cloudiness is then only one to two-tenths.

There is a slight difference in the period of maximum rainfall in different parts of Bangladesh. In most places, the maximum rainfall is recorded in June, though July and August record nearly as much. Dinajpur and the north-west of the North-Bengal, Kushtia and Noakhali get their maximum rainfall in July. Many places such as Comilla, Bogra and Srimangal have a slight tendency to record "double maxima" in July and in September.

In this region the monsoon period is divided into three (Das, 1995): a) pre-monsoon (March-May), b) monsoon (June-September), and c) post-monsoon (October-November). June to August is well known as peak-monsoon months. In pre-monsoon period severe thunderstorms locally called "Kalbaishakhi" develop and proceed mainly from the northwest. In the monsoon period the country has moisture in flux from the Bay of Bengal and cloud develops in association with the low-level south-westerly or south/south-easterly. In this season the country gets heavy rain with maximum rainfall usually in July and the annual rainfall is about 2200 mm ranging from about 1200 mm to about 5800 mm at different sectors of the country. The low-level zonal (meridional) wind is easterly (northerly) in off-monsoon period and turns to westerly (southerly) in monsoon period. The meridional component is more active in monsoon period that carries water vapor

from the Bay of Bengal, which is one of the causes of heavy rainfall in that region. The socio-economic conditions of the people in this region are intimately related with the monsoon. Bangladesh is one of the parts of tropical monsoon areas. Clouds and precipitation, particularly in the world's tropical regions, play an important role in driving the atmospheric circulation (Anagnostou and Kummerow, 1997). Therefore, accurate knowledge of the precipitation types and the period of maximum precipitation are the important issues to discuss.

2.5 Radar Rainfall Measurement

2.5.1 Introduction

The radar reflectivity depends, among many other factors, on the drop size distribution, hydrometeor phase and content variability within the sampling column. The sources of errors with radar rainfall estimation technique are outlined to the following subsections:

2.5.2 Issues Radar Rainfall Measurement

a. Atmospheric and Physical Constraint

i) Attenuation

Two kinds of attenuation may be identified, attenuation by atmosphere gases in the clear atmosphere and attenuation by the precipitation itself. Attenuation caused by atmospheric gases is accurately known (1.5dB per 100 km at 5cm wavelength). Except for the small attenuation caused by water vapor, it is roughly constant and may usually be corrected for by including it in the range normalization. Attenuation caused by rain is described by Ulaby *et al.* (9181) and may vary strongly according to the rain rates along the path, but in many applications it plays a minor role compared to other errors provided a wavelength of 5cm or longer is used. Attempts have been made to correct for attenuation during the data analysis by feedback technique using the reflectivity measured along the path (Geotis, 1975b). However, as Hitschfeld and Bordan (19540 pointed out the correction can very easily become unstable because of errors in the radar calibration, variability in the relationship between reflectivity and attenuation, and/or by echo fluctuation. The correction should therefore be limited to a maximum of the order of 5 dB.

The radar corrects for gaseous attenuation, leaving intervening precipitation as the principal attenuators of microwave return to and from the target. Vertically pointing or slant range measurements from aircraft or satellite may well be useful in regions not covered by land-based radars (Kozu *et al.*, 1986; Menegehini *et al.*, 1986).

ii) Frozen Hydrometeors and the Melting Layer

Rayleigh scattering is assumed, which means that the precipitation particles are presumed small when compared to the wavelength (10 cm for the Doppler Radar) of the incident radiation. Further, the weather radar equation is used, which presumes scatterers that are spherical liquid drops, evenly distributed throughout the sampled volume. To describe actual received power that would be received from scatterers meeting the aforementioned constraints, the effective reflectivity factor Z_e is introduced in place of Z.

The most prominent violations of the assumptions come from large frozen hydrometeors - melting snow just below the freezing level (the bright band) and hail. Most studies show a Z_e enhancement of 5-10 dB in the bright band, and thus R can be up to five times too large there (Austin 1987; Joss and Waldvogel 1990). Fabry and Zawadzki (1995) found differences up to 16 dB. Thus, the bright band remains a major obstacle to precipitation estimation.

iii) Anomalous Propagation (AP)

The Ground Radar displays beam heights assuming standard atmospheric refraction, which is rarely the case. Severe deviations from the standard atmosphere occur in layers with large vertical gradients of temperature and/or water vapor. The role of vapor gradients should not be overlooked, since they can substantially change refractivity where there is abundant moisture. This is usually in the lower troposphere and, unfortunately, often accompanies precipitation. Whatever their cause, certain refractivity lapse rates produce super refraction or sub refraction of the beam and inaccurate calculations of actual beam height. The former is usually the more serious problem, because it can cause ducting or interception of the beam by the ground. This produces persistent and quasi-stationary returns of high Z_e, yielding extreme estimates of (false) precipitation accumulation. This has more operational impact and is more difficult to suppress when AP echoes are imbedded in precipitation echoes

iv) Beam Blockage

This is a major problem where radars are situated near mountains, something that is practically unavoidable in many locations. Installing the radar on a peak may mitigate the problem, but then its lowest elevation slices are so high above valleys (where population is greatest) that near-surface precipitation is not "seen".

v) Range Effects

1) Elevation of Beam - Far Range

Earth curvature and standard refraction dictate that the beam becomes more elevated above the surface with increasing range. This effect is akin to blockage, in that the radar does not sample the layers near the surface. This is termed beam overshoot or inability to sample the full vertical reflectivity profile. It represents a probability of detection (POD) problem.

Kitchen and Jackson (1993) indicted detection failure as a major cause of underestimated rain accumulation. They found a rapid drop in POD beginning at 60 nm, falling to 0.4 (0.3 in winter) at 124 nm in range (the maximum display range for WSR-88D precipitation products). Interestingly, they suggest that when rain is detected at these far ranges, underestimation of the rate Rr (hence Z_e) is smaller than the underestimation of accumulation resulting from low POD.

2) Elevation of Beam - Near Range

Several Doppler radar sites have reported discontinuities in precipitation amounts at constant ranges. The cause for these apparently artificial patterns is uncertain. Smith and Krajewski (1994) documented deficits in WSR-88D precipitation accumulations close to the radar ("holes"), where data originate from higher tilts of the hybrid scan.

The holes could also represent deficits only in a relative sense, when compared to amounts at further ranges. At those ranges, spurious enhancements may be produced by the bright band and/or "bi-scan maximization". The latter would be suspected if the hole's maximum range was the same as the minimum range of this maximization, currently about 27 nm. As Ahnert *et al.* (1983) predicted, the maximization sometimes coincides with the bright band, amplifying the overestimation of Z_e and R_r.

b. Beam Spreading

The average Doppler radar half-power beam width =0.95. This translates to a beam diameter r (where r is range to target) of roughly 1 nm at r = 62 nm and 2 nm at r = 124 nm, the maximum precipitation processing subsystem (PPS) range. The sampled volume quadruples for every doubling of range. This resolution degradation also limits detection of severe weather signatures (e.g., Hunter *et al.* 1993). It increases the likelihood that precipitation fills only part of the beam. Since it is assumed that scatterers fill the sample volume completely and uniformly, one may expect sample volume averaging of received power to yield reduced reflectivity over that of a nearer volume. It will weaken the bright band but distort it in the vertical (Fabry *et al.* 1992). Spreading will also cause overestimation of echo top height.

2.5.3 Radar vs. Rain Gauge Estimates

i) Rain Gauges

The rain gauge is often assumed to be "ground truth" in studies using other measurement technologies, such as radar. The validity of this assumption is undermined by several errors in gauge measurement. Since these are well known, only brief mention will be made here. They include wind/turbulence losses and tipping bucket losses with high rainfall rates (Alena *et al.* 1990). The wind/turbulence errors are usually around 5 % but can be as large as 40 % in high winds, such as with thunderstorm outflows (Wilson and Brandes 1979).

Although gauge accuracy is usually high, the main problem is that the measurement is for essentially a point, compared to a radar sample volume that yields rainfall over a much larger area. The latter is more relevant to hydrology, in which rain over a fixed catchment area is desired. To facilitate comparison between radar (Rr) and gauge (Rg), many experiments have used networks of gauges. This too has limitations, as subsequently related.

ii) Radar/Gauge Sampling Differences

The customary use of gauge data is to "adjust" Rr through various statistical techniques, so that the (usually) superior accuracy of Rg is applied to the greater areal coverage of radar Rr. The integration of these two types of data is problematic. The temporal sampling of the Ground Radar is every 5 or 6 minutes; for gauges it is nearly continuous (although data communication to an

office often lags). More important is the spatial disparity of the two measurements. Not only is the radar sample volume larger, as stated before, but also it is elevated above the gauge. The more elevated the beam, the more likely Rr will deviate from Rg, which is of course from the desired ground level. Physical processes such as evaporation, coalescence, and precipitation displacement by horizontal wind may become important with increasing overshoot.

Even if the beam is sufficiently low to supply a good estimate of the surface precipitation rate over a gauge, how does one apply the Rg/Rr ratio at this point (and others) to the remainder of the Rr field? This question has been the subject of many studies. Brandes (1975) proposed using data from several gauge locations to obtain a single calibration factor (average Rg/Rr) or bias that is applied to the entire Rr field. This should make the total field volumetric water estimate match the true value. Ahnert *et al.* (1983) used a similar scheme but passed the ratios through a Kalman filter. This is incorporated into the PPS rain gauge (bias) adjustment algorithm. The effectiveness of this technique is in direct proportion to the sampling effectiveness of the gauge network. There must be a sufficient number of gauges to faithfully represent the rainfall field under the radar umbrella. POD is also increased by uniformity in gauge spacing (Grosh 1993).

Finally, the technique implicitly assumes that the bias is uniform under the umbrella. If these conditions are not met, gauge adjustment may degrade the accuracy of the Rr field in localized areas (Lin and Krajewski 1990; Zawadzki 1984). This phenomenon is more probable during isolated, convective precipitation, where gauges are less likely to be under precipitation shafts, or they may lie under large reflectivity gradients.

2.5.4 Physics towards Radar Rain Measurement

- **Radar Equation** (Source: Uijlenhoet *et al.*, 2003)

$$P_r = \frac{P_0 G^2 \lambda^2 \sigma}{(4\pi)^3 R_t^{\ 4}}$$

P_0 = transmitted power [W]

P_r = backscattered power [W]

G = antenna gain (engineering term to enlarge signal return)

σ = Radar scattering of rain drop cross section [m^2]

R_t = distance between radar and target [m]

λ = wavelength of radar [m]

- Radar cross-section per unit area:

$$\sigma^0 = \left\langle \frac{d\sigma_i}{dA_i} \right\rangle_{A_0}$$

σ_i = radar cross section of a i-th single raindrop (as a scatterer) [m^2]
dA_i = differential geometrical area of the i-th raindrop [m^2]
A_0 = total area of a radar sensor resolution element (=pixel) [m^2]
<> = denotes the statistical average

- Relation between σ and σ^0

$$\sigma = \sigma^0 A_0$$

- Radar cross section per unit volume σ_v (= Radar spectral scattering coefficient $\kappa_{s,\lambda}$):

$$\sigma_v = \left\langle \frac{d\sigma_i}{dV_i} \right\rangle_{V_0}$$

σ_i = radar cross section of a i-th single raindrop (as a scatterer) [m^2]
dV_i = differential geometrical volume of the i-th raindrop [m^2]
V_0 = resolution volume (=pixel) [m^2]

- Relation between σ and σ_v

$$\boxed{\sigma = \sigma_v V_0 = \kappa_{s,\lambda} V_0}$$

- Radar cross section of the i-th single raindrop of a cloud

$$\boxed{\sigma_i = \begin{cases} \dfrac{2\pi^5}{3\lambda^4}|K|^2 D^6 & D \le 0.05\lambda \\ Mie \quad scattering & \text{For any } \lambda \end{cases}}$$

$$K = \frac{\varepsilon - 1}{\varepsilon + 2}$$

ε = the relative dielectric constant of scatterer (rain drop or ice crystal)
D = diameter of raindrop
λ = wavelength

- Radar cross section per unit volume σ_v: For a precipitable cloud with a raindrop-size distribution (RSD) N (D)

$$\sigma_v = \kappa_{s,\lambda} = \int_0^\infty \sigma_i(D) N(D) dD$$

$$= \frac{2\pi^5}{3\lambda^4}|K|^2 \int_0^\infty N(D) D^6 dD$$

N(D) = the number of raindrops per unit volume at diameter between D and D+dD. D ranges from 0 to infinity.

- **Radar Reflectivity**
- Radar measurements of power of electromagnetic waves backscattered by raindrops are directly related to radar reflectivity, Z, in unit of mm^6/m^3 (Source: Uijlenhoet *et al.*, 2003)

Defining the radar reflectivity

$$Z = \int N(D) D^6 dD \quad [\text{mm}^6\ \text{m}^{-3}]$$

Then we have

$$\sigma_v = \kappa_{s,\lambda} = \frac{2\pi^5}{3\lambda^5}|K|^2 Z$$

$$Z = \frac{3\lambda^5 \sigma_v}{2\pi^5 |K|^2}$$

$$\sigma_v = \sigma / V_0$$

$$\sigma = \frac{(4\pi)^3 R_t^4 P_r}{G^2 \lambda^2 P_0}$$

Finally we have

$$Z = \frac{3\lambda^5 \sigma_v}{2\pi^5 |K|^2} = \frac{96\lambda^3 R_t^4 P_r}{\pi^2 |K|^2 V_0 G^2 P_0}$$

- **Precipitation Rate:**

Precipitation rate R ($mm\ h^{-1}$):

$$R = \frac{\pi}{6} \int_0^\infty D^3 N(D) v(D) dD$$

$v(D)$ = the raindrop fall speed [$mm\ h^{-1}$]. For instance, in still air, raindrop speed $v(D) = CD^{0.67}$, with C = 17.76 $m\ s^{-1}\ cm^{-0.67}$ if D is in cm. For this case we have $R = \frac{17.67\pi}{6} \int_0^\infty D^{3.67} N(D) dD$

2.5.5 Z-R Relationships

The most widely used description of the size distributions of raindrops is that of Marshall and Palmer (1948), who found that the exponential shape fits measured raindrop spectra reasonably well. In fact, the more averaging done in time or space, the better the agreement with the exponential distribution (Joss and Gotri, 1978). Individual drop size distribution may differ

considerably because of physical differences in the processes such as drop sorting, aggregation, coalescence, and breakup during their development.

Empirical values of Z-R relations and variations from storm to storm and within individual storms have been the subject of many studies over the past 40 years. Strictly speaking, a Z-R relation is obtained by calculating Z and R from measured drop-size distributions. These relationships vary from one experiment to the next, and thus number in the hundreds (Battan 1973 lists 69). The DSD is determined by a complex interaction of microphysical processes. It fluctuates daily, seasonally, regionally, and even within the same cloud. In addition to this variability, the aforementioned uncertainties of radar estimates of Rr, and increase the magnitude of the problem.

An alternative is to compare Z measured aloft by the radar (it is then called the "equivalent radar reflectivity factor" and labelled Ze) with R measured at the ground. Such a relation attempts to reflect any differences between the precipitation aloft and that which reaches the ground, and may also include errors in the radar calibration, so it is not strictly a Z-R relation. This technique has been used in the climatological approaches proposed by Miller (1972) and Calheiros and Zawadski (1981). Their relationships are deduced by comparing the overall probability that Ze exceeds given levels with the intensity distribution curve for R as measured by gauges in many storms. In the relation a range effect must be included to account for average variations in the vertical profile of reflectivity. All Z-R relations assume the same things as in the calculation of Ze notably that the scatterers are liquid drops that are small compared to the radar wavelength. These are particularly troublesome assumptions, as bright band and hail contamination are common.

Radar measurement of surface rainfall has a history almost as long as radar meteorology itself. The radar measures power return from precipitation field which is proportional to the radar reflectivity factor Z (provided that the particles are spherical and small compared with the wavelength), the function $|K|^2$ (a function of the dielectric constant of the particles), and the radar constant C, and inversely proportional to the square of the distance r and attenuation A produced by rain and atmospheric gases:

$$P = \left(\frac{C}{A}\right)\left(\frac{Z\,|\,K\,|^2}{r^2}\right) \tag{2.1}$$

The radar constant C depends on the transmitted power, the wavelength, the pulse duration, the beam width, and the gain of the antenna. All particles of precipitation field within the sampled volume of the radar contribute to the radar return. Each particle contributes proportionally to its backscattering cross section. The cross section is a function of the wavelength of the radar, and the size, the shape, orientation (if not spherical) and dielectric properties of the particle. The dielectric constant is very different for ice and water and varies with temperature. As long as particles are smaller than one-third of the wavelength (Rayleigh region; Battan 1973), the backscattering per unit volume of the atmosphere is roughly proportional to the radar reflectivity factor Z. This is usually converted to a radar estimate of rain rate, Rr, through an empirical Z-R relationship. Surface rainfall is most often measured by rain gauges, resulting in a rate Rg.

From the weather radar equation, Z is proportional to Di^6, where Di is the diameters of individual raindrops in the illuminated sample volume. Rg, on the other hand, is proportional to Di^3. This means that the radar measurement is biased toward larger drops. Moreover, different drop size distributions (DSD's) can yield the same Z but different R. This non-unique relationship and the inability (in operational settings) to directly measure the DSD prohibit exact specification of the actual R and precipitation accumulation.

Even if we knew the DSD precisely, there could be measurement errors by the radar (Z), by the gauge (Rg), and by comparison of the two platforms (because of inherent differences in the nature of each measurement). These errors may cause Rr to vary from the true rate R by a typical factor of two (Wilson and Brandes 1979). Correction schemes for Rr may be characterized as analytic (mainly radar-only), statistical/physical, and gauge adjustment (Kitchen *et al.* 1994).

2.6 Satellite Based Rainfall Measurement

2.6.1 Introduction

The approaches used in making quantitative estimates of rainfall by using satellites can be divided into two main streams and the algorithms are grouped according to the type of satellite data being used, and only their common principles and limitations are summarized:

- Visible and infrared techniques
  - Cloud indexing techniques
  - Bispectral methods
  - Life-cycle methods
  - Cloud models
- Microwave radiometry
  - Passive microwave
  - Precipitation radar
  - Hybrid or data fusion (multi-sensors)

The following satellite orbiting systems and sensors being utilized for meteorological purposes:

Geosynchronous	P**olar Orbiting**
GOES-12 by 4/2003	DMSP 3 satellites (SSM/I – 11, 13, 14)
GOES-10 at 135 degrees West	POES 3 satellites: NOAA-14, 15, and 17
Meteosat-7 at 0 degrees	NASA 3 satellites: TRMM, TERRA, AQUA
GMS-5 at 140 degrees East	NOAA 15 & 16 satellites**:** AMSU & AMSU-B
Meteosat-5 at 63 degrees East	EOS- AQUA satellite : AMSR-E
GOES-9 to replace GMS-5 by mid-2003	ADEOS-II satellite : AMSR

2.6.2 Satellite Rainfall Estimation Issues

The geostationary meteorological satellite data are spatially continuous and also highly repetitive. Satellite passive microwave algorithms and satellite-borne rain radar are able to provide accurate estimation of instantaneous rain rates, but the poor temporal sampling of low earth orbiting satellites makes these techniques most suitable for estimation of perhaps a month or more. Although active and passive microwave sensors onboard orbiting satellite provide observations strongly connected to precipitation, there temporal resolution (once or twice a day) limits considerably their utility in many applications. Moreover, it is well known that estimates from polar-orbiting satellites are subject to bias in regions where the diurnal cycle of rainfall is pronounced (Morrissey and Janowiak 1996). Satellite IR algorithms benefits from the high temporal sampling of geostationary satellites, but IR radiances from cloud tops have only weak,

indirect relationship with surface rainfall. Therefore, many simple IR algorithms rely on the effects of scale averaging to improve accuracy (Martin C. Todd *et al.* 2001).

Over land, rain retrieval from microwave radiometer (passive microwave) data is further complicated by variable surface emissivity introduced by vegetation, surface wetness, water bodies and terrain. The errors on rain rate retrievals from SSM/I data, that spatial resolution is not the only cause of such errors but the ability to discriminate the nature of ice hydro-meteors is also an important factor. Multi-spectral, dual polarization measurements made by satellite-borne microwave radiometers do not contain enough independent pieces of information to derive the amount and the vertical distribution of liquid, mixed phase, and frozen hydrometeors present in the atmosphere. This leads to uncertainties in quantitative estimation of rain rate pertaining to convective and stratiform rain based purely on radiative transfer theoretical consideration (Prabhakara C. *et al.* 2000).

During the past three decades, many studies have been conducted using these satellite data, and a large number of algorithms for satellite rainfall retrieval have been proposed, making use of either Infrared data or microwave data, passive or active, or also combination of different types of data. Growing operational use of satellite remote sensing data on precipitation it is clear that limitations on the quality and utility of such data remain, due to numerous factors, including the following (Barrett E. C., 2001) :

- The temporal, spatial and spectral characteristics of the satellite observing systems – which are less than optimal for such a variable phenomena.
- The varied and variable, interactions between electromagnetic radiation and its environment – particularly over land areas.
- The availability and suitability of collateral data for calibration and validation – which are still generally deteriorating.

In many parts of the world (over oceans, remote areas and economically disadvantaged regions) conventional observations do not provide the rainfall as required by the different applications. The alternative has been rainfall estimation from space-based platforms. Many rainfall estimation techniques and algorithms are developed for a particular region and for very different time-space

scales. The most common satellite rainfall estimation techniques rely on cloud top temperature infrared (IR) measurements only (Martin *et al.,* 1990), microwave (MW) measurements (Negri *et al.*, 1994) or on the combination of IR and MW (Vicente, 1994). Lighting Information with Infra-red data helps to detect convective systems of rainfall (Grecu *et al.* 2000 and Tappia *et al.* 1998).

Some emission rainfall algorithms rely upon the amount of extra radiation emitted by the precipitation particles against a radiometrically cold ocean surface. Because land surfaces have emissivities in the range 0.8-0.95, these emission rainfall algorithms are not suitable for over-land applications as the high surface emissions effectively mask the precipitation attenuation (Kidd *et al.* 1998). The scattering rainfall algorithms, on the other hand, rely on the general cooling in the high-frequency channels due to the scattering of ice in the upper portions of many raining clouds (Kummerow and Giglio 1994).

The radiative transfer processes of rain can be separated into two regimes: the attenuation regime and the scattering regime (Wilheit *et al.* 1991). The microwave Tbs observed in the attenuation regimes represents observations of the liquid hydrometeors within the rain cloud, which may be considered direct measurements of the rainfall. Conversely, the microwave Tbs observed in the scattering regime depends on the many details of the ice layer. Therefore, the satellite microwave Tbs may be divided into attenuation-based measurements and scattering based measurements. The factors determining the type of attenuation encountered are the size of precipitation particle, the phase of the particle (ice or liquid), and the wavelength of the radiation (Kidd *et al.* 1998).

The IR-only technique is the most indirect approach because it relies on the statistical interpretation of cloud top temperature. They provide very high temporal resolution for the estimate since the temperature measurements are made by a satellite on a geosynchronous orbit. The MW technique provides the most accurate measurement of instantaneous rainfall rates, because the precipitation amounts are physically related to the cloud MW radiation emission and scattering. However, this technique can only provide estimates a few times a day over a narrow area because they rely on measurements made from a polar orbiting satellite. The techniques that use both IR and MW try to take advantage of the strengths of both measurements.

A combined Infrared, and passive MW technique for rain estimation is also developed at scales smaller than the existing monthly/2.5 deg products. A new combined PMW/IR - microwave/ infrared algorithm (MIRA) for estimation of small-scale rainfall (down to the instantaneous / pixel scale) that addresses the primary limitations of the GPI (Martin C. Todd *et al.* 2001).

2.7 Monte Carlo Simulation

A technique which has had a great impact in many different fields of computational science is a technique called "Monte Carlo Simulation (MCS)." This technique derives its name from the casinos in Monte Carlo - a Monte Carlo simulation uses random numbers to model some sort of a process. This technique works particularly well when the process is one where the underlying probabilities are known but the results are more difficult to determine.

The Monte Carlo method is just one of many methods for analyzing **uncertainty propagation**, where the goal is to determine how *random variation*, *lack of knowledge*, or *error* affects the *sensitivity*, *performance*, or *reliability* of the system that is being modeled. Monte Carlo simulation is categorized as a **sampling method** because the inputs are randomly generated from *probability distributions* to simulate the process of sampling from an actual *population*. So, we try to choose a distribution for the inputs that most closely *matches data we already have*, or best represents our *current state of knowledge*. The data generated from the simulation can be represented as probability distributions (or histograms) or converted to *error bars*, *reliability predictions*, *tolerance zones*, and *confidence intervals*.

Step 1: Create a parametric model, y = f(x1, x2, ..., xq).
Step 2: Generate a set of random inputs, xi1, xi2, ..., xiq.
Step 3: Evaluate the model and store the results as yi.
Step 4: Repeat steps 2 and 3 for i = 1 to n.
Step 5: Analyze the results using histograms, summary statistics, confidence intervals, etc.

2.8 Kalman Filtering

The Kalman filter method, which was created by Kalman in 1960 and is an efficient recursive filter that estimates the state of a dynamic system from a series of incomplete and noisy measurements. Its use in Hydrology began in 1973, when Hino applied the Kalman filter to identify the parameters of a linear, lumped, discharge model from serial observations, then used the new parameters updated by new observations to forecast stream flow. A linear system in which the mean squared error between the desired output and the actual output is minimized when the input is a random signal generated by white noise.

Consider the problem of estimating the variables of some system. In dynamic systems (that is, systems which vary with time) the system variables are often denoted by the term *state variables*. Assume that the system variables, represented by the vector x, are governed by the equation $x_{k+1} = Ax_k + w_k$ where w_k is random process noise, and the subscripts on the vectors represent the time step. For instance, if our dynamic system consists of a spacecraft which is accelerating with random bursts of gas from its reaction control system thrusters, the vector x might consist of position p and velocity v. Then the system equation would be given by Equation 2.2:

$$\begin{bmatrix} p_{k+1} \\ v_{k+1} \end{bmatrix} = \begin{bmatrix} 1 & T \\ 0 & 1 \end{bmatrix} \begin{bmatrix} p_k \\ v_k \end{bmatrix} + \begin{bmatrix} T^2/2 \\ T \end{bmatrix} a_k \tag{2.2}$$

Where a_k is the random time-varying acceleration, and T is the time between step k and step $k+1$. Now suppose we can measure the position p. Then our measurement at time k can be denoted $z_k = p_k + v_k$ where v_k is random measurement noise.

The question which is addressed by the Kalman filter is this: Given our knowledge of the behavior of the system, and given our measurements, what is the best estimate of position and velocity? We know how the system behaves according to the system equation, and we have measurements of the position, so how can we determine the best estimate of the system variables? Surely we can do better than just take each measurement at its face value, especially if we suspect that we have a lot of measurement noise.

The Kalman filter is formulated as follows. Suppose we assume that the process noise w_k is white with a covariance matrix Q. Further assume that the measurement noise v_k is white with a covariance matrix R, and that it is not correlated with the process noise. We might want to formulate an estimation algorithm such that the following statistical conditions hold:

- The expected value of our state estimate is equal to the expected value of the true state. That is, *on average,* our estimate of the state will equal the true state.
- We want an estimation algorithm that minimizes the expected value of the square of the estimation error. That is, *on average,* our algorithm gives the *smallest* possible estimation error.

It so happens that the Kalman filter is the estimation algorithm which satisfies these criteria. There are many alternative ways to formulate the Kalman filter equations. One of the formulations is given in the Equations 2.3-2.6 as follows:

$$S_k = P_k + R \tag{2.3}$$

$$K_k = AP_kS_k^{-1} \tag{2.4}$$

$$P_{k+1} = AP_kA^T + Q - AP_kS_k^{-1}P_kA^T \tag{2.5}$$

$$\hat{x}_{k+1} = A\hat{x}_k + K_k(z_{k+1} - A\hat{x}_k) \tag{2.6}$$

In the above equations, the superscript *–1* indicates matrix inversion and the superscript *T* indicates matrix transposition. *S* is called the covariance of the innovation, *K* is called the gain matrix, and *P* is called the covariance of the prediction error.

Equation 2.6 is fairly intuitive. The first term used to derive the state estimate at time *k+1* is just *A* times the state estimate at time *k*. This would be the state estimate if we didn't have a measurement. In other words, the state estimate propagates in time just like the state vector (see Equation 2.2). The second term in Equation 2.6 is called the *correction* term, and it represents how much to correct the propagated estimated due to our measurement. If the measurement noise is much greater than the process noise, *K* will be small (that is, we won't give much credence to

the measurement). If the measurement noise is much smaller than the process noise, *K* will be large (that is, we will give a lot of credence to the measurement).

2.9 Artificial Neural Network

Artificial Neural Network (ANN) has become extremely popular for prediction and forecasting as it provides a convenient and powerful means of performing nonlinear classification and regression (Tsintikidis, *et al.*, 1997). It is composed of individual processing elements called units or nodes. The nodes are connected by links or weights. An ANN can have multiple layers of nodes interconnected with other nodes in the same or different layers. The layers are classified as input layers, hidden layers and output layers (Figure 2.1). The input nodes are connected by the output nodes through hidden nodes. The hidden nodes capture the non-linearity in the mapping between input and output information. The inputs are processed using interconnecting weights by weighted summation functions to produce a sum that is passed through a transfer function and the output of this transfer function is the output of the node. ANN learning can be supervised or unsupervised. In the supervised learning scheme, the ANN training is done by adjusting the input weights on each node in such a manner that the output of the network is consistent with the desired output. In unsupervised learning scheme, no external criteria are used by the network output for ANN training. The most popular supervised learning scheme is back propagation.

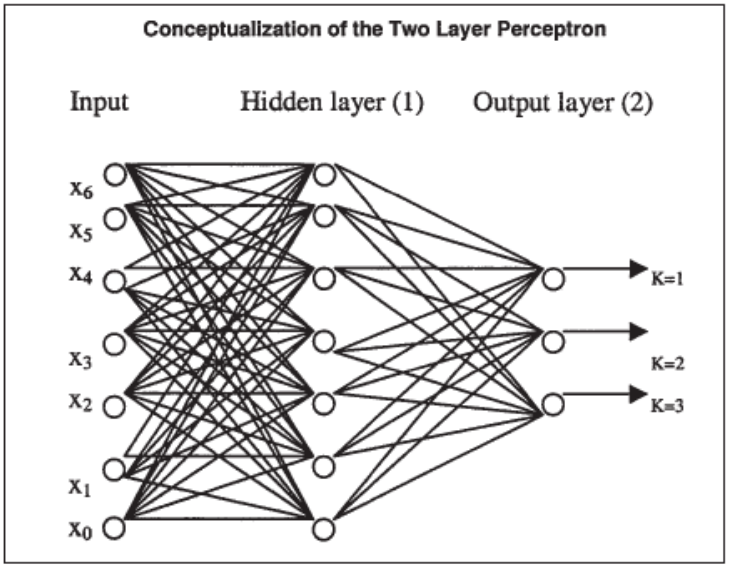

Figure 2.1 Conceptualization of the Two Layered Perception

The steps in ANN algorithm for back propagation (Faisal *et al.* 2003) are outlined below:

Step 1: Initialize w_{ji}^{L} – the weight vector for each class C_j of Layet L

Step 2: Start iteration, ii = 1, 1000 (say)

Step 3: Forward Propagation

Step 4: Back Propagation (Computing local gradients at each node)

Step 5: Repeat steps 3 to 4 till the error function minimize.

2.10 Multiple Regression Model

A. **Goal:** Estimate the mean of Y for the subpopulation with explanatory variables $X_1 = x_1, \ldots, X_p = x_p$

B. **Applications:** Prediction of Y given $X_1 = x_1, \ldots, X_p = x_p$, estimation of causal effect of a variable X_1 on Y controlling for confounding variables.

C. **Data:** For each of n units, we observe a response variable Y and explanatory variables $X_1, \ldots, X_p$. So we observe $(Y_1, X_{11}, \ldots, X_{1p}), (Y_2, X_{21}, \ldots, X_{2p}), \ldots, (Y_n, X_{n1}, \ldots, X_{np})$.

D. **Ideal Multiple Regression Model Assumptions**:

a. $\mu\{Y \mid X_1 = x_1, \ldots, X_p = x_p\} = \beta_0 + \beta_1 x_1 + \cdots + \beta_p x_p$ (linearity)

b. $SD\{Y \mid X_1 = x_1, \ldots, X_p = x_p\} = \sigma$ (constant variance)

c. Distribution of Y for each subpopulation $X_1 = x_1, \ldots, X_p = x_p$ is normally distributed (normality)

d. Observations are independent

E. **Estimation:** The coefficients are estimated by choosing $\hat{\beta}_0, \ldots, \hat{\beta}_p$ to make the sum of squared prediction errors as small as possible. These are called the least squares estimates. $\sigma = SD(Y \mid X_1 = x_1, \ldots, X_p = x_p)$ Estimated by $\hat{\sigma} =$ root mean square error of residuals.

F. **Predictions and Residuals:** Predicted value of Y given $X_1 = x_1, \ldots, X_p = x_p$ is the estimated mean of Y for the subpopulation $X_1 = x_1, \ldots, X_p = x_p$, $\hat{\mu}\{Y \mid X_1 = x_1, \ldots, X_p = x_p\} = \hat{\beta}_0 + \hat{\beta}_1 x_1 + \cdots + \hat{\beta}_p x_p$. The residual for observation i is the error in using $\hat{\mu}\{Y \mid X_1 = x_{i1}, \ldots, X_p = x_{ip}\}$ to predict Y_i, $res_i = Y_i - \hat{\beta}_0 - \hat{\beta}_1 x_{i1} - \cdots - \hat{\beta}_p x_{ip}$.

G. Errors in Prediction and Residuals: Assuming ideal multiple linear regression model holds,

a. Approximately 68 % of the residuals res_i will be within $\hat{\sigma}$ of Y_i. Approximately 68 % of predictions of a future Y based on $X_1,\ldots,X_p$ (i.e., predict Y_{new} by $\hat{\mu}\{Y \mid X_1 = x_{new,1},\ldots,X_p = x_{new,p}\}$) will be off by at most $\hat{\sigma}$.

b. Approximately 95 % of the residuals res_i will be within $2\hat{\sigma}$ of Y_i. Approximately 95 % of predictions of a future Y based on $X_1,\ldots,X_p$ will be off by at most $2\hat{\sigma}$.

H. Interpreting Regression Coefficients:

$\mu\{Y \mid X_1 = x_1,\ldots,X_p = x_p\} = \beta_0 + \beta_1 x_1 + \cdots + \beta_p x_p$. Interpretation of β_1: Increase in mean of Y that is associated with a one unit increase in X_1 (from x_1 to $x_1 + 1$), holding fixed $X_2 = x_2,\ldots,X_p = x_p$. Interpretation of multiple regression coefficients on a variable X_1 depends on what other explanatory variables are in the model.

Source: On the Web, D. Small, Review of Multiple Regression (Lectures 22-27), Stat 112 Course

CHAPTER 3

3. RAINFALL RETRIEVAL METHODOLOGIES

3.1 Introduction

The aim of the following sections is to present a brief overview of the different types of rainfall retrieval methodologies using ground radar observations and various satellite data, to give their respective advantages and drawbacks, and to indicate the appropriate range of temporal and spatial scales of the rainfall estimates they produce. In fact, measuring rainfall is important in various applications such as agriculture, hydrology, economy, meteorology or climatology, but in each case, different time and space scales are concerned.

3.2 Radar Rainfall Estimation Algorithm

3.2.1 Radar Z-R Relationship

It is difficult to find sound scientific rationale for changing Z-R, however, especially when faced with operational time and data constraints. Fluctuations of DSD are often so rapid and localized that it is nearly impossible to select a single representative Z-R relation for the entire radar umbrella, or for any length of time.

There are some instances, for example long-lived and widespread stratiform rain events, where the DSD is stable enough to be characterized by a single Z-R relation. These instances must be identified by considerable local research, defining the relationship for each precipitation system in question.

3.2.2 Bright Band Corrections

Correction algorithms have been advanced by Cheng and Collier (1993), Smith (1986), and Kitchen *et al.* (1994). The latter two identify the bright band by its pronounced vertical discontinuity in Ze. This vertical profile is then modeled, from which a "background" Ze is calculated. This value is proposed as that which would exist in the absence of the bright band

enhancement. Both methods are the subject of continuing research by NWS OH for possible inclusion into the WSR-88D (Seo *et al.* 1995). This research indicates that much additional data analysis is required before any such scheme is implemented.

This conclusion is supported by the findings of Fabry and Zawadzki (1995), who report larger variability in bright band intensities than previously known. They add that even the physical cause of bright band enhancement is still open to debate, as the classical explanation of large water-coated snow aggregates could only account for 50 % of their observations. Such uncertainties complicate the development of robust correction techniques.

3.2.3 Anomalous Propagation Corrections

The seriousness of Anomalous Propagation (AP) contamination has given impetus to a high-priority NWS investigation of AP rejection algorithms (Interagency MOU 1995). Weber *et al.* (1993) and Moskowicz *et al.* (1994) presented identification/rejection methods that could provide a foundation for development of WSR-88D algorithms. Such methods are needed to combat loss of credibility by users of PPS products.

3.2.4 Gauge Data Adjustment Techniques

This field embraces a large array of procedures, several originating as far back as the 1970's. Most are statistical, but there are wide variations in analysis mode. The sampling problems addressed in Section 3a affect all of them. Whichever one is used in the bias adjustment algorithm should minimize these problems as much as possible for estimation of heavier rainfall, which is of primary concern in flood forecasting.

The bias adjustment algorithm will eventually be activated in the WSR-88D. It has been tested in a few cases and was shown not to degrade the Rr field, even with input from as little as three gauges (Seo *et al.* 1995). It will continue to be evaluated in the field, however, and might be changed or simplified if problems are found. If its benefits do not outweigh its liabilities, the scheme should be overhauled, augmented, or replaced. A few prototypes for potential augmentation or replacement follow.

Modification of adjustment for specific meteorological regimes or physical factors has been done by Collier *et al.* (1983) and Austin (1987). Classification of a precipitation system as stratiform or convective should be feasible at the very least.

A good candidate for classification might be "tropical" systems. There is much evidence that the PPS underestimates rainfall with these systems (Natural Disaster Survey Report 1995; Ruthi *et al.* 1993; Hitchens *et al.* 1993, Woods *et al.* 1995). This may result from their high precipitation efficiencies, DSD's weighted toward small sizes or, less likely, from a hail threshold that is too small for these cases. In response to the evidence, the Operational Support Facility (OSF) submitted a new relation, for use in the field during "tropical rain" events. This relation, $Z=250R^{1.2}$ (from Rosenfeld *et al.* 1993), provided good Rr estimates in four tropical rainstorms in Texas and Florida. It will be interesting to follow the performance of this relation upon a larger sample of tropical systems, across the world. Finally, Rosenfeld *et al.* (1994) proposed that Rr be adjusted ***locally***, in small windows surrounding a gauge. A bigger obstacle is a sparity of gauges under many radar umbrellas.

3.2.5 Vertical Reflectivity Profile (VRP) Corrections

This category could also be termed "range dependent corrections", since the portion of the VRP observed by a radar is determined by its range. The bright band strongly affects the ***shape*** of the VRP. The bright band ***height*** divides layers with very different Ze profiles. The sampling of these profiles is range dependent and so is discussed later in this subsection. An even more serious consideration is those effects that prevent the radar from "seeing" the lower portion of the VRP, the most representative portion for precipitation estimation.

Joss & Waldvogel (1990) assert that VRP measurement is "***...the main problem in using radar for precipitation measurements and hydrology in operational applications.***" This is affirmed by several researchers, including Koistinen (1991), Galli and Joss (1991), Andrieu and Creutin (1991), and Smith (1990). Joss and Waldvogel (1990) reinforce the importance of VRP correction by asserting that it should be done ***before any other adjustment***, as with gauge data.

3.3 Satellite Based Rainfall Estimation over the Globe

3.3.1 Introduction

Satellite remote sensing of rainfall has started in the seventies. First, Visible (VIS) and Infrared (IR) imagers onboard geostationary satellites were used (for example, Meteosat-1 launched in 1977); then microwave (MW) passive radiometers have been available; for example the Special Sensor Microwave /Imagers (SSM/I) have been carried on board the series of DMSP polar orbiting satellites, starting in 1987. Finally the first mission specially dedicated to precipitation measurement, the Tropical Rainfall Measuring Mission (TRMM) was launched in 1997, on a tropical orbit (35 deg N – 37 deg S), carrying on board VIS, IR and MW radiometers and the first space born precipitation radar. The following sub-sections describe the approaches used in making quantitative estimates of rainfall by satellite observations.

3.3.2 VIS and Infrared Algorithms

Cloud indexing techniques assign a rainrate level to each cloud type as identified from the satellite imagery. The simplest and perhaps most widely used is the one developed by Arkin (1979) during GATE on the basis of a high correlation between radar-estimated precipitation and fraction of the area covered by pixels colder than 235 K in the IR. The scheme, named GOES Precipitation Index (GPI) (Arkin and Meisner 1987), assigns these areas a constant rainrate of 3 mm h^{-1}, appropriate for tropical precipitation over 2.5°×2.5° areas. GPI is a standard for climatological rainfall analysis (Arkin and Janowiak 1991) and is regularly applied and archived for distribution. A family of cloud indexing algorithms was developed at the University of Bristol based on the Polar-Orbiter Effective Rainfall Monitoring Integrative Technique (PERMIT) (Barrett and Bellerby 1992). Originally developed for polar-orbiting NOAA satellites, they are now adapted to geostationary satellite imagery.

Many other techniques, which are more sophisticated, have been developed; they aim to improve the IR temperature-rainfall relationship and to better identify the precipitating area in the cloud. Among them, the following approaches should be mentioned: techniques that vary the threshold temperatures according to regions and seasons; techniques using visible (VIS) radiances in order to discriminate cirrus clouds (Bi-spectral VIS/IR techniques). Bispectral methods are based on the

very simple, though not automatic, relationship between cold and bright clouds and high probability of precipitation, e.g. the cumulonimbus case. Lower probabilities are associated to cold but dark clouds (cirrus) or bright but warm (stratus). The RAINSAT technique (Lovejoy and Austin 1979; Bellon *et al.* 1980) screens out cold but not highly reflective clouds or those that are highly reflective but have a relatively warm top. The number of false alarms of the pure IR techniques is then reduced. The algorithm is based on a supervised classification trained by radar to recognize precipitation from both VIS brightness and IR cloud top temperature. Results of an optimization of RAINSAT using METEOSAT over the UK were published (Cheng *et al.* 1993; Cheng and Brown 1995). Clustering similar to that applied to bispectral cloud classification was applied by Tsonis and Isaac (1985) and Tsonis (1987). Rain areas are determined by classifying pixel clusters in the VIS/IR histogram of the image scene and radar data are used as "ground truth" for the validation of the method.

The role of VIS data in improving IR rainfall estimates has been examined by King *et al.* (1995) during the First Algorithm Intercomparison Project (AIP/1) over Japan. Results show a higher correlation with validation data using VIS/IR over the IR alone for the case of warm, orographically induced rainfall. For cold, bright clouds (e.g. cumulonimbus) the correlations were similar. Other approaches have used pattern recognition techniques applied to VIS/IR data sets. O'Sullivan *et al.* (1990) used brightness and textural characteristics during daytime and IR temperature patterns to estimate rainfall over a 10×10 pixel array in three categories: no rain, light rain, and moderate/heavy rain.

Most of Satellite (IR) rainfall algorithms experimentally relate the rainfall amounts to parameters associated with the cloud-top fraction or cloud area (Negri *et al.* 1984; Arkin and Xie 1994; Goodman *et al.* 1994; Ebert *et al.* 1996; Kurino 1997; Vicente *et al.* 1998; Alder *et al.* 2001) using techniques such as the Griffith-Woodley technique (Griffith *et al.* 1978), the auto-estimator (Vicente *et al.* 1998), and the Geostationary Operational Environmental Satellite (GOES) Precipitation Index (GPI) (Arkin 1979; Arkin and Meisner 1987). Their applications concentrate primarily on climate analysis and model initialization. Few of them focus on the instantaneous rainfall observations and real-time flash flood watches (Vicente *et al.* 1998). The addition of satellite visible (VIS) data efficiently improves the infrared (IR) rain algorithm in reducing high clouds without rains. However, IR radiometers sense radiation emitted from or reflected by the

cloud top. Thus, there is no information available on the vertical cloud structure and the near-surface rain layers (Bauer *et al.* 1998; Hong *et al.* 1999). Satellite VIS data are only available in the daytime, which limits the improvement space for some algorithms.

Techniques oriented towards convective cloud systems are the life-history methods. They take into account the cloud's life cycle which is particularly relevant for convective clouds. One for all so called Griffith-Woodley technique (Griffith *et al.* 1978) tracks clouds through their life cycle before assigning precipitation. A major problem is that often cirrus anvils of neighboring clouds screen the cloud life cycle leading to underestimates early in the day and overestimates towards the evening. Negri *et al.* (1984) have simplified the technique eliminating cloud tracking and producing a precipitation scheme that treats each cloud as if existing only in one image. The scheme is proved to perform at the same level of the Griffith- Woodley's. Advantages and limitations of the technique when applied to frontal precipitation leading to flood episodes were examined by Levizzani *et al.* (1990). The Scofield-Oliver technique (Scofield and Oliver 1977; Scofield 1987) involves direct interaction by a meteorologist and is currently used by NOAA-NESDIS for operational nowcasting of heavy rainfall and flash floods (Scofield and Naimeng 1994; Robinson and Scofield 1994; Vicente and Scofield 1996).

Cloud life-cycle techniques, which distinguish the growing phase producing heavy rain and the dissipating phase accompanied by light rain; techniques using cloud models in order to delineate the convective and stratiform parts of the system; and techniques using other IR channels (water vapor or near IR or the «split window«), which help to detect cirrus cloud. Cloud models are used to improve estimation results by trying to build the physics of clouds into the retrieval process. Gruber (1973) first introduced a cumulus convection parameterization to relate fractional cloud cover to rainrate. Wylie (1979) used a cloud model to adjust calibration coefficients. The Convective Stratiform Technique (CST) (Adler and Negri 1988) relies upon a 1D cloud model to relate cloud top temperature to rainrate and rain area. Local minima in the IR temperature are sought and screened to eliminate thin, non precipitating cirrus. Precipitation is assigned to convective areas by means of the cloud model. To every other element colder than the stratiform threshold a fixed stratiform rainrate of 2 mm h-1 is assigned. These methods were originally developed for a particular location and their adaptation to other areas of the globe or climate regimes is not trivial (e.g. Marrocu *et al.* 1993).

All these methods make use of data from IR/VIS radiometers on board geostationary satellites, which have a very good temporal and spatial coverage, providing an image every half an hour with a spatial resolution of 5 km, for example, for Meteosat. Because of the resulting very good sampling of the data, and despite the IR/VIS measurements have no direct physical connection with surface precipitation, infrared techniques provide however, reliable estimation of the rainfall amount accumulated during long time periods and averaged over large areas. These techniques are mostly appropriate for large and climatic scales.

3.3.3 Others IR Algorithms

Rainfall can be inferred from Infrared satellite observations. The thermal infrared (10-12 μm) brightness temperature measured over a cloudy area is related to the cloud top height. Clouds with very cold top indicate deep convection. Such convective cells are associated with surface precipitation; in fact the convective systems produce the major part of rainfall in the tropics. Actually the relationship between IR temperature and rainfall is indirect, which is not physically based. Moreover, it is not possible to discriminate the convective part of the system producing heavy rainfall from the stratiform part of the system or cirrus clouds, also with a cold cloud top, which do not produce any rain. Nevertheless, if time integration and/or large surface area are considered, then there is a good correlation between the corresponding cumulated and averaged rainfall and the computed IR index. Arkin (1979) found a relationship between fractional coverage of high cloud and rainfall accumulations. The so-called GOES Precipitation Index (GPI) is the percentage of the pixels having an IR temperature colder than the threshold temperature (235 K) in a 2.5°x2.5° grid box multiplied by a constant rain rate of 3 mm/h. Although this calibration value should vary for the different climatic regimes, the GPI is commonly used and archived for climatologically studies. (Arkin and Meisner, 1987; Arkin and Janowiak, 1991).

IR and near-IR channels other than the 10.5-12.5 mm window region show some potential for application to rainfall estimations. Techniques for the instantaneous delineation of convective rainfall areas using split-window data were conceived for the AVHRR (Inoue, 1987a, b, 1997). These techniques initially detect non-precipitating cirrus and low-level cumulus clouds using the split-window 10.5-11.5 and 11.5-12.5 μm channels. Kurino (1997a, b) has applied a split-window technique to data from the Japanese Geostationary Meteorological Satellite (GMS). He used three parameters: the 11 μm brightness temperatures, the difference between 11 and 12 μm, and the

difference between 11 and 6.7 μm. The technique was statistically characterized against digital radar data on 1°×1° boxes over a considerable amount of time for nowcasting applications. Vicente (1996) developed a simple and fast algorithm for rainfall retrieval using the 11 and 3.9 μm channels with the advantage of night-time use. The 11 μm channel is more sensitive to the presence of ice while the 3.9 μm to that of water vapour. The difference can be used as a tool to select cloud areas associated to a higher probability of producing rain.

3.3.4 Microwave Algorithms

Rainfall can be inferred from passive or active microwave satellite observations. Passive microwave (MW) radiometers physically sense drops and hydrometeors within precipitating clouds, which allows correct multi channel MW measurements of rain regions under the clouds (Ferraro *et al.* 1994; Wilheit *et al.* 1991). Although, MW rain retrieval methods use measurements that are more direct than those used for IR rain retrievals, and the instantaneous MW rain estimates are more accurate than IR rain estimates (Ebert et al. 1996), they are, however, limited by the microwave remote sensing technology. Poor temporal scan resolution strategy and narrow scan-swath limit the application of polar-orbiting satellites in both flash flood watches and oceanic heavy rainfall warnings. The microwave radiometers have several channels at 4 different frequencies for SSM/I, and 5 frequencies for TRMM Microwave Imager (TMI), which range from 10 to 86 GHz and which are polarized horizontally and vertically. Interactions between ground surface and hydrometeors with the MW radiation depend on frequency, polarization and surface emissivity (0.4–0.6 for the ocean and 0.8–0.9 for land). In short, at low frequencies (below 60 GHz), when interacting with clouds or precipitation, the absorption/ emission from liquid water is the predominant effect, while at high frequencies (above 60 GHz), scattering by large ice crystals present in the upper layer of the convective clouds is the most important effect. For the emission mode, the MW signal is directly related to rain drops and thus to rain rate, but it is measurable only over the ocean. For the scattering mode, the relationship between the MW signal and rain rate is indirect, however, since the scattering signal is independent of the background, it allows estimating rainfall over land.

At passive MW frequencies precipitation particles are the main source of attenuation of the upwelling radiation. MW techniques are thus physically more direct than those based on VIS/IR radiation. The emission of radiation from atmospheric particles results in an increase of the

received signal. At the same time the scattering due to hydrometeors reduces the radiation stream. Type and size of the hydrometeors depend upon the frequency of the upwelling radiation. Above 60 GHz ice scattering dominates and the radiometers can only sense ice while rain is not detected. Below about 22 GHz absorption is the primary mechanism affecting the transfer of MW radiation and ice above the rain layer is virtually transparent. Between 19.3 and 85.5 GHz, the common passive MW imagers' frequency range, radiation interacts with the main types of hydrometeors, water particles or droplets (liquid or frozen). Scattering and emission happen at the same time with radiation undergoing multiple transformations within the cloud column in the sensor's field of view. At different frequencies the radiometers observe different parts of the rain column. As for other parts of the spectrum MW radiation is absorbed (but not scattered) by cloud droplets, water vapour and oxygen making precipitation estimates based on absorption potentially difficult.

Precipitation drops strongly interact with MW radiation and are detected by radiometers without the IR strong biases. The biggest disadvantage is the poor spatial and temporal resolution, the first due to diffraction and the latter to the fact that MW sensors are presently only mounted on polar orbiters, a clear consequence of the first. The matter is further complicated by the different radiative characteristics of sea and land surfaces underneath. A sea surface has a relatively constant low emissivity (e=0.4) so that the radiation emitted from it is small and precipitation (e=0.8) will increase the amount of radiation detected by the sensor through emission. The high polarization of sea surface also contrasts very much with the low polarization of rain. Land surfaces have a high and variable emissivity (e=0.7-0.9) close to that of precipitation and low polarization (Levizzani, V). The emissivity is dependent upon the characteristics of the surface including vegetation cover and moisture content. Rainfall over land will increase the upwelling radiation stream but at the same time absorb radiation inducing errors in the identification of rain areas. Scattering is thus the key to MW rainfall estimation techniques over land and the 85.5 GHz channel of the Special Sensor Microwave/Imager (SSM/I) is very sensitive to scattering from small particles. The applicability of passive MW rainfall retrieval methods needs to be clearly defined, specially when operational applications are at stake (Ferraro *et al.*, 1994; Berg *et al.*, 1998). Wilheit *et al.* (1994) provide a fairly complete overview of the field and Petty (1995) concentrates on rainfall estimation over land. One study refers that maximum rainfall rate occurs at a considerably lower altitude when low liquid-emission or low ice-scattering signatures are observed. It is also found that the liquid and ice water amounts in tropical rains are correlated

over scales the size of a satellite pixel and for a given surface rainfall rate, the brightness-temperature differences among the pixel groups are large, highlighting the importance of vertical precipitation profile in determining upwelling microwave radiation (Yunfei *et al.* 2001).

Methods vary from relatively simple polarisation techniques (Spencer *et al.*, 1989; Kidd, 1998) to more complex approaches based on time-dependent cloud-radiation models (Smith *et al.*, 1992; Mugnai *et al.*, 1993). The simplest microwave methods are based on statistical regressions using some of the brightness temperatures or combination of them to derive a rain index, which is then related to rain rate. Examples of such indices are the Scattering Index (SI) proposed by Grody (1991) or the Normalized Polarization Difference (NPD) proposed by Petty (1994). In general, algorithms are differentiated according to their use over land or ocean surface. Some other methods are more based on an inversion algorithm using a database (Kummerow and Giglio, 1994 or Mugnai and Smith, 1988). Yeh *et al.* (1990a) used a radiative transfer model along with radar reflectivity-derived hydrometeors to information about particle size distribution and phase. High frequencies are sensitive to the upper layers of the cloud (ice crystals) and the low frequencies are influenced by the larger precipitation particles. Vertical Profile of rainfall gives an opportunity to study vertical structure of rain corresponding to a particular rain-rate and it was derived from TRMM Microwave 10 GHz channels and PR data. It will help to characterize the rain structure in cloud system over land, oceans because rain has different characteristics over different surface (P.K, Pal et al 2001). Many regional and seasonal biases are identified and applicability of new features to the other microwave sensors are studied using TMI, SSM/I and AMSR-E data where foot print between TMI and SSM/I is different but AMSR-E is the same as the TMI and frequencies of these instruments are very similar (Jeffrey *et al.* 2003). Area average rain retrieval methodology was developed to land area based on ATI concepts outlined by Doneaud et al (1984) where variance drops to 55 % (C. Prabhakara, *et al.* 1999). A probabilistically based convective-stratiform rainfall classification scheme was developed, which relates a quantity called variability index (VI), computed from 85-GHz brightness observations, to the precipitation types that is independent of any rainfall retrieval scheme (Emmanouil *et al.* 1996). Beside this another scheme was also developed to classify convective and stratiform precipitation over oceans using multi channel brightness temperatures of passive microwave because convective precipitation has high spatial variability as well as high intensity (Ye Hong *et al.* 1999).

More over, there are difficulties that are common to all MW methods, related to the coarse spatial resolution of the data. Because of the high spatial variability of rain rate, there are large in homogeneities of the rain rate field inside such large pixels. Also the pixel areas can be covered partially by precipitation. Another characteristic of microwave data is that MW radiometers are used only on board low earth-orbiting satellites, because of the present technology of antennas. A study of estimation errors on the monthly rainfall averaged on different spatial scales, which are due to the under sampling of MW satellite data, was conducted by Weng *et al.* (1994). It indicates that the error is at least 25 % over ocean and more over land. Particularly, when the diurnal cycle is important, the rainfall estimates are overestimated or underestimated according to the satellite over passing time being close to the maximum or the minimum of the diurnal cycle.

Rainfall estimation methods using active MW data derive the vertical profile of instantaneous rain rates from precipitation radar reflectivities (Iguchi *et al.*, 2000). The limitations of these methods are similar to the limitations of other MW techniques, but the limitation due to poor spatial coverage is even more severe, because the swath of the precipitation radar (on board TRMM) is limited to only 220 km compared to the radiometer swath, which is 760 km. On the other hand, the spatial resolution of the radar pixels is better, with a pixel size of 4 km. It is necessary also to mention the difficulties due to the calibration of space radar, which contribute significantly to rain rate estimate uncertainties. At last, there are methods combining active and passive microwave data (Haddad *et al.* 1997).

To conclude, the passive and/or active microwave techniques are mainly designed to estimate instantaneous surface rain rates or rain rate profiles. Some MW techniques are used to provide accumulated averaged rain rates, like monthly averages of satellite-estimated rainfall with grid resolution of 1°-5° square. The uncertainties of such products depend on various factors like location, season or type of rain, but are always large because of the sampling error due to the poor coverage by low-orbiting satellites. Bell and Kundu (2000) give an interesting review of the work that has been devoted to the problem of attaching error estimates to these products.

3.3.5 Multi-source Combined IR / MW Methods

Various methods have suggested combining the observations delivered by satellite instruments of different type to improve averaged rainfall estimation by using multi-source data. For example,

the methods combining IR data from geosynchronous satellite and MW data from low-orbit satellites attempt to take advantage of both IR and MW techniques. They benefit from the excellent time and space coverage of IR images and from the direct connection of the MW observations with precipitation. As an example, RACC (Rain and Cloud Classification) proposed by Jobard and Desbois (1994) is the method of such IR/MW combining approach. It is based on an automatic classification procedure. The learning phase, applied to a set of IR images and MW data from coincident orbits, uses a dynamic clustering technique to find out classes characterizing different types of cloud. The MW data allow assigning a rainfall amount to each class characterized as precipitating. The application phase using only the IR images, leads to cloud classified images, from which rainfall images are derived. These half-hourly rainfall images, with 5-km pixels, are then cumulated and/or spatially averaged to produce accumulated averaged surface rainfall for any desired time and space resolutions according to the users' own requirements.

One of the important findings of AIP-3 (Ebert et al, 1998) was that for monthly rainfall products, the combined techniques performed better than the SSM/I-only techniques, whereas for instantaneous rain retrieval, the SSM/I-only techniques showed a better correlation with the validation data than did the combined algorithms (Smith *et al.*, 1998). Statistically blend low-Earth orbiting (LEO) passive microwave based rainfall estimates from the Special Sensor Microwave Imager (SSM/I) and the Tropical Rainfall Measuring Mission (TRMM) microwave imagers together with geostationary-Earth orbiting (GEO) infrared satellite data in a near real-time, operationally-oriented fashion. The idea of blending LEO microwave and GEO infrared data together to introduce additional temporal sampling was proposed shortly after the launch of the first SSM/I and is an active area of research (Adler *et al.*, 1993, 1994; Todd *et al.*, 1998; Xu *et al.*, 1999; Miller *et al.*, 2000). A major advantage of blending in the microwave-based data into the stream of geostationary data collection is the possibility of an hourly (or less) global rain rate analysis which avoids the spatial and temporal coverage gaps characteristic of swath-limited, low-Earth orbiting orbits.

A near real-time adjustment of the thermal infrared (IR) co-localized with MW-based rainrates is operationally very promising. Numerical weather prediction (NWP) model data need to be incorporated within the rapid-update scheme in order to accommodate orographic precipitation, a

common error source (Levizzani *et al.* 2003). Large time scale rainfall estimates based on geostationary satellite Infrared (IR) data have been shown a good agreement with observations at the monthly time scale (K. Ramage *et al.*). Multi-source data algorithms are also developed to produce, in near real-time, 3-hour global rainfall analyses blending IR data from any geostationary imager with co-localized MW derived rain rates from all available SSM/I‘s and TMI (Turk *et al.*, 2000). Another approach proposed by Vincente *et al.* (1998) is to retrieve from GOES thermal IR data, 6-hour rainfall estimates, which are then adjusted for different moisture regimes using percipitable water and relative humidity fields from a numerical weather prediction model and SSM/I measurements.

Another approach proposed by Adler *et al.* (1994), the Adjusted GPI technique, is based on the IR GPI index: the monthly rainfall derived from the GPI is adjusted by a factor, which is the ratio between the monthly rainfall estimated from MW data and monthly rainfall derived from the subset of IR images having a coincident MW image. This technique has been now upgraded by including information from rain gauges. The AGPI monthly rainfall is adjusted with the gauge analyses provided mostly over land, by the Global Precipitation Climatology Project (GPCP). The merging technique is described in Adler *et al.* (2000). The merged satellite/gauge estimates of surface precipitation are produced operationally in TRMM (as labelled product 3B-43) for calendar months on a 1°x1° latitude-longitude grid. A similar multi-source data approach has been developed for producing precipitation estimates on a daily 1°x1° lat/lon grid with a global coverage: this is the One-Degree Daily (1DD) GPCP dataset, available from 1997 to nearly present (the product is computed a few months after real time). This satellite-gauge product is described in Huffman *et al.* (2001); it is actually derived from the histograms of geosynchronous satellite IR temperatures on a 1°x1° grid covering 40°N-40°S.

The superior spatial and temporal resolution of geostationary satellite rainfall estimates on one hand and better physical insight of MW retrievals on the other are directing research efforts towards investigating hybrid techniques where MW retrievals are used in the same way as ground truth. Adler *et al.* (1993) combined Special Sensor Microwave/ Imager (SSM/I) and Geostationary Meteorological Satellite (GMS) measurements of rainfall over Japan: the aim was to obtain mean monthly values for climate studies. Negri and Adler (1993) modified the cloud area threshold and adopted an empirical discrimination threshold between raining and non-raining

clouds. Levizzani *et al.* (1996) conducted a simultaneous rainfall analysis using SSM/I and METEOSAT data for two storms over northern Italy that caused damaging floods. Their results, though very preliminary, suggest that an IR-based rainfall analysis derived from half-hourly geosynchronous images can be improved with a calibration approach using a MW algorithm sensitive to vertical cloud structure and its inhomogeneities. A calibration attempt of IR geosynchronous data using SSM/I retrievals over the Pacific Ocean was made by Vicente and Anderson (1994): their approach involves two multi-linear regressions a day allowing a twice a day calibration between MW rainfall rate and IR cloud top temperature. Laing *et al.* (1994) focused their attention to Meso-scale Convective Systems (MCS) in Africa deriving a relationship between SSM/I-derived precipitation characteristics and METEOSAT IR data.

Hybrids method of Turk *et al.* (1998a,b) attempts to statistically fuse these two types of satellite data in real time for the retrieval of instantaneous and accumulated rain rates at the geostationary time scale, i.e. half an hour or less. A probability matching is done between SSM/I rain rates from the closest passage in time and the geostationary IR brightness temperatures. The matching is automatically updated as new SSM/I data are ingested in real time. Several other IR+MW methods have been proposed trying to take advantage of the higher physical content of MW measurements and the spatial and temporal coverage of geostationary satellites. Among them Jobard and Desbois (1992), Laing *et al.* (1994), and Vicente and Anderson (1994) are widely used.

A different approach based on the synergetic use of GOES-8/9 thermal IR data, radar instantaneous rainfall estimates and model output is the Auto-Estimator technique of NOAA National Environmental Satellite Data and Information Service (NESDIS) (Vicente *et al.*, 1998). The method is based on a power-law regression algorithm to compute real-time precipitation values. The regression is based on a statistical matching between radar-derived instantaneous rainfall estimates and satellite IR brightness temperature field. Adjustments are performed for different moisture regimes using real-time fields of precipitable water and relative humidity as computed by the Eta Model of the National Center for Environmental Predictions (NCEP). The technique is being used as an operational tool for flash flood forecasting, numerical modeling and hydrology.

3.4 Rainfall Estimation, Diurnal Cycle and Variability in and around Bangladesh

Most previous works comparing the tropical rainfall diurnal cycle over the ocean and the land surfaces agree that the amplitude of the diurnal cycle of rainfall over the continent is larger than that of over the open oceans (Gray and Jacobson, 1977; Chen and Houze, 1997). However, studies conducted over different regions of the tropics have found significant differences in the character of the diurnal cycle, leading to different hypothesized causal mechanisms (Nesbitt and Zipser, 2003). Diurnal variability and convective organization are poorly understood in the tropics in general and especially in Bangladesh and the Bay of Bengal. In and around Bangladesh the exact pattern of the diurnal variation of convective activity is also not yet clear enough. The diurnal variation observed by TRMM PR (Precipitation Radar) informed that precipitation dominates in the afternoon on land and in the morning over water near coast (TRMM report, 2002). However, exception is seen over Bangladesh, morning precipitation dominated over the country in 1998 and 1999.

There are some studies on the diurnal variations with raingauge data in some parts of India (Prasad, 1974; Bhattacharya and Bhattacharyya, 1980; Harlar *et al.*, 1991). Wahid and Islam (1999) reported the morning and afternoon/evening peak in the north-eastern part (Sylhet) of Bangladesh using raingauge rainfall data of 1996. Ohsawa *et al.* (2001) reported early morning peak in the northeast (0400-0600 LST) and in the southern coastal region (0300-0600 LST) with an afternoon peak in the southeast-southwest regions of Bangladesh using raingauge rainfall data of 1995. There is no comprehensive research work on diurnal variation of cloud activity over Bangladesh using high-resolution data. Zuidema (2003) also suggested the study of diurnal cycle using data with higher temporal resolution.

It is difficult to understand the nature and variability of precipitation on a microclimate scale, mainly because of the coarse temporal and spatial resolution of global datasets. Meisner and Arkin (1987) reported that the diurnal cycle over the tropical continents during summer was much larger than over the oceans. Chang *et al.* (1995) analyzed rainfall observations made by SSM/I measurements. They found that over the tropical oceans in general and inter-tropical convergence zone (ITCZ) in particular, the rainfall during morning hours was significantly higher (about 2 %) than that during evening hours. In an earlier study using SSM/I data, Sharma *et al.* (1991) had also noticed that the morning rainfall was larger than afternoon rainfall over the

region between 50 deg N – 50 deg S. Chen *et al.* (1999) found that the maximum daily rainfall over Taiwan occurs at about 1600-1700 LST, which is 2-3 hour after the maximum horizontal convergence of surface air mass flux. They interpreted this time lag as a regulating effect of the interaction between mountainous terrain of the region and the land-sea-breeze circulation. Diurnal variations of convective activity were investigated using GMS satellite (GMS-5) and rain gauge data from Bangladesh, Thailand, Vietnam and Malaysia and found a strong possibility that the late night-early morning maximum of convective activity and rainfall have a great effect on energy and water balance in tropical Asia (Teruo Ohsawa *et al.* 2001).

Averaging of rainfall using different grid size (0.5 deg or 01 deg) from GMS-5 data over south east Asia does not effect to the result (C. M. Mukammel Wahed et al 2000). Other study refers using TRMM data for mountainous region in Nepal that PR performs better on low elevation stations than high altitude stations and PR 3D rain profiles gives a strong interaction between mesoscale convective systems and steep terrain at elevations of 1-2 km (A. P Barros *et al.* 2000). Using GMS-5 Infrared detects higher rainfall intensity in north east region in Bangladesh and sea, offshore areas received almost uniform rainfall compared to land areas, where it fluctuates with horizontal distance (C. M. Mukammel et al 2000). A relationship was derived between cloud top temperature and cyclone near coastal region of Bangladesh using GMS-5 Infra-red data by statistical regression analysis (D. A. Quadir, *et al.* 1999).

Two rain index namely RI1 and RI2 were developed based on Cloud Cold Duration (CCD) technique using METEOSAT Infra-red data and applied for semi-humid (Senegal) and humid region (Bangladesh) but neither produces better results than GPI in Bangladesh but in the Senegal river basin RI1 model performs best (Gorm Dybkjaer et al, 2003). Some other studies have been done towards Satellite rainfall estimation over Bangladesh using Geostationary Meteorological Satellite (GMS) Infrared data. In one study, Convective and Stratiform Technique (CST) was applied to calculate 3-hourly rainfall using GMS-5 Infrared data and found better correlation near coastal region (South Eastern part of Bangladesh) but not at inland area (Nazrul *et al.* 2002). Adjusted Geostationary Operational Environmental Satellite Precipitation Index (AGPI) was also used in Flood Forecasting and Warning System Project of Bangladesh to estimate 3-hourly rainfall using METEOSAT 5 data (FFWC Project report, Bangladesh, 2001).

3.5 Future Mission to Rainfall Estimation

Advancement of TRMM, and recognizing the need for more comprehensive global precipitation measurements, NASA and NASDA has now planned a new mission, i.e., the Global Precipitation Measurement (GPM) mission. The primary goal of GPM is to extend TRMM's rainfall time series while making substantial improvements in precipitation observations, specifically in terms of measurement accuracy, sampling frequency, Earth coverage, and spatial resolution. GPM represents the next generation of space based precipitation estimation and builds upon valuable knowledge and experience gained during the TRMM era. In the GPM era, up to nine constellation satellites will provide more accurate and physically-based microwave precipitation estimates on a global basis with ~5 percent bias and ~20 percent precision uncertainty for 3-hourly products. Such direct measurements of precipitation and hydrometeor structure mitigate errors introduced by non-precipitating clouds, diverse macro cloud physics, and varying precipitation types. GPM's novel Dual Frequency Precipitation Radar (DPR) and its up to nine passive microwave radiometers (PMRs) on the constellation fleet provide an excellent means to cross-calibrate similar precipitation-measuring instruments in space and on the ground (e.g., from carefully instrumented ground validation sites). Thus, GPM will enable improved measurements of light rain, warm rain, snow, and other modes of frozen precipitation. The DPR will better detect explicit precipitation microphysics than was possible from the single frequency TRMM Precipitation Radar (PR), thereby leading to improvements in latent heating algorithms and mass spectra properties associated with the highly varying drop size distribution (DSD).

CHAPTER 4

4. STUDY AREA AND DATA DESCRIPTION

4.1 Introduction

This chapter contains the general description of the study area, data availability and description of different data set. Different satellite sensors, products and it applications related to rainfall products are described to the following subsections. A brief climatology in Bangladesh is also outlined in this chapter.

4.2 General Description of Study Area

Bangladesh is one of the South Asian countries and total area is about 147000 sq km. It is located in the north eastern part of South Asia between 20^0 34" and 26^0 38" north latitude and 88^0 01" and 92^0 41" east longitude (Figure 4.1). Bangladesh is one of the most densely populated places on earth with 1,000 people living in just a single square kilometer. About 80 % land area of Bangladesh is located within the floodplains of three great rivers: the Ganges, Brahmaputra and Meghna, and their tributaries. The Meghna basin experiences the highest rainfall intensity in the world.

The source of water vapour, the Bay of Bengal is located in the south, while the Himalayas and the Tibetan Plateau, high elevation areas are situated in the north. The organization and diurnal phasing of precipitation systems during the summer monsoon in and around Bangladesh is affected by these orographic characteristics situations, south-westerly wind, the anomalies of land-sea thermal temperature and sea-breeze circulation (Liu and Yanai, 2001).

The land of Bangladesh is very flat: elevation is about 1-10 m above sea level except small portions in the southeast (elevation ~200 m), which is border with Myanmar, and in the northeast (elevation ~100 m), which is border with Shillong hill of India. There are few mountains in the country higher than 1000 m. The Shillong Plateau and Chittagong Hill Tracts, located near the

north-eastern and south-eastern borders with India, respectively, have great effects on the amount of rainfall in the adjacent areas.

Bangladesh has a subtropical monsoon climate characterized by wide seasonal variations in rainfall, moderately warm temperatures, and high humidity. Regional climatic differences in this flat country are minor. Three seasons are generally recognized: a hot, humid summer from March to June; a cool, rainy monsoon season from June to October; and a cool, dry winter from October to March. In general, maximum summer temperatures range between 32°C and 38°C. April is the warmest month in most parts of the country. January is the coldest month, when the average temperature for most of the country is 10°C.

Winds are mostly from the north and northwest in the winter, blowing gently at one to three kilometers per hour in northern and central areas and three to six kilometers per hour near the coast. From March to May, violent thunderstorms, called northwesters by local English speakers, produce winds of up to sixty kilometers per hour. During the intense storms of the early summer and late monsoon season, southerly winds of more than 160 kilometers per hour cause waves to crest as high as 6 meters in the Bay of Bengal, which brings disastrous flooding to coastal areas.

Heavy rainfall is characteristic of Bangladesh. With the exception of the relatively dry western region of Rajshahi, where the annual rainfall is about 160 centimeters, most parts of the country receive at least 200 centimeters of rainfall per year. Because of its location just south of the foothills of the Himalayas, where monsoon winds turn west and northwest, the region of Sylhet in north-eastern Bangladesh receives the greatest average precipitation. The annual rainfall exceeds 5000 mm near the Shillong Plateau (Ohsawa *et al.* 1997a) because the Shillong Plateau works as a topographic barrier to the prevailing southerly monsoon wind, the amount of rainfall is extremely high on the southern slope of the Shillong Plateau.

Monsoon rainfall accounts for approximately 80 % of the total annual rainfall from June to September in Bangladesh (McGregor & Nieuwolt 1998). The northerly monsoon from the Bay of Bengal extends across the country to the foothills of the Himalayan mountain range in the north. Rain typically falls as showers from a pronounced cloud cover throughout the monsoon, but can be also associated with heavy rainstorms and tropical cyclones (McGregor & Nieuwolt 1998). About 80 percent of Bangladesh's rain falls during the monsoon season. The monsoons result

from the contrasts between low and high air pressure areas that result from differential heating of land and water. During the hot months of April and May hot air raises over the Indian subcontinent, creating low-pressure areas into which rush cooler, moisture-bearing winds from the Indian Ocean. During June to September, Bangladesh is influenced by the humid northerly monsoon, resulting in relatively homogeneous climatic conditions. Dividing against the Indian landmass, the monsoon flows in two branches, one of which strikes western India. The other travels up the Bay of Bengal and over eastern India and Bangladesh, crossing the plain to the north and northeast before being turned to the west and northwest by the foothills of the Himalayas.

From the past fifty year statistical average, annual rainfall over Bangladesh is 2360 mm and ranges from 1650-2930 mm. At a particular place (i.e. north east area) it is from 1200-5600 mm. Temperature in Bangladesh ranges from less than 5^0 C to more then 43^0 C. The peak in April-May but exceeds 43^0 C in the western parts of the Northwest Region. Extreme minimum temperatures observe in January-February and 1.7^0 C in Srimongal within Northeast Region of Bangladesh. Table 4.1 outlines the long term monthly average temperature and precipitation in Bangladesh.

Table 4.1 Monthly Average Temperature and Precipitation in Bangladesh, Source: BMD

	Jan	Feb	Mar	Apr	May	Jun	Jul	Aug	Sep	Oct	Nov	Dec
Max. Temp (°C)	25.4	28.1	32.3	34.2	33.4	31.7	31.1	31.3	31.6	31.0	28.9	26.1
Min. Temp (°C)	12.3	14.0	19.0	23.1	24.5	25.5	25.7	25.8	25.5	23.5	18.5	13.7
Rainfall (mm)	07.0	19.8	40.7	110.7	257.5	460.9	517.6	431.9	289.9	184.2	35.0	09.4

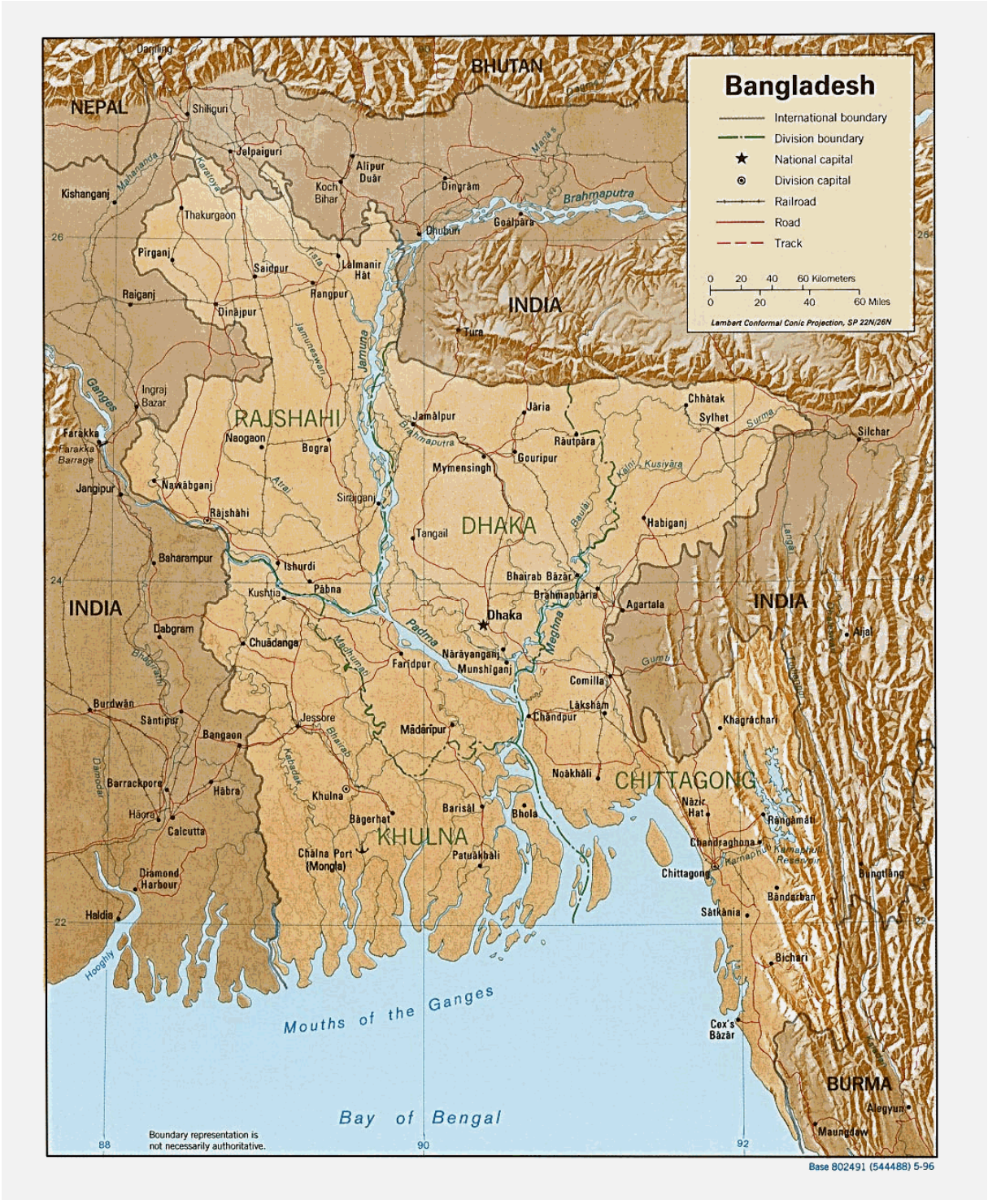

Figure 4.1 Location Map of Bangladesh (Source IFCDR Flood Study Report, Topic No. 1, 1997)

4.3 Data Availability

4.3.1 Meteorological Data

The meteorological data used in this study have been taken from IFCDR/JICA Rainfall Experiment, conducted between 1999 and 2003 in Northeast area of Bangladesh, deployed among S-Band Radar in Dhaka. In addition to this, 5-minute intervals rainfall data were collected from 15 tipping bucket type rain gauges in Dhaka and Sylhet area. Moreover, the Bangladesh Meteorological Department (BMD) also collects 3-hourly intervals rainfall data from several standard rain gauge type stations (star marks in Figure 4.2 and blue dot marks in Figure 4.3) over whole country.

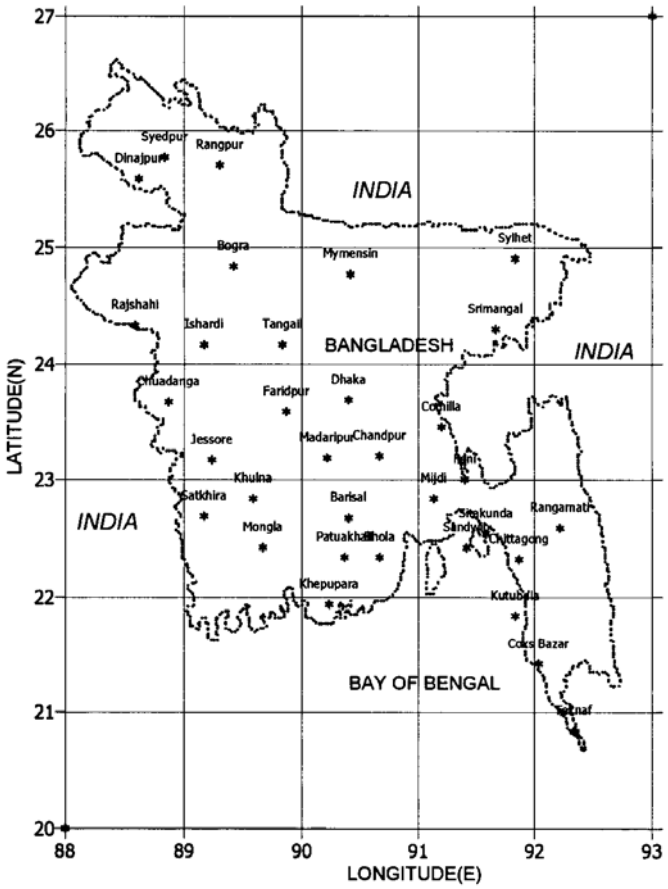

Figure 4.2 BMD 3-hourly rain-gauge locations over Bangladesh (Total 33 Stations).

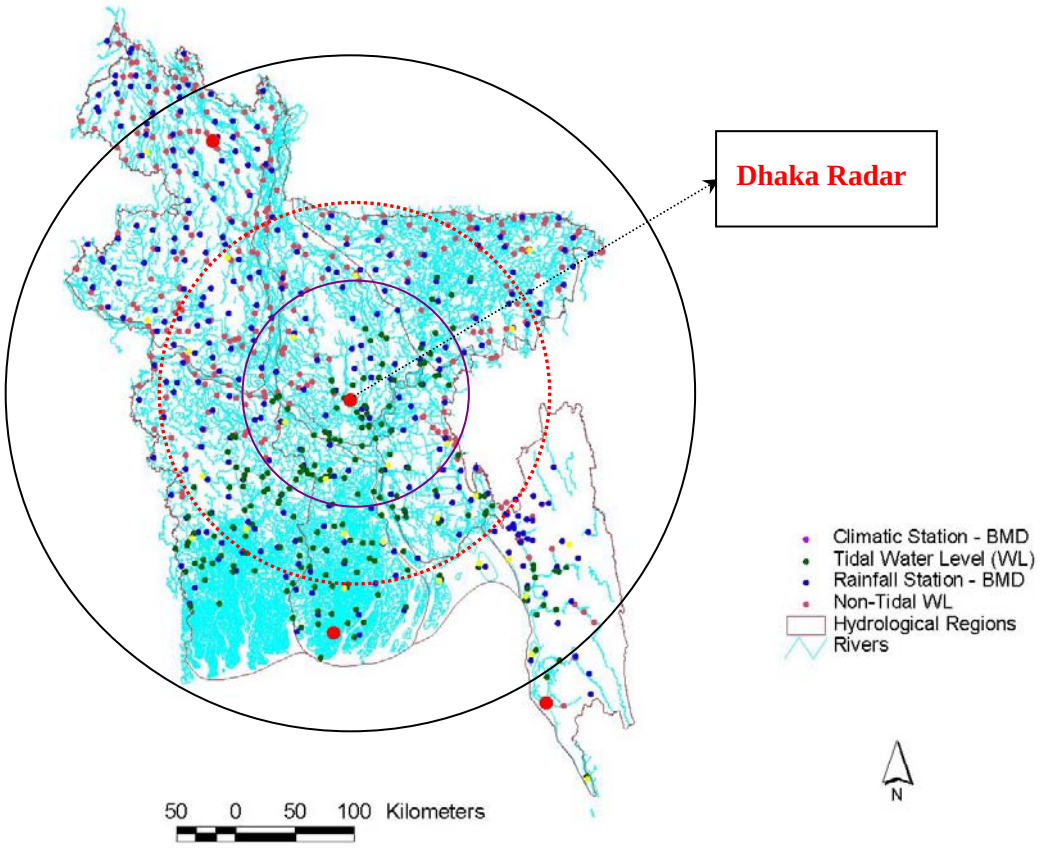

Figure 4.3 Radar Locations in Bangladesh (The blue dots represent the rain-gauge locations over Bangladesh and the big red dots represent the radar)
(Source: Data come from the Bangladesh Meteorological Department)

The BMD installed an S-band weather radar (wavelength: ~10 cm) at Dhaka (90.4°N, 23.7°E) on the roof of a building with height 60m (Figure 4.3), which provides a coverage of 600 km by 600 km rectangular area. Hereafter, this radar is called as Dhaka radar. It is noted that Dhaka radar covers almost the whole of Bangladesh including some neighbouring parts of India and Myanmar. This radar is designed to cover a radious of 400 km, at present the maximum effective radius being about 250 km. The 100 km, 150 km and 250 km radius circles are shown respectively at Dhaka radar site. It operates at a frequency of 2700-2900 MHz with a beam width of 1.7°. Moreover, the Dhaka radar operates with only zero elevation angles and collects PPI scan data (pixel size: 2.5 km mesh) at 2-3-minute intervals continuously for 1 hour with a 2-hour break during operation. Sometimes radar is operated for a few continuous hours without any break. The

radar stops operation at 03 LST everyday. There are about 20 PPI (plan position indicator) scans data available during each operation hour. For this study purpose, the PPI scan from Dhaka radar was archived from 16 April to 30 August 2000. A precipitation map in a 10 km grid generated from radar rain status (i.e. category) data on April 28, 2008 is shown in Figure 4.4.

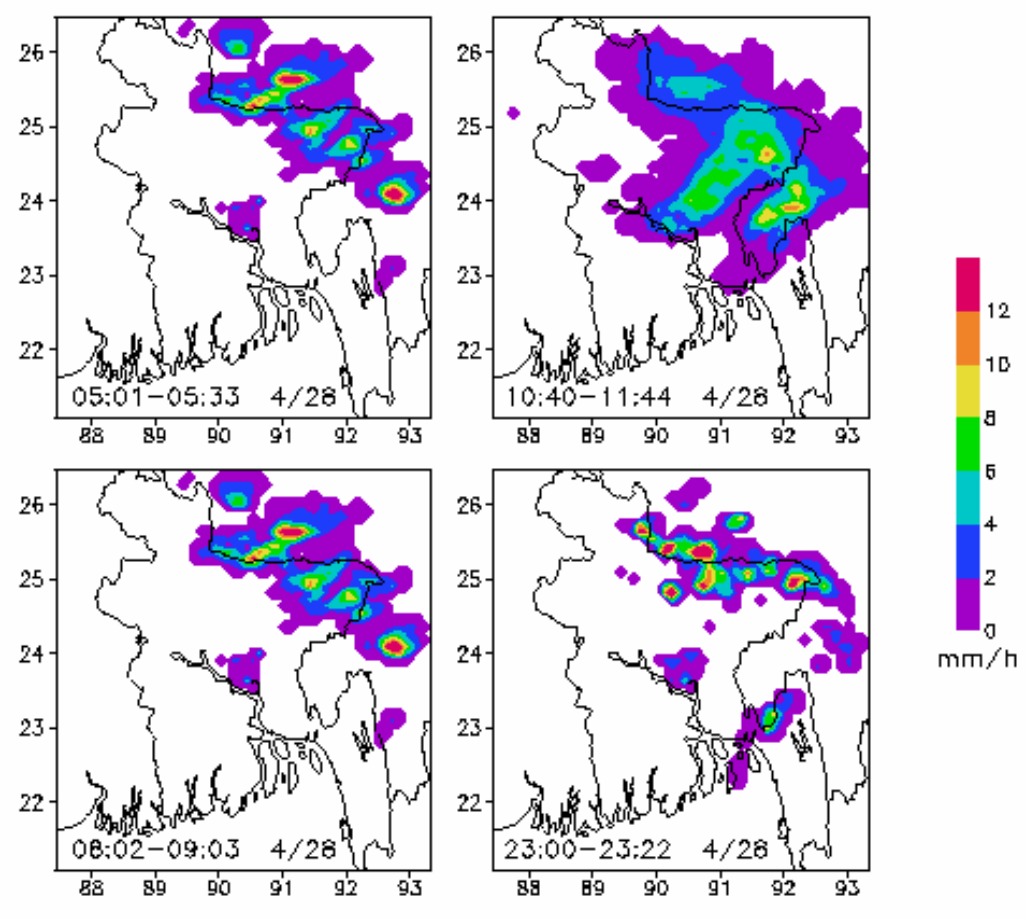

Figure 4.4. Radar Rain in 28 April 2000, Rain rate (mm/hr) in a 10 km Grid

4.3.2 Satellite Data

The satellite data were collected from Global Hydrological Research Centre (GHRC), NASA and DAAC, NASA for 1998-2004. The collected data is mainly covered the Ganges, Brahmanputra, Meghna (GBM) region and Southern part of USA. The TRMM satellite data consist of ascending and descending both passes over GBM and US regions. The following satellite dataset in Table 4.2 are used in this research:

Table 4.2 List of Satellite Data used in this Study

Satellite Data Product	Parameters	Period
TRMM TMI 1B11	Multifrequency and polarization brightness temperature	2000-2003
TRMM TMI 2A12	TMI Rain Product, Precipitation Water, Hydrometeor Profile.	2000-2003
TRMM PR 2A23 and 2A25	Attenuated Reflectivity Profiles, Path-integrated Attenuation (PIA), Rainfall-Rate Profiles, Bright Band, Bright Band Height and Rain Classification.	2000-2003
TRMM 3B42 V5 and V6, 3B42RT	TRMM and other Satellites Rain Product (Daily and 3-hourly)	1998-2004
TRMM 3B43 V5 & V6	3B42 and Rain Gauges Product	1998-2004
GMS-5 IR	1/2 – hourly Cloud Temperature Data	April 2000 – Sept. 2000

4.3.3 GIS and Hydrometeorological Data

- Hydro-meteorological data are available for Bangladesh (Appendix A)
- GIS coverages for whole Bangladesh are available (Appendix A)
- Gauge rainfall data in Bangladesh from 1998 to 2004 are available in different intervals: 5 min, 30 min, hourly, 3-hourly, and daily etc. (Appendix B).
- Rainfall data from Mesonet site (Oklahoma) in USA for 2000-2002 in 5-min intervals.

4.4 Satellite Sensors and Products Description

4.4.1 Geostationary Meteorological Satellite (GMS-5)

The Japanese Geostationary Meteorological Satellite (GMS-5) hourly equivalent black body temperature (T_{BB}) data of infrared channel 1 (IR1) are utilized for the domain of 10°-30°N and 80°-100°E. To quantify the frequency of occurrence and cloud embedded area (coverage of cloudy pixels having 10 km mesh size in an image) from satellite data, objective analysis is performed on T_{BB} data of GMS-5 in two domains each having coverage of 600 km × 600 km: one is over Bangladesh (land) and the other is over the north of the Bay of Bengal (ocean). The

GMS-5 data are sampled for 0.1°×0.1° mesh from April to September 2000, the year in which radar data are available.

To obtain monthly mean values about 720 GMS IR images are used in averaging. Depending on the interest of findings, there is a range of temperature thresholds used by many researchers (Spencer *et al.*, 1989; Goldenberg *et al.*, 1990; Mapes and Houze, 1993; Machado *et al.*, 1998; Islam *et al.*, 1998; Negri and Adler, 1987). Besides, the frequency of occurrence for the large domain is obtained from GMS-5 data using threshold temperatures <263K and <220K. The threshold <263K of T_{BB} is used to get information about low-level clouds while the threshold <220K of T_{BB} is used to obtain information about upper-level convection.

4.4.2 TRMM Sensors and Products

The TRMM satellite was launched in November 1997 (Kummerow *et al.*, 1998), it is designed to make measurements in the tropics and sub-tropics (35 deg N – 35 deg S), but since the orbit has been increased to 403 km altitude in August 2001 the swaths of TRMM Microwave Imager (TMI) now cover the southern Mediterranean Sea up to 39° N. The PR is the first space-borne rain radar (13.8 GHz), sensitivity is under 0.7 mm /hr (Kummerow, 1998) and the only instrument on TRMM platform directly providing vertical distribution of rain profiles, which has an attenuated frequency 13.8 GHz (2.2 cm wavelength) with horizontal polarization, swath width 220 km, 4.3 km spatial resolution at near-nadir and 250 m vertical resolution. A normal sensitivity threshold of about 17 dBz, has been demonstrated by the NASDA of Japan to be consistent stability within 0.8 dB. It has also TMI radiometer similar to the SSM/I, except that it has two additional spectral channels (vertical and horizontal polarization) at 10.7 GHz. The TMI improves upon the SSM/I heritage with the addition of a polarized 10.7 GHz channel, and improved spatial resolution by a factor of about 2.5 (Kummerow *et al.*, 1998). TRMM samples the tropics in a non-sun synchronous, low inclination orbit and the local sampling time progresses throughout the month.

The horizontal polarization is preferred because of the surface emissivity effect, which gives it a larger dynamic range over land and ocean compared to the vertical polarization data. Furthermore, because of the lower altitude of the TRMM satellite, the spatial resolution of the TMI radiometer is about two times finer than SSM/I and it offers an opportunity to discriminate

convective rain from stratiform rain. The TRMM PR will be especially helpful in resolving the shallow orographic rain that is different to detect with passive microwave technique.

TRMM Microwave Imager

The TMI (of DMSP SSM/I heritage) is a multichannel passive microwave radiometer operating at five frequencies: 10.65, 19.35, 37.0, and 85.5 GHz at dual polarization and 22.235 GHz at single polarization. The TMI provides information on the integrated column precipitation content, cloud liquid water, cloud ice, rain intensity, and rainfall types (e.g., stratiform or convective).

Summary of Features of the TMI instrument:

- ☒ uses a scan angle of 65 degrees
- ☒ collects data over a swath width of 760 km.
- ☒ can perceive rain through clouds
- ☒ makes quantitative measurement of rain intensity (mm/h) as integrated column precipitation content and areal distribution

TRMM Microwave Imager – 2A12

The TRMM 2A12 hydrometeor profile provides the level 2 data product for the TMI. The profiling techniques of the algorithm use the Goddard Cumulus Ensemble Model, and generate vertical hydrometeor profiles on a pixel by pixel basis. For each pixel, cloud liquid water, precipitation water, cloud ice water, precipitation ice, and latent heating are given at 14 vertical layers based upon the nine channels of the TRMM microwave imager (TMI). The top of each layer is given at 0.5, 1.0, 1.5, 2.0, 2.5, 3.0, 3.5, 4.0, 5.0, 6.0, 8.0, 10.0, 14.0, and 18.0 km above the surface. The surface rainfall and the associated confidence indicator are also calculated. Each data granule is one orbit plus 50 scan lines of pre-orbit overlap and 50 scan lines of post-orbit overlap. Each data granule consists of two parts: metadata and swath data.

Precipitation Radar (PR)

The PR, the first of its kind in space, is electronically scanning radar, operating at 13.8 GHz that measures the 3-D rainfall distribution over both land and ocean, and define the layer depth of the precipitation. There are three levels of 2A products for PR, 2A-21 – surface cross section, 2A-23 – PR qualitative and 2A-25 – PR profile. 2A-23 produces a Rain/No-rain flag. If rain is present, this algorithm will detect the bright band, determine the heights of the bright band and the storm, and classify rain types. 2A-25 produces an estimate of vertical rainfall rate profile for each radar beam. The rainfall rate estimate is given at each resolution cell of the PR radar. To compare with ground-based radar data, the attenuation corrected Z profiles is also given. Other output data include rain rate at different altitude, near surface rain, maximum Z (i.e. reflectivity) and parameters of Z-R relationship.

One of its most important features will be its ability to provide vertical profiles of the rain and snow from the surface up to a height of about 20 kilometers. The Precipitation Radar will be able to detect fairly light rain rates down to about 0.7 mm/hr. The Precipitation Radar is able to separate out rain echoes for vertical sample sizes of about 250 meters when looking straight down.

The PR will determine the vertical distribution of precipitation by measuring the "radar reflectivity" of the cloud systems and the weakening of a signal as it passes through the precipitation. Thus, it will measure the 3-D rainfall distribution over both land and ocean. More specifically, this instrument will define the layer depth of the precipitation and provide information about the rainfall reaching the surface, the key to determining the latent heat input to the atmosphere.

Summary of Features of the PR sensor:

- ☒ can perceive rain through clouds
- ☒ makes quantitative measurements of rain (mm/h) over land and ocean with a sensitivity better than 0.5 mm/h
- ☒ measures rain from the ground to an altitude of 20 km, with a vertical ("range") resolution of 250 m.
- ☒ provides 3-dimensional rainfall distribution

Table 4.3 TRMM Instrument Characteristics

	Visible Infrared Scanner	TRMM Microwave Imager (TMI)	Precipitation Radar (PR)
Frequency/ Wavelength	0.63, 1.6, 3.75, 10.8, 12 um	10.65, 19.35, 37.0, 85.5 GHz dual polarization, 22.35 GHz vertical polarization	13.8 GHz horizontal polarization
Scanning Mode	Cross track	Conical	Cross track
Ground Resolution	2.1 km	Ranges from 5 km at 85.5 GHz to 45 km at 10.65 GHz	4.3 km at nadir
Swath Width	720 km	760 km	220 km
Temporal Resolution		Max. two passes/day – ascending and descending	Max. two passes/day

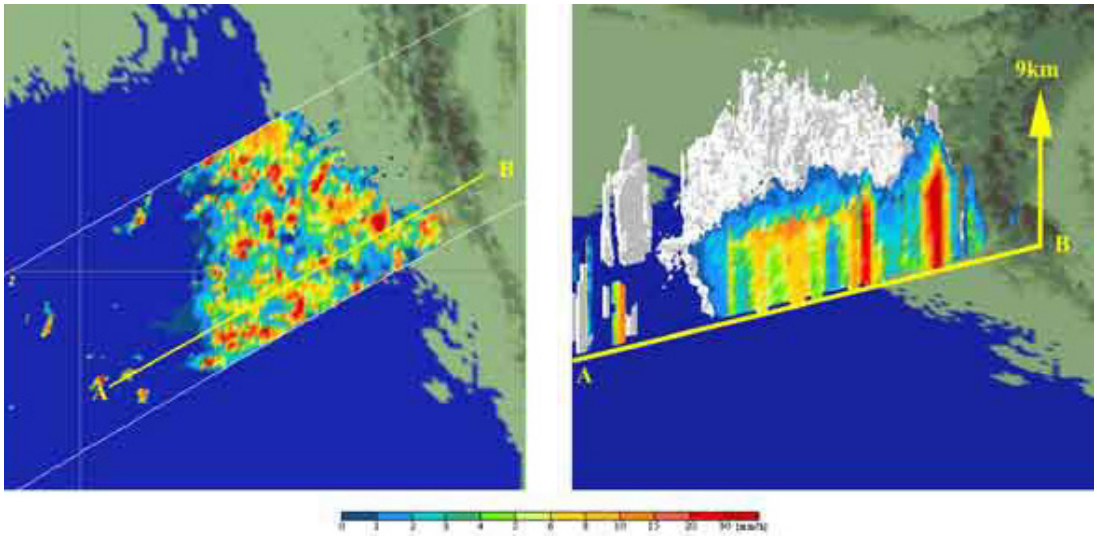

Horizontal X-Section of Rain at 2 km Height **3 D Rain Structure at A-B**

Figure 4.5. Sample TRMM PR Rain over Bangladesh on August 29, 2002 1:29-1:32 (UTC)

Source : www.trmm.nasa.gsfc.gov

4.4.3 Global IR Data and TRMM Calibrated Data Products

The primary source of IR data is the international constellation of geosynchronous-orbit meteorological satellites - the Geosynchronous Operational Environmental Satellites (GOES, United States), the Geosynchronous Meteorological Satellite (GMS, Japan), and the Meteorological Satellite (Meteosat, European Community). There are usually two GOES platforms active, GOES-EAST and -WEST, which cover the eastern and western United States, respectively. Gaps in geosynchronous coverage (most notably over the Indian Ocean prior to June 1998) must be filled with IR data from the NOAA-series polar- orbiting meteorological satellites. TRMM-based precipitation estimates are provided on a global 0.25°x0.25° grid over the latitude band 50°N-S within about six hours of observation time. Three products are being provided: A TRMM-calibrated merger of all available TMI and SSM/I precipitation estimates (three-hourly accumulations); a geosynchronous infrared estimate which is calibrated by the merged-microwave data (hourly estimates); and a combination of the first two fields (three-hourly accumulations).

3B40RT (High Quality, or HQ): A merger of all available SSM/I and TMI microwave precipitation estimates into a "high-quality" (HQ) precipitation estimate. The SSM/I estimates are computed with the GPROF 5.0-SSMI algorithm and the TMI estimates are computed with the GPROF 5.0-TMI algorithm (the real-time TRMM 2A12 product). Before merger the SSM/I are calibrated to the TMI using separate global land and ocean matched histograms**.**

3B41RT (Variable Rain Rate Infrared, or VAR): Precipitation estimates from geostationary infrared (IR) observations using spatially and temporally varying calibration by the HQ. The algorithm is a probability-matched threshold approach that ensures that the histogram of gridbox-average IR precipitation rates matches the histogram of gridbox-average HQ precipitation rates locally. We refer to this as the variable-rain rate (VAR) infrared algorithm. Source: Web and Huffman G. J., 2003.

3B42RT (Merger of HQ and VAR): A merger of 3B40RT (HQ) and 3B41RT (VAR). The current scheme is simple replacement - for each gridbox the HQ value is used if available, and otherwise the VAR value is used. Adler *et al.* (2000) used a combination of TRMM and geosynchronous Infrared IR (geo-IR) data to provide 3-hourly estimates of precipitation over 50°N-50°S using an

approach based on TRMM post-real-time multi-satellite algorithm 3B42. The combined instrument rain calibration algorithm (3B-42) uses an optimal combination of 2B-31, 2A-12, SSM/I, AMSR and AMSU precipitation estimates (referred to as HQ), to adjust IR estimates from geostationary IR observations. Near-global estimates are made by calibrating the IR brightness temperatures to the HQ estimates. The 3B-42 estimates are scaled to match the monthly rain gauge analysis used in 3B-43. The output is rainfall for 0.25x0.25 degree grid boxes every 3 hours. Source: TSDIS-P907, Vol. 4; Release 4.07, May 1999 and Huffman *et al.*, 2007.

3B43RT: It provides a "best" precipitation estimate in the TRMM region from all global data sources, namely TRMM, IR, SSM/I microwave, and rain gauges. The 3b43 dataset merges the daily 3b42 dataset with the GPCC rain gauge analysis. The resulting 3B43 rain rates are monthly averages gridded over 0.25x0.25 degree lat/lon boxes. The 3B43 retrieval algorithm used for this product is based on the technique by Huffman *et al.* [1995, 1997] and Huffman [1997]. Source: TSDIS-P907, Vol. 4; Release 4.07, May 1999 and Huffman *et al.*, 2007.

Both 3B42RT and 3B42 were upgraded to include AMSR-E and AMSU-B precipitation estimates in late 2004. The new version of 3B4XRT began operational use in February 2005, and current data processing for Version 6 3B42/43 began in July 2005. The entire available archive of AMSR-E and AMSU-B estimates is incorporated in the Version 6 3B42.

3B42 Product: The combined instrument rain calibration algorithm (3B-42) uses an optimal combination of 2B-31, 2A-12, SSMI, AMSR, and AMSU precipitation estimates (referred to as HQ), to adjust IR estimates from geostationary IR observations. Near-global estimates are made by calibrating the IR brightness temperatures to the HQ estimates. The 3B-42 estimates are scaled to match the monthly rain gauge analysis used in 3B-43. The output is rainfall for 0.25x0.25 degree grid boxes every 3 hours.

3B43 Product: The 3B43 dataset merges the daily 3B42 dataset with the GPCC rain gauge analysis. The resulting 3B43 rain rates are monthly averages gridded over 0.25x0.25 degree lat/lon boxes. The 3B43 retrieval algorithm used for this product is based on the technique by Haffman *et al.* [1995, 1997] and Haffman [1997].

CHAPTER 5

5. METHODOLOGY

5.1 Introduction

Although three seasons in Bangladesh in terms of climate conditions are described in Section 4.2 but in our analysis, March-April-May, June-July-August-September and October-November are considered as pre-monsoon, monsoon and post-monsoon seasons in Bangladesh respectively. The month of April, July and October are selected for detail analysis as the peak month of pre-monsoon, monsoon and post-monsoon periods, respectively from each year.

Radar rainfall in Bangladesh is analyzed based on short period of radar rain-status and gauge rainfall. The rain status has been converted into rain-rate and the methodology has been described in sub-section 5.2. Performance of radar data and TRMM rain products are evaluated using gauge rainfall. Study of diurnal cycle of rainfall is examined using GMS-5, Radar and TRMM rain products. A statistical approach has been investigated in order to improve Gr. Radar rainfall in Bangladesh. TMI data has been calibrated using space-borne radar rain product and validated using TMI rain profile as well as gauge rainfall in Bangladesh. Detailed research steps along with the data used for each objective are outlined to the following subsections.

5.2 Characteristics of Rainfall System over Bangladesh using Radar and Gauge Data (Objective # 1)

Radar PPI (Plain Position Indicator) scans and 3-hourly rainfall data from the BMD rain-gauges throughout the country were used. Radar data (pixel size 2.5km x 2.5km) are available for the analysis of the period April 16 to August 30, 2000. The BMD radar collects reflectivity (dBZ) data and automatically converts it to the precipitation rate (mm/h) and stores data in six statuses; 1 (1-4 mm/h), 2 (5-16 mm/h), 3 (17-32 mm/h), 4 (33-64 mm/h), 5 (65-128 mm/h), and 6 (>128 mm/h). A procedure is employed to retrieve rain rate from rain status as depicted in Figure 5.1. Figure 5.1 is the sample of 5 × 5 pixels in a PPI scan of BMD radar data. Actually the

radar data coverage is divided in 60 × 60 grid boxes, each box contains 16 pixels, each pixel having 2.5 km resolutions. So, one grid box is 10 km length along abscissa or ordinate that contains 4 × 4 = 16 pixels. Each pixel is the candidate of different status and knowing the status relative to rain rate and pixel area, the rain rate is retrieved for each 10 km grid boxes.

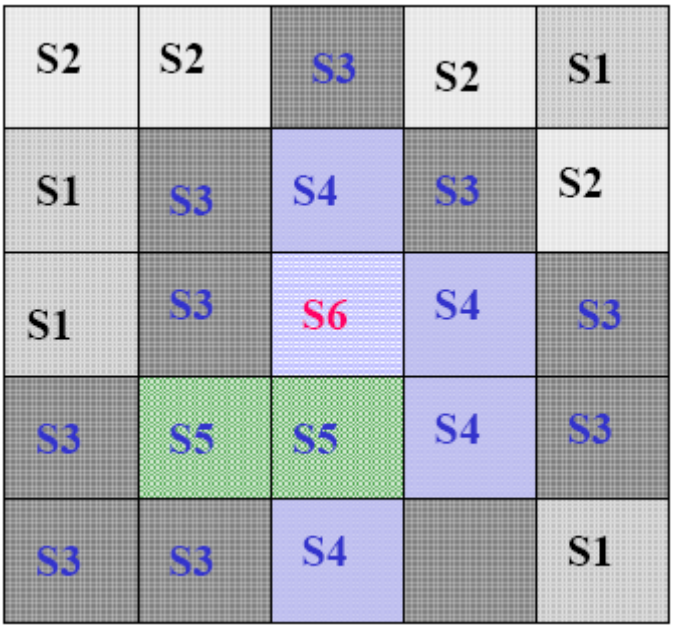

Figure 5.1. Schematic diagram for the radar analysis. Different pixels show different status identity each pixel is 2.5 km by 2.5 km in size

Rain rates are retrieved from rain statuses as discussed here. This retrieval result is used to estimate real-time rainfall (Anagnostou and Karajewski, 1999). The space-time averaged rain rate is estimated as follows. The instantaneous rain rate R_I is defined as

$$R_I = (1/A_R)\sum_{r=1}^{r=6} S_r A_{R,r} \tag{5.1}$$

where r is the rain status, S_r is possible rain-rate corresponding to each status and A_R is the rainy area of each rain status in a 10 km grid box. In this analysis, we use S_r values as 2.5, 10.5, 24.5, 48.5, 96.5, and 129 mm/h for r =*1, 2, 3, 4, 5*, and *6,* respectively.

The spell rain rate R_S is defined as

$$R_S = (1/N)\sum_{I=1}^{I=N} R_I \tag{5.2}$$

where R_I is the instantaneous rain rate in a 10 km grid box calculated from equation 5.1 and N is the total number of PPI scans during the spell duration. The precipitation system in R_I comprises a single continuous rain area in which relatively intense precipitation cores are interconnected with higher precipitation area. Spell rain contains lower rain rate than instantaneous rain.

The hourly rain rate R_H is defined as

$$R_H = (1/N)\sum_{t=1}^{t=N} R_t \tag{5.3}$$

where N is the total number of scans in an hour and R_t is the instantaneous rain rate of a 10 km grid box per unit area instead of rainy area with

$$R_t = (1/A_G)\sum_{r=1}^{r=6} S_r A_{R,r} \tag{5.4}$$

where A_G is the grid area, which is 100 km^2 in this analysis. Daily rainfalls were then calculated from 6 are sampled in each PPI scan and employed all available PPI scans in an hour to obtain hourly value. Then hourly values are used to obtained daily and monthly values for different parameters. In radar analysis the echo embedded area (EEA) is the raining pixels coverage having rain rate >1 mm/h. The frequency of occurrence (FO) is the number of echoes or echo-systems determined from all employed PPI scans. The echo length, lifetime, propagation speed and direction of the echo systems are subjectively obtained using 2-3 min interval PPI scans data. The pattern matching technique (Islam *et al.*, 1997) is used to detect the clouds during their life time.

The precipitation areas observed over Bangladesh are categorized into solitary and merged types. Solitary type includes echoes, which are developed and disappeared individually, never merge to

maintain the system. On the other hand, merged type includes echoes, which are gathered by merging effect to maintain the system. Each precipitation type is again subcategorized into oval, line and arc types.

5.3 Performance Evaluation of Radar Rainfall Estimation over Bangladesh using Gauge Data (Objective # 2)

The data utilized in this work include the rainfall amount from the rain gauges, calculated radar rain rate from Section 5.2. For spatial comparison purpose, the hourly radar rain rates at each pixel and BMD 3-hourly gauge rainfall data at each station are summed into daily total. These have been done for the month of April, May, June, July and August (AMJJA) 2000. The daily average rain rate (mm/day) for each radar pixel and gauge data at each gauge station are calculated for AMJJA respectively. The daily average rainrate for 33 BMD rain gauges are interpolated in 10 km grid cell using ArcGIS Spatial Analyst software in order to create a surface. Finally, both surfaces are compared in terms of spatial distribution of rainfall over Bangladesh. Finally, relationships between rainfall calculated by radar and rain-gauge data in different months are established using regression analysis.

5.4 Performance Evaluation of TRMM Rain Retrieval over Bangladesh (Objective # 3)

In order to evaluate performance of TRMM rain product, firstly, TRMM 3B42 daily rainfall data are analyzed from pre-monsoon to monsoon periods for the years 1998-2002 in Bangladesh. Rain-gauge (RNG) 3-hourly rainfalls collected by BMD at 33 stations over Bangladesh are used for the same analysis. Zero mm rainfall within 3 hours is included in obtaining daily amount. Any (zero) amount of rainfall within 3-hours (24-hours) decided the day as rainy (rainless). Rainy day simultaneously detected by both TRMM and RNG is called matched day. Time sequences of daily rainfall (mm) for 5 years have been determined by both TRMM and averaged rainfall from rain gauges over the country.

Secondly, TRMM V5 3B42, V5 3B43, V6 3B42 and V6 3B43 data for 1998–2002 were also analyzed to obtain daily and monthly rainfall amounts in Bangladesh. Bangladesh ground-based rain-gauge (BG) data collected at 33 stations (Figure 4.2) by the Bangladesh Meteorological Department (BMD) are utilized for the calibration of TRMM products. The availability of

reliable 3-hourly BG data for the years 1998–2002 is considered to compare TRMM calculated rainfall with rain-gauge data. The daily data from TRMM V5 3B42 products estimated gridded rainfall of 1° × 1° resolution. Scattered plots of monthly and daily TRMM products are established in order to determine the correlation between rain gauge and 3B42 rainfalls.

The 2A25 data, with a nominal 4.3 km spatial resolution and 250 m vertical sampling from the surface to 20 km altitude (Kidd and McGregor, 2007), is used in this analysis. The period of PR data is different from 3B data and BG data, but the effect of different integration time is small. TRMM 2A25 data are analyzed in the domain of 87–94 °E and 18–28 °N to obtain the vertical variations of rain intensities and spatial distribution of location of maximum rain rates in different rainy periods from 2000 through 2003. The rain rates derived from the radar reflectivity of TRMM PR using the algorithms of TRMM science data and information system (TSDIS) are considered as rain intensities. Some good cases, 34 in April, 82 in July and 36 in October, which includes rain in and around Bangladesh, are manually selected from 2A25 overpass. The number of selected cases is few due to only a single overpass of the TRMM PR during a 24-h period. If there is a TRMM pass in the analysis domain with no considerable convection, the overpass is excluded from the analysis. Among the selected overpasses, the maximum rain rate and its position are extracted from each overpass. The maximum rain rate is defined as the most intense rate in an overpass. The 2A25 has 80 layers, each of which is 250 m thick. Using these layers, the vertical extension of the precipitation field up to 20 km from the surface is obtained along with the maximum precipitation area. The echo top is defined as the top of the vertical extension of the precipitation field for a specific threshold rain rate. In this analysis, echo tops for different rain thresholds 5, 10, 15, . . ., 50 and 60 mm/h are determined manually. First, the vertical extension of the precipitation field is created and determined by the echo top height for each specified threshold. The months of April, July and October are selected from each year for detailed analysis as the peak months of the pre-monsoon, monsoon and post-monsoon periods, respectively. Performance of a TRMM product is defined by the difference between the TRMM and BG values divided by the BG value, and is expressed in percentage.

5.5 Study of Diurnal Cycle and Seasonal Variations of Rainfall in and around Bangladesh (Objective # 4)

For better understanding the diurnal cycle in and around Bangladesh, the detail of the diurnal variation are examined using high temporal (hourly) and spatial (0.1°) resolutions GMS-5 data, PPI scans of radar data, and TRMM rain products. Daily rainfall (mm/d) determined by TRMM-3B42RT averaged for 1st June to 31st September from 2002 to 2004 at 06 LST and 18 LST. Daily rainfalls from 2002 to 2004 for 33 BMD rain gauges (Figure 4.2) are averaged to determine inter-seasonal variations of rainfall over Bangladesh.

Hourly equivalent Black Body Temperature (T_{BB}) data of GMS-5 IR Channel 1 (IR1) are processed for the 10 km mesh in a domain of 80-100ºE, 10-30ºN from April to September 2000 in order to see the large-scale cloud activity and to compare with the radar observations. The frequency of occurrence (FO) of cloud calculated from GMS-5 hourly T_{BB} data. The cloud embedded area (CEA) calculated using the same data set over the land and the ocean. Spectral analysis is performed on the hourly T_{BB} data to obtain the cloud activity in the analysis region. T_{BB} data are averaged in a 1°×1° grid from 100 pixels with a size of 0.1° mesh. The cloud area is defined as area where T_{BB} is below the threshold temperature of 263K. The regions above the threshold temperature are defined as clear sky. The time of maximum activity is obtained when the minimum T_{BB} area becomes the largest.

To observe the precipitation types related to cloud activity developed there, radar data available for the year 2000 are also utilized in this study. Available radar data to analyze are from 16 April to 30 August 2000. Radar data are sampled in each PPI scan and employed all available PPI scans in an hour to obtain hourly value. Then hourly values are used to obtain daily and monthly values for different parameters. In radar analysis the Echo Embedded Area (EEA) is the raining pixels coverage having rain rate >1 mm/h. The Frequency of Occurrence (FO) is the number of echoes or echo-systems determined from all employed PPI scans. The echo length, lifetime, propagation speed and direction of the echo systems are subjectively obtained using 2-3 minutes interval PPI scans data. The pattern matching technique (Islam *et al.*, 1997) is used to detect the clouds during their lifetime. In this analysis cases are tried to take when continuous PPI scans are available.

However, when radar data are missing for continuous 2 hours, GMS-5 data are used as supporting document to detect the system in next available PPI scan.

5.6 Develop a Statistical Procedure to Determine Ground Based Radar Rain Algorithm Parameter Estimation in Bangladesh (Objective # 5)

5.6.1 Introduction

Obtaining the actual precipitation distribution over Bangladesh and making BMD radar useful is a challenging task. At present, there is no reliable way to retrieve precipitation from the Bangladesh Meteorological Department (BMD) radar data. There are two problems in using BMD radar data. One is that the data provide only a six-range rain status, the other is that a lack of precise Z (Reflectivity) - R (Rain rate) relationship for this region. In this work, attempts have been made to obtain the precipitation rate from the BMD radar data.

The dataset used in this study consists of PPI scans from Dhaka radar station and rain gauge rainfall measurements over Bangladesh. The relative location of ground radar with respect to the rain gauges is shown in Figure 4.3. The rain gauge network is virtually divided into three clusters with 100 km, 150 km and 250 km radius circles formed at Dhaka radar (Figure 4.3). The ranges among the different clusters make their rain measurements spatially independent at scales less than one hour. Hourly rainfall (mm/hr) accumulation from tipping buckets type rain measurement is used in this analysis and radar bias adjustment using Kalman filter technique.

The standard Z-R relationship ($Z=200R^{1.6}$) is used in order to convert rain rate into its reflectivity. Marshall *et al.*, 1948 developed this standard Z-R relationship for stratiform rain, where a general Z-R relationship was $Z=300R^{1.4}$. Fullon *et al.*, 1998 also developed another Z-R relationship ($Z=250R^{1.2}$) for tropical rainfall estimation. Reflectivity data is used to estimate radar rain algorithm parameter values using equation 5.8.

The parameters in the Z-R relationship have been considered stochastic. As a result, 4000 parameter sets have been produced using Monte Carlo simulation from uniform distribution. Using these parameters, rainfall has been estimated. The efficiency of each parameter set in estimating rainfall has been evaluated using the following relation ship.

$$Eff = 1 - \frac{Variance\,of\ Error}{Variance\,of\ Ra\inf all} \tag{5.5}$$

An efficiency threshold of 0.5 has been chosen. Above this threshold the parameter sets are assumed to perform better in estimating rainfall. According to these criteria 1944 parameter sets have been selected. For each of these parameter sets rainfall estimation has been done for the three clusters discussed above. An arithmetic average of the rain gauge estimated rainfalls (RG) have been computed for each cluster and comparison has been done with the estimated radar rainfall (RR) in order to determine the biasness of the estimated radar rainfall compared to the gauge rainfall.

5.6.2 Conversion of Reflectivity to Rainfall Rate

The reflectivity value of each radar cell, which exceeds a specified minimum reflectivity threshold (Z_{min}), is converted to rainfall rate through the following non-linear relationship:

$$R_p(s,t,\theta,r) = B_{cls} \cdot \left[\frac{Z_c(s,t,\theta,r)}{A}\right]^{1/B} \quad , \text{ for } Z_c > Z_{min} \tag{5.6}$$

Where Z_c and R_p are the corresponding integrated reflectivity (mm^6m^{-3}) and rainfall (mmh^{-1}) values at hour *s*, scan *t*, radar cell azimuth θ and range r (in km); A and B are the parameters of the Z-R relationship, presented in the conventional form (i.e., $Z=AR^B$); Z_{min} is the minimum reflectivity value to be converted to rainfall; B_{cls} is the parameter that differentiates the convective and stratiform multipliers of the Z-R relationship:

$$B_{cls} = \begin{cases} bc & for\ convective\ rain \\ 1 & for\ stratiform\ rain \end{cases} \tag{5.7}$$

The values of Z-R (A and B) and classification (bc) parameters are applied globally to the whole dataset. Estimation of these parameter values is described in the next section.

5.6.3 Errors Adjustments in Radar Rain Estimation

The Dhaka radar collects PPI scan data with azimuth zero. Therefore, the rain-path attenuation is not part of the radar rainfall estimation algorithm.

a. Bias Calculation

Operational radar rainfall estimates rarely match the amounts recorded by rain gauges [Battan, 1973; Wilson and Brades, 1979; Austin, 1987; Joss and Waldvogel, 1990; Smith *et al.*, 1996a, b; Baeck and Smith, 1998; Fulton *et al.* 1998; Johnson *et al.*,1999]. For many practical purposes therefore the radar rainfall estimates are adjusted using the information provided by rain gauges. This may be accomplished in various ways, the simplest being a removal of the average difference (i.e. bias) between the radar and estimates at rain gauge locations and the corresponding gauge rainfall amounts [e.g. Steiner and Houze, 1997]. That is, the bias–adjusted radar rainfall estimates are obtained by using a power law relationship between $Z(mm^6/m^3)$ and R(mm/h) of the form

$$Z = \overline{A}R^b = AB^{-b}R^b \tag{5.8}$$

where $\overline{A}$ is the adjusted multiplicative factor (A is the initial choice), B is the bias defined by:

$$B = \frac{\frac{1}{n}\sum_{i=1}^{n} Gi}{\frac{1}{n}\sum_{i=1}^{n} Ri} \tag{5.9}$$

and Gi and Ri are the gauge accumulated and radar accumulated storm rainfall totals, respectively, at gauge location i,. A and b are positive empirical constants. Typical values of the multiplicative factor A may range from a few tens to several hundreds [Battan, 1973], while the power factor b is limited to $1 \le b \le 3$ [Smith and Krajewski, 1993], with typical values ranging between b=1.2 and b=1.8 [Battan, 1973; Ulbrich, 1983].

b. Mean-field Systematic Error (Bias) Adjustment

The mean-field systematic error (bias) adjustment is applied to the rainfall estimates to account for some variations in the Z-R relationship. This approach has been followed by many studies in the past and is becoming a practice even in real-time radar rainfall algorithm operations (e.g., Fulton *et al.*, 1998; Anagnostou and Krajewski, 1999). The estimation of mean-field systematic error (B_s) is done at the hourly time scale based on corresponding radar and rain gauge rainfall accumulations. Due to the large difference in the sampling geometry of radar and rain gauges and the high rainfall variability, determination of Bs through direct radar-gauge comparisons can be quite noisy even at scales larger than hour (Kitchen and Blackall, 1992; Anagnostou *et al.*, 1998).

In this study a stochastic filtering approach was devised based on the Kalman filter technique (Gelb, 1974), where prior mean-field bias information and radar-gauge bias evaluation from the most recent hour are combined statistically accounting for bias propagation variability and sampling error (Smith and Krajewski, 1991). The bias propagation equation is defined as in Anagnostou and Krajewski (1999):

$$\beta_s = \beta_{s-1} + W_s \tag{5.10}$$

Where β_s is the natural logarithm ($\log_e$) of Bs, and Ws~N (0, Q) is the propagation model error that is normally distributed with zero mean and variance Q. This model error represents variability in the mean-field bias, which is mainly due to variations in the drop size distribution and beam power fluctuations. The predicted bias is linked to data based on bias calculations (Ys) through the observation equation:

$$Y_s = \beta_s + M_s \tag{5.11}$$

Where the observation error is defined as a normally distributed variable, N ($0,R_M$), with zero mean and variance R_M. The observed bias was calculated at every hour s as:

$$Y_s = \log_e \left[\frac{\sum_{j=1}^{N} R_g(s, u_j)}{\sum_{j=1}^{N} A_c(s, u_j)} \right] \quad (5.12)$$

where R_g and A_c are the rain gauge and radar estimated rainfall accumulations at hour s and Cartesian grid locations, u_j, with available gauges. The bias estimation parameter values are adjusted recursively based on a procedure first presented by Mehra (1972). A data based study by Anagnostou *et al.* (1998) has shown that this approach can obtain optimal estimates for Q and R_M. The $\log_e$-bias (β_s) statistics can be related to the multiplicative mean-field bias factor (B_s) statistics as:

$$\overline{B}_s = \exp\left\{\hat{\beta}_s + 0.5V_s\right\} \quad (5.13)$$

$$\Sigma_{B_s} = \overline{B}_s\left(\exp V_s - 1\right) \quad (5.14)$$

where $\hat{\beta}_s$ and Vs. are the mean and variance of β_s determined by the Kalman filter equations (Gelb, 1974), and $\overline{B}_s$, Σ_{B_s} are the mean and variance of B_s; The value of Σ_{B_s} can be used for determining confidence intervals for the estimated radar rainfall fields (Anagnostou *et al.*, 1999).

c. Bias Adjustment using Kalman Filter

Due to lack of knowledge of the time varying behaviour of the mean field radar rainfall bias, the quantity β_t is assumed to follow an Autoregressive order one (AR1) process (Smith and Krajewski 1991):

$$\beta_t = \rho_\beta \times \beta_{t-1} + W_t\,;\; W_t \sim N(0, \sigma_W^2) \quad (5.15)$$

where ρ_β is the lag-one correlation coefficient of the mean field bias, and *Wt* is a independent normally distributed random variable with mean zero and variance σ^2_w. A stationary process variance, σ^2_w, is set to have the following form:

$$\sigma^2_w = (1-\rho^2_\beta) \times \sigma^2_\beta \quad (5.16)$$

where σ^2_β is a stationary variance of the logarithmic bias process. The errors associated with the observed rainfield lead to a deviation between the observed and true values for β_t. This is represented as:

$$Y_t = \beta_t + M_t;\ M_t \sim N(0, \sigma^2_M) \tag{5.17}$$

where *Yt* is the observed mean field bias and *Mt* is an independent normally distributed random variable with mean zero and variance σ^2_M that represents the observation error. While σ^2_{Mt} represents the time varying variance of the $(Yt - \beta_t)$ process, it can be specified as $\sigma^2_{Mi,t}$ for rain gauge *i* at time *t.* Assuming spatial independence in the observation errors (Ripley 1981), the time varying variance σ^2_{Mt} can be estimated as:

$$\begin{aligned}\sigma^2_{M_t} &= \sigma^2_{\tilde{\beta}_t} - \sigma^2_{\beta} \\ &= \frac{1}{n}\sum_{i=1}^{n} \sigma^2_{\tilde{\beta}_{i,t}} - \sigma^2_{\beta}\end{aligned} \tag{5.18}$$

where $\sigma^2_{B,t}$ is the variance of the measured $\log_{10}$(G/R), estimated as the average across all rain gauge locations for hour *t, n* is the total number of rain gauge available for that hour. The variance of the measurement noise is represented as the difference between the variance of the measured β (denoted β ~ in above equation) and the stationary variance of the logarithmic bias process, σ^2_β. Chumchean *et al.* (2003a) proposed a model for estimating the variance of the measured β, for the case where storm classification has been performed. This is expressed as:

$$\sigma^2_{\tilde{\beta}_{i,t}} = -0.015 \times \overline{G_t} + 0.14\ ; \qquad \text{for } r_i \le 55 \text{ km} \tag{5.19}$$

$$\sigma^2_{\tilde{\beta}_{i,t}} = -0.015 \times \overline{G}_t + 0.13 \times \frac{(r_i - 55)}{P} + 0.14\ ; \quad \text{for } r_i > 55 \text{ km} \tag{5.20}$$

Where $\sigma^2_{Bi,t}$ is the variance of $\log_{10}$(G/R) at gauge *i* for hour *t*, *Gt* (mm) is the conditional mean of rain gauge rainfall at hour *t*, the mean being estimated based on all rainfall values that are greater than the rain gauge resolution, *ri* (km) is the observation range for the i^{th} rain gauge and *P*

is the number of pulses used in reflectivity measurement at each range bin [see Chumchean *et al.* (2003a) for details].

The observation error model used in this study depends on the following: (a) the number of observation rain gauges at that hour; (b) the location of the observation rain gauges; (c) the conditional mean of rain gauge rainfall; and (d) the number of pulses used for reflectivity measurements. This allows the observation error model to account for changes in the reliability of measured reflectivity due to increases in observation volume with range.

The recursive equations for the operation of the Kalman filter are illustrated in Figure 5.2. At time t = 0, β_0 and P_0 are assumed to equal their expected values which are respectively the climatological mean field bias (0) and the stationary process variance, σ^2_w . In the case that no rain gauge observations available for any hour, the σ^2_β was used as a default for the variance of the logarithmic bias process. The Kalman filter updates the estimate for the process variance at each time step based on the newly observed values of β. This time varying variance is denoted as P_t in the remainder of this paper. It should be noted that σ^2_w represents the stationary variance of β, whereas P_t is an update of this variance based on the projected value of β using the Kalman filtering methodology.

To obtain optimality in the Kalman filter, the innovation ($Yt - \beta^- t$) sequence should be white noise (Anagnostou *et al.* 1998). In this study, it is assumed that the innovation is white noise and exhibits time invariance when the lag-one correlation coefficient of the innovation sequence is less than 0.05. From Figure 5.2, only two variables are unknown, these being the lag-one correlation coefficient of the process model ρ_β, and the variance of logarithm bias process, σ^2_β. Thus the simulations were repeated by varying these unknowns until the lag-one correlation of the innovation sequence was less than 0.05. Since the bias model is defined in terms of the log bias process βt, state estimators for *Bt* were consequently derived in terms of state estimators for βt. Equation 5.15 was used to convert the estimated βt into *Bt* (Smith and Krajewski 1991):

$$B_t = 10^{[\beta t + 0.5 P_t]} \qquad \text{Where, } P_t \text{ is the error variance of } B_t. \qquad (5.21)$$

State estimate are obtained on an hourly basis from an hourly basis from corresponding rain gauge and radar rainfall accumulations. Bias estimations and 1-h-ahead predictions are based on Kalman filter equations, which optimally combine observations and model estimates, taking into account uncertainties associated with both measurements.

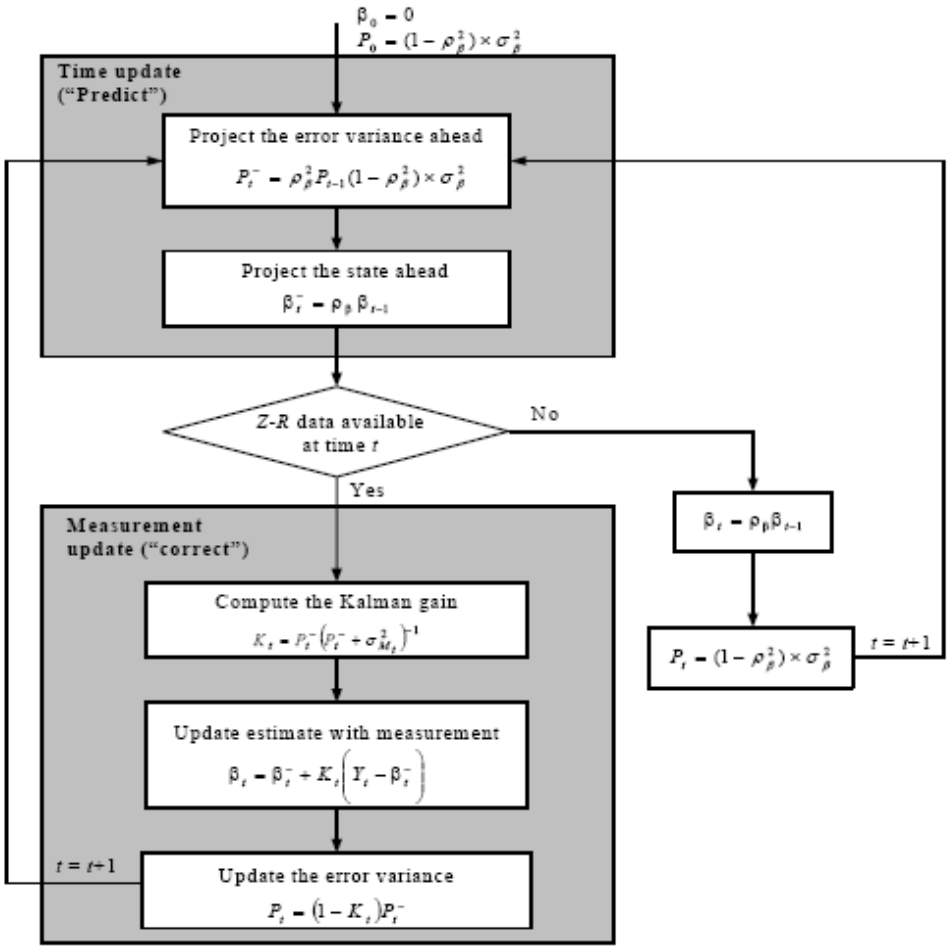

Figure 5.2. Flowchart of Operation of Kalman Filter

Figure 5.2 shows a flowchart of the operation of the Kalman Filter. (t represents hour, β^-_t is initially estimated mean field bias at time t, βt is the estimated mean field bias, Kt is the Kalman gain, Yt is the observed mean field bias, σ^2_{Mt} is the observation error variance. σ^2_β is the process error variance, P^-_t is the priori estimated error variance of the β^-_t, P_t is posteriori the estimated error variance of βt, and β ρ is the lag-one correlation coefficient of the process model. Note that ρ_β and σ^2_β are specified externally for the filter to operate.

d. Root Mean Square Error (rms) Adjustment

The algorithm has **six parameters**: Z_{min}, A, B, bc, Q, and R_M, that control its different processing components. The Q and R_M are determined recursively as discussed above. Parameter A is assigned an arbitrary constant (i.e., 200) since its value is adjusted every hour through the mean-field bias coefficient, while parameters Q and R_M were estimated as part of the stochastic filtering/updating approach described in a previous section. Consequently, implementation of the above algorithm in radar data required evaluation of three free parameter values, namely Z_{min}, B and bc. The parameter estimation is formulated as an optimization problem with cost function defined as the **root-mean-square** (rms) difference of radar and rain gauge hourly accumulations:

$$\mathrm{rms} = \left(\frac{1}{N_s N_g} \sum_{s=1}^{N_s} \sum_{j=1}^{N_g} \left[R_g(s,j) - R_c(s,j) \right]^2 \right)^{0.5} \tag{5.22}$$

Where all variables have been defined above. This approach has been proven quite successsful in past radar rainfall algorithm calibration studies (Ciach *et al.*, 1997; Anagnostou and Krajewski, 1998; and Anagnostou and Krajewski, 1999). Due to the high zero intermittence of rainfall at the hourly scale (Seed and Austin 1990; Crane 1990) point rain gauge measurements cannot represent accurately very low pixel averaged rainfall intensity. Consequently, only gauge-radar pairs conditional to gauge rainfall greater than 0.1 mm/h were considered in the rms calculations. The above process has been repeated for each parameter sets. Periods of non-zero gauge rainfalls have been selected so that we can get the radar estimates for the same period of non-zero rain from rain gauge.

The similarity between the gauge observations has been investigated with respect to the **relative distance** between the rain gauges stations.

$$r = \frac{\sum(\log(Ri) - \log(\bar{R})) * (\log(R_j) - \log(\bar{R})) - \frac{\sum(\log(R_i) - \log(\bar{R})) * \sum(\log(R_j) - \log(\bar{R}))}{N}}{\sqrt{(\sum(\log(R_i) - \log(\bar{R}))^2 - (1/N)(\sum(\log(R_i) - \log(\bar{R})))^2)(\sum(\log(R_j) - \log(\bar{R}))^2 - (1/N)(\sum \log(R_j) - \log(\bar{R})))^2)}} \tag{5.23}$$

A common way of assessing the accuracy of radar rainfall estimates is through comparison with observations from rain gauge networks. Although rain gauge observations are considered to accurately represent rainfall at a point, their accuracy in representing mean – areal rainfall of size of radar pixel is low (Ciach and Krajewsky 1999). Ciach and Krajewski (1999) show that in the Tropics, the contribution of the hourly area-point (AP) rms difference to the radar-to-rain gauge (RG) rms difference is over 50 % for hourly accumulations. Therefore, one can easily realize that RG rms difference is not an actual representation of the difference between radar and true mean-areal rainfall (RT). To retrieve the variance of the desired error variable RT, the variance of AP difference should be separated from the variance of the RG difference.

To make validation for the radar observation we need to have a true value for rainfall observation. However, as explained above, the gauge rainfall can't be a true representation of the rainfall over certain area (the limitations are discussed above). Therefore, an adjustment for the gauge observation was required. The rain gauge error is defined as:

$$Rt = Ri * \varepsilon i \tag{5.24}$$

Where Rt is the true gauge rainfall and Ri is observed rainfall rate at time i. The random variable εi(s, u) represents the multiplicative gauge rainfall error.

This skewness nature leads us to make lognormal transformation, which is resulted in probability distribution function (pdf) of a lognormal error rainfall, which is normally distributed with parameters expectation of error in the rainfall and that variance of the error:

$$f(x;\theta,w) = \begin{cases} \dfrac{1}{\sqrt{2\pi w x}} e^{\left[\ln(x)-\theta\right]^2/(2w^2)} & x \geq 0 \\ 0 & x < 0 \end{cases} \tag{5.25}$$

$$\sigma_{\varepsilon}^{\ 2} = \exp(2*\theta + w^2) * (\exp(w^2) - 1) \tag{5.26}$$

Where

$$w^2 = \text{var}\left\{\log \overline{R} - \log Ri\right\}$$
$$\theta = E\left\{\log \overline{R} - \log Ri\right\} \quad (5.27)$$

Where E is expectation and var is variance.

Equation 5.24 can be generalized to any number of stations in a cluster to give an existing true areal rainfall so that comparison with the radar observation (which is areal by nature) could be easier. For two stations the true rainfall can be estimated using the following relationship.

$$R_t = 0.5R_1\varepsilon_1 + 0.5R_2\varepsilon_2. \quad (5.28)$$

$$Var(R_t) = 0.5^2 R_1^2 Var(\varepsilon_1) + 0.5^2 R_2^2 Var(\varepsilon_2) + 2*0.5^2 R_1R_2 Cov(\varepsilon_1\varepsilon_2) \quad (5.29)$$

Where, Var (Rt) is variance of a true rainfall at time t. Equation 5.29 can be generalized for n stations in a given cluster as:

$$Var(R_t) = 0.5^2(R_1^2 Var(\varepsilon_1) + R_2^2 Var(\varepsilon_2).....R_n^2 Var(\varepsilon_n)) + 2*0.5^2(R_1R_2 Cov(\varepsilon_1\varepsilon_2) + R_1R_3 Cov(\varepsilon_1\varepsilon_3)...$$
$$....R_1R_n Cov(\varepsilon_1\varepsilon_n) + R_2R_3 Cov(\varepsilon_2\varepsilon_3) + ...R_2R_n Cov(\varepsilon_2\varepsilon_n) + ... + R_{n-1}R_n Cov(\varepsilon_{n-1}\varepsilon_n)$$

This is in generalized form:

$$Var(R_t) = 0.5^2(\sum_{i=1}^{n} R_i^2 Var(\varepsilon i) + 2*\sum_{i=1}^{n}\sum_{j=i+1}(RiRjCov(\varepsilon i\varepsilon j) \quad (5.30)$$

But, $Cov(\varepsilon_i\varepsilon_j) = \rho_{ij} * Var_i * Var_j = \rho_{ij} * \sigma_\varepsilon^2$

Where ρ_{ij} is correlation between stations i and j and σ_ε^2 is variance (computed above).

This true variance has been used to define 95 % of confidence interval for true rain at any time t, using the following relationship.

$$R_{ti} = Ri \pm 1.96 * sqrt(Var(Rt)) \quad (5.31)$$

Where R_{ti} is a true rainfall interval at time i, and Ri observed rainfall at time i. If the radar rainfall falls in this interval, one can just take it as a hit for the radar and any observation out of the interval can be considered as an exccedance for a radar observation compared to the true rainfall.

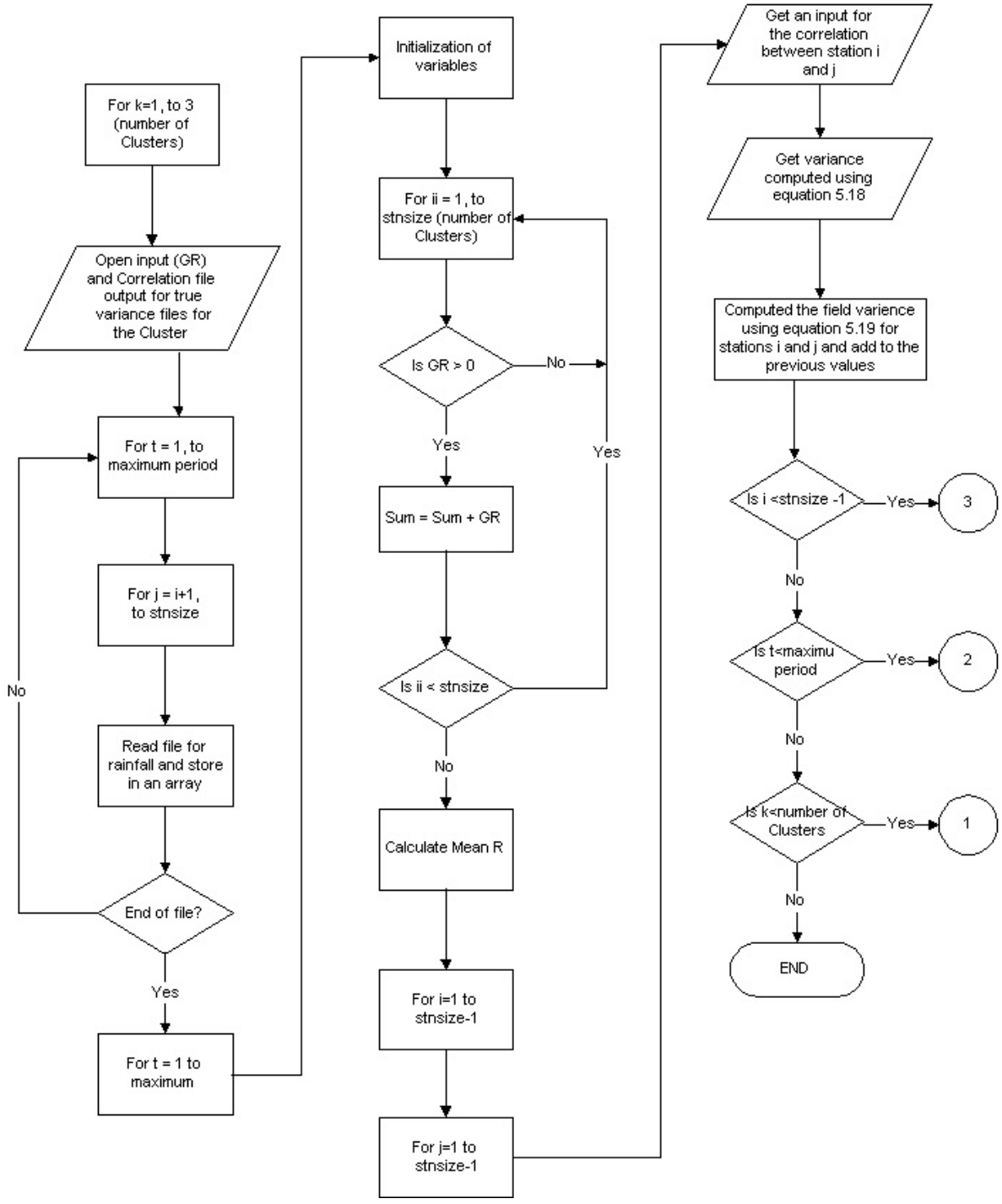

Figure 5.3. Flow Chart for the Implementation of Equation 5.30

e. Excedence Probability

The 50 % quantile of the radar rainfall has been observed to depict the gauge rainfall cumulated over time. The quantiles of radar rainfall ±5 % of the 50 % quantiles have been computed. For these quantiles the excedence has been computed as the number of radar rainfall in these intervals being out of the 95 % C.I of rain gauge rainfall. This excedence probability is calculated by taking the ratio of the counts of radar observations falling beyond this Confidence interval to that of the total observation. See Figure 5.4.

The error in the calculation of the excedence probability has been verified by plotting the histogram of the number of times the radar exceeded the confidence interval for various variances computed at each time of observations.

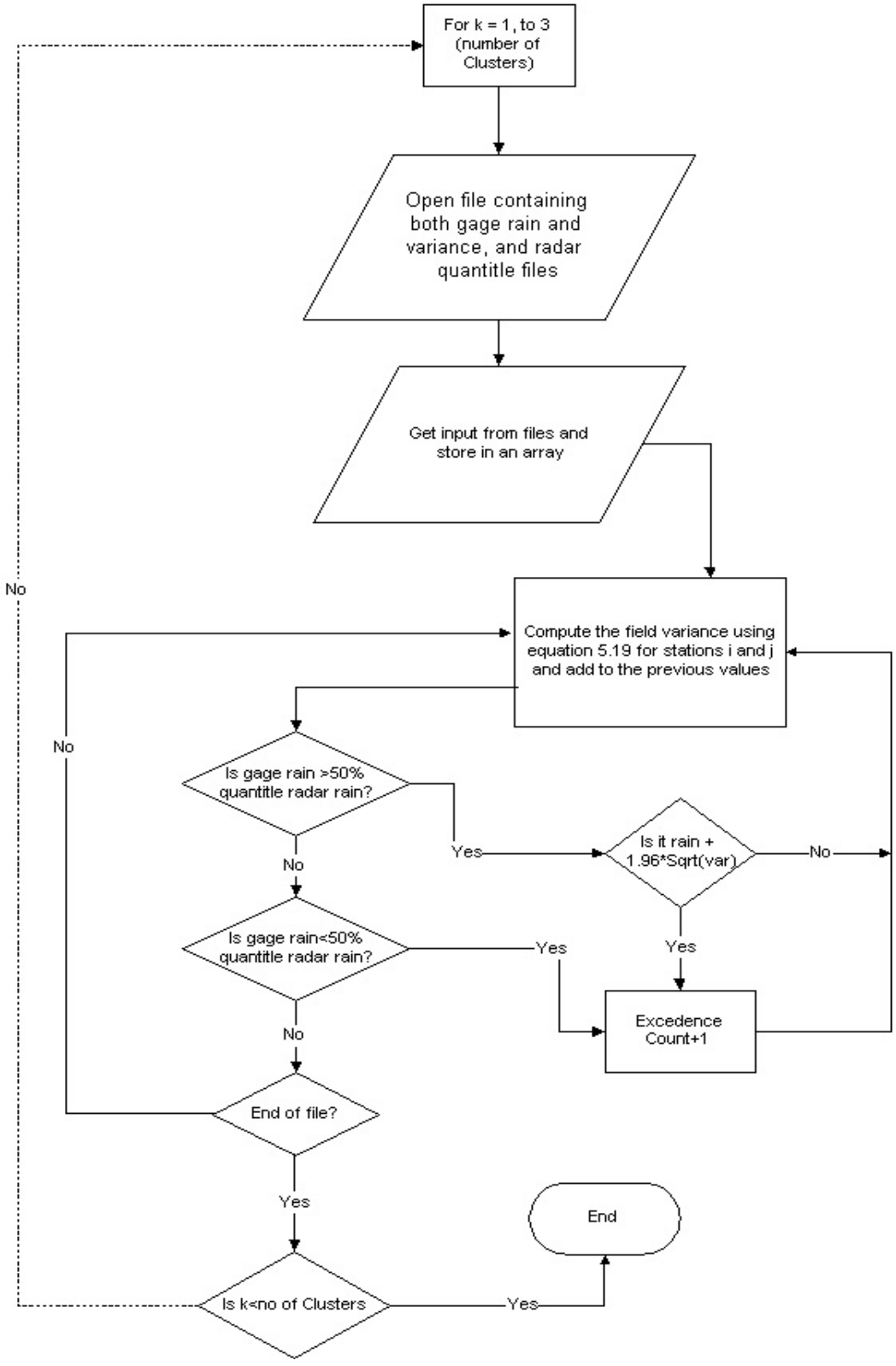

Figure 5.4. Flow Chart for Excedence Probability

5.7 Investigate Calibration Procedure of TRMM Satellite Based Rain Retrieval over Bangladesh (Objective # 6)

5.7.1 Coincident PR and Gauge Data Preparation

The data used in this study are the i) multifrequency and polarization brightness temperature observation from TMI, ii) attenuated reflectivity profiles from PR, iii) PR path-integrated attenuation (PIA), iv) rainfall-rate profiles, v) bright band heights, and vi) rain regime classification from PR. The PIA, rain-rate profile, bright-band height, and precipitation classification are products retrieved from the TRMM Science Data and Information System (TSDIS) 2A25 and 2A23 algorithms documented in Iguchi *et al.* (2000). TSDIS products, 2A12 (TMI rain profile), 2A25 (PR quantitative) and 2A23 (PR qualitative), are used in this study.

We have used the PR-qualitative product 2A23, this product provides a qualitative level of certainty in classification of rain into either convective or stratiform types. For comparison, we have sorted all TRMM observations as per their observations time. The observations falling within a 1–hour time period (local) is considered to have the same observation time. TRMM observations are compared with only those gauge stations that fall inside the instantaneous field of view (IFOV) of that particular TRMM observation. The IFOV is considering 10-km circle surrounding the geolocation coordinates of a given TRMM observation.

In this study, we have used two methods of TRMM PR rainrate/rain type data acquisition. It includes the center value of TRMM data within 10-km diameter circle in particular gauge location and the average value of TRMM data of surrounding pixels in 10-km circles of same gauge location. We collect the rain rate and rain type from surface, and at different levels (e.g. 1-km, 2-km, and 3-km above the surface) of TRMM PR (2A25 and 2A23) observations. It is understood that the over-land rain retrieval effects by surface emission. Considering high space-time variability of rainfall, we have used a relaxed criterion for the comparison of rain observations from these two systems. If at least 50 % of the gauge network that falls within a TRMM IFOV at the time of satellite over pass match with the TRMM observations within 10 % (of the TRMM value) or 1 mm /hr (whichever is greater), then the match between satellite and in situ observations is considered to be good. The tipping buckets type rain gauges are considered in this case because only tipping buckets collect 1-minute interval rain in Bangladesh but these

rain gauges are only located in Dhaka and Sylhet areas. Therefore, the match cases between satellite and in situ observations are very limited for detail statistical analysis.

Two regions (i.e. Ganges, Brahmaputra and Meghna (GBM) basin, and USA) are considered to investigate TRMM rain retrieval. Coincident PR and TMI data from four respective summer months (June – September) of 2000 are used for the calibrations. Each TRMM data is remapped to a common 10 km grid for calibrations and comparisons. For each TMI multifrequency brightness temperature array, we determine the corresponding PR precipitation profile using a geometrical matching scheme. The matching yielded a database of about 20230 coincident pixels.

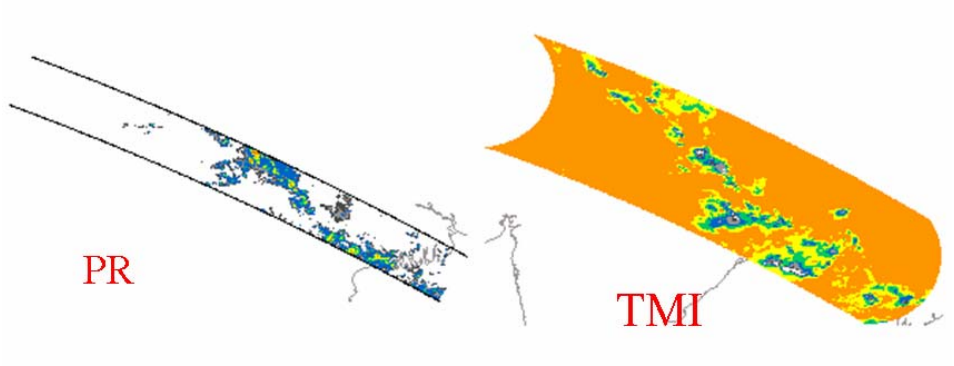

TRMM PR rain rate **TRMM TMI-Tb**

Figure 5.5. Sample of Coincident TRMM PR-TMI Data over Bangladesh

5.7.2 Procedures to Determine Coincident Dataset

- Extract PR rain rate from 8 surrounding pixels in different levels: surface, 1-km, 2-km, 3-km etc. and extract the convective/stratiform classification for the said pixels.
- Create database for coincident precipitation in time and space i.e. 5 (or 15-minute) gauge rainfall rates (mm/h) and TRMM PR rain rates from the corresponding PR grid (centre point, average of 8-neighbour pixels) at 1, 2, 3 km etc. level and at surface
- Contingency Table, i.e. Gauges >= 0.0 and PR >= 0.0; Gauges > 0.0 and PR > 0.0; Gauges = 0.0 and PR > 0.0; Gauges > 0.0 and PR = 0.0
- Probability of PR rain detection error : N (Gauges > 0.0 and PR = 0.0) / N(Gauges > 0.0) and show frequency histogram of the gauge rainfall rate when the corresponding PR = 0.0

- Probability of PR non-rain detection error: N(Gauges = 0.0 and PR > 0.0) / N(Gauges = 0.0) and show frequency histogram of the PR rainfall rate when corresponding gauges = 0.0
- Show the frequency histograms of Gauge and PR rainfall rates for the cases we have both Gauge and PR > 0.0
- Show the following conditional probabilities N(Gauges > R_{thres} and PR > R_{thres}) / N(Gauge > R_{thres}) as function of R_{thres} for 0.5, 1.00, 2.00, 5.00, 10.00, 15.00 and 20.00
- Repeat all these at different PR levels and for surface rain.

5.7.3 Rain Retrieval Statistical Evaluation Techniques

If the satellite-based and the radar/gauge-based precipitation fields are on the same grid, then the following comparisons and statistical analysis can be performed to characterize their uncertainty for both random and bias. Probability of detection (POD), False Alarm Rate (FAR), Cumulative Success Index (CSI), Bias, Fractional Standard Error (FSE), Efficiency (Eff) and Correlation coefficient (r) are used to evaluate satellite data over radar/gauge measurement.

i) Continuous Verification Statistics

$$a \quad Mean\ Error(bias) = \frac{1}{N}\sum_{i=1}^{N}(F_i - O_i) \tag{5.32}$$

Measures: Average difference between estimated and observed values

$$b \quad Root\_Mean\_Squar\_Error(RMSE) = \sqrt{\frac{1}{N}\sum_{i=1}^{N}(F_i - O_i)^2} \tag{5.33}$$

Measures: Error magnitude, with large errors having a greater impact than in the MAE

$$c \quad Correlation\_Coefficient(r) = \frac{\sum(F-\overline{F})(O-\overline{O})}{\sqrt{\sum(F-\overline{F})^2}\sqrt{\sum(O-\overline{O})^2}} \tag{5.34}$$

Measures: Relationship between estimated and observed data (i.e. between two variables), independent of mean bias.

ii) Categorical Statistics

$$Bias\_Score(BIAS) = \frac{hits + false\ alarms}{hits + misses} \quad or, \quad BIAS = \frac{Nsc + Nfa}{Nsc + Nfl} \tag{5.35}$$

Measures: Ratio of estimated area (frequency) to observed area (frequency)

$$POD = \frac{hits}{hits + misses} \quad or, \quad POD = \frac{Nsc}{Nsc + Nfl} \tag{5.36}$$

$$FAR = \frac{false\ alarms}{hits + false\ alarms} \quad or, \quad FAR = \frac{Nfa}{Nsc + Nfa} \tag{5.37}$$

$$TS = CSI = \frac{hits}{hits + misses + false\ alarms} \quad or, \quad CSI = \frac{Nsc}{Nsc + Nfl + Nfa} \tag{5.38}$$

$$Eff = 1 - \frac{\sqrt{(sum(estimated - obs.)^2)}}{\sqrt{(sum(obs.^2))}} \tag{5.39}$$

Where, N_{sc} = Number of Successs, N_{fl} = Number of Failures, N_{fa} = Number of False Alarms etc.

Table 5.1 Contingency Table in Each of the Four Possible Situations

	Yes/No	**Estimated (NN)**	
Observed PR or Rain Gauge RG		Yes	No
	Yes	Hits (N_{sc})	Misses (N_{fl})
	No	False Alarm (N_{fa})	Correct Negative

5.7.4 ANN Based Rain Retrieval Algorithm

Although overland Passive Microwave (PM) rainfall algorithms have been intensively studied, both their performance and their error characterization may be improved through the use of TRMM data. This is because TRMM provides statistically significant coincident active (radar, PR) and passive (TMI) microwave observations, which allows a comprehensive investigation of many of the existent PM algorithms using as reference the more definitive satellite radar (PR) retrievals (2A-25, V5). The PR-based TMI calibration is done for two different regions (Bangladesh and USA). The calibration process consists of:

i. developing rain area delineation (rain/no rain),
ii. convective/stratiform rain classification scheme based on Artificial Neural Network (Grecu, 2001) and
iii. multiple linear regression (MLR) models to estimate convective and stratiform rain rates. The NN features are obtained from TMI channels and are trained using PR rain profile (product 2A25) and rain type (2A23) data.

The ANN architecture used in this study consists of an input layer, a hidden layer, and an output layer (as shown in Figure 5.6). A discrimination scheme is developed herein based on the available TMI and PR data. A set of descriptors are optimally combined within a back propagation NN scheme to determine rain areas from TMI multi-frequency data. For rain/no rain discrimination, Slope, Correlation, Scattering Index, T_{19v} and T_{19h} polarization differences, the T_{85v} and T_{37v} linear combination, Gradient of T_{85v}, Standard deviation of T_{85v}, Mean of T_{37v}, are processed for ANN. Once the pre-processing of the data is done, the original data is randomly divided into three parts training, calibration\validation and testing.

For Calibration of the NN scheme, each TMI multifrequeny brightness temperature array, we determined the corresponding PR precipitation profile using a geometrical matching scheme. The 2A25 PR rainfall products were used to classify a matched pixel as rainy or no rainy; the nine classification descriptors were calculated from the corresponding TMI data. “0” for no rain and “1” for rain are used from PR rain classification. The histograms of the different descriptors for rain and no-rain situations derived from the above matched dataset. The validation results are given in the form of a contingency array. The values in the table represent the number of pixels in each of the four possible situations using Table 5.1.

A strategy similar to that used rain/no-rain discrimination was devised for the rain-regime classification. A set of descriptors was determined and fed to an NN, which was trained to predict the regime type (stratiform vs. convective rain). The calibration/validation setup for this classification scheme is the same as rain/no-rain scheme. For each matched TMI-PR pixel, the 2A-23 PR rain classification product was used as reference. The validation results of four possible situations are given as a contingency array. Finally, NN features obtained in US region have been applied for GBM region to develop TMI overland rain retrieval.

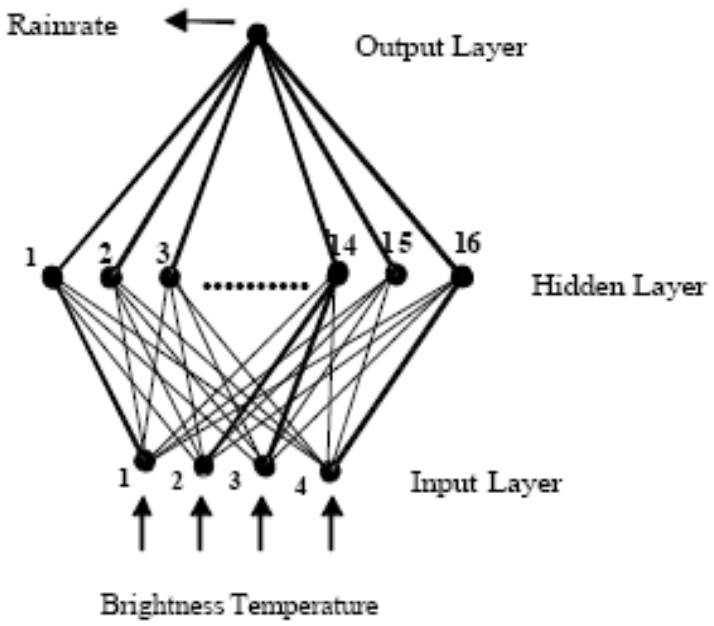

Figure 5.6 ANN Architecture showing the Input and Output Connections through the Hidden Units

5.7.5 Multiple Regression Model

We investigated rain estimation from TMI observation, based on algorithms of varying complexity and error characteristics. A common feature of the investigation algorithms is to use of multilinear regression to relate their predictors to rain estimation. MLR is basaed on a linear combination of the 85-GHz vertically brightness temperature, the 37-GHz vertically polarized brightness temperature, and their product. That is,

$$\text{Rain} = a_0 + a_1 T_{85v} + a_2 T_{37v} + a_3 T_{85v} T_{37v} \tag{5.40}$$

Where, a_0, a_1, a_2, and a_3 are coefficients to be determined by a linear regression.

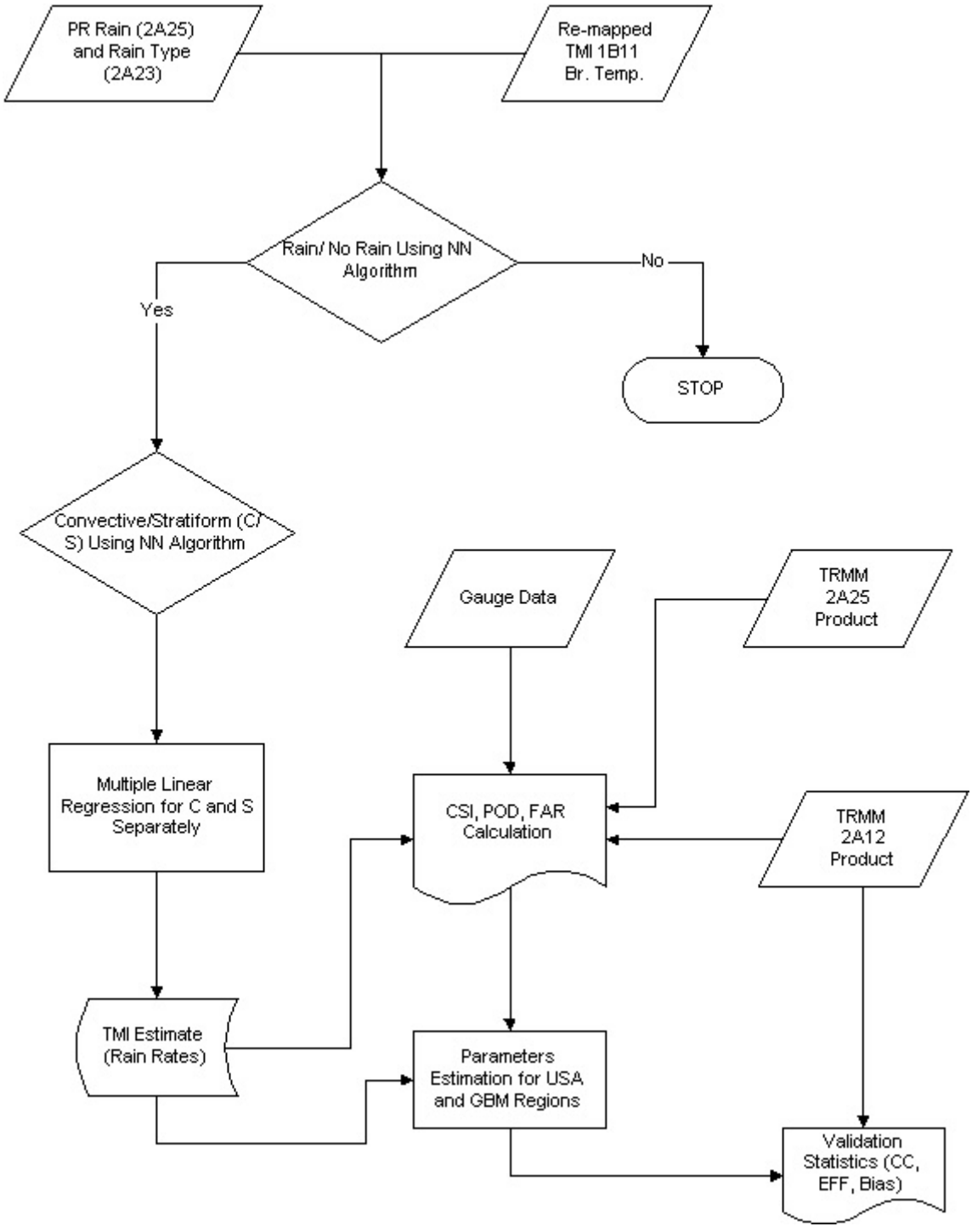

Figure 5.7. Flow Chart for Passive Microwave based Rain Algorithm

CHAPTER 6

6. RESULTS AND DISCUSSION

6.1 Characteristics of Radar Rainfall over Bangladesh (Objective 1)

6.1.1 Introduction

The Dhaka radar system automatically produces the converted rainfall intensity data. However, the intensity is classified into only 6 categories, 1-4, 4-16, 16-32, 32-64, 64-128, and over 129 (units are in mm/hr). There is a difficulty in determining the rain intensity from the categorized data. In this section, characteristics of precipitation in relation to cloud activity, hourly and daily precipitation distributions, time of maximum rainfall are derived from radar data.

6.1.2 Characteristics of Precipitation in Relation to Cloud Activity

The details of the statistics for all precipitation types are tabulated in Table 6.1. In this analysis 185 cases are identified inspecting 20846 PPI scans available from 16 April to 30 August 2000 for Dhaka radar. Analysis has been done on 107 solitary cases out of 185 and the rest 78 are merged cases. Average lifetime for solitary and merged type is 4.0 and 7.5 hours, respectively. More long-lasting convection is found in April, May and August than in June and July. The mean length shows similar trend to lifetime. The propagation speed is found faster in all other months compared to July and the speed in pre-monsoon months is the fastest. The maximum length represents the dimension of an individual cloud or a mesoscale convective system at least in one-direction, which is 88.4 km for solitary and 190.3 km for merged type. The average speed is found 5.2 m/s and 4.9 m/s for solitary and merged type respectively. It is interesting to see that the development side of the echo is almost northern in pre-monsoon months and it is becoming central and southern in the peak-monsoon months. The propagation direction of echo seems almost north (0) - east (90) and east - south (180). Hence it is obvious that many begin in the north and move east-northeast or east-southeast. The single cell, multicell and squall line categories (Houze, 1993) are also observed in precipitation areas of Bangladesh.

Table 6.1 Characteristics of Precipitation Areas over Bangladesh Observed by Dhaka Radar

Month	Type	Case	Lifetime (hour)	Max. Length (km)	Speed (m/s)	Propagation direction (%)					Development Side (%)		
						0-90	90-180	180-270	270-360	ML	N	C	S
APR	Solitary	O-3 L-14 A-1	4.3	116.9	7.8	39	56	5	…	…	94	6	…
	Merged	O- L-7 A-8	8.2	234	7.4	33	67	…	…	…	87	13	…
MAY	Solitary	O-12 L-11 A-1	4.3	86.7	5.9	38	54	8	…	…	58	33	8
	Merged	O-6 L-8 A-7	6.2	219.5	4.9	5	67	14	…	14	62	24	14
JUN	Solitary	O-9 L-16 A-…	3.7	90.6	19.08	64	8	8	12	8	48	28	24
	Merged	O-6 L-13 A-2	7.0	178.5	5.2	62	29	10	…	…	52	19	29
JUL	Solitary	O-10 L-10 A-…	4.3	62	3.8	65	15	5	5	10	65	10	25
	Merged	O-2 L-5 A-2	8.0	130	0.4	56	22	22	…	…	33	11	56
AUG	Solitary	O-14 L-6 A-…	3.9	85.7	3.8	55	10	10	10	15	65	20	15
	Merged	O-4 L-6 A-2	7.8	189.2	4.4	33	33	17	17	…	33	33	33
AMJJA	Solitary	107	4.0	88.4	5.2	56	30	8	6	7	69	22	16
	Merged	78	7.5	190.3	4.9	27	36	9	3	3	44	16	18

Note: O=Oval, L=Line, A=Arc, N=Northern, C=Central, S=Southern, ML=Motion less

In this analysis, we have tried to use available continuous PPI scans, but when radar data are missing for a continuous two hours, Global Infrared (IR) data were used as supporting information to detect the system in the next available PPI scan. The dynamics behind the above types are not clear because of the lack of observational data. Only PPI scans data may not be enough to discuss the cloud dynamics in Bangladesh.

Time sequences for EEA, determined by the BMD radar that covers the whole of Bangladesh and surrounding areas are presented in Figure 6.1 together with the amount of rainfall averaged for 33 rain-gauge stations located throughout the country. With few exceptions, the EEA and rainfall provide very similar patterns for all the days. Some days, the EEAs were not as large as the high

amount of rainfall; e.g., on May 23 and 24 the amounts of rainfall were high but the EEA was not very large. This situation continued for many days in July. The reasons for the differences include the fact that the low-density rain-gauge network (25-140km) throughout the country is insufficient for catching the rainfall from tiny clouds. Sometimes when the precipitation rate is very high, a small echo area provides a large amount of rainfall.

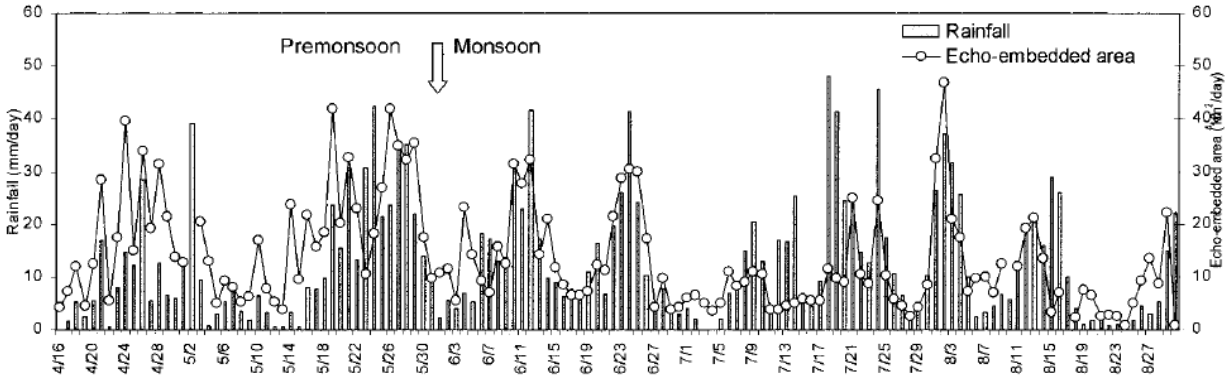

Figure 6.1. Time Sequences of Daily Rain-Gauge Rainfall (mm) showing Echo-Embedded Area (EEA) Detected by the BMD Radar from 16 April to 30 August 2000

Figure 6.2 shows the cluster size distribution and frequency of occurrence (FO) during the analysis period. Small size echoes contribute markedly below the cluster size of ~80km^2. Alternatively, convective activity becomes less organized for producing large clusters. Large clusters, however, contribute to the total precipitation due to their huge coverage. Figure 6.3 shows the propagation speed and direction of the 185 cases analyzed. Propagation speed varies from 0.4 to 19.08m/s, but on average is ~6.5m/s. The propagation direction, with few exceptions is almost east-northeast or east-southeast. The lifetime averaged of all 185 cases is ~5.7 hours (not shown) for the five month period from April to August (AMJJA).

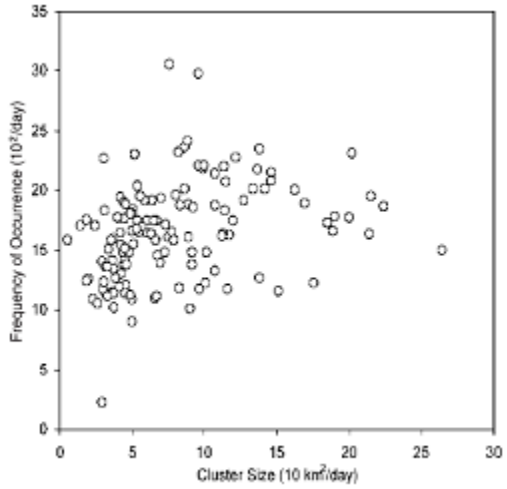

Figure 6.2. FO and Cluster Size Determined by the BMD Radar for 185 Cases in 2000

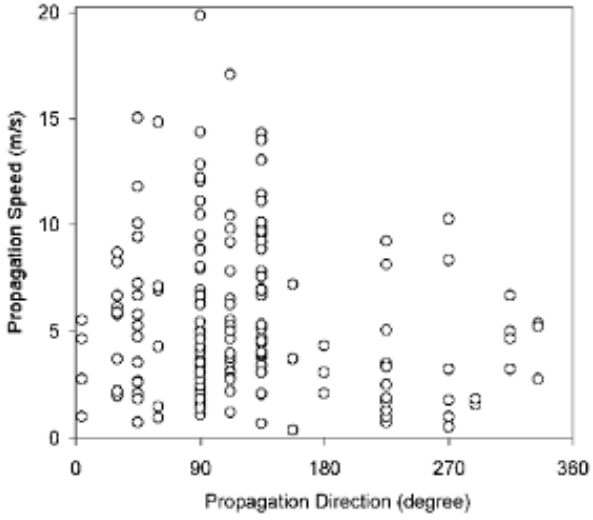

Figure 6.3. Propagation Speed and Direction of the 185 Cases Analyzed in 2000

6.1.3 Lifetime and Size of Precipitation Systems in Bangladesh

Characteristics of precipitation such as lifetime and size of echoes in relation to cloud activity are discussed here using 135 days consecutive radar data over Bangladesh. The cloud life cycles for time clusters obtained from 3-hourly satellite data were also reported by Zuidema (2003).

Larger cloud systems tend to have longer lifetimes as shown in Figure 6.4. The solitary types are concentrated below the length of 120 km and lifetime about 6 hours while the merged types are concentrated below length of about 270 km and lifetime about 10.5 hours. In the present work the maximum lifetime for solitary and merged type is found 11.5 and 27.5 hours respectively. The maximum lengths are found 215 and 580 km for solitary and merged type respectively.

The size of the clusters is investigated in detail using 4800 PPI scans (coverage of each scan is 600 km × 600 km) available in July (Figure 6.5). The log distribution shows that the accumulated frequency is a straight line above the certain size of echo area 50 km^2. The curve deviates at the smallest echo sizes. This deviation is the characteristic of a truncated log distribution. Hence, this result suggests that the precipitation area about 50 km^2 is necessary for maintaining the mesoscale convective systems in that region. Knowing that about 56 % of the tropical cloud is precipitable and about 90 % of the precipitable portion reach to the surface (Islam *et al.*, 1998), one can convert echo size 50 km^2 to cloud size 100 km^2 i. e. cloud size is just the double of echo size. The size of echo (cloud) area ~50 km^2 (~100 km^2) significantly informs that after this certain size the echoes (clouds) gather to maintain the mesoscale convective systems.

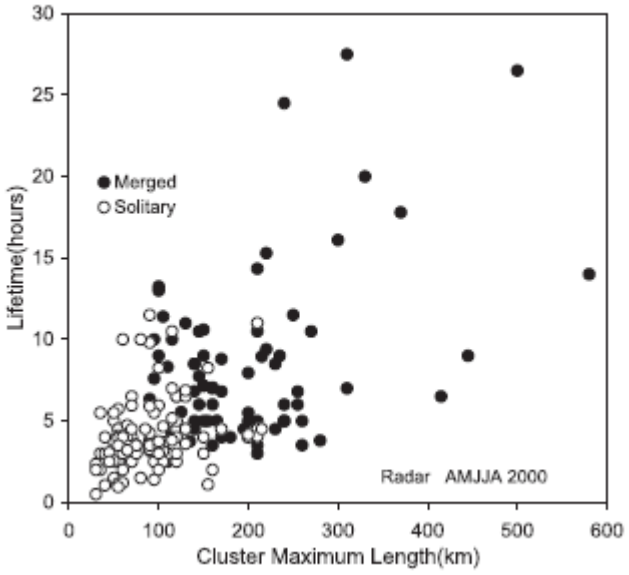

Figure 6.4. Lifetimes of Clusters Plotted Against Maximum Length of the Cluster

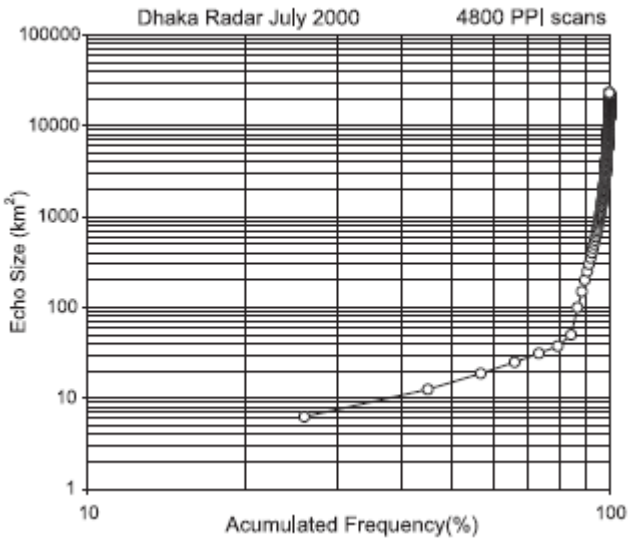

Figure 6.5. Distributed of the size of cluster over Bangladesh determined by Dhaka Radar

6.1.4 Distribution of Hourly and Daily Rainfall

The instantaneous and spell rain rates, excluding rainless grids (mm/h), are calculated using Equations 5.1 and 5.2, respectively. The spell rain rate is lower than the instantaneous rain rate. The precipitation system in spell rain comprises a single continuous rain area, in which relatively intense precipitation cores are interconnected with lighter precipitation area. Hourly and daily rainfall (mm) is calculated from Equation 5.3.

Figure 6.6 represents an example of distributions of hourly and daily rainfall (mm) calculated on 25 April 2000. On this day, the BMD reported 9.6 mm rainfall averaged over the country. Surface wind blew easterly in the north and south-westerly to the south of the country. Low temperature and pressure persisted to the north and high temperature and pressure to the south. Cloud coverages were high percentage (~80 %) in the west and low (~10 %) in the south. Figure 6.6 shows hourly-averaged rainfalls obtained from all available PPI scans within that hour, while rainless grids are excluded. For example, at 06 LST, all PPI scans from 05 LST to 06 LST are used for average. Daily rainfall is obtained from accumulation of the hourly values for the rainy grids. The area-averaged rainfall excluding (including) rainless grids at 00, 06, 09, 12, 15, 18, 21 LST and daily rainfall are 10 (2), 22 (3), 6 (1), 7 (0.4), 8 (0.4), 43 (3), 27 (6), and 18 (2.2) mm.

Hourly rainfalls of all area are strong from evening (18 LST) to morning (06 LST). At 21 LST and 00 LST, rainfalls at each grid are not so strong, but rainfall area is larger in this case.

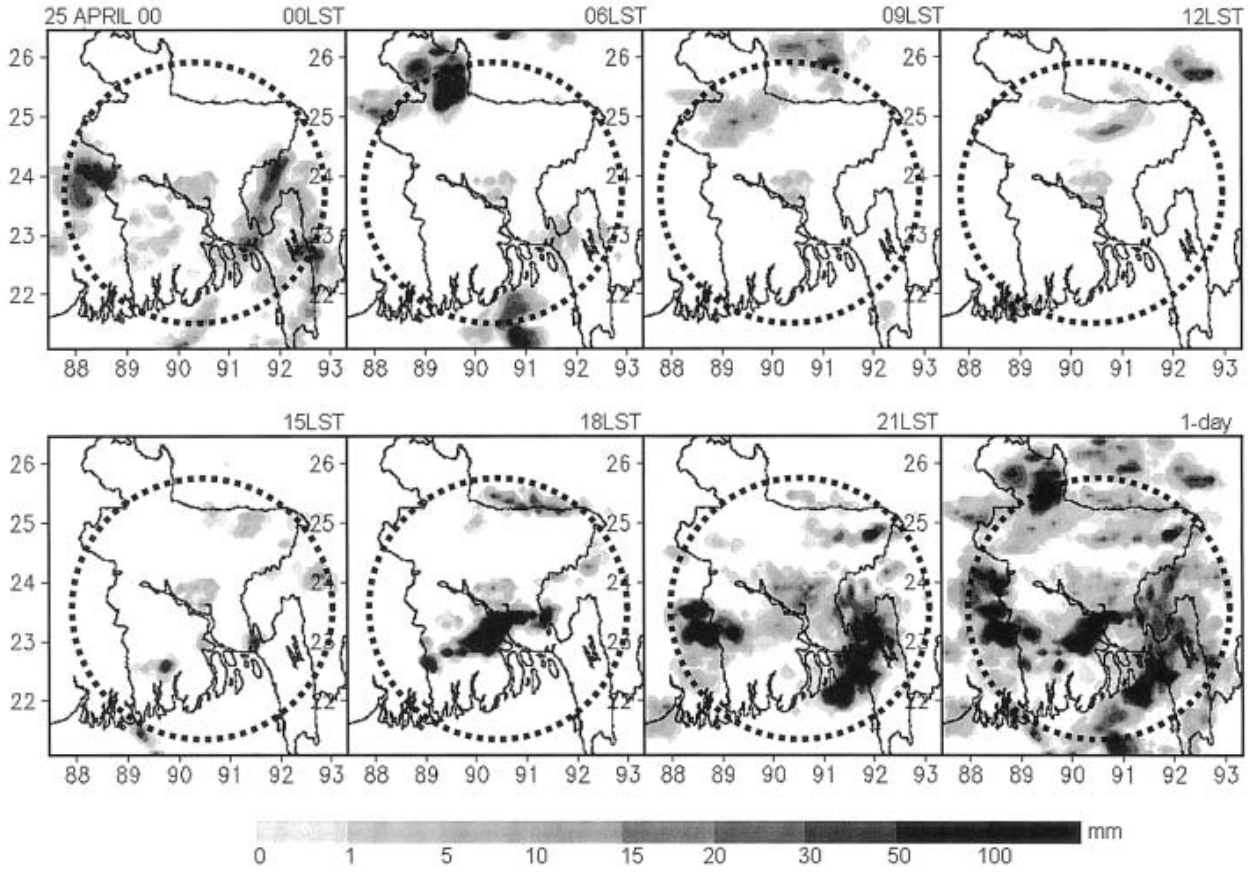

Figure 6.6. Calculated Hourly and Daily Rainfall (mm) over Bangladesh on 25 April 2000

In Figure 6.6, the top panel, left to right, for 00, 06, 09 and 12; bottom panel, left to right, for 15, 18, 21, and 1 day. The hourly values are accumulated for a day in 1 day. Dotted circle denotes the Dhaka radar effective range of observations.

6.2 Performance Evaluation of Radar Rainfall using Gauge Network (Objective 2)

6.2.1 Comparison Study Radar vs. Gauge Rainfall

The retrieved rainfall averaged for 16 April to 30 August 2000 is shown in Figure 6.7. From the rainfall distribution, it is seen that rainfall is high in the NE and east parts of the country. The low

rainfall dominates in the western parts. The low rainfall in the extreme SE region may not be accurate one because this portion is out of radar effective coverage (250 km from radar centre).

The rainfall distribution estimated by BMD rain-gauge is shown in Figure 6.8 for the same period of radar. The pattern is similar to that detected by radar except the amounts are higher than radar estimates (e.g. 2.2 mm/day vs. 11.6 mm/day). It seems that radar underestimates (Figure 6.7) in rainfall estimation compared to rain-gauge values.

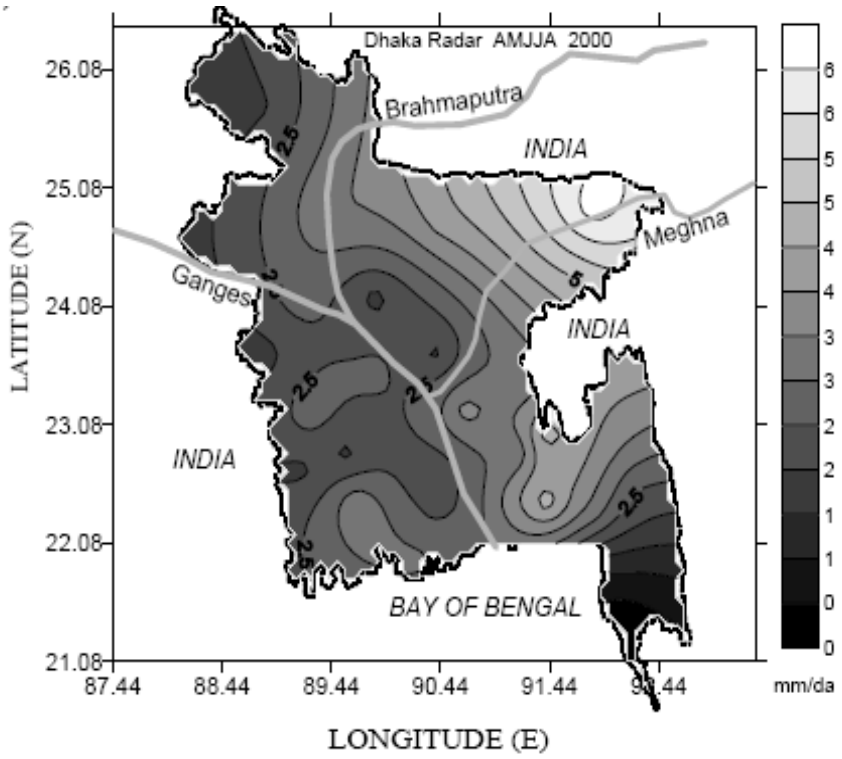

Figure 6.7. Radar Estimated Rainfall Averaged for 16 April to 30 August 2000

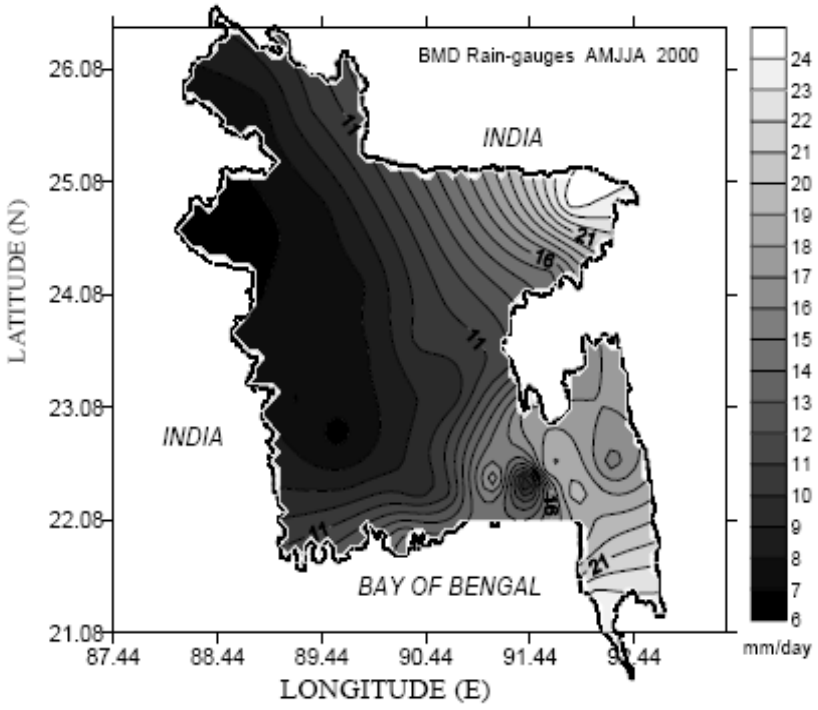

Figure 6.8. Estimated Rainfalls Averaged for 16 April to 30 August 2000 from Rain-Gauge

The daily rainfall (mm) estimated by radar and rain-gauge averaged from 33 stations (as shown in Figure 4.2) at different months in 2000 is tabulated in Table 6.2. The percentage (%) indicates how much of total rainfall the radar can detect when compared to rain gauges. Radar can detect from 8.81 % (Jul) to 45.58 % (Apr) of rain-gauge rainfall. In average for all four months it is 24.41 %. This means that radar estimates about one fourth of the rain-gauge rainfall. One may think that radar grossly under estimates of rainfall for the year 2000. The fact is that in 2000, most of the rain comes from SE coastal regions (Figure 6.8). The radar effective radius is 250 km and it can not catch well the precipitation in these remote distances. On the other hand, rain-gauge provides point information while data is averaged in a 10 km grid for radar analysis. Another cause of underestimation is that the standard Z-R relationship ($Z=200R^{1.6}$) is used in radar data processing. The Z-R relationship is regional and cloud type dependent. Therefore, further investigation is carried out to find a best fit Z-R relationship for this region. Radar rain algorithm parameters are described and estimated in Sections 5.6 and 6.5 respectively.

Table 6.2 Relation between Daily Rainfall Estimated by Radar and Rain-Gauge Averaged from 33 Stations at Different Months in 2000

Month	Radar (mm/d)	Rain-Gauge (mm/d)	%	Average %
Apr	3.83	8.41	45.58	24.41
May	4.14	14.30	28.95	
Jun	2.70	13.70	19.70	
Jul	1.22	13.89	8.81	
Aug	2.20	11.59	19.01	

Figure 6.9(a) shows daily rainfall estimated by the Dhaka radar at each rain gauge site averaged for 135 days from 16 April to 30 August 2000. The time of maximum daily rainfall at each rain gauge site are also shown using arrows. Note that rainless grids are included to obtain hourly as well as daily and monthly rainfall in the rest of the analysis. Figure 6.9(b) shows daily rainfall estimated from rain gauge data using similar approach of Figure 6.9(a).

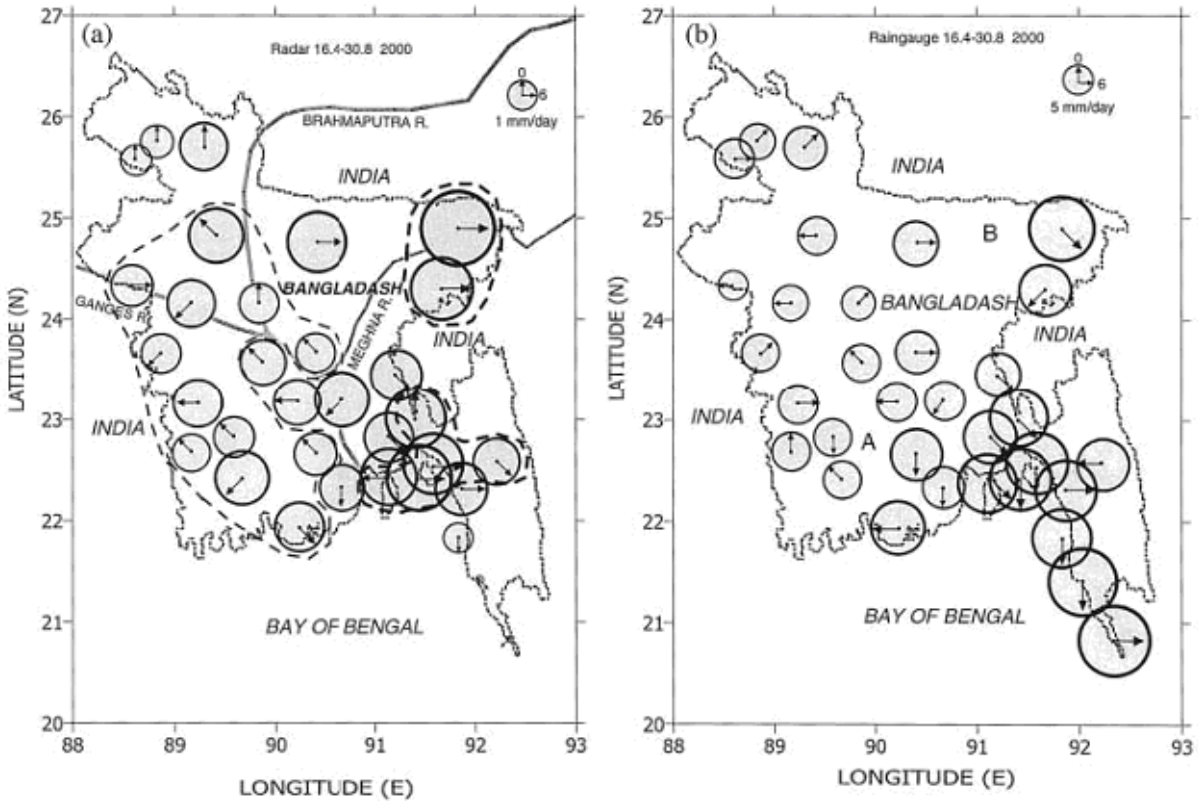

Figure 6.9. Daily Rainfall averaged for 16 April to 30 August of 2000 in Bangladesh (a) estimated by the Dhaka radar and (b) Estimated by Rain Gauge

The area of circle in Figure 6.9 (a) and (b) is proportional to the volume of daily rainfall. The orientation of arrows indicates the time of maximum rainfall. Arrows pointing to the north, east, south and west denote 00 LST, 06 LST, 12 LST, and 18 LST, respectively. Rainfall scale of the rain gauge is 5 times of the radar rainfall.

The quantity of rainfall estimated by the Dhaka radar was much lower than that measured by each rain gauge. The rainfall discrepancy between the two may come from inconsistency of temporal and spatial averaging of the radar and the rain gauge data. It may come from rainfall calculation from rain status based on single Z-R relations. In case of the radar analysis, rainfalls of 16 pixels (each 2.5 km mesh) in a grid box including rainless pixels are averaged. On the other hand, no spatial average is taken for the rain gauge. As seen in Figure 6.9(a), rainfalls estimated by the radar of south-easterly stations are very less than those in Fig 6.9(b). This is because these stations are located far from the radar and out of the effective range of the radar (250 km). The reduction of the reflectivity is very clear on the outside of the radar's effective radius. The northwest rain gauge stations are located on the border of the radar's effective range. The rainfall estimated by the radar is consistent with the rain gauge result with an increasing tendency in the northern stations.

Time of maximum rainfalls obtained by the radar analysis differs remarkably from that obtained by the rain gauges, especially at stations enclosed with dashed lines in Figure 6.9(a). Since the Dhaka radar was not operated during 03 LST, we cannot confirm the time of maximum rainfall at the northwest stations.

The spatial distribution of rainfall amount over the country in Figure 6.9 is similar to pattern of rainfall in 1995 reported by Ohsawa *et al.* (2001). Much of the rain comes from the southeastern coastal and north-eastern regions. However, the time of maximum rainfall in 2000 somewhat differs from that of 1995 at many stations. The dissimilarity may come from the type of data coverage; radar data are analyzed in 100-km^2 coverage, while rain gauges only indicate a point value. The larger area averaging of the radar may conceal the variation of the time of maximum rainfall measured by the rain gauges in the averaging area. The year-to-year change of diurnal variation of rainfalls in 1995 and 2000 may be another reason.

6.2.2 Distribution and Time of Maximum Precipitation in Bangladesh

Figure 6.10 presents the distribution of the averaged daily rainfall (mm) as estimated from BMD radar data (left panel) and that estimated by the rain-gauge system (right panel) during the entire analysis period. The radar-estimated precipitation is calculated for a 100 km^2 grid box with 2.5km pixel resolution at each rain-gauge site. Precipitation in the northeast and southeast parts of Bangladesh is significantly high. In the southeast corner, precipitation is low due to the long distance from the radar center, and one station is beyond radar coverage. There are a number of stations located outside the effective radar radius of 250km (circle, Figure 6.10). Precipitation varies greatly with location in the country, and this distribution pattern coincides with rain-gauge results, however, the rain-gauge provides a large amount of rainfall compared to radar.

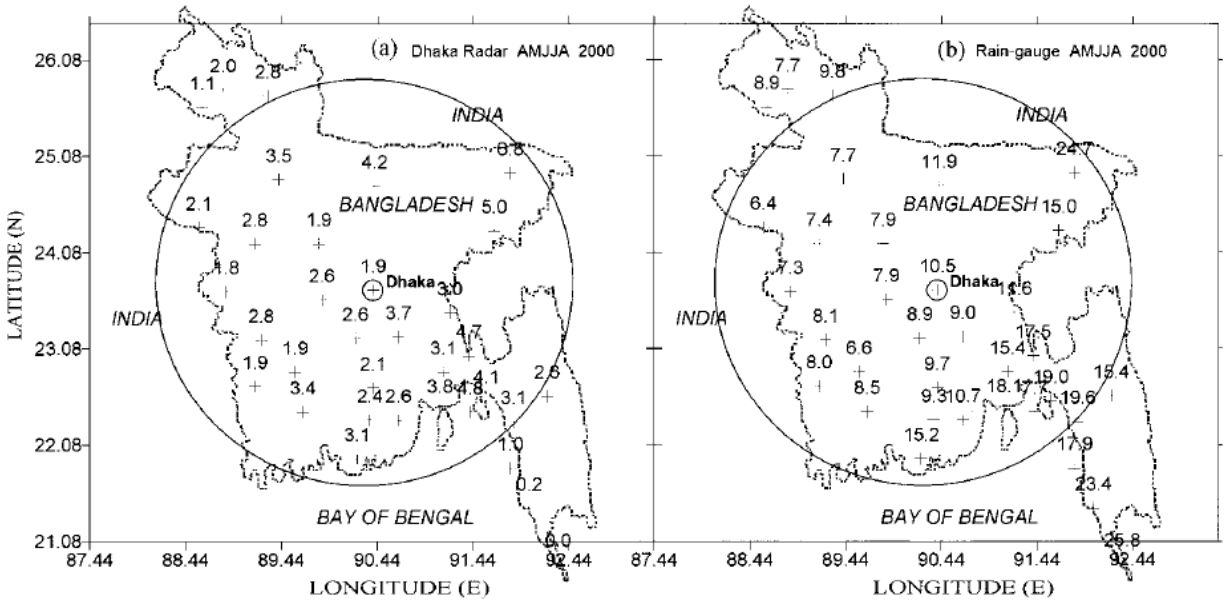

Figure 6.10. Distribution of precipitation (mm/day) obtained from (a) BMD radar and (b) Rain-gauge data. Average for 16 April to 30 August 2000. Large circle represents the effective radius of BMD radar

The right panel in Figure 6.10 shows the relationships between rainfall calculated from the rain-gauge and radar data averaged from April-August 2000 inside the effective BMD radar coverage (<250km). Clearly, the radar data underestimates rainfall by about one-fourth that of the rain-gauge value. The discrepancy between the rainfall estimations based on the BMD radar and rain-gauge systems is due to the following: (i) radar rainfall is estimated from the areal average of 100 km^2 grid boxes, whereas rain-gauges indicate point values; (ii) there is inconsistency in the

temporal and spatial averaging of the radar and rain-gauge data; (iii) rain status is calculated based on a single Z-R relationship, details of spatial variation in the precipitation in Bangladesh are discussed in Islam *et al.* (2005). The northern border of Bangladesh, close to the Shillong Hills of India, is the region with the highest rainfall, the second highest rainfall occurring along the eastern border.

Rain-gauge rainfall versus radar rainfall scatter plot (left panel, Figure 6.11(a)) shows the relationships between them for the entire BMD radar coverage in different months (April-August) of 2000. The correlation coefficients for the different months (0.63-0.89) are tabulated in Table 6.3. For all five months (April-August) the correlation coefficient is 0.64. The coefficient increases in magnitude (0.70) inside the effective radius of the BMD radar (right panel, Figure 6.11(b)). If a new best-fit Z-R relationship is obtained for BMD radar that considers the same temporal and spatial averaging then the correlation further increases. The discrepancy in the rainfall values estimated by radar and rain-gauge, as shown in Figure 6.10, will be reduced.

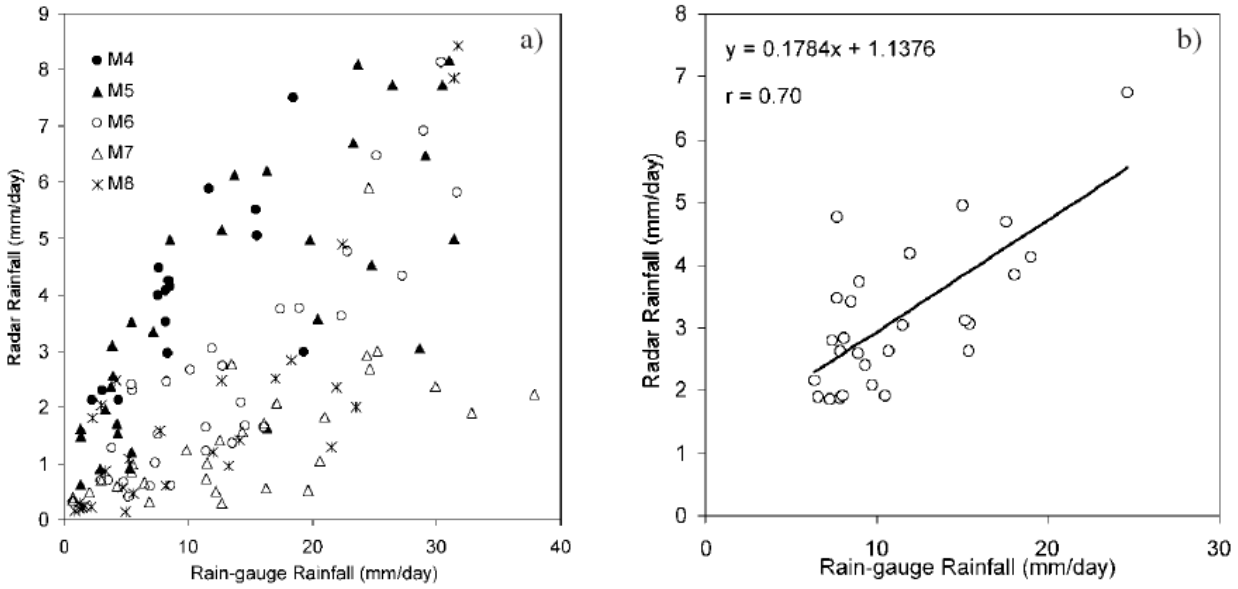

Figure 6.11. Relationships between rainfalls calculated by radar and rain-gauge data, (a) In different months of 2000 and (b) averaged for all months (March-August) in 2000 inside radar effective radius. Symbols in (a) represent for different months (i.e. M4 = April, M5 = May, M6 = June, M7 = July, and M8 = August)

Table 6.3 Relationship between Rainfall obtained by Radar and Rain-gauge

Months	Regression Equation	Correlation Coefficient
April	Y= 0.1952X + 2.1434	0.878
May	Y=0.176X + 1.4876	0.767
June	Y = 0.212X – 0.2329	0.892
July	Y= 0.0779X + 0.309	0.634
August	Y = 0.1791X + 0.0794	0.809
April–August (Radar Data Coverage)	Y = 2.771X + 5.5005	0.644
April-August (Radar Effective Radius)	Y = 0.178X + 1.1376	0.700

6.3 Performance Evaluation of TRMM Rain Product over Bangladesh (Objective 3)

6.3.1 Introduction

There is not much research work on the estimation of rainfall in Bangladesh using remote sensing data. Some preliminary works are reported by Islam *et al.* (1997, 1998, and 2002) and Wahid *et al.*, 2000. There is almost no validation work on the rainfall estimated by TRMM over Bangladesh. So, an attempt is made to compare the rainfall determined by TRMM 3B42 with the same estimated by rain-gauge in Bangladesh.

Cause of the variations of rain intensities in different parts of the rainy season is not clear enough. The existence of the liquid contents at various altitudes may be one of the candidates in finding the possible reasons of the variations of rain intensities in different periods. The study of the vertical structure of the liquid contents is not possible using available data from the rain-gauge and radar plan position indicator (PPI); the volume scan radar data is not available yet in Bangladesh. In such a situation of data paucity, the tropical rainfall measuring mission (TRMM) data products help studying the vertical variations of rain intensity of the precipitation fields in Bangladesh. Therefore, attempts are made to clarify the vertical variations of rain intensity using the TRMM 2A25 data in order to understand one of the basic characteristics of rainfall in and around Bangladesh that different rain intensities occurred during the different rainy periods.

6.3.2 Compare of TRMM Products with Gauge Rainfall

Daily rainfall (mm) determined by TRMM 3B42 (right) and RNG (left) averaged for 1 March to 30 November from 1998-2002 at each station over Bangladesh is shown in Figure 6.12. TRMM underestimates rainfall in the north-east and south-east regions which are the heavy-rainfall regions in Bangladesh. In the rest parts of the country rainfall amounts are almost similar. Rainy days and daily rainfall (mm) determined by TRMM and RNG in each year at five selected stations named Dhaka (centre), Khulna (south-west), Rangpur (north-west), Sylhet (north-east) and Teknaf (south-east), as mentioned in Figure 6.12. It is seen that the numbers of rainy days determined by TRMM are higher than the same determined by RNG while the numbers of match day are alike to RNG. Daily rainfalls determined by TRMM are higher than the same determined by RNG at Dhaka and Khulna. In other three stations situations are fully opposite. TRMM underestimated rainfall regions are the wet regions (not shown) over the country.

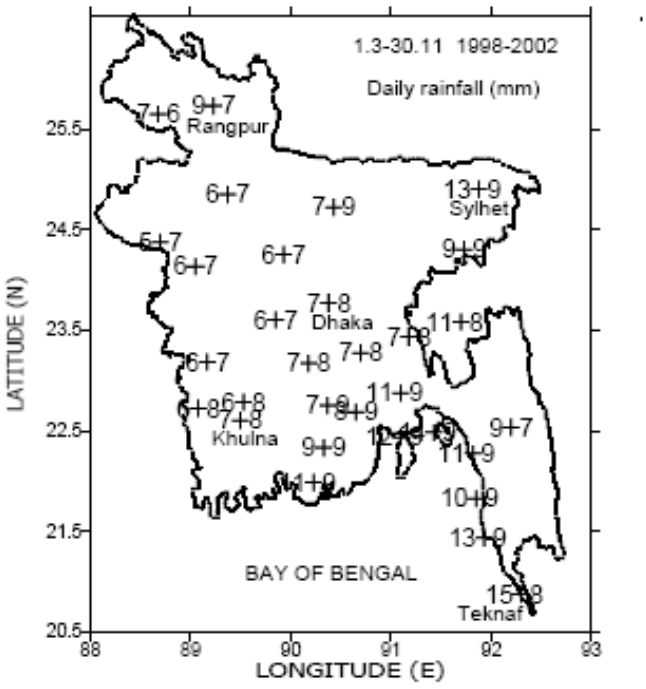

Figure 6.12. Daily rainfall estimated by TRMM (right) and RNG (left). The plus mark represents the location of rain-gauge station

Daily rainfall (mm) determined by TRMM and RNG averaged for selected 5 stations (Dhaka, Sylhet, Rangpur, Khulna, and Teknaf) from 1998-2002 for pre-monsoon, monsoon and post-monsoon periods are shown in Figure 6.13. TRMM underestimates rainfall during monsoon period while the other two periods estimate similar. When rainfall averaged for all 31 stations then TRMM underestimates during monsoon period but overestimates during pre-monsoon period (Figure 6.14).

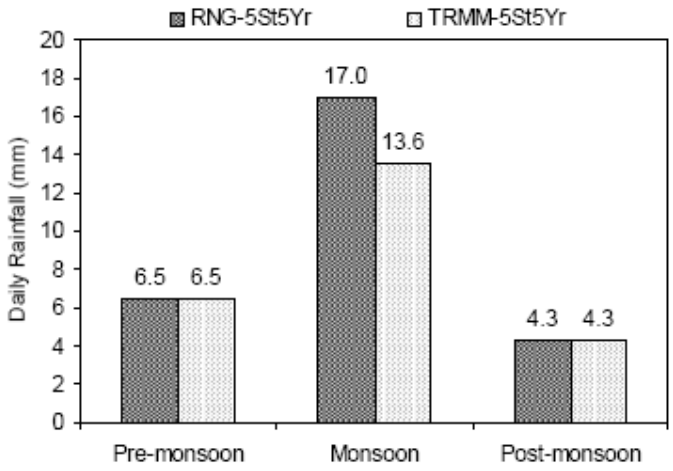

Figure 6.13. Daily rainfalls averaged for 5 stations from 1998-2002

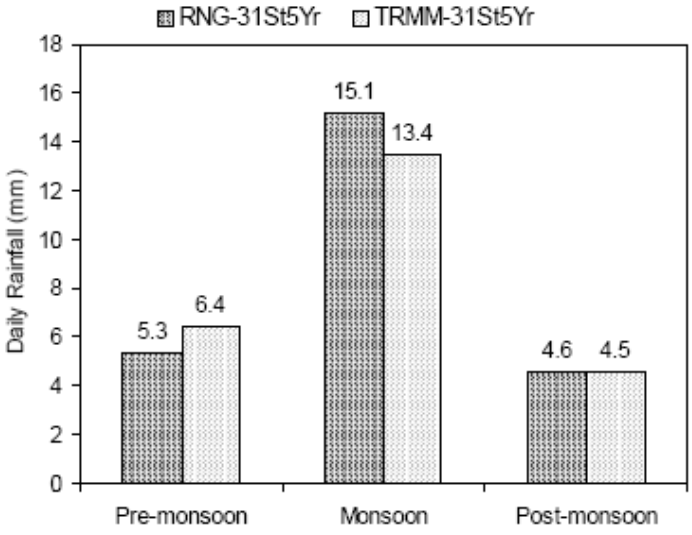

Figure 6.14. Daily rainfalls averaged for 31 stations from 1998-2002

Daily rainfall (mm) and percentage of rainy days averaged for 31 stations over the country in different years are shown in Figure 6.15. Daily rainfall anomaly (individual year average minus all years average) among different years lies between -0.61 to 0.52 mm for RNG and between -0.41 to 0.52 mm for TRMM. TRMM estimates rainfall very close to the RNG amount. In different years, rainfall difference determined by TRMM and RNG lies between -0.08 to 0.51 mm. Percentages of rainy days determined by TRMM and RNG represent that TRMM can accurately detect the rainy days, as determined by RNG. In average for 1998-2002, the match days between TRMM and RNG is 95.99 %.

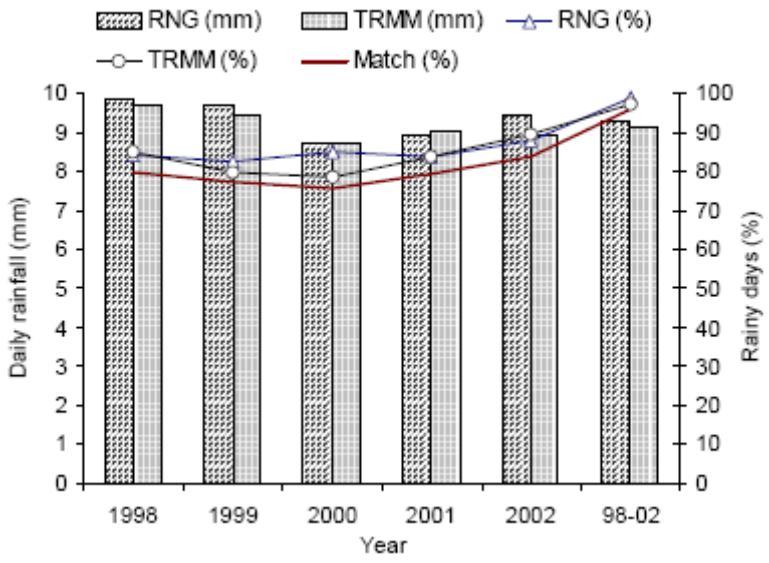

Figure 6.15. Daily rainfall and rainy days determined by both TRMM and RNG in different years

Day-by-day variations of rainfall determined by RNG and TRMM at station Dhaka from 1 March to 30 November 1998 are shown in Figure 6.16. Dhaka station is situated in dry region and rainfall patterns determined by both RNG and TRMM are very similar except RNG or TRMM overestimates for a few days. The station Sylhet (north-east region of the country) is situated in the heavy rainfall region of Bangladesh and the rainfall patterns for 1 March to 30 November 1998 shows that TRMM underestimates in many days (Figure 6.17). When rainfall determined by RNG and TRMM is averaged over 31 stations for 1 March to 30 November 1998 it is clearly seen that TRMM underestimates during monsoon period (Figure 6.18). This result supports Figure 6.13 and Figure 6.14. The patterns of rainfall determined by RNG and TRMM are much more comparable when averaged for 1998-2002 (Figure 6.19).

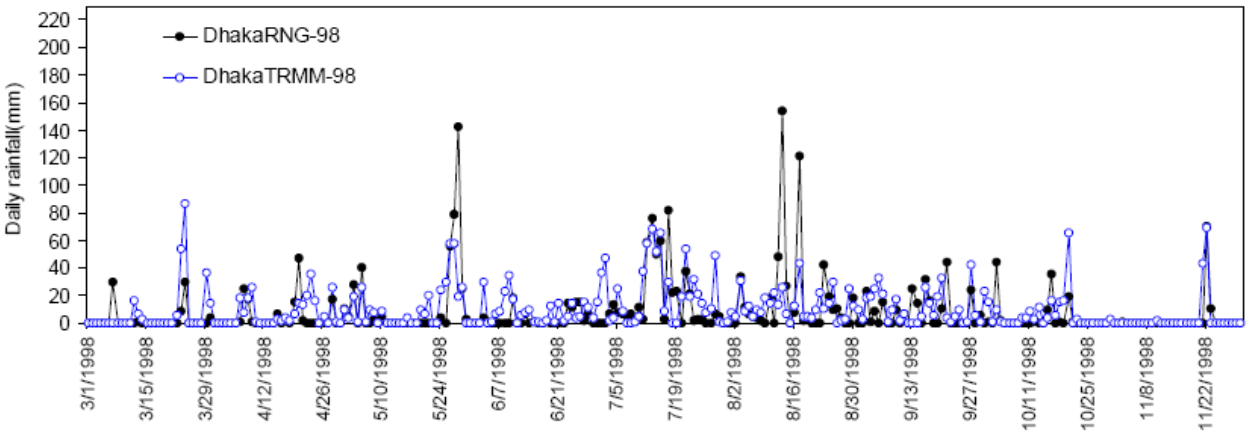

Figure 6.16. Time sequences of daily rainfall (mm) determined by both TRMM and RNG at station Dhaka in 1998

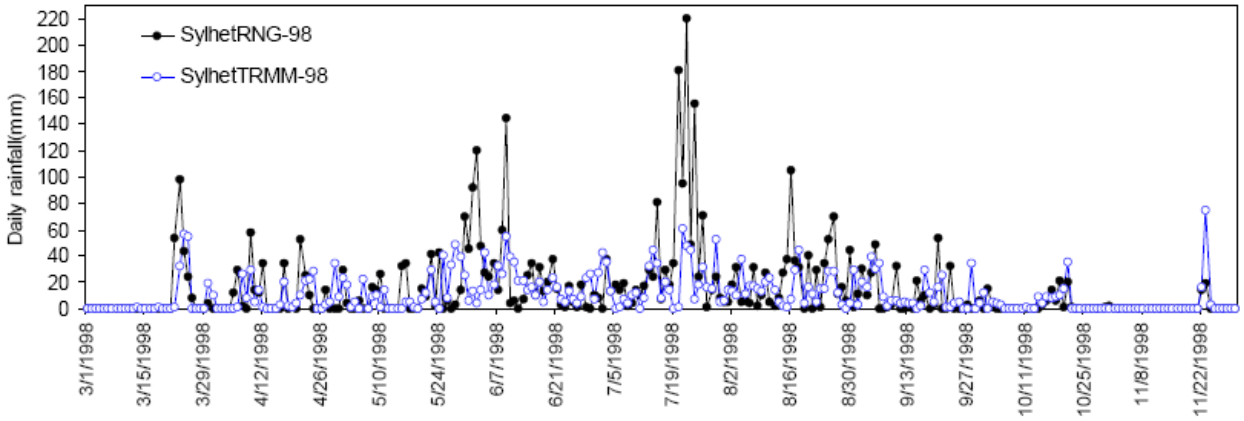

Figure 6.17. Time sequences of daily rainfall (mm) determined by both TRMM and RNG at station Syllet in 1998

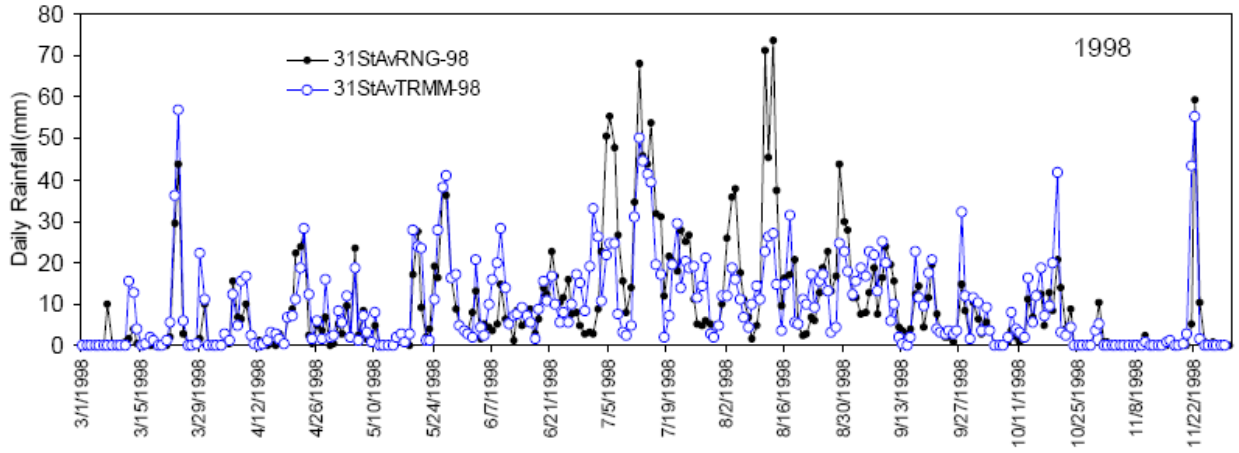

Figure 6.18. Time sequences of daily rainfall (mm) determined by both TRMM and averaged rainfall in 1998 from 31 stations over the country

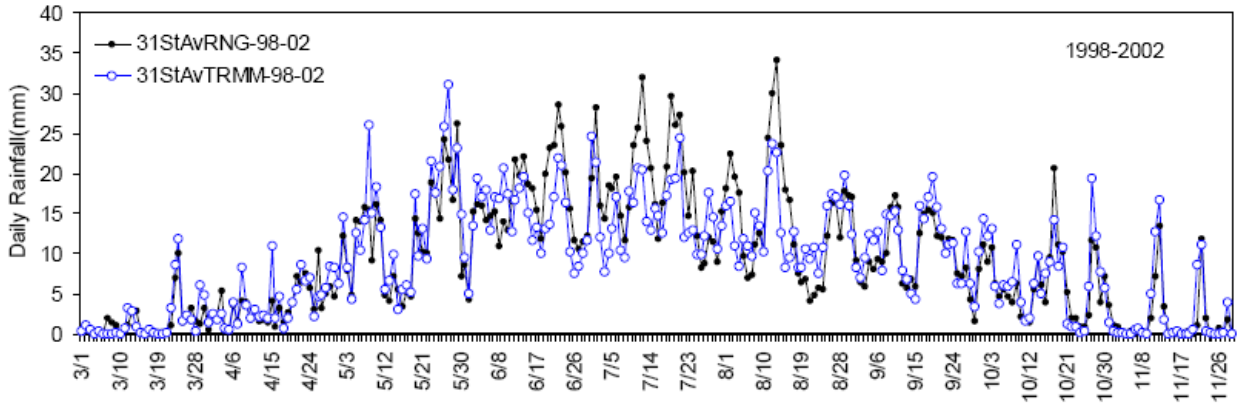

Figure 6.19. Time sequences of averaged rainfall (mm) for 5 years (1998-2002) determined by both TRMM and from 31 stations over the country

Figure 6.20(a) shows the comparison of seasonal rainfall obtained from TRMM V5 3B42, V5 3B43, V6 3B42, V6 3B43 and RNG. Rainfall in each season is averaged from 1998 to 2002. The V5 3B42 overestimated rainfall in the pre-monsoon and post-monsoon periods and underestimated it in the monsoon period. The V5 3B43 underestimated rainfall in all periods. The V6 3B42 and V6 3B43 estimated rainfall amounts are very close to the RNG-estimated one. The rain rates have been scaled to match the monthly rain gauge analysis. It is therefore to be expected that the correlationship between 3B42 and the gauge rain rates would be high.

The V5 3B42, V5 3B43, V6 3B42 and V6 3B43 performances obtained for 1998–2002 are about −2.8, −10.1, −6.8 and −4.2 %, respectively. But the fact is that V5 3B42 substantially overestimates the gauge measurement in the pre-monsoon and underestimates it during the monsoon, whereas V6 measures are closer to the observed value in both periods (Figure 6.20(a)). Hence, the performance of V5 3B42 is the best. All TRMM products underestimated the monsoon rainfall. Figure 6.20(b) shows the scatter plots of monthly rainfall measured by V5 3B42, V5 3B43, V6 3B42 and V6 3B43 with BG during 1998–2002. The V5 3B42 overestimated low rainfall and underestimated high rainfall totals. The degree of underestimation is much higher for V5 3B43. Overall, V6 3B43 is better in all measurements. The TRMM has some false detection for low rainfall totals and limitations in detecting very high rainfall. The V5 has large false over detection whereas V6 has small false under detection (Islam and Uyeda, 2007). The fact is that the low bias of V5 3B43 may be due to the non-inclusion of some rain events in the operational gauge analyses that are used in the production of V5 3B43 (Chiu *et al.*, 2006). The reduction of rainfall is overestimated in both pre-monsoon and post-monsoon periods, and underestimated in monsoon periods. The V6 (compared to V5) results in better agreement between RNG estimates and TRMM V6 products. The correlations between RNG and TRMM rainfall estimations are 0.95, 0.96, 0.97 and 0.98 for V5 3B42, V5 3B43, V6 3B42 and V6 3B43, respectively. These correlations are better than 0.65, 0.81, 0.84 and 0.86 for V5 3B42, V5 3B43, V6 3B42 and V6 3B43, respectively, obtained by Chokngamwong and Chiu (2006) for Thailand who analyzed V5 data for 1998–2004 (March) and V6 data for about 1998–2005. This is due to the different rainfall climatology in Thailand and Bangladesh and the integration time of data. The scatter plots between daily rainfall measured by V5 3B42 and V6 3B42 with RNG for 1998–2002 are displayed in Figure 6.20(c). The correlations between RNG and 3B42 daily rainfalls are 0.91 and 0.89 for V5 and V6, respectively. Hence, the correlation is reduced only by 4–8 % for daily rainfall compared to the monthly data. BG stands for the rain gauges in Bangladesh (i.e. RNG). Figure 6.20(b) shows the bias in extreme values and Figure 6.20(c) shows the scatter in extremes.

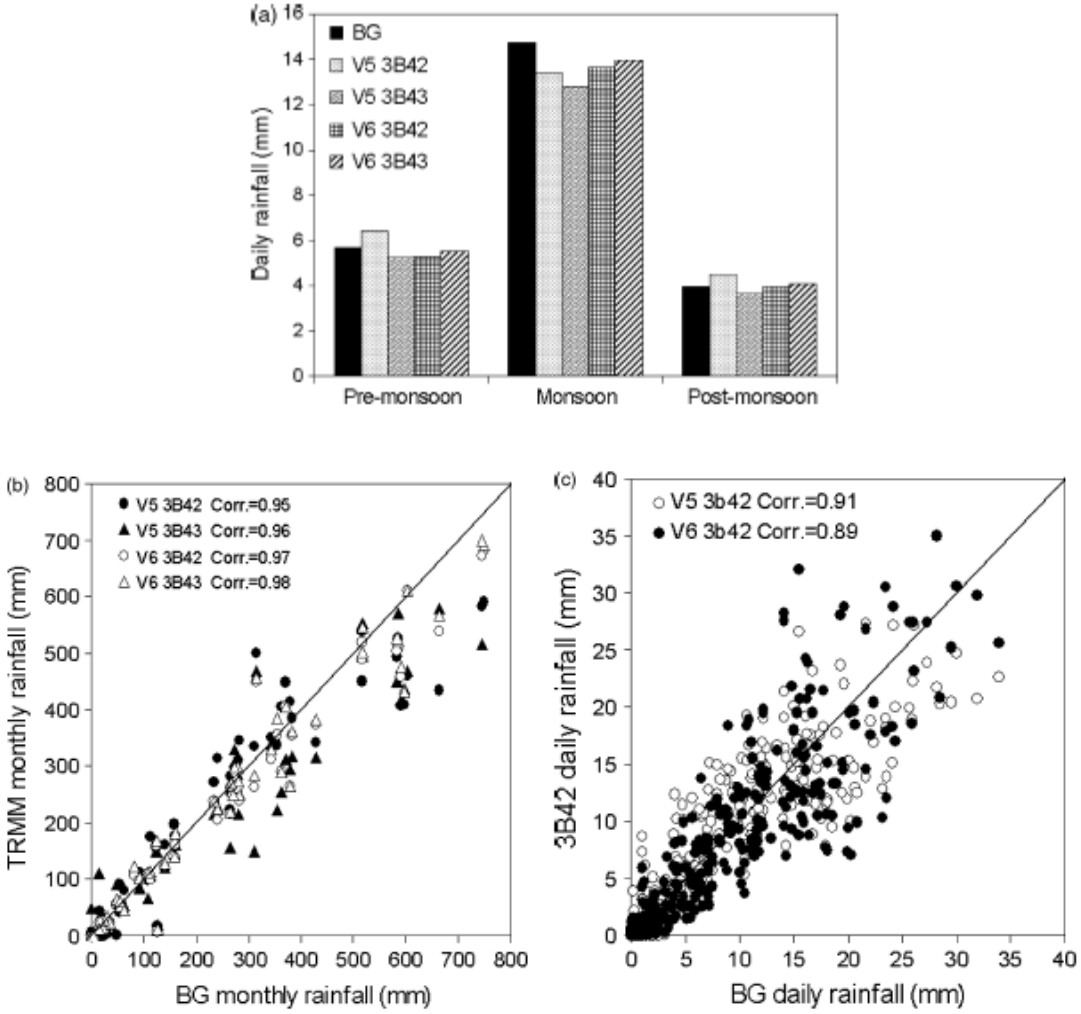

Figure 6.20. (a) Seasonal rainfall obtained from TRMM datasets and BG, (b) Scatter plots of TRMM products* versus *BG rainfall and (c) Scatter plots of V5 3B42 and V6 3B42* versus *BG rainfall

6.3.3 Vertical Variations of Rain Intensity

To understand the distinction of intensity in different periods, maximum rain rates and echo top heights are calculated for 34 cases in April, 82 cases in July and 36 cases in October using 2A25 datasets during 2000–2003. Averages from the above mentioned cases, show that rain rates are high in April compared to other months, and low in October (Figure 6.21). Echo top height is also higher in April than in other months, and low in October. Figure 6.22 shows the echo top heights for different thresholds calculated from the same number of cases used in Figure 6.21. In April, a pre-monsoon month, high echo tops are found for large threshold rain rates (Figure 6.22 (a)).

On the other hand, low echo tops are found for large threshold rain rates in July, a monsoon month (Figure 6.22(b)), and in October, a post-monsoon month (Figure 6.22(c)). Above 5 km, a small number of echo tops are observed in July and October beyond the threshold limit of 20 mm/h. For April, many echo tops are found above 5 km beyond the same threshold limit. It is clear that heavy rainfall has higher echo top height corresponding to strong rain rate in the pre-monsoon than in other rainy periods. Thus, this explains the high rain intensity of maximum rain rate events in pre-monsoon convective systems. Results from the manual detection of echo top may be useful in developing an automatic echo top detection program.

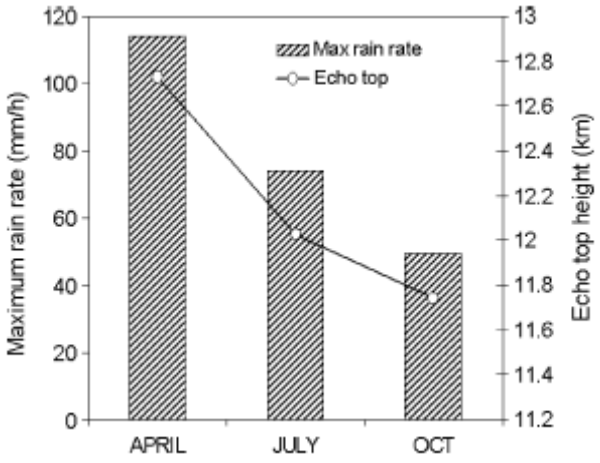

Figure 6.21. Maximum rain rates and echo tops are calculated by using 2A25 data in April, July and October

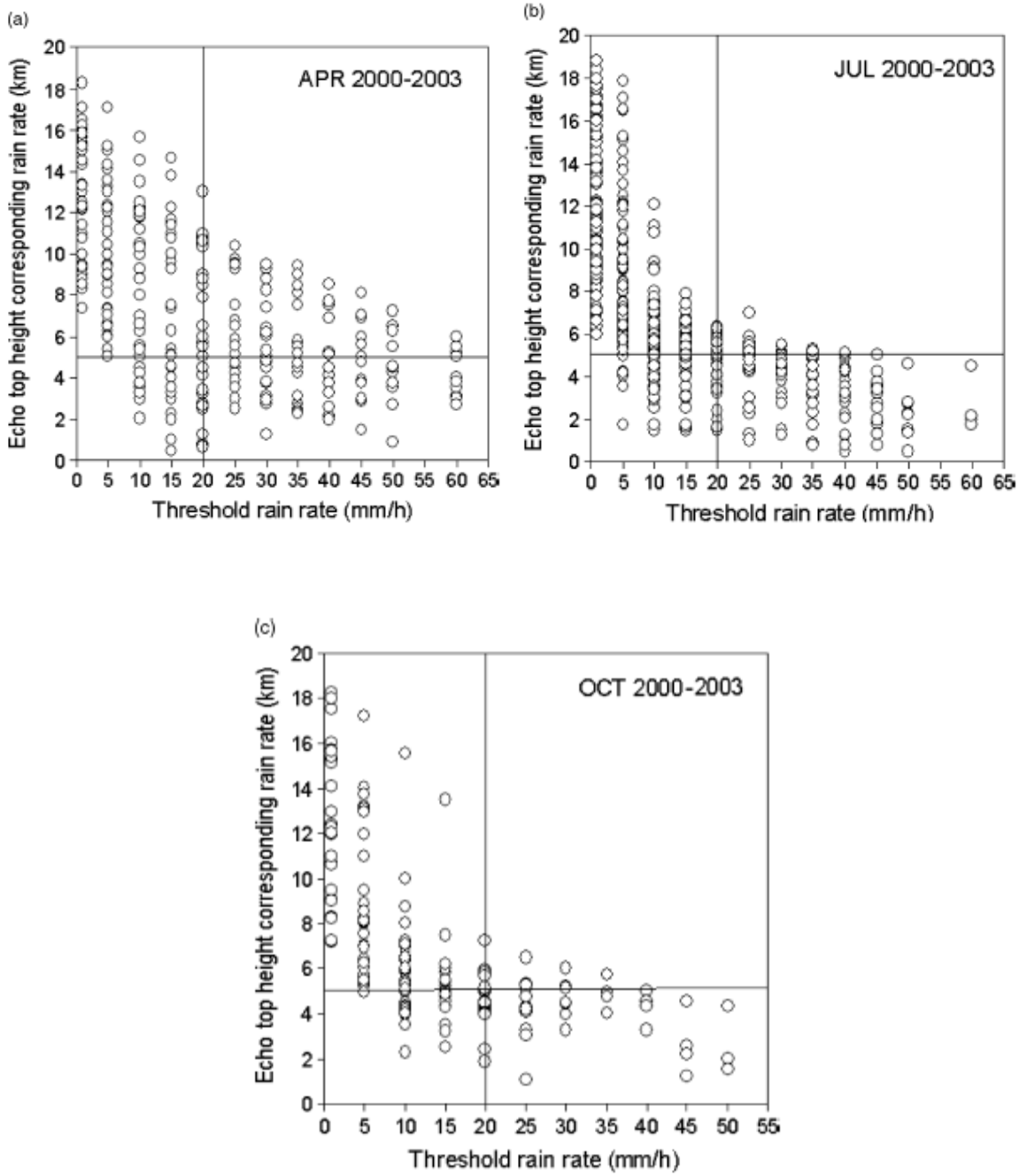

Figure 6.22. Echo tops calculated at different threshold rain rates by using 2A25 data in (a) April, (b) July and (c) October. The horizontal and vertical lines represent 5 km and 20 mm/h, respectively

Vertical extension of precipitation field determined by TRMM-2A25 in and around Bangladesh in different periods of 2001 is shown in Figure 6.23. Usually, intensified regions are embedded relatively higher altitudes for pre-monsoon echo (Figure 6.23a) compared to monsoon (Figure 6.23b) and post-monsoon (Figure 6.23c). On the other hand, less intensified regions are embedded at higher altitudes for monsoon and post-monsoon echoes compared to pre-monsoon.

The echo top heights versus threshold rain rates for April (14 cases), July (29 cases) and October (12 cases) in 2000 are shown in Figure 6.24. It is clear that 10 mm/h or higher rain rates are found from about 2 to 14 km for April whereas the same rates are found from about 2 to 7.5 km for July. In October, rain rates are comparatively lower than that of other months. These results are very consistent with the explanation of Figure 6.23.

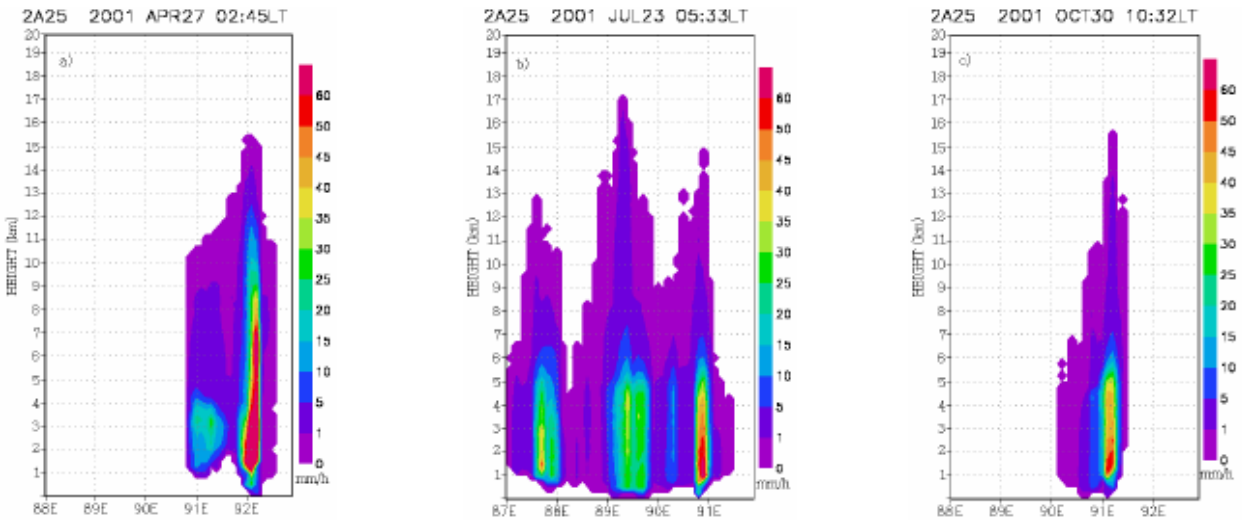

Figure 6.23. Vertical extension of precipitation field obtained by TRMM-2A25 a) 27 April over Bangladesh, b) 23 July and c) 30 October over Bay of Bengal in 2001

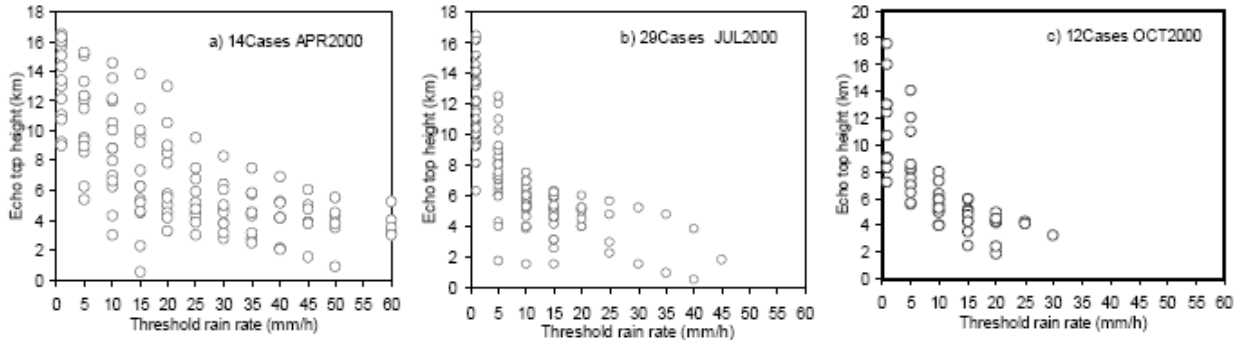

Figure 6.24. Echo top height at different threshold rain rates determined by TRMM-2A25 data in a) April, b) July and c) October 2000

The echo top height is about 16 km or higher for many cases in July and low rain rates are also found for some cases in April. The fact is that these depend on the development site, time and stage of the echo. The echo base and top height, maximum rain rate are tabulated in Table 6.4. From single scan of TRMM-2A25 data in a day, it is difficult to obtain the stage of the echo whether it is in developing, mature or dissipating.

Analyzing a number of cases as presented in Table 6.4, it is found that there are similarities in precipitation parameters in year to year and dissimilarities in month to month. Some exceptions are also found due to different stages, development sites and echo born-time. Averages from 4 years (2000-2003) data, it is found that echo base height is 0.45, 0.34, 0.57, echo top height is 12.73, 12.02, 11.74 and maximum rain rate is 114.19, 73.88, 49.28 in April, July and October respectively. Hence, rain rate is higher (lower) in pre-monsoon (post monsoon) month April (October) for all years. Echoes are developed at higher altitudes in post-monsoon period compared to other periods.

Table 6.4 Echo Parameters Determined By TRMM-2A25

	No Cases	Echo base height (km)	Echo top height (km)	Max rain rate (mm/h)
APR2000	12	0.34	13.23	120.58
APR2001	6	0.31	11.95	119.82
APR2002	8	0.78	10.96	100.71
APR2003	7	0.36	14.78	115.67
JUL2000	23	0.46	11.86	57.72
JUL2001	25	0.39	11.11	72.01
JUL2002	13	0.18	13.14	77.91
JUL2003	19	0.34	11.99	87.86
OCT2000	12	0.56	11.02	47.05
OCT2001	10	0.30	12.93	59.15
OCT2002	6	0.82	11.99	40.02
OCT2003	9	0.60	11.03	50.89

6.4 Study of Diurnal Cycle of Rainfall in and around Bangladesh (Objective 4)

In order to get the spatial pattern of the diurnal cycle in and around Bangladesh the frequency of occurrence of cloud activity are discussed first before discussing diurnal variations. The frequency of occurrence has been counted from the individual clouds and mesoscale convective systems. The details of the properties of precipitation areas related to cloud in Bangladesh are discussed in subsequent sections in this chapter.

6.4.1 Frequency of Occurrence of Cloud using GMS-5 Data

The frequency of occurrence (FO) of cloud calculated from GMS-5 hourly T_{BB} data for a large domain of 10°-30°N and 80°-100°E is described here. The FO of cloud activity calculated using the threshold temperature <263K (FO263) and <220K (FO220) at different hours averaged for June-July-August (JJA) 2000. During the evening (1800 LST) to midnight (0000 LST) the land of India is devoid of FO263 relative to Bangladesh and the north of the Bay of Bengal. During the morning (0600 LST) to noon (1200 LST) the situation is opposite. These are consistent with large amounts of percent high cloudiness <235K of infrared temperature (Zuidema, 2003). There is a noticeable contrast in FO263 over the ocean in between midnight and evening. Close to Andaman Islands, FO263 is significantly high during all hours. Deep convection (FO220) over the ocean increases from morning to noon and then decreases from evening to midnight. This is consistent with large amount of percent high cloudiness <210K of infrared temperature (Zuidema, 2003). In

Bangladesh, FO220 shows minima at noon, slightly significant in the morning. Hence it is found that over the north of the Bay of Bengal, FO220 and FO263 are high at noon and evening respectively. Over Bangladesh, both FO263K and FO220K are slightly high in the morning and evening. The FO220 for deep convection in close to Andaman Islands is not seen during evening to midnight.

The cloud embedded area (CEA) calculated using the same data set over the land and the ocean are shown in Figure 6.25 for the domain of 600 km × 600 km in and around Bangladesh. Below a certain size of CEA 70,000 km^2 the deep (shallow) convection dominates on the land and shallow (deep) convection dominates over the ocean. One can calculate FO 69 % on the land and 53 % over the ocean below CEA 50,000 km^2 for threshold temperature <214K. The percentages on the land and over the ocean become 28 % and 31 % respectively for the threshold temperature <243K. Above the CEA 35,000 km^2 the percentages are 17 % on land and 30 % over ocean for threshold temperature <214K, while 66 % on land and 56 % over ocean for threshold temperature <243K. Hence it is obvious that small size deep convection dominates on the land while small size shallow convection dominates over the ocean. In contrast, large size deep convection dominates over ocean and large size shallow convection dominates on the land. However, very large size shallow convection (CEA >170,000 km^2) is more frequent over the ocean than on the land. The existence of large deep convection and very large shallow convection over the ocean suggests that convection is much more organized and long-lasted over the ocean than on the land. This is consistence with the result of Zuidema (2003).

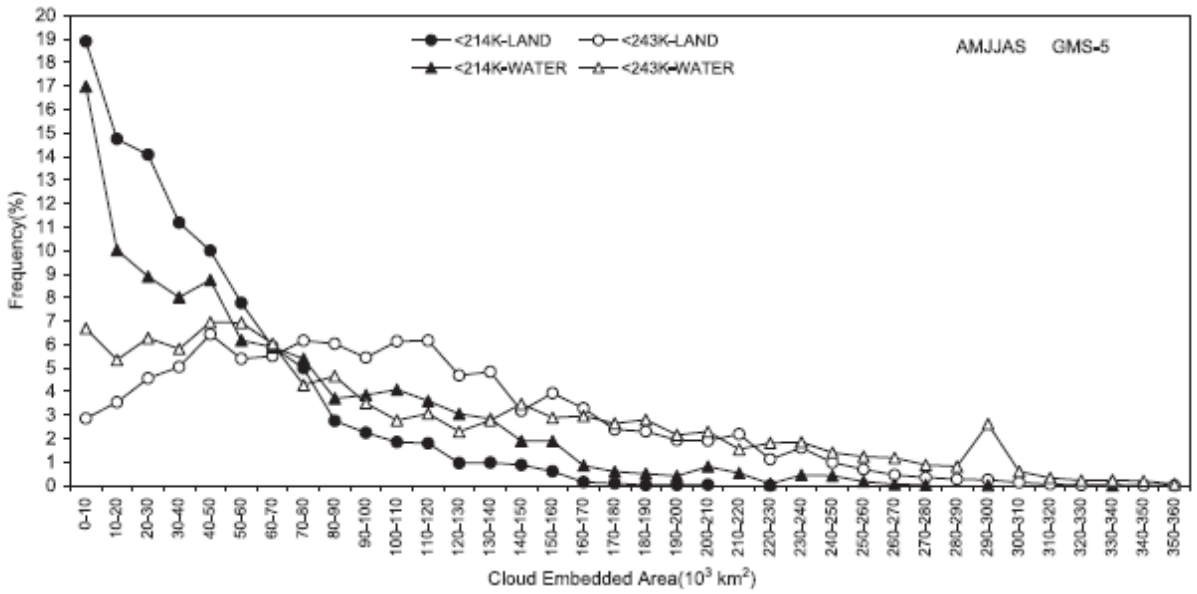

Figure 6.25. Cloud embedded area and frequency of occurrence of convection calculated from GMS-5 data over Bangladesh (land) and the north of the Bay of Bengal (ocean)

6.4.2 Diurnal Variations of CEA and FO using GMS-5 Data

Figure 6.26 shows the diurnal variation of cloud embedded area (CEA) calculated from GMS-5 data over the land and the ocean. The early morning and afternoon peaks are observed on the land. The shallow (<243K) convection dominates the former while both shallow and deep (<214K) convection dominates the latter. On the other hand, only afternoon peak is observed over the ocean. The afternoon peak of CEA over the ocean (87.44-93.33°E; 15.7°-21.08°N) in this analysis is consistent with Zuidema (2003, Figure 13-f) and differs from the large coverage of the Bay of Bengal. It is interesting to see that the peak of deep convection over the ocean is about 2 hours earlier than that of shallow convection. This suggests that the above time lag is necessary to change the status from convective cloud component to stratiform one. The time lag of 2 hours slightly differs from 1-1.5 hours reported by Anagnostou *et al.* (1999) for the Amazon region. The results of land and ocean of the present analysis differ from the conception that land areas have a much larger rainfall cycle than that of over the ocean, with a marked minimum in the mid-morning hours and a maximum in the afternoon (Nesbitt and Zipser, 2003). However, heavy rain events contributed to the night-time maximum precipitation over the western Pacific (Gray and

Jacobson, 1977), predawn maximum and afternoon minimum in the cold cloud cover and surface rainfall over most of earth's tropical oceans (e. g. Janowiak *et al.* 1994) are reported.

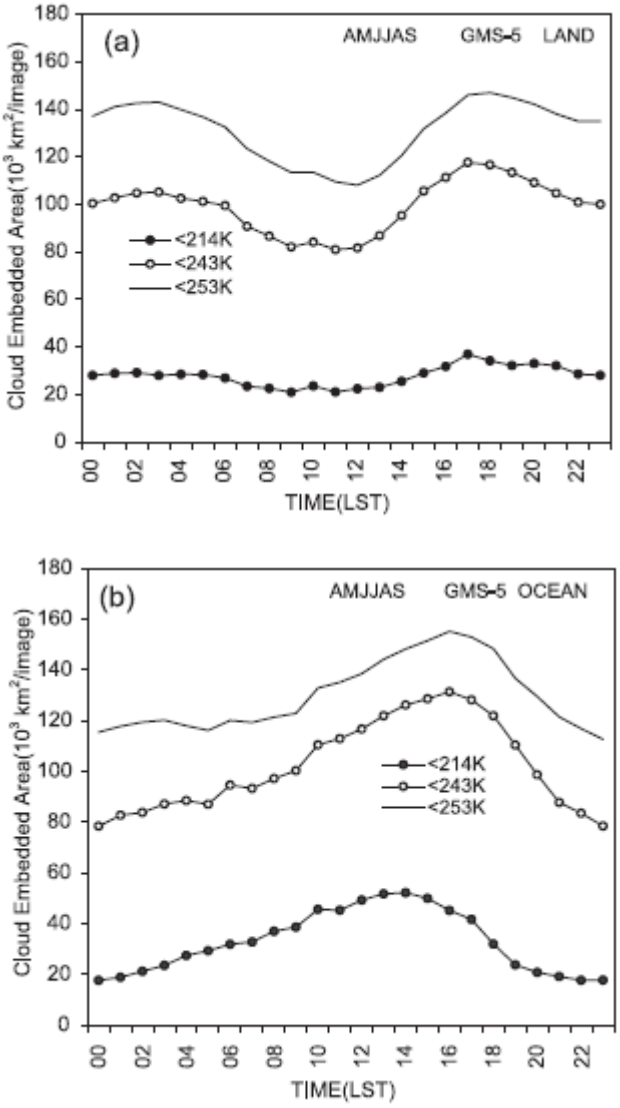

Figure 6.26. Diurnal variations of cloud embedded area (CEA) at different thresholds averaged for AMJJAS 2000 determined by Global IR over the land (upper panel) and the ocean (lower panel)

The frequency of occurrence (FO) on the land and over the ocean determined from GMS-5 data is shown Figure 6.27. The afternoon peak is observed on the land for both deep and shallow convection. The afternoon peak for FO indicates the initiation times of land-based clusters in Bangladesh and is consistent with Zuidema (2003). The afternoon peak of FO over the ocean is very clear for deep convection while a less sharp early morning peak is also observed. The

morning peak of AMJJAS is due to 0300 LST of April (not shown). The afternoon peak of CEA and FO over the ocean differs from morning rainfall as reported from TRMM result (TRMM report, 2002; Nesbitt and Zipser, 2003). The afternoon peak of FO in the analyzed ocean (87.44^0-93.33°E; 15.7°-21.08°N) differs from the initiation times of water-based clusters for the large coverage of the Bay of Bengal (Zuidema, 2003). Near-continent variations in the diurnal cycle have been linked to coastline effects and gravity wave forcing by the nearby continental diurnal cycle (Silva *et al.*, 1987; Yang and Slingo, 2000). Thus the result obtained in the present analysis encourages more analysis in the Bay of Bengal using long time series.

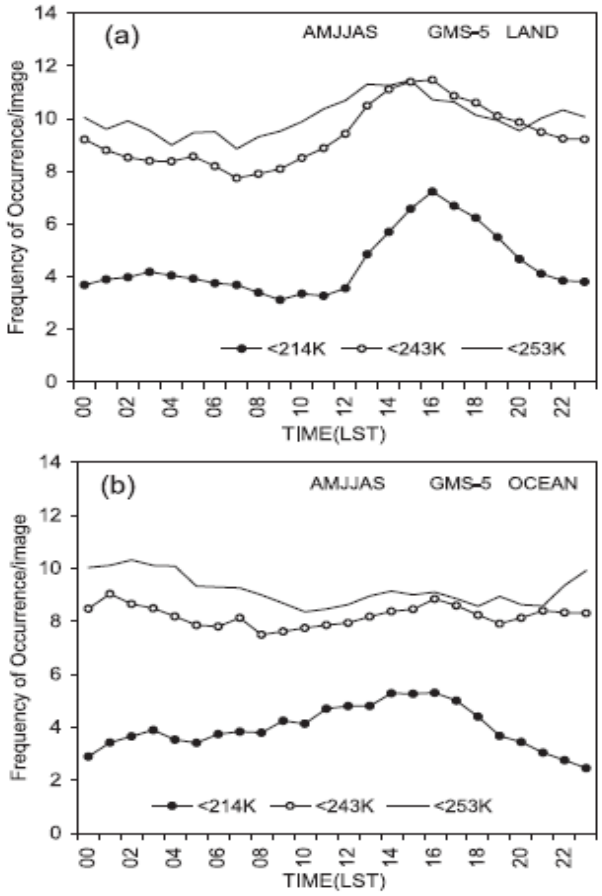

Figure 6.27. Frequency of occurrence at different thresholds averaged for AMJJAS 2000 determined by GMS-5 over the land (upper panel) and the ocean (lower panel)

6.4.3 Diurnal Variation of Precipitation Using TRMM Products

In and around Bangladesh, precipitation substantially varies with space and time as shown in Figure 6.28. Daily rainfall (mm/d) determined by TRMM-3B42RT averaged for 1 June to 31 September from 2002 to 2004 at 06 LST (left panel) and 18 LST (right panel) is shown in Figure 6.28. TRMM-3B42RT determines heavy rainfall in the northeast region of the Bay of Bengal at 06 LST. At this time the northern and the southern parts of Bangladesh, which are the heavy-rainfall regions in the country, also show high rainfall. At the same time, very low rainfall is observed over India. On the other hand, high rainfall over India and low rainfall over Bangladesh are observed at 18 LST.

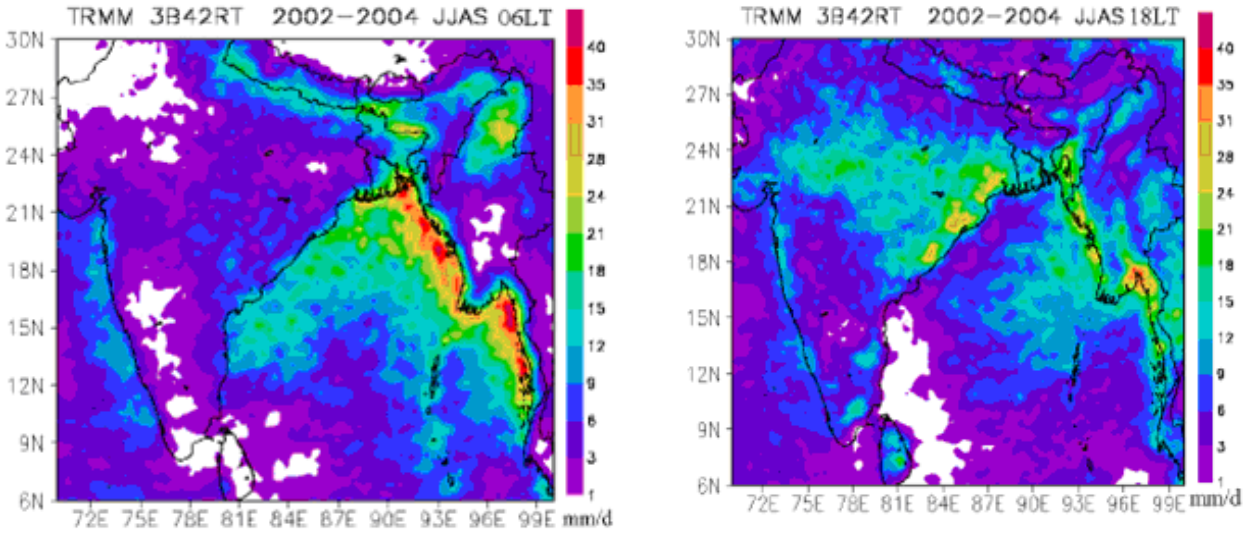

Figure 6.28. Diurnal variation of precipitation determined by TRMM-3B42RT at 06 LST (left panel) and 18 LST (right panel) during monsoon period (JJAS)

Daily rainfall at different hours in different seasons obtained by TRMM-3B42RT and RG averaged for 33 locations over Bangladesh and from 2002 to 2004 is tabulated in Table 6.5. Daily rainfall determined by TRMM is higher than the same determined by RG in pre-monsoon. In monsoon, TRMM underestimates rainfall while in post-monsoon TRMM measures almost similar to RG. These deviations come from different intensities of precipitation at various altitudes in corresponding periods in and around Bangladesh.

Table 6.5 Rainfall (mm/day) Determined by Rain-Gauge (RG) and TRMM-3B42RT in Different Periods and Averaged from 2002 to 2004

LT	RG MAM	3B42RT MAM	RG JJAS	3B42RT JJAS	RG ON	3B42RT ON
00	5.97	10.90	9.62	10.64	3.65	2.67
03	6.63	8.28	13.94	13.74	4.83	2.70
06	7.01	6.96	19.08	16.33	5.93	5.06
09	5.97	6.35	17.03	13.12	4.99	5.03
12	5.12	6.40	15.89	11.10	5.20	5.12
15	5.39	6.99	16.73	14.26	7.99	5.14
18	5.75	9.29	13.76	11.60	7.49	3.56
21	6.26	9.60	9.48	8.38	5.25	3.45
Daily	6.01	8.1	14.44	12.4	5.67	4.09

Figure 6.29 shows the diurnal variation of rainfall (mm/day) determined by TRMM-3B42RT and RG in pre-monsoon (upper panel), monsoon (middle panel) and post-monsoon (lower panel) periods. Rainfalls are obtained by averaging from 33 stations (2002–2004) in corresponding periods. In pre-monsoon, rainfall dominates from evening to early morning whereas monsoon rainfall dominates from morning to afternoon. In the case of post-monsoon, rainfall dominates during day time. The patterns of the variation of rainfall determined by both TRMM and RG are almost similar.

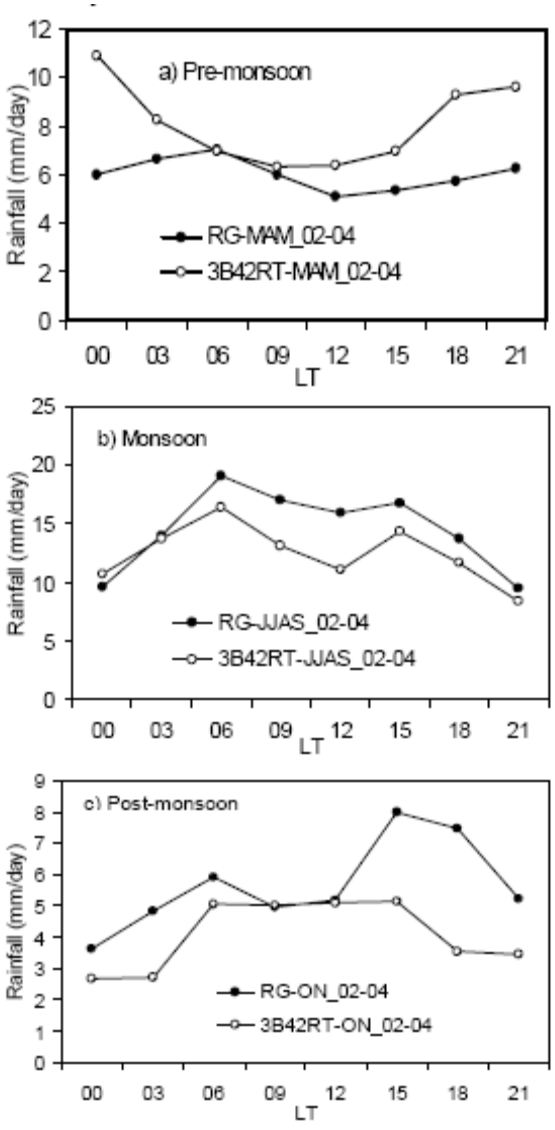

Figure 6.29. Diurnal variation of rainfall determined by TRMM-3B42RT and RG

For the entire rainy season (March to November), diurnal variation of rainfall (mm) determined by TRMM-3B42RT and RG averaged for 33 stations and from 2002 to 2004 (Figure 6.30), shows the maximum rainfall in Bangladesh occurred at 06 LST and the secondary maximum rainfall peak appeared at 15 LST.

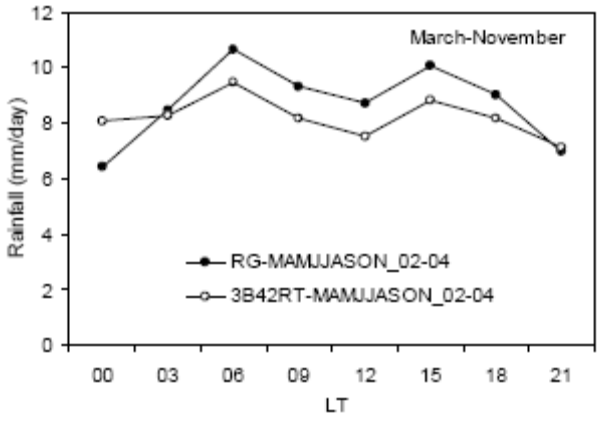

Figure 6.30. Averaged diurnal variation of rainfall for the entire rainy season determined by TRMM-3B42RT and RG

6.4.4 Diurnal Variations of Convection in Bangladesh using Radar Data

The diurnal variation of echo embedded area (EEA) determined by Dhaka radar accumulation over radar coverage in all analyzed months is shown in Figure 6.31(a). The EEA shows a clear morning maximum at 0600 LST for April-August. This morning maximum is obviously dominant in pre-monsoon and monsoon months while pre-monsoon months are more prominent. In addition, a secondary peak is observed for peak monsoon-months (JJA): afternoon peak at 1500 LST for July and August while evening peak is at 1800 LST for June. The morning (0600 LST) maximum EEA for AMJJA is different from the afternoon maximum rainfall, over most of South and Central America (Mapes *et al.*, 2003a; Warner *et al.*, 2003). It is also different from the evening (1800 LST) maximum cloudiness amount to the west of Bangladesh, over India (Zuidema, 2003; Figure 14). Short and Wallace (1980) also found an evening maximum in cold clouds over tropical islands, mountains and plateaus, but little variation over lowlands and basins. Nocturnal rainfall maxima over land in Africa, southern and eastern Asia, Indonesia and northern Australia are reported by Ramage (1971 and references therein) and others. The night/morning maximum of rainfall across the west coast of Colombia is reported by Warner *et al.* (2003). The highest morning maximum of coastal convection in the northern South America is also reported by Anagnostou *et al.* (1999). Regional studies of other parts of the tropics, e. g. over the Atlantic Ocean and tropical Africa (Machado *et al.* 1993; Duvel 1989), over the western Pacific (Albright *et al.* 1985), over the eastern Atlantic (McGarry and Reed 1978), reported various diurnal

behaviors in terms of observed times and amplitudes of the diurnal maximum and minimum occurrence of precipitation and/or cold cloud cover. Gray and Jacobson (1977) found a pronounced afternoon maximum in moderate rains over Africa in general, but no such pattern over South America. These regional differences are probably related to the specific regional environment that influences the initiation and life-cycle of the cloud systems (Chen and Houze, 1997).

Figure 6.31(b) shows frequency of occurrence (FO) of convection obtained from Dhaka radar data. The FO shows morning peak at 0600 LST and afternoon peak at 1500 LST: pre-monsoon (AM) convection dominates the former while peak-monsoon (JJA) convection dominates the latter. Both morning and afternoon peaks are equally strengthening for AMJJA while individual month shows different situations: July and August show strong peak in the afternoon, May shows strong peak in the morning, while April and June show strong peak in the midnight instead of morning one. This clear distinction of the dominant months and peak time, using data coverage of over the whole country, is reported in greater details in this comprehensive analysis. Afternoon peak of FO is prominent than that of EEA. This result implies that smaller echoes dominate in the afternoon while larger echoes develop in the early morning.

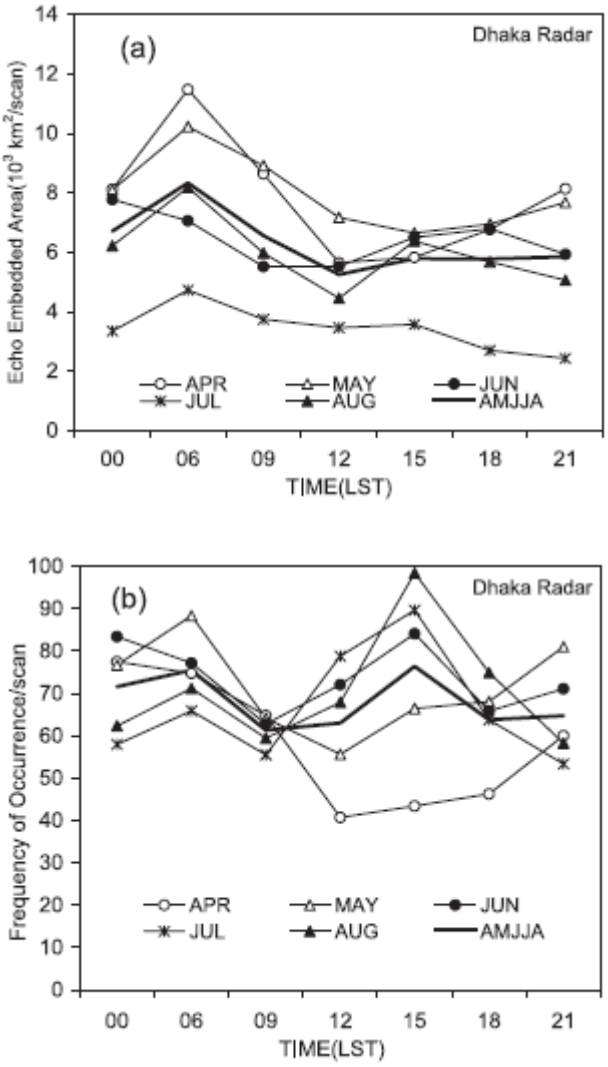

Figure 6.31. Diurnal variations of (a) echo embedded area (upper panel) and (b) frequency of occurrence of convection (lower panel) determined by Dhaka radar in different months of 2000

6.4.5 Regional Variation of Precipitation using Radar Data

Figure 6.32 gives the areal averaged precipitation rates determined by BMD radar in the three predefined regions. The rate has the maximum value at 00-06 LST in the Northern, at 06 and 15-18 LST in the Central, and at 06 LST in the Southern regions. These times are consistent with the results reported by Ohsawa *et al.* (2001) in an analysis of rainfall in Bangladesh but differ from the general characteristics reported for inland rainfall (e. g., Gray and Jacobson, 1977; Riehl, 1978; Meisner and Arkin, 1987; Al-bright *et al.*, 1985; Short and Wallace, 1980; Mapes *et al.*,

2003; Warner *et al.*, 2003). In reality, the precipitation rates in the Northern and Southern regions tend to be much higher because these regions are beyond the BMD radar effective radius (250km). At any rate, the time of maximum rate is very important for determining exact diurnal variations in the tropical convective activity that developed in those regions. Details of diurnal cloud activity variation in Bangladesh are discussed in Islam *et al.* (2004). The nature of the diurnal precipitation cycle in Bangladesh is a morning peak at 0600 LST and a minimum at noon.

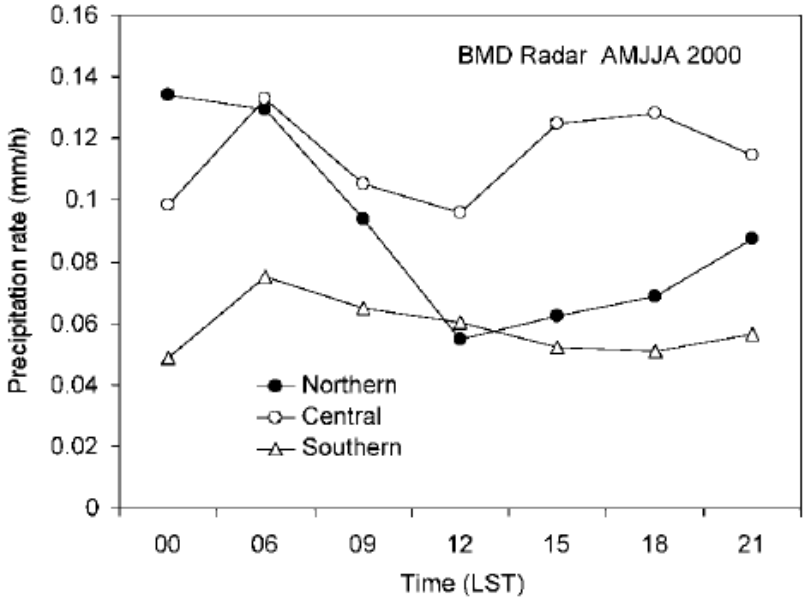

Figure 6.32. Precipitation rates (mm/h) determined by the BMD radar at three regions in Bangladesh. Averages for 16 April to 30 August 2000 (AMJJA 2000)

In order to check regional monthly rainfall, we divided the total radar data coverage (600 km × 600 km) into 9 sectors, each having 200 km × 200 km, denoted by C, E, W, N, S, NE, SE, NW, and SW, as shown in Figure 6.33. The arrows represent the time of maximum rainfall in each sector during 16 April to 30 August (i.e. radar operation months). In each sector, the monthly rain rate is averaged over all pixels including rainless pixels. The times of the maximum rainfall in each sector are shown with the vectors. The N and NE sectors show the maximum rainfall at 00-06 LST, which is caused by influence of the Shillong hill (Prasad, 1974; Ohsawa *et al.*, 2001). The evening rainfall at 18 LST in the western sectors reflects the influences of the land characteristics of India. In the S and SE sectors, rainfalls from 06 to 12 LST are dominative.

The coastal region in the S and SE sectors includes both land and water area. Contrast between land and water influences the diurnal cycle in the coastal regions. This geographical complexity in the coastal region likely makes differential characteristics of cloud activities over the Bay of Bengal (Zuidema, 2003). He showed that the coastal-region rains are brought by small- and medium-sized convections from the Joint Air-Sea Monsoon Interaction Experiment (JASMINE; Webster *et al.*, 2002).

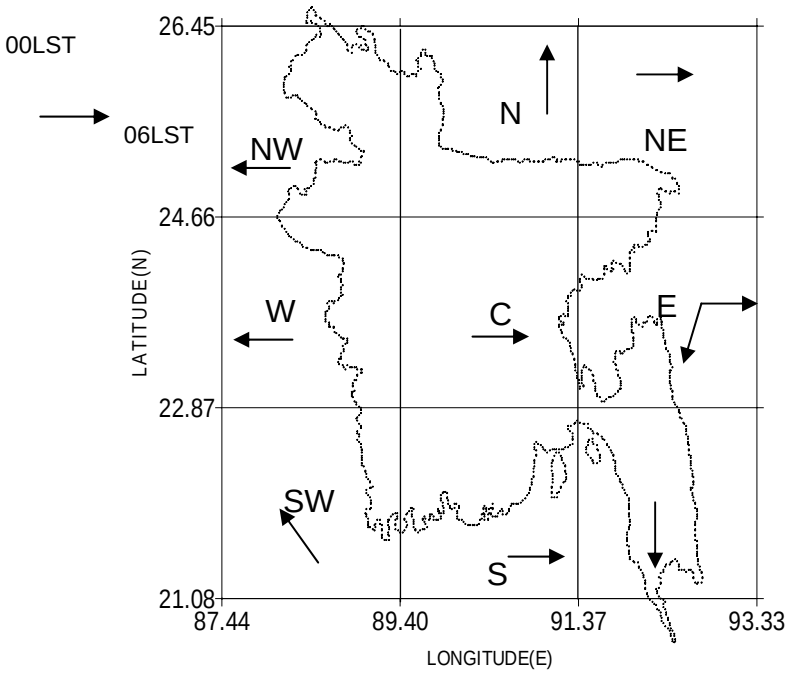

Figure 6.33. Time of Maximum Rainfall in Each Sector of Radar Operation Period (16 April-30 August 2000)

The Figure 6.34 shows that the rain rate in the C, S, E, NE and N sectors are larger for almost all months, and the N and E sectors are especially high rain rate regions as shown in Figure 6.32. As seen in Figure 6.34, the rain rate in July is less than that in other months, while the S sector shows the maximum rainfalls in this month. It is evident that the rain rate during the pre-monsoon months (AM) is higher than in the peak-monsoon months (JJA). It is one of characteristics of precipitation in this region.

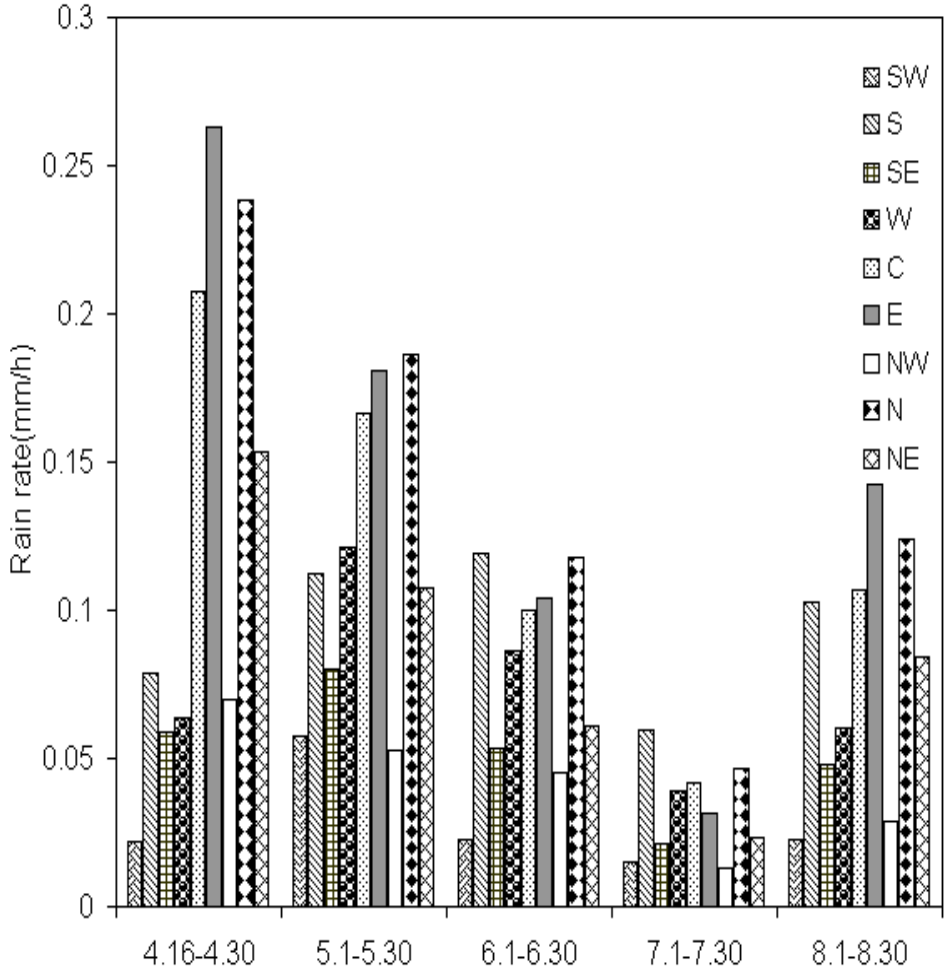

Figure 6.34. Rain rate (mm/hr) estimated by radar for different months in 2000 in different sectors. The arrows represent the time of maximum rainfall in each sector of whole analysis period (16 April-30 August 2000)

From the rain observations of the TRMM PR, precipitation dominates in the afternoon over land and in the morning over water near coasts (TRMM report, 2002). However, eastern areas of Bangladesh show the maximum precipitation in the morning at 06 LST, which is different from the Indian Subcontinent and mountain ranges. This difference could be caused by the geographical features of Bangladesh which is a flat wetland with many ponds, marshes, and rivers. Additionally, most frequency of rainfall from 21 to 09 LST is observed in the northern, eastern and southern regions. It is possibly linked to the local effects such as complex terrain or sea and land breeze circulations.

6.5 Develop a Statistical Procedure to Determine Ground Based Radar Rain Algorithm Parameters in Bangladesh (Objective 5)

6.5.1 Introduction

The standard Z-R relationship (power law: $Z=200R^{1.6}$) used in this analysis may contribute to lower rain rate of the radar analysis. Best-fit Z-R relationships for different geographical features are provided by many previous studies (Steiner *et al.*, 1995; Rosenfeld *et al.*, 1995; Ciach *et al.*, 1997). The rainfall estimates vary with the parameters (200 and 1.6) in power law, which are dependent on local climatic conditions (Iguchi *et al.*, 2000). At present, it is difficult to find the best-fit Z-R relationship for Bangladesh using data of one-season. A statistical approach has been established to find the best-fit Z-R relationship and the error statistics associated with ground radar rain estimation.

6.5.2 Error Statistics of Rain-Gauge Clusters

Table 6.6 shows statistics of the rain gauge data represented by cluster. The statistics include (1) record completeness that is the portion where all gauges for a given cluster are reporting a measurement; (2) unconditional mean and standard deviation of rainfall recorded by each cluster; and (3) statistics showing the representativeness of a single gauge to the cluster's mean values. One of the statistics is the rain detection frequency, which represents the number of times a single gauge would measure non-zero rainfall occurring in the cluster's mean value. Considering that the cluster mean represents as close as possible the area average rainfall, the intent of this analysis is to understand the effect of rain intermittence in single gauge measurements, which with their near point sampling may often observe zero rainfall when coincident radar pixel average rainfall estimates are non-zero. The second statistical measure is the standard error of single gauge rainfall measurement with respect to the cluster mean value. With this conditional statistical measure we attempt to evaluate the effect of small-scale rainfall variability (or else spatial rain de-correlation) in representing radar pixel size area rainfall by single gauge rain measurements. Both statistics show that a single gauge measurement is not an accurate representation of rainfall averaged at the scale of a typical radar grid resolution (e.g., 2.5 km x 2.5 km). It is shown that a single gauge would detect between 60 % and 70 % of the rainfall detected by the cluster average

within a minute, while the standard error of its detected rainfall could be up to 61 %. Averaging at higher time scales reduces this uncertainty significantly.

Table 6.6 Statistics Presented for the Three Gauge Clusters

Cluster Number	**#1**	**#2**	**#3**
Number of gauges	19	16	10
Range from Gr. Radar (km)	100	150	250
Completeness of record (%)	82	85	94
Standard deviation (mm/h)	3.6	3.6	3.1
Rain detection frequency (%)	59	62	70
Standard error (%)	45	61	54

The 50 % quantile of the radar rainfall has been calculated for each rain gauge cluster to show the gauge rainfall cumulated over time. The quantiles of radar rainfall have been computed within 5 % of the 50 % quantiles. For comparison purpose, the 10 % and 90 % quantiles have also been calculated and presented on the same graph. Figure 6.35 shows the cumulative distribution of radar and rain gauge rainfall. Figure 6.36 shows the correlations between the stations in the cluster as a function of time.

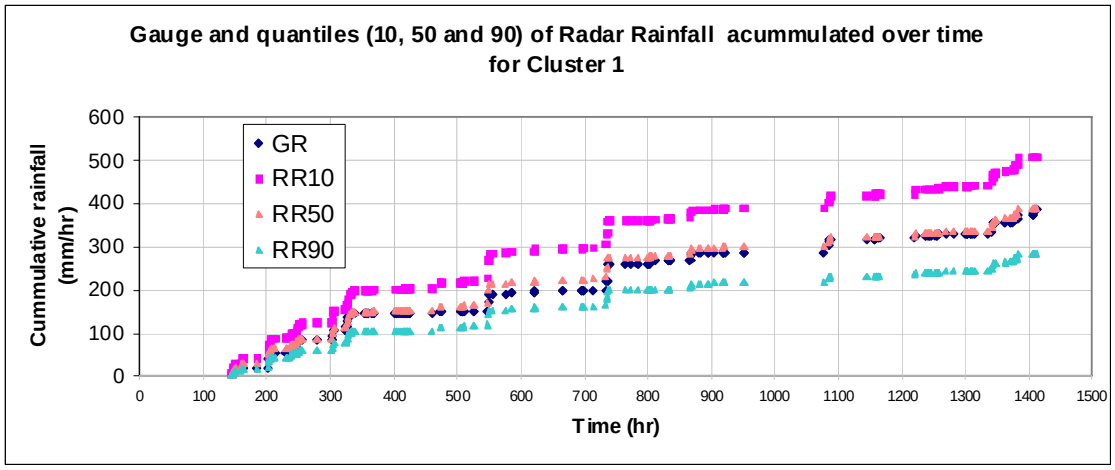

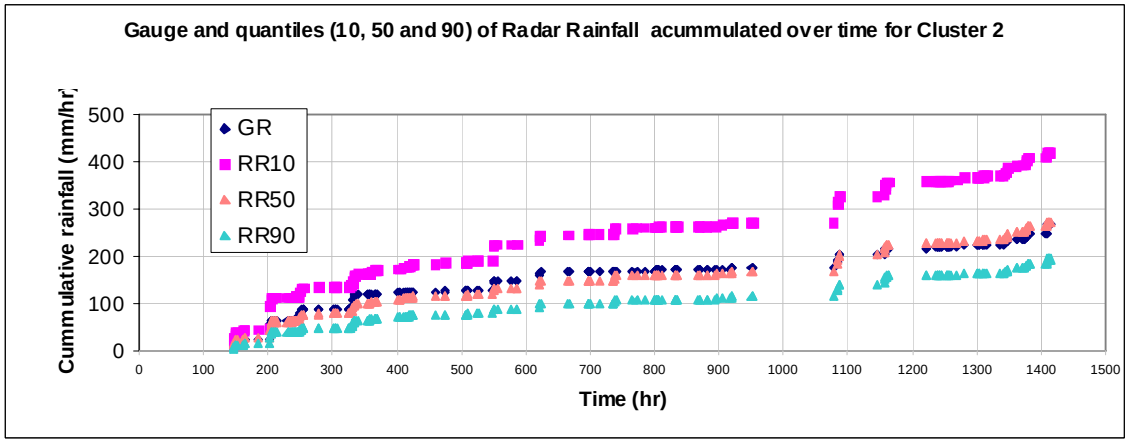

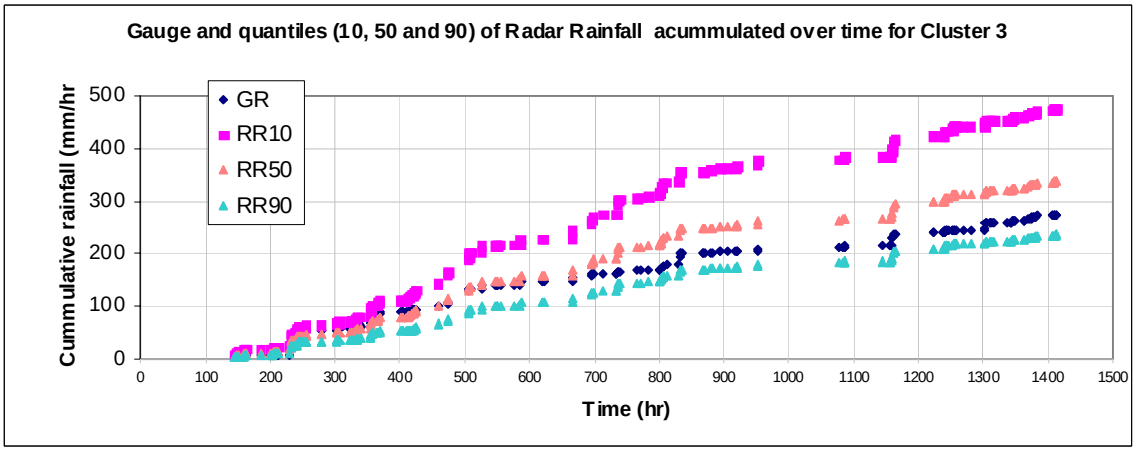

Figure 6.35. Cumulative Distribution of Radar and Gauge Rainfall

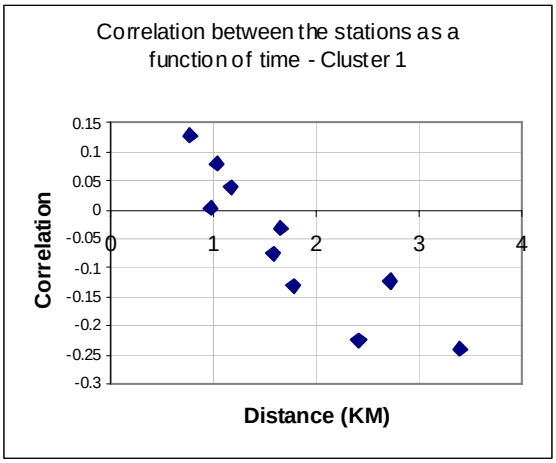

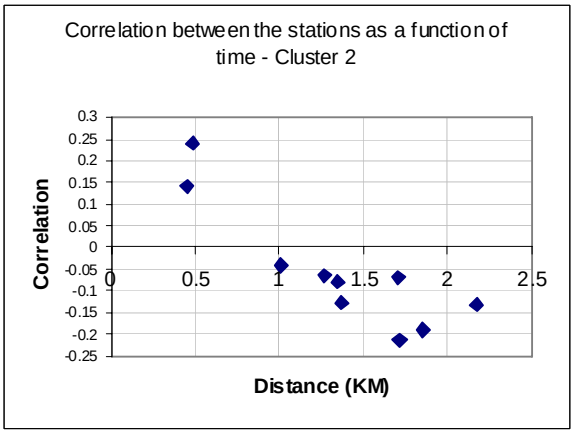

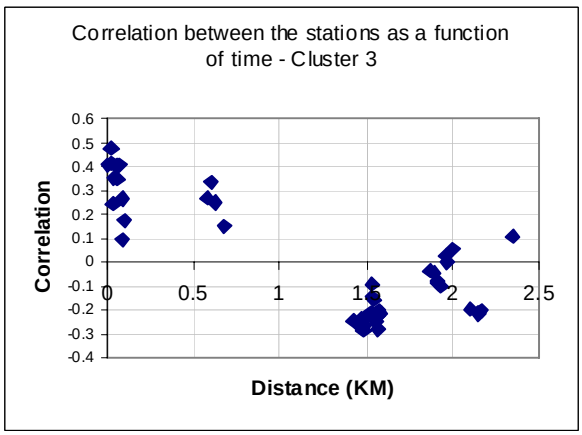

Figure 6.36. Correlations between the Stations in Gauge Cluster

Root mean square errors between radar and gauge rainfall distribution for different quantiles are calculated and shown in Figure 6.37. In cluster 1, the rms error at 50 % quintile is zero (0) but it gets higher with a consistent rate at lower and upper quantiles (e.g. 10 % and 90 %). In cluster 2, the rms error at 50 % quantile remains zero (0) but the rms error at lower quantiles (e.g. 10 %) get higher than the upper quantiles. On the other hand, the rms error shows zero (0) at 75 % quantile in cluster 3 and the rms errors are very high (i.e. 15 or higher) at lower quantiles and very low in upper quantiles (i.e. 5 or lower). It is concluded that the distance between gauge clusters and radar location control the rms errors.

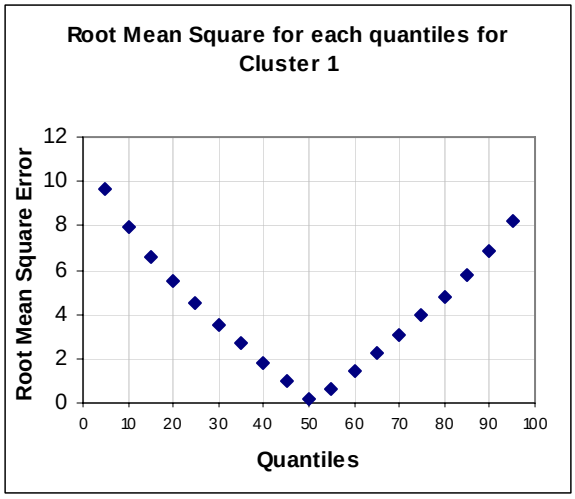

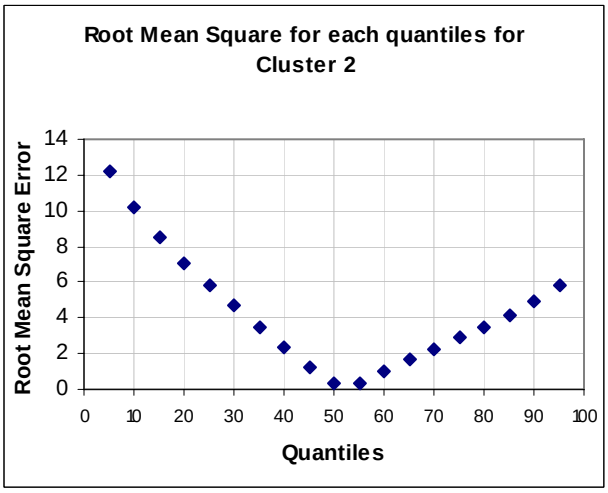

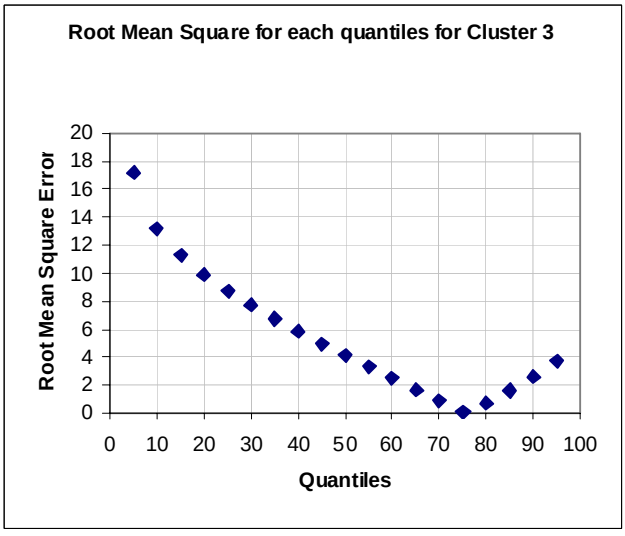

Figure 6.37. RMS Error between Radar and Gauge Rainfall Distribution

The quantiles of radar rainfall +/-5 % of the 50 % quantiles have been computed. The procedure for excedence probability has been demonstrated in Figure 5.2 with a flow chart. The excedence probabilities of radar with respect to the gauge rainfall are shown in Figure 6.38 for each cluster.

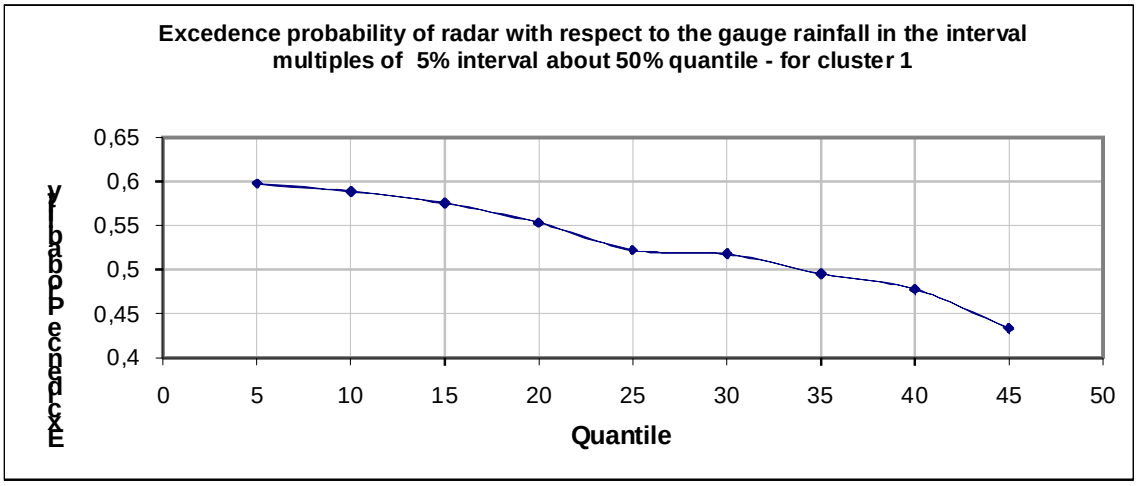

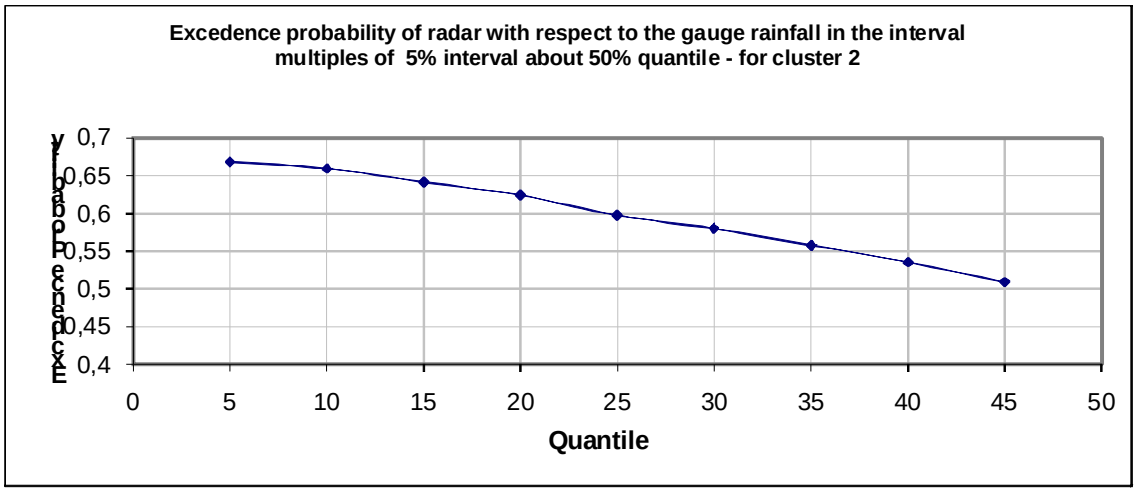

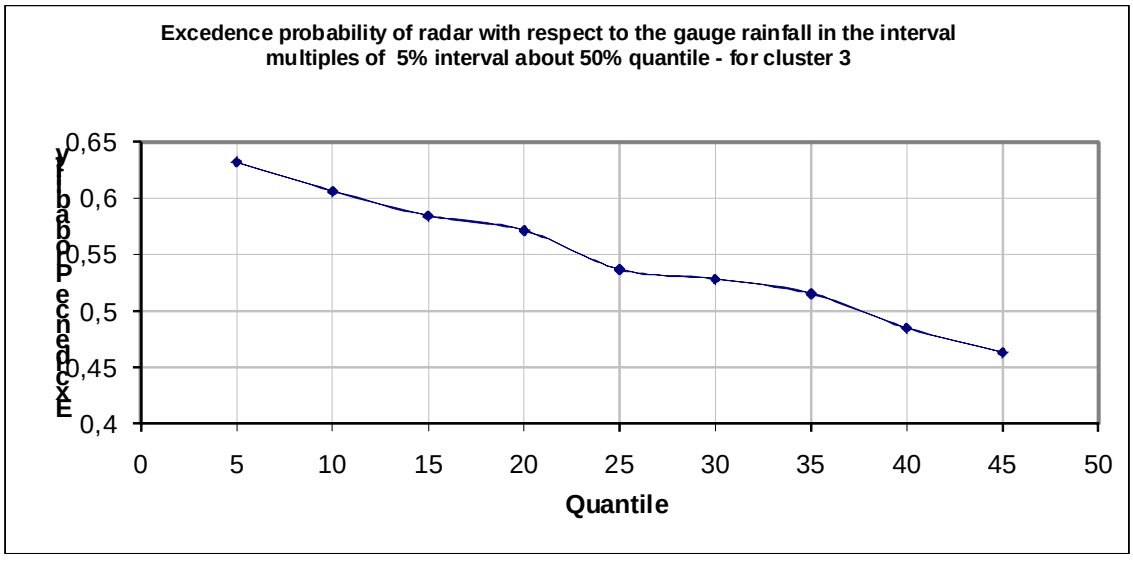

Figure 6.38. Excedence Probability of Radar with respect to the Gauge Rainfall

The error in the calculation of the excedence probability has been shown in Figure 6.39 by plotting the histogram of the number of times the radar exceeded the confidence interval for various variances computed at each time of observations.

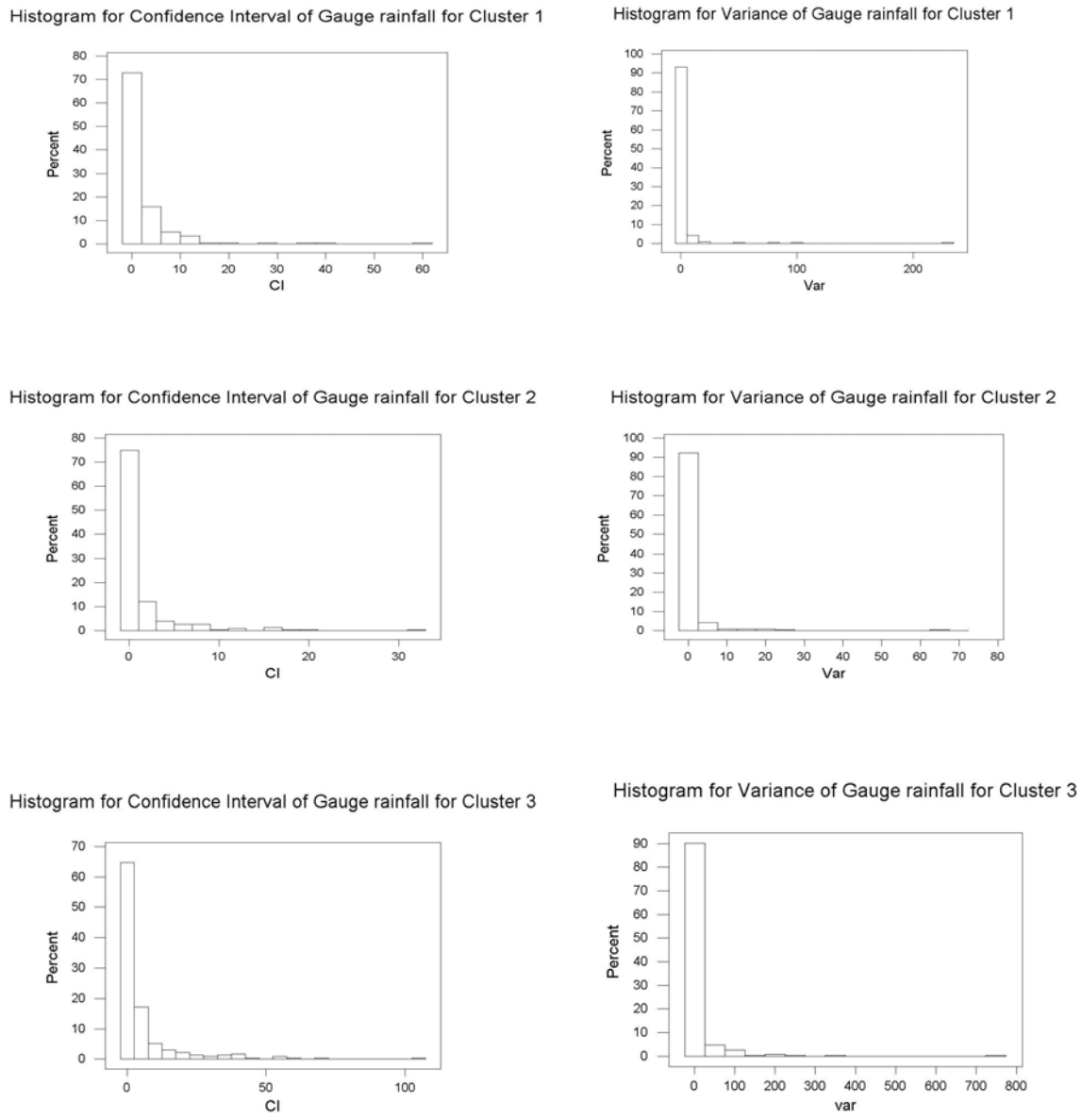

Figure 6.39. Histograms for Confidence Interval and Variance of Gauge Rainfall

6.5.3 Radar Algorithm Parameter Estimation and Error Adjustment

The errors in radar rainfall estimates are associated with reflectivity measurement error and reflectivity rainfall rate (*Z-R)* conversion error. Even if these two sources of error have been corrected based on an understanding in the physical processes of both the reflectivity measurements and the conversion of reflectivity to rainfall rate, there remains error in the radar rainfall estimates when compared to rain gauge measurements. This is because of the differences between the two rainfall measuring sensors. A rain gauge measures point rainfall continuously at the ground while radar measures areal rainfall of a radar size for a specified temporal resolution at some height above the ground. Additionally, changes in rain drops size distribution in both space and time have a different effect on the corresponding rainfall. These residual errors will often produce a uniform multiplicative bias in radar rainfall estimation when compared to rain gauge data (Anagnostou *et al.* 1998; Krajewski and Smith 2002).

An attempt has been made to determine the radar parameters for Bangladesh. The mean-field systematic error (bias) adjustment is applied to the rainfall estimates to account for some variations in the Z-R relationship. The mean and variance are determined as described in section 5.6.3. Parameter A is assigned an arbitrary constant (i.e., 200) since its value is adjusted every hour through the mean-field bias coefficient, while parameters Q and R_M were estimated as part of the stochastic filtering/updating approach described in section 5.6.3. Consequently, implementation of the radar rain algorithm in radar data required evaluation of three free parameter values, namely Z_{min}, B and bc. The parameter estimation is formulated as an optimization problem with cost function defined as root-mean-square (rms) difference of radar and rain gauge hourly accumulations. Finally, the radar algorithm parameters for Bangladesh are optimized and shown in Table 6.7.

Table 6.7 Radar Rain Algorithm Parameter Values

Parameters Description	**Value**
Z-R relationship exponent, B	1.37
Convective rain multiplier, b_c	2.1
Lower reflectivity threshold, Z_{min}	13 dBZ
Bias model variance, Q	0.3
Bias observation error variance, R_M	1.4
Z-R relationship constant, A	265

The rainfall estimation from the method of Z-R relation yielded the largest mean relative error of 43.8 % among the selected algorithms. After adjustments were made to the radar estimated precipitation from Z-R relationship by using rain gauge measurements, the precision of radar rainfall estimations were improved dramatically from average calibration, radar-gauge adjustment, and Kalman filter approach. Especially Kalman filter approach shows much consistent features than ever before. The mean relative error with average calibration, radar-gauge adjustment and Kalman filter approach is respectively 14.5 %, 10.2 % and 7.9 %. The correlations between radar and gauge rainfall for different approaches are 0.584 (not corrected i.e. before error adjustment), 0.902 (with error adjustment but without filtering) and 0.963 (corrected with Kalman filtering) (see Figure 6.40). It was found that the spatial rainfall distributions from the method of Z-R relation were in good consistence with those interpolated by rain gauge network measured precipitation to a large extent, however, the intense rainfall location centers exhibit different patterns compared with those interpolated with rain gauge network measurements. After adjustments were made to the radar estimated precipitation by using in site measurements with the automatic rain gauge networks, radar rainfall estimations were improved dramatically on precision either in the spatial distribution or in the location of intense precipitation centers.

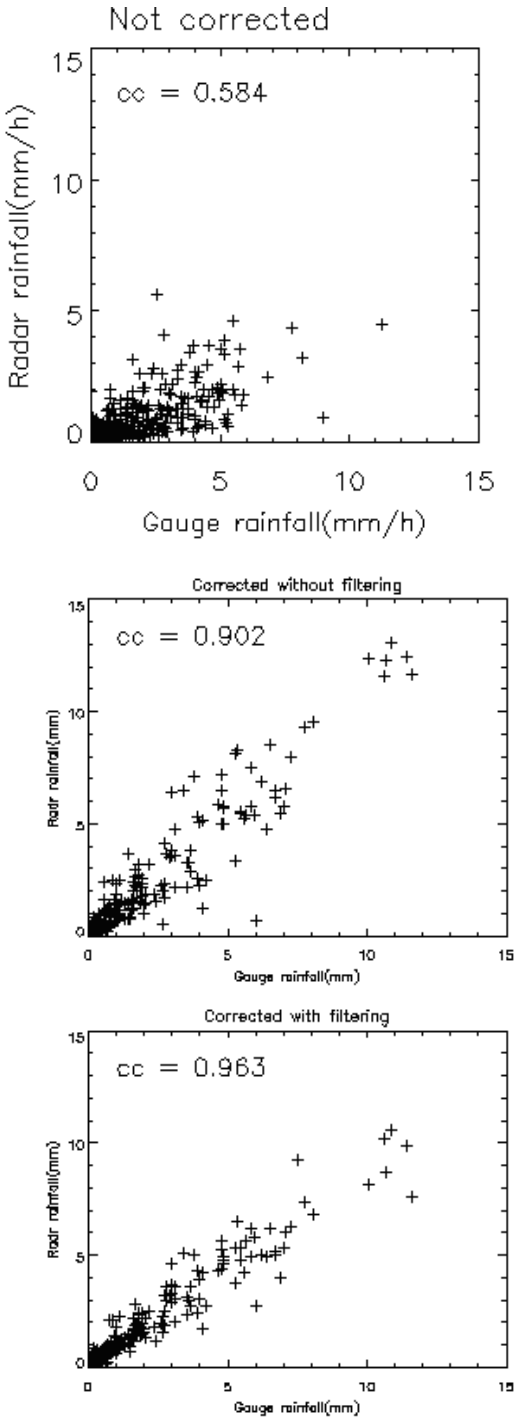

Figure 6.40. Radar Rain Bias Correction using Kalman Filter Technique (a) Before error adjustment, (b) error adjustment, (c) Kalman Filter applying

6.6 Investigate Calibration Procedure of TRMM Satellite based Rain Retrieval over Bangladesh (Objective 6)

6.6.1 Introduction

TMI-2A12 rain algorithm developed by Kummerow *et al.*, 2001 and the NN scheme developed by Grecu *et al.* 2001 were applied over US and GBM (i.e. Bangladesh) regions in order to understand the performance of both schemes. TRMM PR rain estimate were used to improve the calibration of passive microwave (i.e. TMI) algorithm for precipitation estimation at the radiometer footprint scale over Bangladesh. In this study, a passive microwave (PM) calibration scheme developed by Grecu and Anagnostou (2001) has been investigated. This algorithm is known as neural network based scheme which identifies rain/no-rain area and delineates the convectic and stratiform rain types. Finally, multiple linear regressions are used to relate PR rain and TMI brightness temperatures. A flow chart for Passive Microwave based rain algorithm steps are given in Figure 5.7 and further procedures are explained in Section 6.6.3 in this chapter.

6.6.2 TRMM Rain Algorithm Performance

Figure 6.41 shows comparisons of the probabilities of rain detection failure, conditional to a varying PR rain threshold for the two regions. Rain retrieval from TRMM TMI 2A12 (v.5) product is also included for comparison. The GBM region is the worst particularly for the TMI-2A12 product.

As a result, TMI-2A12 rain product can not be used for the GBM region because over there its rain detection is very poor. Rain Comparing the results for two different regions, it has been observed that the GBM region is distinct from USA. The main reason could be that summer rain for this region comes mainly from extensive mid-level stratiform clouds, and the algorithm's performance is not good for this type of clouds.

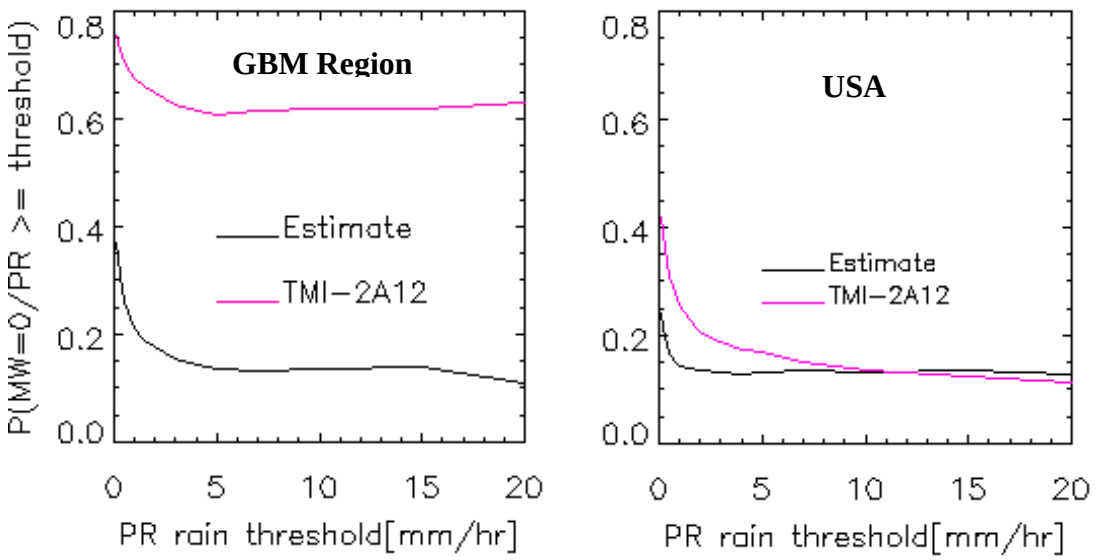

Figure 6.41. TMI rain detection failures as function of PR rain threshold. 'Estimate' is estimated and'TMI-2A12' is surface rain from TRMM 2A12 Ver5.0

In an attempt to explain these differences we make use of the 3D-reflectivity data from PR product 2A25. 2A25 has, as one of the many parameters, attenuation corrected reflectivity from surface to 20 km at a vertical resolution of 250 meters. To make full use of these data we plot the Contoured Frequency by Altitude Display (CFAD) for each region as given in Figure 6.42. We also make use of PR 2A23 rain type classification to display the stratiform and convective rain types separately. This will give more information than plotting the whole data together. Comparing Figure 6.41 and Figure 6.42, we observe that regions with higher detection error are those regions where stratiform rain is dominant, or constitute a significant proportion.

Here the cloud system is dominated by medium level stratiform clouds. The vertical extent of the convection of GBM region is similar pattern as compared to US region. Though not as dominant as the GBM region, mid-level stratiform clouds are also very significant in the USA. In both cases, the more dominant is the convection in Figure 6.42, the less the detection errors in Figure 6.41.

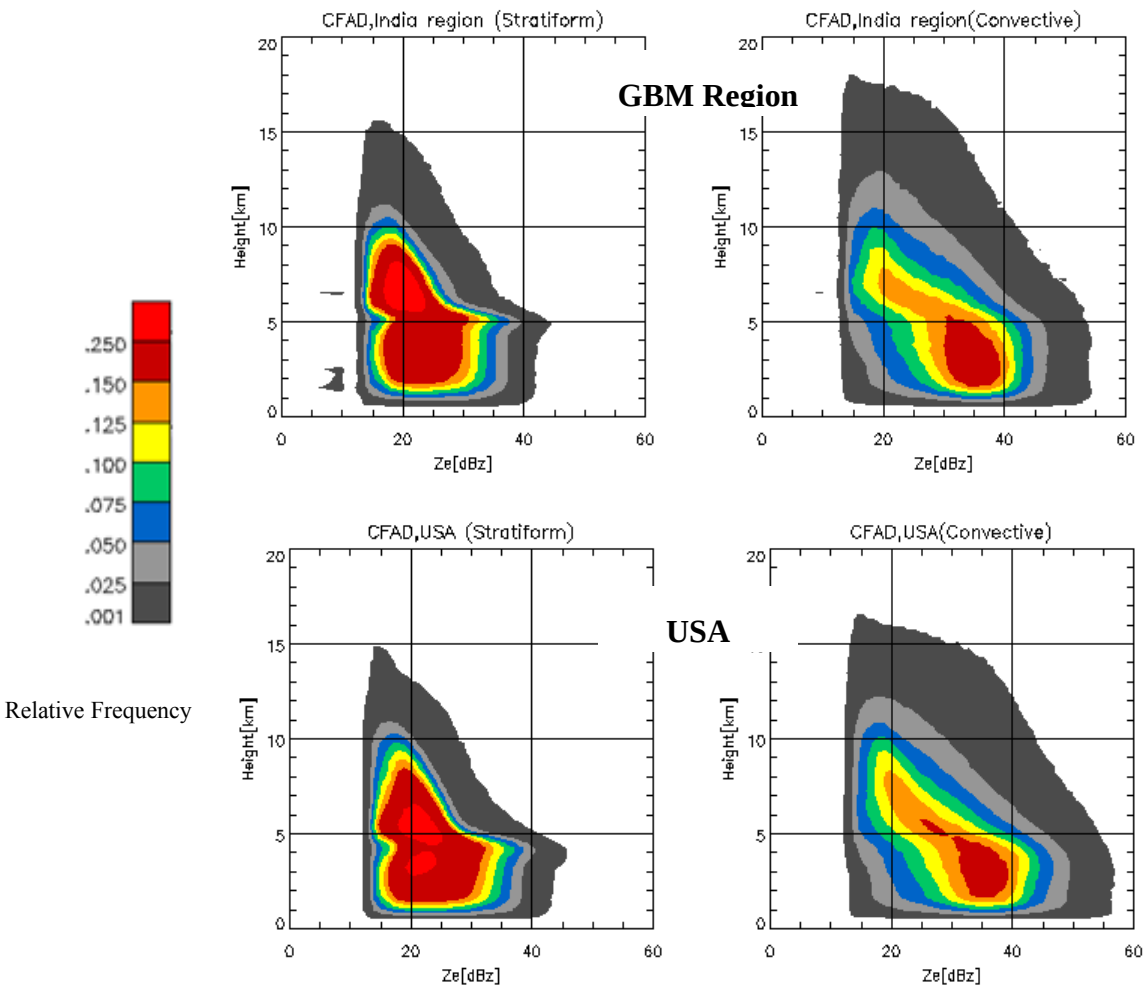

Figure 6.42. Comparison of PR reflectivity profile over the two regions using contoured frequency versus altitude plots (CFAD)

The summer rains over US are dominated by convective activity. Thus, it is no wonder that Figure 6.42 shows both regions as being dominated by convection, and conversely, that MW rainfall detection performs better for these regions. In fact, the GBM region is dominated by stratiform rain. Ramage (1971), who found that the ratio of thunderstorm days to rain is minimum in mid-summer, explains that "synoptic scale converge in the friction layer enhances total rainfall through massive ascent but, by increasing the depth of moist air and diminishing the laps rate, hinders thunderstorm development". The reduced lap's rate can also be seen from Figure 6.42, where for the stratiform use the height of bright band is higher than USA.

Studying satellite data and airborne radar over the Bay of Bengal region, Johnson et al (1987) also observed that the rainfall over this region comes from convective cell embedded in larger region of light rainfall. Raja *et al.* (1999), observed similar phenomena using radar data. They state that the synoptic-scale mass of layered stratiform clouds are results of inertio-gravity waves. Whatever the cause, it is evident that the stratiform cloud observed in Figure 6.42 is a prominent feature of the GBM region summer monsoon.

6.6.3 PR-TMI Calibration and Rain Estimation

Rain/No-rain Classification:

Figure 6.43 shows descriptors (slope, correlation, scattering index, T_{85v} & T_{37v} linear combination, 19-GHz polarization signature, polarized corrected temperature, gradient of 85-GHz temperature and standard deviation of 85-GHz) related to rain/no-rain discrimination used in NN scheme (Grecu and Anagnostou, 2001). The slope relates the T_{85v} and T_{37v} brightness temperatures. This descriptor makes use of the observation that the 85-GHz and 37-GHz brightness temperatures vary differently with respect to rain intensity. That is, a given increase in rain intensity produces larger decrease in the 85-GHz temperature versus the 37-GHz. The correlation indicates variations in brightness temperature caused by precipitation rather than by ground emissivity variability. The scattering index (SI) formula is defined by Grody (1991). It allows the identification of the scattering component in the actual T_{85v} observation.

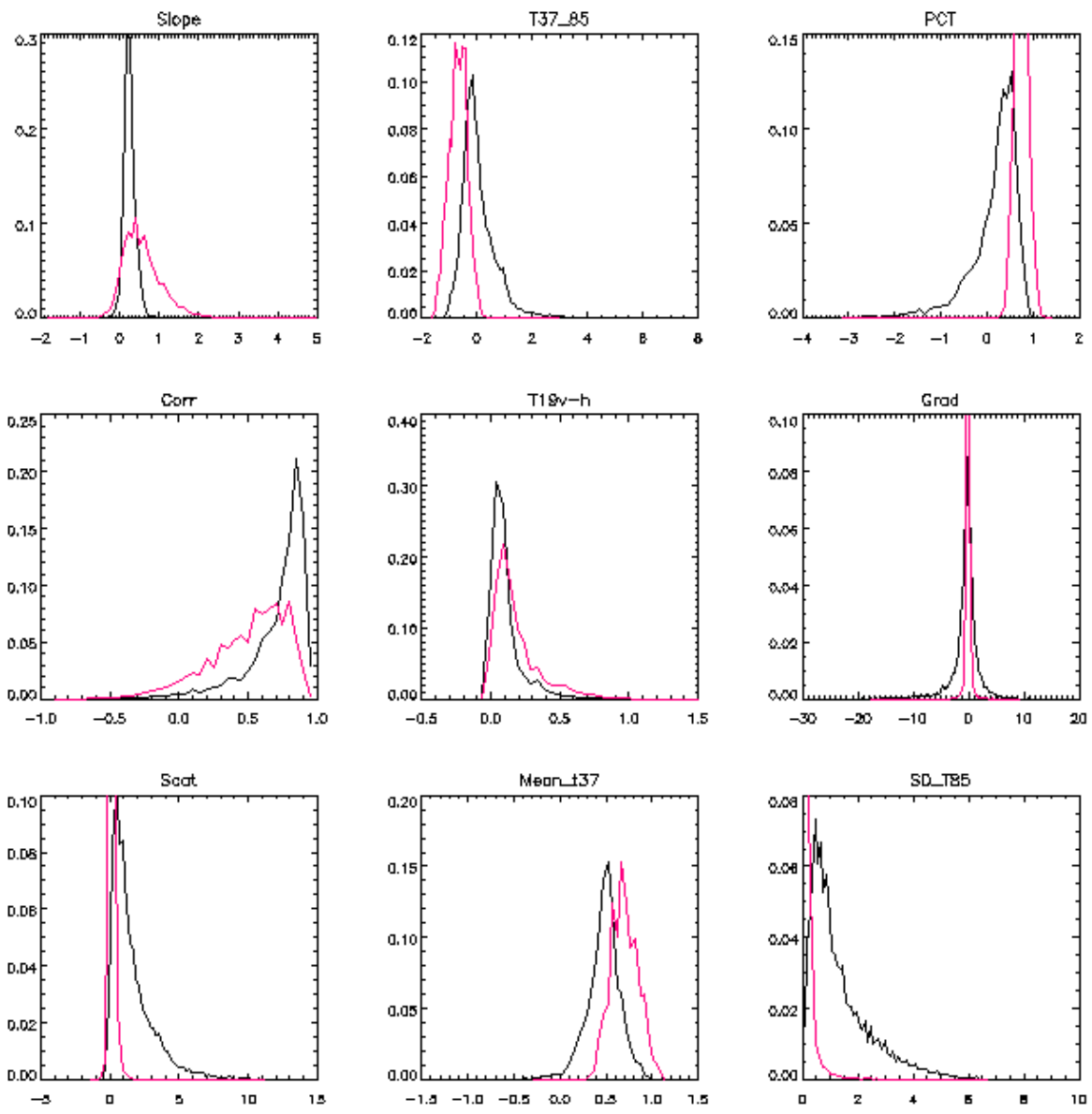

Figure 6.43. Histograms of features for rain/no-rain discrimination (black line represents "rain" and color line represents "no-rain")

The linear combination (LC) is determined by a linear least squares fit of vertically integrated hydrometeor content (VIHC) or 2A12 TMI hydrometeor profile versus T_{37v} and T_{85v} (i.e. LC = 124.28 – 0.36 T_{37v} – 0.1T_{85v}) Only raining pixels were considered in the fitting formula. As a consequence, raining pixels are expected preponderantly to yield positive LC values.

The 19-GHz polarization signature indicates that the differences between T_{19v} and T_{19h} greater than 7 K at 19-GHz frequency are likely caused by ground emissivity rather than rainfall (Ferraro *et al.* 1998). The gradient of T_{85v} is a descriptor defined as the difference between T_{85v} and the mean of T_{85v} in a four-point neighborhood. The standard deviation of T_{85v} was defined based on an eight-point neighborhood. The gradient and the standard deviation of T_{85v} are the descriptors to exploit the observation that T_{85v} is more variable in rain than in no-rain pixels (Anagnostou *et al.* 1997).

The values in the Table 6.8 represent the number of pixels in each of the four possible situations: 1) both NN discrimination and PR observations indicate rain, 2) NN discrimination erroneously indicates rain, 3) NN discrimination erroneously indicates no rain, and 4) both NN and PR indicate no rain. These are determined as ratios of number of pixels in a situation to the total number of pixel. Total number of pixel is 57904.

Table 6.8 Contingency Table for rain/no-rain Discrimination

	Rain/No-rain	PR Rain		
		Rain	No-rain	Total
NN Discrimination	Rain	0.083 (4806)	0.038 (2200)	0.121 (7006)
	No-rain	0.052 (3011)	0.827 (47886)	0.879 (50897)

	NN rain	2A12 rain
POD	0.69	0.63
FAR	0.39	0.32
CSI	0.48	0.56

Convective vs. Stratiform Classification:

A similar approach to that used in rain/no-rain discrimination was formulated for the rain-type classification. A set of descriptors (minimum T_{37v} & T_{85v} temperatures, T_{85v} temperature, scattering index, T_{85v} & T_{37v} linear combination, gradient of T_{85v} temperature and standard deviation of T_{37v} & T_{85v}) was determined and apply to an NN scheme, which was trained to predict the rain type (stratiform vs. convective rain).

Figure 6.44 shows the descriptors used in NN scheme to determine the rain-regime (stratiform vs. convective). The T_{85v} brightness temperature is a strong indicator of rain intensity. The standard deviation of T_{85v} indicates the convective rain is more variable in a small area than is the stratiform rain. The SI descriptor gives a measure of the rain intensity and consequently of the likelihood of convective rainfall. Table 6.9 represents the number of pixels in each of the four possible situations.

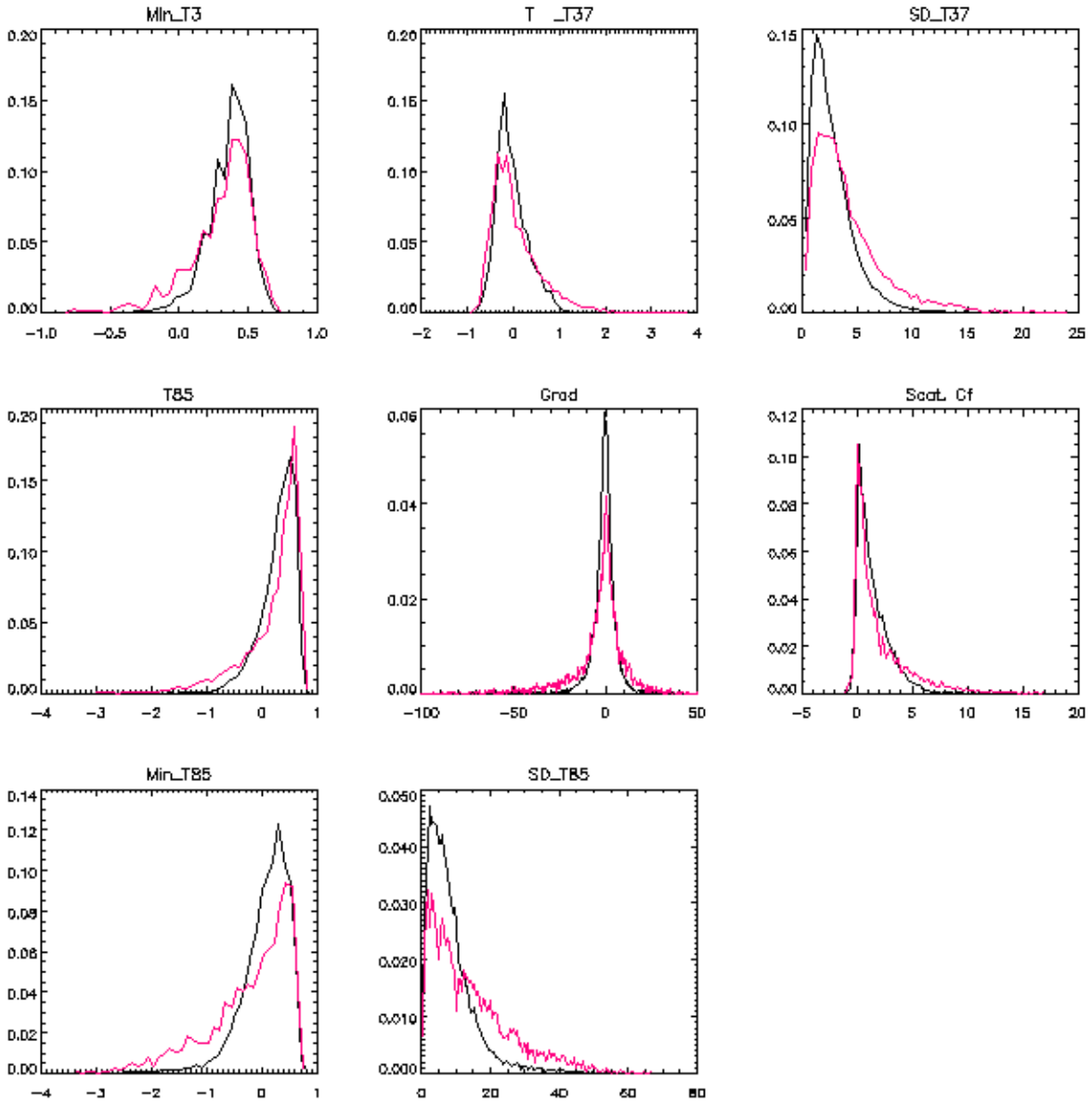

Figure 6.44. Histograms of features for stratiform vs. convective rain classification (black line represents stratiform and color line represents convective rain)

Table 6.9 Contingency Table for Stratiform vs. Convective Rain Classification (N=20230)

	S/C	PR Classification	
		S	C
NN Classification	S	0.518	0.105
	C	0.135	0.241

	NN class	2A23 class
POD	0.83	0.55
FAR	0.18	0.52
CSI	0.68	0.34

PR-TMI Calibration:

PR-2A25 data (rain rate) and 2A23 product (rain type) have been used to calibrate the TMI microwave (MW) channels over USA and GBM. The NN features are obtained from TMI channels, and trained using PR rain profile and rain type data.

- For calibration cases where pr>0 and rnr>0 and pr_cst and NN-cst agree are used
- In estimation only NN-rnr and NN-cst are used
- For validation only data where both PR rnr/cst and NN rnr/cst agree is used

RNR Discrimination Comparison of NN vs. 2A12

Values are:

CSI1 CSI2 CSI1 = CSI (rr > 0), CSI2 = CSI (rr = 0)

POD FAR

Over USA (i.e. Oklahoma)

NN

0.564937 0.932825 CSI

0.735095 0.340174 POD, FAR

2A12

0.483419 0.939991

0.530104 0.154103

Over GBM (i.e. Bangladesh)

NN With US weights

0.541465 0.846502 0.572869 0.864518

0.689647 0.355614 0.734709 0.310567

2A12

0.197586 0.809216

0.223506 0.369849

Rain/no rain discrimination skill and rain rate amount estimation accuracy is compared. PR-2A25 rain is used as a reference, and TMI-2A12 rain is also presented for comparison purposes. To investigate the effect of regional calibration, parameters obtained from USA region are applied over GBM region. In general, parameters obtained using the USA data seem to work well for the GBM region. Table 6.10 shows the comparison of cumulative success index (CST) for rain detection, probability of detection (POD) and false alarm (FAR) for the two regions. NN1 and NN2 (with US parameters over GBM region) refer to neural network calibration using region's own parameter and that of USA, respectively. 2A12 is rain/no-rain discrimination obtained from TMI-2A12 algorithm. For each region and each statistics, relatively best values are shown in bold.

Table 6.10 also compares the effect of using USA calibrations over GBM region for rain/no-rain classification. The statistics used for the comparison are CSI for detecting rain, POD and FAR. From the table we understand that TMI-2A12 performs poorly for the GBM region and in that case the neural network scheme is much better. The region with higher detection failure is the region where stratiform rain is dominant and convective does not penetrate above zero isotherms.

Table 6.10 Comparison of Cumulative Ssuccess Index (CSI) for rain detection, Probability of Detection (POD) and False Alarm (FAR)

Region	CSI			POD			FAR		
	NN1	NN2	2A12	NN1	NN2	2A12	NN1	NN2	2A12
GBM	0.54	**0.57**	0.19	0.69	**0.73**	0.22	0.36	**0.31**	0.37
USA	**0.56**		0.48	0.74		0.53	0.34		**0.15**

Figure 6.45 and 6.46 show similar results presented differently. These figures compare: i) Probability that the microwave rain (MWR) estimate is zero while PR has the values shown in the intervals; and ii) Probability of PR's rain is zero while the MWR is greater than zero. The main features of the figures could be summarized by stating that TMI-2A12 performs poorly for the GBM region and in that case the neural network scheme is much better, where we can use either its own calibration or that of USA.

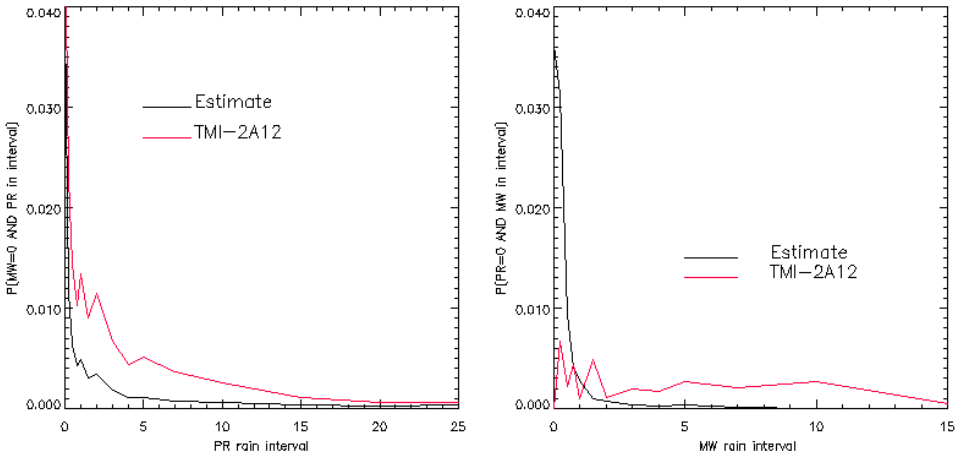

Figure 6.45. Probability (MWR = 0, and PR is not 0) left panel and Probability (PR=0 and MWR is not zero) right panel, for USA

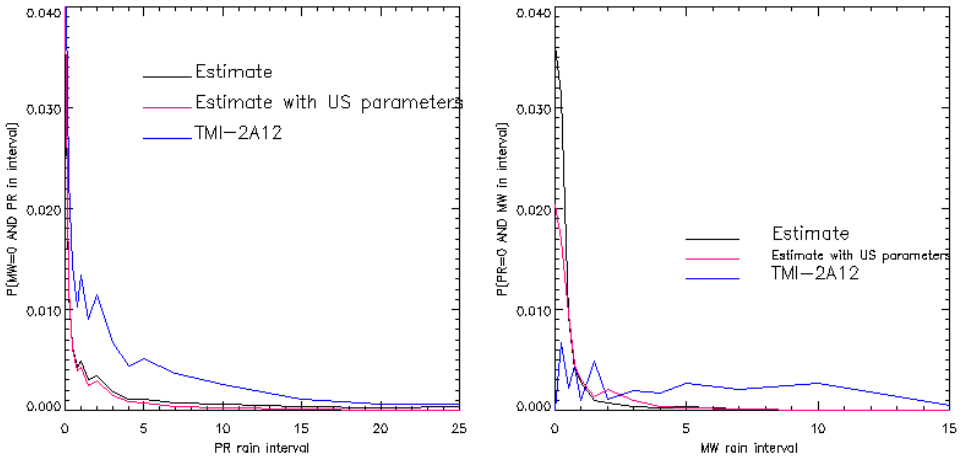

Figure 6.46. Probability (MWR = 0, and PR is not 0), left panel and Probability (PR=0 and MWR is not zero) right panel, for GBM region

Rain Retrieval Validation Statistics:

Figure 6.47 shows the rain detection and false alarm probabilities of PR and TMI-2A12 Version 5 as compared to gauge rainfall. USA NN scheme performs better in terms of rain detection probability, but has also higher FAR for rainfall rates <5mm/hr.

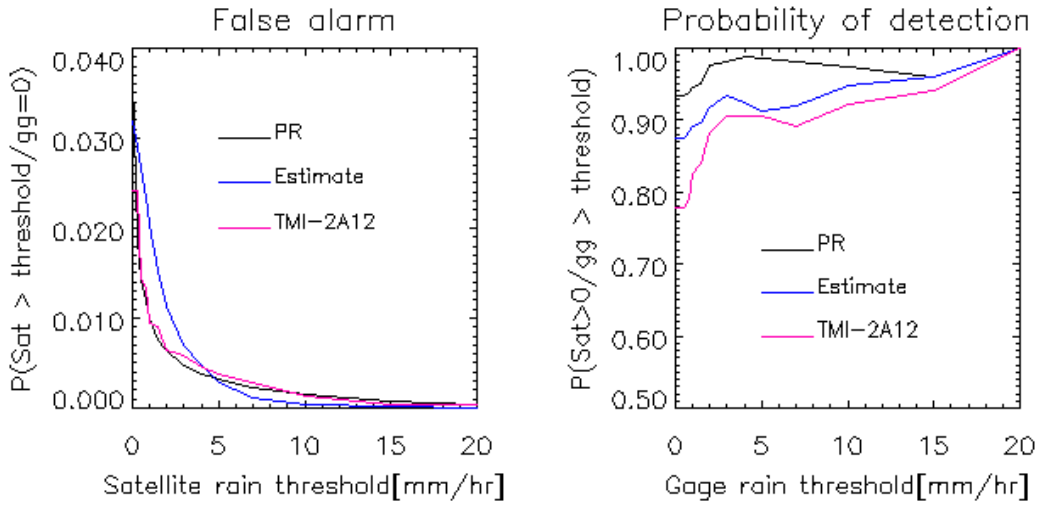

Figure 6.47. Comparison of false alarm and detection probabilities for PR and TMI. "Estimate" is estimated rain rate. The reference data are gauge observations in Bangladesh

Comparison has been done with gauges over Bangladesh. We compared area-averaged (over gauge coverage regime) instantaneous TMI rainfall against area average gauge rainfall. We have used 46 gauges from summer months, covering the whole area in Bangladesh and north-eastern part of India. The statistics used are correlation coefficient (CC), efficiency (Eff) and bias. The results are summarized as follows:

Rain Rate	CC	Eff	Bias
PR	0.57	0.19	1.02
Estimated (EST)	0.74	0.31	1.01
2A12	0.73	0.04	1.01

Figure 6.48 shows the correlations and biases of estimated rain and TMI-2A12 rain retrievals when these retrievals compare with the PR-2A25 rain retrieval. Startiform type rain shows higher correlations than convective type rain. Table 6.11 summerizes the statistics of rainfall estimation using NN and 2A12 rain schemes over GBM and US regions. Rain retrieval (i.e. Estimate) over GBM region with US parameter provides higher correlation and efficiency than 2A12 scheme. Stratiform type rain shows higher correlation and efficiency than convective type. Cumulative and probability distribution functions of estimated and PR rain rates are also plotted in Figures 6.49 and 6.50. See more results for PR-TMI calibration/validation in Appendix – C.

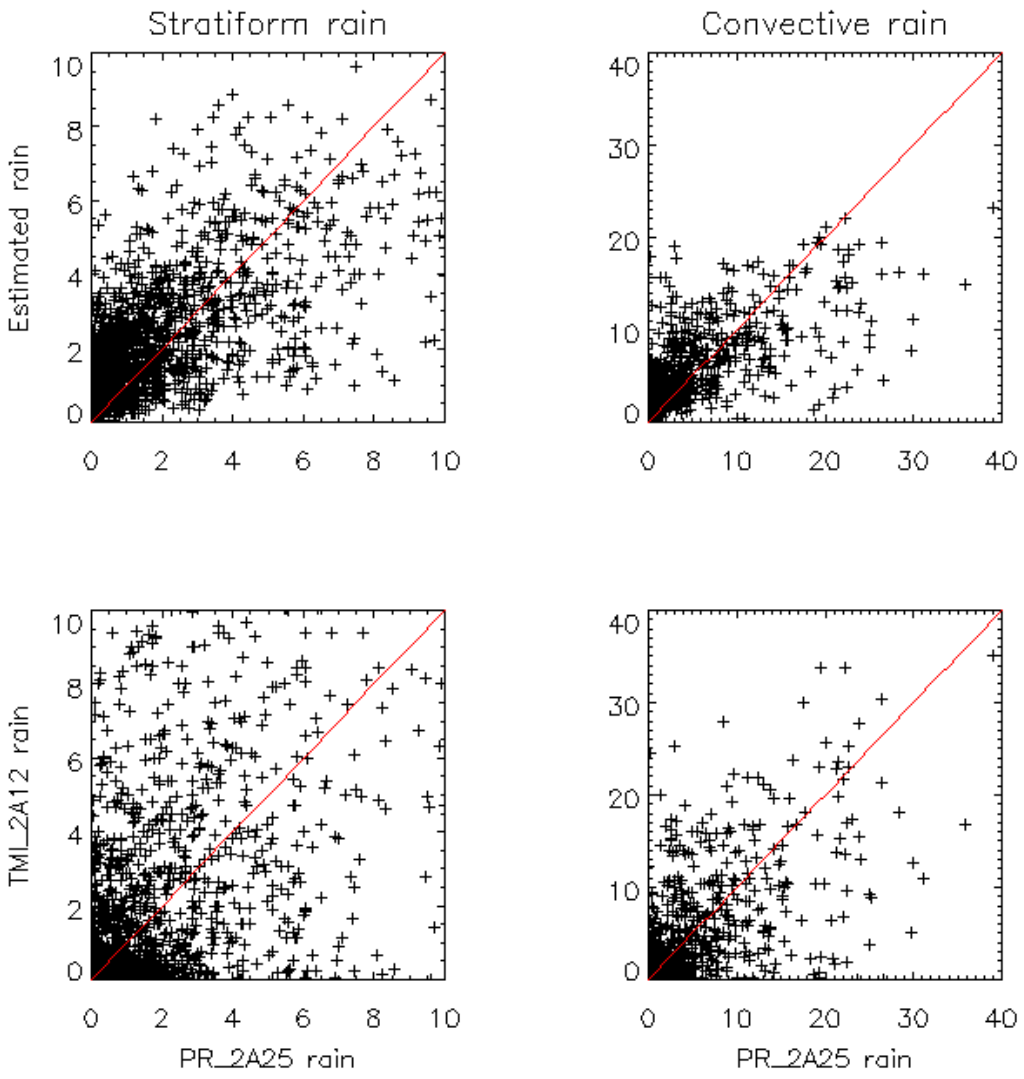

Figure 6.48. PR-TMI Validations for Estimated and TMI 2A12 rain retrievals over Bangladesh

Table 6.11 Rain Retrieval Statistics over Two Regions (i.e. GBM and USA)

Estimate						
Region	**Stratiform**			**Convective**		
	CC	EFF	Bias	CC	EFF	Bias
GBM	0.65	0.25	0.83	0.45	0.13	1.04
USA	0.73	0.31	0.90	0.63	0.39	1.02
2A12						
GBM	0.30	-0.17	0.81	0.03	-0.57	0.38
USA	0.59	-0.07	0.18	0.48	0.15	0.97

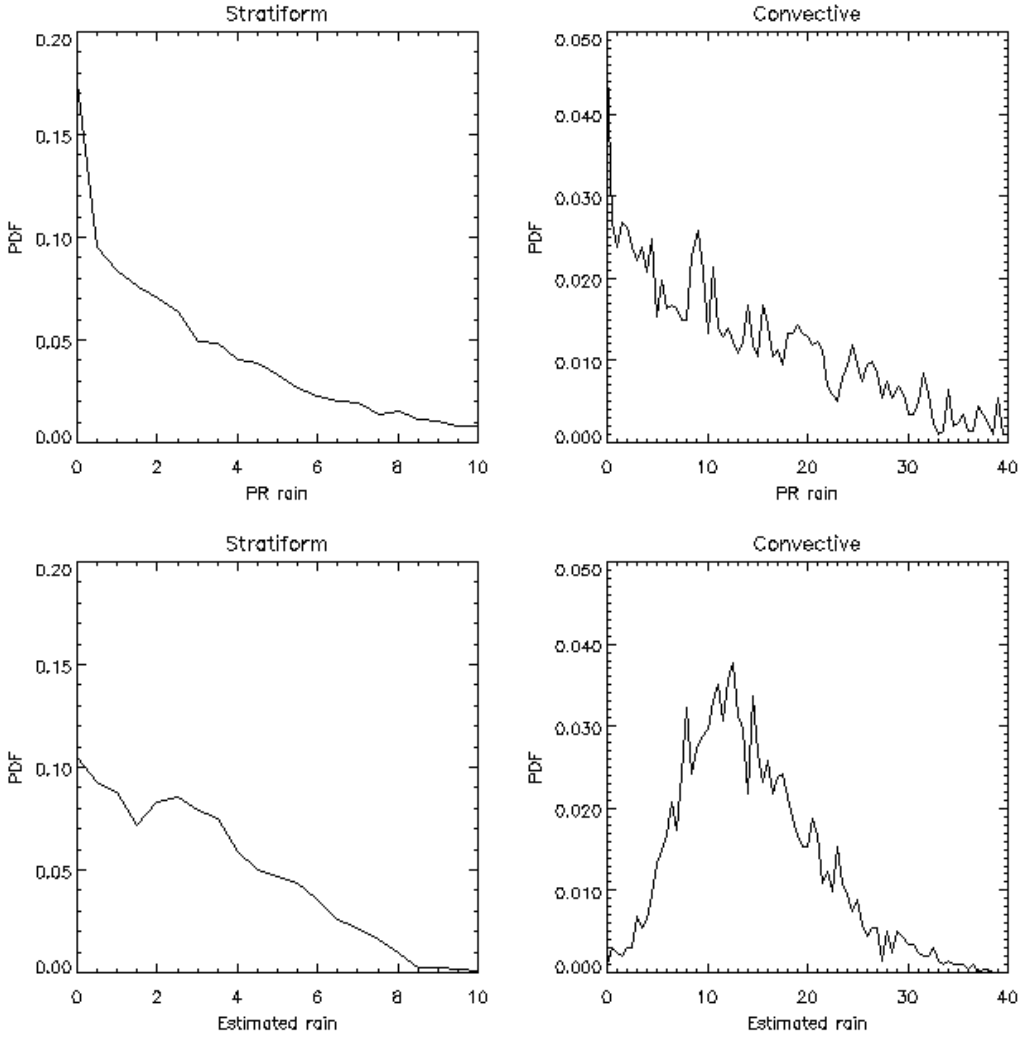

Figure 6.49. Cumulative Distribution Functions of Estimated rain and PR rain rates

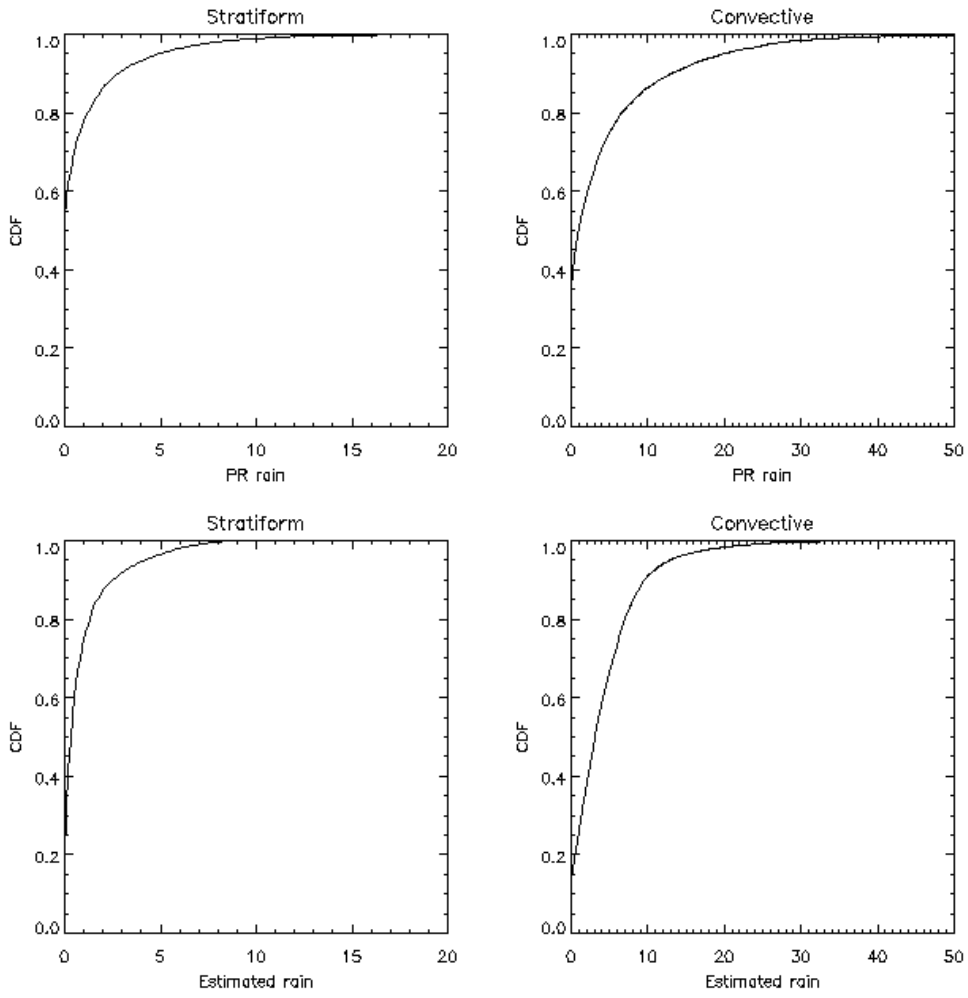

Figure 6.50. Probability Density Functions of Estimated rain and PR rain rates

CHAPTER 7

7. CONCLUSIONS

All the six research objectives of this thesis have been achieved. 1) Characterizations of rainfall system over Bangladesh have been analyzed and presented in relation to clouds activity, distribution of hourly and daily rainfall, as well as time of maximum rainfall. 2) Performance of radar rainfall in Bangladesh has been evaluated using rain gauge data and spatial distribution and times of maximum precipitation are presented. 3) Performance of TRMM rain product has also been evaluated using rain gauge data and the vertical variations of PR rain intensity. 4) Diurnal cycle of rainfall in and around Bangladesh has been determined using TRMM product and radar rainfall. Lifetime, size, place and time of maximum rainfall have been presented using TRMM and radar rainfall. 5) Statistics of three gauge clusters around Dhaka radar have been established and radar rain algorithm parameters have been determined using kalman filter technique. Parameters were estimated using Monto-Carlo statistical solution. Finally, 6) TRMM rain retrieval over Bangladesh has been investigated using ANN algorithm developed by Grece and Anagnostou (2001). The results are summarized below.

The data from BMD radar in Dhaka from 16 April to 30 August 2000 for consecutive 135 days over Bangladesh are utilized in this research work. The BMD radar collects only rain status data in six pre-defined ranges instead of radar reflectivity. It is also understood that there is no radar data available between 03-06 LST of radar operations. Therefore, a methodology has been developed in this study in order to retrieve the precipitation rate from the rain status obtained by the BMD radar data. A correlation between three-days-running averaged rainfall estimated by radar and rain-gauges was calculated and it ranged from 0.63-0.89 over the months of radar operations in 2000. It is found that the radar data were systematically underestimated by about one-fourth the rain-gauge value. It is noted that small size (~80 km2) echoes contribute greatly to the total precipitation, but there were few large size echoes.

Analysis of 185 cases over five months (AMJJA) of 2000, revealed the characteristics of precipitation systems-development locations, sizes, shapes, dimensions, lifetimes, propagation speeds, and directions for the first time in Bangladesh. Most of the precipitation systems were

found to develop in the Northern region then move east-northeast or east-southeast. The average lifetime of these systems is ~5.7 hours and the speed of movement ~5 m/s. Midnight to morning (00-06 LST) is the optimum period for maximum precipitation in the Northern region of Bangladesh whereas it is 06 LST in the Southern region. The optimum times in the Central region are 06 LST and 15-18 LST. The above information on precipitation systems in Bangladesh is important for model parameterization, which should prove useful for forecasting that can be used for water management and for the prevention of natural disasters.

Using the radar data, it was revealed that the peak time of rainfall averaged over Bangladesh is at 06 LST for AMJJA, while different sectors have different local times. The morning maximum rainfall at 06 LST of Bangladesh is very different from the usual characteristics generally observed on land, which may be due to the wetness and oceanic character of Bangladesh. In Bangladesh, the heavy rainfall areas are northern, eastern, and southern regions, and the northern border is the heaviest. The pre-monsoon rain rate is higher than the peak-monsoon rain rate which reveals the basic properties of precipitation in Bangladesh, that is, pre-monsoon thunderstorms are very strong.

The instantaneous and spell rain rate, hourly, monthly, and seasonal rainfall obtained by the radar helped us to understand the detailed distribution of precipitation in this region. The distribution of rainfall obtained by the radar is checked by comparison with that obtained by rain gauge network over the country. The rain distribution obtained by the radar and the rain gauges were similar, while the time of maximum rainfall determined by the radar slightly differed from that determined by the rain gauges. The amount of rainfall determined by the radar was lower than that of the rain gauges. The data coverage of the two may be responsible for the dissimilarities: rainfalls estimated by the radar are averaged over 100-km^2, while the rain gauges provide only point value. The range limitation of the Dhaka radar is also a candidate for the dissimilarities of rainfall amount.

Three-hourly rain data from BMD at 33 gauge locations are also utilized to analyze the radar results. It is found that the distributions of rainfall obtained by both the radar and the rain gauges are similar in pattern, but the time of the maximum rainfall determined by the radar is a few hours earlier than that determined by the rain gauges. The distribution of rainfall over the whole radar domain suggests that the most likely time for rainfall to occur in Bangladesh is between 21 to 09

local standard time (LST), while 06 LST is the most likely time for maximum rainfall to occur over the entire country. The occurrence of 21 to 09 LST rainfall is possibly linked to the local effects such as complex terrain and sea and land breeze circulations. The morning maximum rainfall at 06 LST in Bangladesh is different from that of the Indian subcontinent or of the mountain area where, generally, maximum rainfall occurs in the afternoon. The northern border of Bangladesh, close to the Shillong hill of India, is the region with the highest rainfall, while the second highest volume of rainfall occurs on the eastern border. Furthermore, the radar data over Bangladesh are also utilized to obtain the diurnal variations and characteristics of precipitation in relation to cloud activity. The nature of the diurnal cycle of precipitation in Bangladesh is that there is a morning peak at 0600 LST with minimum at noon. The frequency of the echoes exhibits two peaks-one in the afternoon (~ 1500 LST) and the other in the morning (0600 LST) hours. The smaller echoes dominate in the afternoon while larger echoes develop in the early morning.

The Japanese Geostationary Meteorological Satellite (GMS-5) high resolution (10 km mesh) hourly data were also used in this study. The GMS-5 data analysis in a large domain helped us to understand the cloud activity in relation to rainfall in Bangladesh from pre-monsoon to monsoon seasons. It revealed that cloud activity over Bangladesh was active through May to August 2000 except in July, which supports the rainfall data obtained by the radar. In July 2000, most of the rainfall comes from the coastal regions that demonstrate maximum daily rainfall during 03 to 06 LST. The GMS-5 hourly data are sampled in 1°×1° grid boxes in the domain of 600 km × 600 km over Bangladesh (land) and the north part of the Bay of Bengal (ocean) to obtain diurnal cycle of cloud activity. The cloud embedded area (CEA) shows afternoon (~1700 LST) and morning (~0300 LST) peaks over land typically composed of relatively small deep (<214K) and large shallow (<243K) convective cloud systems. In contrast, only afternoon (1400-1600 LST) peak is observed over ocean typically composed of small shallow and large deep convective cloud systems. Meanwhile the frequency of the cloud systems exhibits the clear afternoon (~ 1600 LST) peak over the land and the ocean that indicates that afternoon is the initiation times of land-based clusters over Bangladesh and water-based clusters in the analyzed ocean (87.44°-93.33°E; 15.7°-21.08°N). The northwestern part of Bangladesh was largely affected by pre-monsoon clouds, while the whole country was affected by the peak monsoon activities.

Diurnal variation of cloud activity in and around Bangladesh is obtained using GMS-5 hourly data. Radar data for consecutive 135 days from 16 April 2000 are utilized to verify the diurnal variation obtained from satellite data over Bangladesh. Radar data is also utilized to obtain the characteristics of precipitation in relation to cloud activity in Bangladesh.

The satellite data revealed the distinct features of occurrence between cloud activity over Bangladesh (land) and the north of the Bay of Bengal (ocean). Small size shallow convection is observed over the ocean with large size deep convection and very large size shallow convection. In contrasts, small size deep convection observed on the land with large size shallow convection. The existence of large deep convection and very large shallow convection over ocean suggests that convection is much more organized and long-lasting over the ocean than that on the land. The cloud embedded area (CEA) on the land shows morning and afternoon peaks while only afternoon peak is obtained over the ocean. Large echo embedded area (EEA) obtained from radar data supports the morning maximum of CEA on land. The morning maximum on the land and afternoon maximum over the ocean differ from the reported values in other studies. Over the land and ocean, the phases of Fourier components are in opposite but the amplitudes are similar in magnitude. However, the amplitude on the land (over ocean) is lower (higher) than that of in the subcontinent (Open Ocean). The surface characters of Bangladesh and north of the Bay of Bengal differ from those of usual land and ocean, respectively. After all, a very clear morning maximum is found at 0600 LST for the precipitation area in Bangladesh.

The certainty of the time of maximum precipitation, the time of maximum frequency of cloud activity, the characteristics of precipitation types such as lifetime, size, propagation speed and direction may help to improve the knowledge in future planning like Global Precipitation Measurement (GPM) and for the validation of model output and the like.

Radar data from the Bangladesh Meteorological Department (BMD) are analyzed to retrieve rain rate from rain status. Radar PPI scans data for the year 2000 are successsfully employed to estimate daily rainfall and compared with rain-gauge and TRMM 3B42 products estimated rainfalls. Radar underestimates rainfall due to Z-R relationship and limited data coverage. Historical data indicates that rainfall in Bangladesh increasing in pre-monsoon and post-monsoon seasons.

Comparing TRMM 3B42 products rainfall with surface-based rain-gauge rainfall obtained by Bangladesh Meteorological Department (BMD) over Bangladesh for the years 1998-2002, it is found that rainy days detected by TRMM match 95.99 % of the same detected by rain-gauge. On an average for 5 years data over 31 stations it is found that daily rainfall determined by TRMM and RNG are 9.16 and 9.32 mm respectively. Hence, TRMM can determine about 98.24 % of the rain-gauge rainfall. TRMM overestimates rainfall during pre-monsoon period, and underestimates during monsoon period and heavy rainfall regions.

A comparison of rainfall amounts determined by TRMM and BG shows that the performance of V6 3B43 is useful for understanding rainfall climatology (monthly rainfall) in Bangladesh. Also, V6 3B42 is useful for estimating short-term (daily) rainfall. In addition, pre-monsoon convection activities are observed over land, whereas monsoon and post-monsoon activities are distributed over the Bay of Bengal and land. One of the basic characteristics of rainfall in and around Bangladesh is that pre-monsoon rainfall is more intense than that during other rainy periods. The analysis of TRMM 2A25 products reveals that intensified echo regions extend up to relatively higher altitudes for pre-monsoon echoes than for those in other periods. On average, the echo top height is high in pre-monsoon events. These results can explain the vertical variations of rain intensities in different rainy periods. This availability of analyses of rain intensity manually judged the TRMM 2A25 data encourages our future plan to analyze TRMM 2A25 data in preparing a routine to detect three-dimensional echo cells automatically.

Analyzing TRMM-2A25 data from pre-monsoon to post monsoon of 2000-2003, it is found that precipitation is strong in pre-monsoon compared to monsoon and post-monsoon. The fact is that intensified echo regions are embedded relatively higher altitudes in pre-monsoon compared to other periods. On average, echo top height is high in pre-monsoon and echo base height is high in post-monsoon events. Comparing rainfall determined by TRMM-3B42RT and RG, it is found that TRMM overestimates rainfall during pre-monsoon period, and underestimates during monsoon, which is due to the various vertical structure of precipitation field in corresponding periods. TRMM-3B42RT data product determines that the diurnal variation of rainfall over Bangladesh differs from the same over India. TRMM well determines the maximum rainfall peak at 06 LT in Bangladesh that is confirmed by RG. The information of the vertical structure and

diurnal variation of rainfall over Bangladesh will be helpful in planning for the forthcoming Global Precipitation Measurement (GPM) project.

This research work presents development of statistical procedure for quantitative estimation of rainfall in Bangladesh from combination of radar observations and rain gauge measurements. The uncertainty bounds associated with those estimates is also evaluated at a given space and time resolution. There are six parameters controlling the various processing stages. Sensitivity analysis showed that there is a host of parameter values coming from different regions in the parameter space that are equally acceptable as predictors of rainfall. Consequently, a methodology is devised to assess the uncertainty arising from errors in algorithm structure and parameter selection. Within this methodology, the algorithm calibration problem is formulated into the estimation of posterior probabilities of acceptable algorithm responses, thereby avoiding the concept of determining a likelihood values associated with errors between observed and estimated precipitation amounts derived through repetitive sampling of parameter space on the basis of Monte Carlo technique. Those likelihood values along with assumed prior distribution of parameter set are used to build its posterior distribution, which reflects the algorithm performance. An advantage with this approach is that the posterior distribution is systematically updated within the Bayesian framework allowing incorporation of new information from observations at different time periods (or radar sites).

The rainfall estimation from the method of Z-R relationship yielded the largest mean relative error of 43.8 % among the selected algorithms. The Kalman filtering technique was also applied in order to adjust radar rain estimation errors. The mean relative error with average calibration, radar-gauge adjustment and Kalman filter approach is respectively 14.5 %, 10.2 % and 7.9 %. The correlations between radar and gauge rainfall for different approaches are 0.584 (not corrected i.e. before error adjustment), 0.902 (with error adjustment but without filtering), and 0.963 (corrected with Kalman filtering). It is found that there is very little error adjustment made by the Kalman filter.

The PR-TMI calibration results has been presented for two regions, which are the GBM and USA. The results compared are the rain detection errors between TMI-2A12 and PR estimated rains. USA region has shown better result than the GBM region. Using CFAD plots of 3D PR reflectivities, for stratiform and convective rains, it has shown the Bangladesh region is

dominated by medium stratiform clouds. The USA region is also dominated by convection during the summer season, but it seems there is also a significance of medium stratiform clouds. It has been argued that over-land microwave rainfall estimation algorithms perform better for deep convection rain systems. Our algorithm performs better than that of 2A12, particularly over Bangladesh, because the neural network approach for rain area delineation, which makes use many channels and different features of the cloud system.

Both the algorithms we are using (Grecu and Anagnostou, 2001) and that of 2A12 version 5 (Kummerow *et al.*, 2001) are mainly scattering-based algorithms. Scattering-based rain retrieval algorithms use the scattering by ice particles at cloud top. This approach assumes that a larger amount of ice particles at cloud top are associated with heavy precipitation. Thus, this retrieval algorithm is most suited for deep convective clouds. That seems to be the reason why the MW algorithms perform better for the regions where convection is dominant. As a result, NN scheme perform better than the 2A12 because NN takes many aspects of cloud system into consideration (Grece and Anagnostou, 2001).

The PR rain estimates are used for calibrating an overland TMI rain algorithm. The algorithm consists of 1) multichannel-based rain screening and convective/stratiform (C/S) classification schemes, and 2) nonlinear (linear) regressions for the rain-rate retrieval of stratiform (convective) rain regimes. This algorithm is the Neural Network (NN) scheme developpel by Grecu *et al.*, 2001. This study examines the differences in the algorithm performance between two areas. The U.S. southern Plains (USA), and the Ganges-Brahmaputra-Meghna River basin (GBM) in south Asia. Data from three summer months of 2000 and 2001 are used for calibration; validation is done using summer 2002 data. The current algorithm is also compared with the latest [version 6 (V6)] TRMM 2A12 product in terms of rain detection, and rain-rate retrieval error statistics on the basis of PR reference rainfall. The 2A12 rain algorithm was developed by Kummerow *et al.*, 2001. The performance NN algorithm is different for the two regions. The reduction in random error (relative to 2A12 V6) is about 26 % and 135 % for USA and GBM respectively. Validation statistics show that this NN scheme outperforms the existing TMI retrievals (2A12) both in terms of rain detection and systematic/random differences as compared to ground validation gauge measurements.

The NN scheme performs better than that of 2A12, particularly over Bangladesh, because the neural network approach for rain area delineation makes use of many channels and different features of the cloud system. Rain retrieval over GBM region with US parameter provides higher correlation and efficiency than 2A12 scheme. Stratiform type rain shows higher correlation and efficency than convective type of rain.

It is confirmed that characterizations of rainfall system can improve radar and satellite based rainfall algorithm development in Bangladesh. TRMM rain retrieval over Bangladesh has been determined based on cloud type and its variability over land in monsoon season. Statistical approaches have been used in radar and satellite rain performance evaluations, parameter estimations, and error estimations. Statistical methods have also been used to determine different predictors in rain/no-rain discrimination and stratiform vs. convective rain classification. TRMM rain retrieval over Bangladesh provides rain estimation in low temporal resolution but radar rain estimation can provide in high temporal resolution. It is understood that the Dhaka radar does not operate continuously and we can not improve nearly real time rain estimation using its present controlling system. It is expected that the rain product from multi sensors satellite can improve nearly real time rainfall estimation in Bangladesh. In this study, we did not develop a hydrological model using low temporal resolution rain data from radar and satellite estimation.

Finally, the three outlined hypothesis were confirmed or resolved. Characterization of rainfall, its variability and the study of diurnal cycle of cloud system in and around Bangladesh improve rainfall estimation. Many statistical methods were used in order to estimate algorithm parameters, predictors, rainfall error estimation. Those statistical procedures can be applied to improve rainfall estimation using ground radar and satellite data as well as rainfall calibration and validation purposes. ***In conclusion, satellite based rainfall estimation can help to investigate improvements of near real time rainfall estimation in Bangladesh.***

CHAPTER 8

8. RECOMMENDATIONS

Rainfall characteristics, its variability and diurnal cycle in and around Bangladesh have been investigated using Gr. Radar, GMS-5 and TRMM rainfall data. Radar rain algorithm parameters were calculated based on radar rain-status category and TMI data was calibrated using TRMM PR for microwave rain estimation over Bangladesh. An up-grade (recording reflectivity and volume scans) of the BMD radar system has been proposed, and in the near future it will be possible to obtain quantitative amounts of rainfall from BMD radar data. Long term radar data are necessary to find a best fit Z-R relationship and to calibrate radar results with rain-gauge values.

The local orographic effect was not examined in this study. Therefore, the local orographic effect to the monsoon rainfall in Bangladesh should be examined in more detail using the radar observation and microwave passive rain retrieval. In this analysis, we do not find strong contrast between the amplitudes of diurnal variations of cloud activities over the land and the ocean, which differ from the reported diurnal cycle over the tropical continents and the other continents during summer (Meisner and Arkin, 1987). Therefore, this study encourages more analysis using long time-large coverage data to verify the present result and to clarify the real form of diurnal cycle of cloud activity in and around Bangladesh.

Bangladesh is one of the places where maximum rainfall comes at morning and at its northern parts received maximum rain from mid night to early morning (Ohsawa *et al.*, 2001; Prasad, 1974). However, the details of the storm clustering and cluster longevity to be obtained from high temporal and spatial resolution data, the mechanism behind the development of convection are still open to discussion. Because of the lack of long-term observational data the model simulation like MM5 as used by Warner *et al.* (2003) and Mapes *et al.* (2003b) for the study of diurnal pattern of rainfall in north-western South America may be used in near future to extend the present study.

It is not possible to investigate any hydrological scenarios due to temporal limitation of TRMM satellite data but TRMM rain product is found very useful to calibrate other satellite product. Therefore, it is recommended to calibrate SSM/I (and/or AMSR, AMSU-B data) passive microwave data using current calibrated TRMM TMI data over Bangladesh. We have also Global IR data in ½-hourly interval and it is also recommended to calibrate IR data using multi-sensor microwave rain product. Finally, this product can be used in hydrological model to investigate error propagation in different hydrologic fluxes through model simulation and observe data.

At present, the F-13, F-14 and F-15 satellites are operational. The SSM/I is a seven-channel, four frequency, linearly-polarized, passive microwave radiometric system which measures atmospheric, ocean and terrain microwave brightness temperatures at 19.35, 22.235, 37.0 and 85.5 GHz. Each DMSP satellite has a 101 minute, sun-synchronous near-polar orbit at an altitude of 830km above the surface of the earth, inclination 98.8 deg and swath width 1400 km providing global coverage twice per day. The combination of day/night and dawn/dusk satellites allows monitoring of global information such as clouds every 6 hours. The polar orbit provides nominal coverage over the latitudes 85N-S, although limitations in retrieval techniques prevent useful precipitation estimates in cases of cold land (scattering), land (emission), or sea ice (both scattering and emission). The SSM/I is an operational sensor, so the data record suffers the usual gaps in the record due to processing errors, down time on receivers, etc. Over time the coverage has improved as the operational system has matured.

Optimally, the differences between the various satellite estimates should be random at small spatial and short time scales and negligible at large spatial and long time scales. Unfortunately, this is not the case with most of the current overland microwave sensor estimates. With this in mind, we need to formulate an effective methodology to investigate and eliminate the systematic differences between microwave rain estimates and, thus, build a unified database of rain products from a combination of various passive microwave (PM) instrument estimates. The PM database will be used to consistently train a high-frequency rain retrieval that combines satellite infrared, which would produce jointly with the infrequent PM estimates optimal rain estimates at various spatial (0.1-0.5 degree) and temporal (hourly to 6-hourly) scales over South east Asia.

We propose a “bottom-up” approach, in which the effort focuses on connecting (or partially transferring) the information derived in instantaneous high-resolution rainfall estimation to longer

time scales and larger spatial scales. Specifically TRMM PR rain estimates will be used to improve the calibration of a number of passive microwave (TMI, SSM/I, AMSR and AMSU-B) algorithms for precipitation estimation at the radiometer footprint scale. A Bayesian formulation could be proposed to optimally determine this combination, as well as the uncertainty associated with the merged products. The coincident rainfall estimates from a dense rain gauge network available in Bangladesh would be used to determine the covariance matrices associated with this formulation. It is expected that the PM retrievals would be unbiased with respect to PR rainfall, but the random error would probably vary from sensor to sensor. The different PM sensor error statistics would be assessed using the rain gauge rainfall measurements. Finally, the end rain product can be used in hydrological model (e.g. HYDROTEL, HSP-F, Mike SHE) to investigate error propagation in modeling hydrologic variables over different time and space scales.

An up-grade of the BMD radar system is highly recommended, and in near future it will be possible to obtain quantitative amounts of rainfall from BMD radar. The TRMM PR and calibrated PM rain products can be used to calibrate BMD radar in order to estimate real-time rainfall for flood forecasting model (currently used Mike 11) development in Bangladesh.

REFERENCES

Adler, R.F., G.H. Huffman and P.R. Keehn, 1994. Global Tropical Rain Estimates from Microwave-adjusted Geosynchronus IR Data. *Remote Sens. Rev.*, 11: 125-152.

Adler, R.F., A. J. Negri, P.R. Keen and I.M. Hakkarinen, 1993. Estimation of monthly rainfall over Japan and surrounding water from a combination of low-orbit microwave and geosynchronous IR data. *J. Appl. Meteor*., 32: 335-356.

Adler, R.F. and A.J. Negri, 1988. A satellite infrared technique to estimate tropical convective and stratiform rainfall. *J. Appl. Meteor.,* 27: 30-51.

Adler, Robert F., George J. Huffman, David T. Bolvin, Scott Curtis, Eric J. Nelkin, 2000. Tropical Rainfall Distributions Determined Using TRMM Combined with Other Satellite and Rain Gauge Information. *Journal of Applied Meteorology*, 39(12): 2007–2023.

Ahmed, R. and S. Karmakar, 1993. Arrival and withdrawal dates of summer monsoon in Bangladesh. *Int. J. Climatol*., 13: 727-740.

Albright, M. D., Recker, E. E., Reed, R. J. and Dang, R., 1985. The diurnal variation of deep convection and inferred precipitation in the central tropical Pacific during January-February 1979. *Mon. Wea. Rev*., 113: 1663-1680.

Amorati, R., Alberoni, P.P., Levizzani, V. and Nanni, S. 1999. Satellite and radar rainfall estimates of convective storms over Northern Italy. Submitted to *Meteorol.Appl*.

Anagnostou E.N, Christan Kummerow, 1996. Stratiform and Convective Classification of Rainfall Using SSM/I 85-GHz Brightness Temperature Observations, *Journal of Atmospheric and Oceanic Technology*, 14: 570-575.

Anagnostou E.N., Negri. A. J. and Adler, F A., 1999. Statistical Adjustment of Satellite Monthly Rainfall Estimates over Amazonia, *Journal of Applied Meteorology*, 38: 1590-1598.

Anagnostou, E. N. and W. F. Karajewski, 1999. Real-time radar rainfall estimation. Part II: Case study. *J. Atmos. Oceanic Technol*., 16: 198-205.

Anagnostou, E.N. A.J. Negri and R.F. Adler, 1999. A satellite infrared technique for diurnal rainfall variability studies. *J. Geophys. Res*., 104 (D24): 31,477-31,488.

Anagnostou, E.N., C. Morales and T. Dinku, 2001."The Use of TRMM Precipitation Radar Observations in Determining Ground Radar Calibration Biases," *Journal of Atmospheric and Oceanic Technology*, 18: 616-628.

Arkin, P.A. and B.N. Meisner, 1987. The relationship between large scale convective rainfall and cold cloud over the western hemisphere during 1982-1984. *Mon. Wea. Rev.*, 115: 51-74.

Arkin, P.A. and J. Janowiak, 1991. Analysis of the Global Distribution of Precipitation. *Dyn. Atmos. Oceans*, 16: 5-16.

Arkin, P.A., 1979. The Relationship between Fractional Coverage of High Cloud and Rainfall Accumulations during GATE over the B-Scale Array. *Mon. Wea. Rev.*, 107: 1382-1387.

Arkin, P.A., R. Joyce, J.E. Janowiak, 1994. The estimation of global monthly mean rainfall using infrared satellite data: The GOES Precipitation Index (GPI). *Rem. Sens. Rev*., 11: 107-124.

Ba, M. and A. Gruber, 2001. GOES Multispectral Rainfall Algorithm (GMSRA). *J. Appl. Meteor*., 40(8): 1500–1514.

Ba, M.B., Rosenfeld, D. and Gruber, A., 1998. AVHRR multispectral derived cloud parameters: Relationship to microwave scattering signature and to cloud-to-ground lightning. *Prepr. 9th Conf. Satellite Meteorology and Oceanography*, AMS, 408-411.

Barbe, L. L., Lebel T and Tapsoba D., 2002. Rainfall Variability in West Africa During the years 1950-90, *American Meteorological Society*, 15(2): 187-202.

Barrett, E.C. and D.W. Martin, 1981. The Use of Satellite Data in Rainfall Monitoring. Academic Press, p. 340.

Barrett, E. C., D'Souza, G., Power, C. H. and Kidd, C., 1988. Toward trispectral satellite rainfall monitoring algorithms. In Tropical Precipitation Measurements, Proc. Int. Symp., Tokyo, Japan, NASS/NASDA (eds J. S. Theon and J. Fugono), A.Depak, Hampton, VA, pp. 285-292

Barrett, E.C., 2001. Satellite remote sensing of precipitation: progress and problems, *Remote Sensing Hydrology 2000*, IAHS Publ. No. 267: 3-10.

Barros, P, M. Joshi, J. Putkonen and Burbank, 2000. A Study of the 1999 monsoon rainfall in a mountainous region in central Nepal using TRMM products and rain gauge observations, *Geophysical Research Letter*, 27(22): 3683-3686.

Bell, T. L. and P.K. Kundu, 2000. Dependence of Satellite Sampling Error on monthly Averaged Rain Rates: Comparison of Simple Models and Recent Studies. *J. Climate*, 13: 449-462.

Bell, T. L., P.K. Kundu and Kummerrow C. D, 2001. Sampling errors of SSM/I and TRMM rainfall averages: Comparison with error estimates from satellite data and a simple model, *Journal of Applied Meteorology*, 40: 938-954.

Bellon, A., Lovejoy, S. and Austin, G.L., 1980. Combining satellite and radar data for the shortrange forecasting of precipitation. *Mon.Wea.Rev.*, 108: 1554-1556.

Bellon, A., S. Lovejoy and G.L.Austin, 1980. Combining satellite and radar data for the short-range forecasting of precipitation. *Mon.Wea.Rev.*, 108: 1554-1556.

Berg, W., Olson, W., Ferraro, R., Goodman, S.J. and LaFontaine, F.J. 1998. An assessment of the first- and second-generation Navy operational precipitation retrieval algorithms. *J.Atmos.Sci*., 55: 1558–1575.

Bhat, G. S., S. Gadgil, P. V. Hareesh Kumar, S. R. Kalsi, P. Madhusoodanan, V. S. N. Murty, C. V. K. Prasada Rao, V. Ramesh Babu, L. V. G. Rao, R. R. Rao, M. Ravichandran, K. G. Reddy, P. Sanjeeva Rao, D. Sengupta, D. R. Sikka, J. Swain and P. N. Vinayachandran, 2001. BOBMEX, the Bay of Bengal Monsoon Experiment. *Bull. of the Amer. Meteor. Soc.,* 82(1): 2217-2243.

Bhattacharya, P. K. and Bhattarcharyya, S. G., 1980. Diurnal variation of rainfall in the upper catchments of north Bengal rivers, *MAUSAM*, 31: 51-54.

Brimes, D I F, Iguzquiza E. P and Bonifacio R, 1999. Optimal area rainfall estimation using raingauge and satellite data, *Journal of Hydrology*, 222: 93-108.

Buechler, D., H.J. Chirstian, S.J. Goodman, 1994. Rainfall estimation using lightning data. Seventh Conf. Satell. Meteor. and Ocean., *Amer. Meteorol. Soc.*, June 6-10, pp. 171-174.

Canadian Space Agency, 2002. Canadian Global Precipitation Measurement Mission Proposal v12, NASA and Canadian Scientists.

Chen, C. S. and Chen Y. L., 2003. The Rainfall Characteristics of Taiwan, *Monthly Weather Review*, 131: 1323-1341.

Chen, M X, Zeng XB, Dickinson RE, 1998. Adjustment of GCM precipitation intensity over the United States. *Journal of Applied Meteorology*, 37: 876-887.

Chen, S. S. and Houze, Jr. R.A., 1997. Diurnal variation and life-cycle of deep convective systems over the tropical Pacific warm pool. *J. R. Meterol. Soc.*, 123: 357-388.

Chen, T. C., M. C. Yen, J. C. Hsieh and R. W. Arritt, 1999. Diurnal and seasonal variations of the rainfall measured by the automatic rainfall and meteorological telemetry system in Taiwan. *Bull. Amer. Meteor. Soc.*, 80: 2299-2312.

Cheng, M. and Brown, R., 1995. Delineation of precipitation areas by correlation of METEOSAT visible and infrared data with radar data. *Mon.Wea.Rev.*, 123: 2743-2757.

Cheng, M., R.Brown, and C.G.Collier, 1993. Delineation of precipitation areas using METEOSAT infrared and visible data in the region of the United Kingdom. *J.Appl.Meteorol.,* 32: 884-898.

Ciach, G. J., W. F. Krajewski, E. N. Anagnostou, M. L. Baeck, J. A. Smith, J. R. McColum and A. Kruger, 1997. Radar rainfall estimation for ground validation studies of the tropical rainfall measuring mission, *J. Appl. Meteor.,* 36: 736-747.

Ciach, J.G. and W.F. Krajewski, 1999. On the estimation of radar rainfall error variance, *Advances in Water Resources*, 22(6): 585-595.

Costa, M. H. and J. A. Foley, 1998. A comparison of precipitation datasets for the Amazon basin, *Geophysical Research Letters*, 25: 155-158.

Dai, A., Giorgi, F. and Trenberth, K. E., 1999. Observed and model simulated precipitation diurnal cycle over the contiguous United States. *J. Geophys. Res.*, 104: 6377-6402.

Das, P. K., 1995. The Monsoons, Third Edition published by the Director, National Book Trust, New Delhi, India.

Droegemeier, K.K., J.D. Smith, S. Businger, C. Doswell III, J. Doyle, C. Duffy, E. Foufoula Georgiou, T. Graziano, L.D. James, W. Krajewski, M. LeMone, D. Lettenmaier, C. Mass, R. Pielke Sr., P. Ray, S. Rutledge, J. Schaake, E. Zipser, 2000. Hydrological aspects of weather prediction and flood warnings:

Report of the Ninth Prospectus Development Team of the U.S. Weather Research Program, *Bulletin of the American Meteorological Society*, 81(11): 2665–2680.

Duvel, J. P., 1989. Convection over tropical Africa and the Atlantic Ocean during northern summer. Part I: Interannual and diurnal variations. *Mon. Wea. Rev.*, 117: 2782-2799.

Ebert E.E. and M.J. Manton, 1998. Performance of Satellite Rainfall Estimation Algorithms during TOGA-COARE. *J. Atm. Sciences*, 55(N09): 1537-1557.

Ebert, E. E., M. J. Manton, P. A. Arkin, R. J. Allam, G. E. Holpin, and A. Gruber, 1996. Results from the GPCP algorithm intercomparison programme. *Bull. Amer. Meteor. Soc*., 77: 2875-2887.

Fernández, J.M., Legléau, H., Zwatz-Meise, V. and Dybbroe, A., 1998. The Satellite Application Facility (SAF) of EUMETSAT to support nowcasting: An Introduction. Prepr. 9th Conf. Satellite Meteorology and Oceanography, *AMS*, pp. 319-322.

Ferraro, R. J., Grody, N. C. and Kogut, J. A., 1986. Classification of geophysical parameters using passive microwave satellite measurements. *IEEE Trans. Geosci. Remote Sensing*, GE-24: 1008-1013.

Ferraro, R., Grody, N. and Marks, G., 1994. Effects of surface conditions on rain identification using the DMSP-SSM/I. *Rem.Sens.Rev*., 11: 195-209.

Ferraro, R.R, F. Weng, N.C. Grody and L. Zhao, 2000. Precipitation characteristics over land from the NOAA-15 AMSU Sensor. *Geophy. Res. Let.*, 27: 2669-2672.

FFWC Project Report, Bangladesh, 2000. Daily Rainfall Mapping using Satellite based Rain Cloud Duration Technique, Flood Forecasting and Warning Centre, Bangladesh.

Follansbee, W.A., 1973. Estimation of average daily rainfall from satellite cloud photographs. NOAA Tech. Memorandum NESS 44, Dept. of Commerce, Washington, D.C., 39 p.

Gao, X, S. Sorooshian *et al.*, 2003. SST Data Improve Modelling of North American Monsoon Rainfall, EOS, Transaction, *American Geophysical Union*, Vol. 84, Number 43, October.

George, J. Huffman David T. Bolvin, 2003. Trmm Real-Time Multi-Satellite Precipitation Analysis Data Set Documentation Laboratory for Atmospheres, NASA Goddard Space Flight Center and Science Systems and Applications, 10 October.

Goldenberg, S. B., Houze, Jr. R. A. and Churchill, D. D., 1990. Convective and stratiform components of a winter monsoon cloud cluster determined from geo- synchronous infrared satellite data. *J. Meteor. Soc. Japan*, 68: 37–63.

Goodfellow, G., 2002. Dept. of Mathematics, University of Waterloo, 200 University Ave. W. Waterloo, Ontario Canada, N2L 3G1, 519.885.1211, www.math.uwaterloo.ca.

Gorm, Dybkjaer and Geografisk Tidsskrift, 2003. A Simple self-calibrated Cold Cloud Duration technique applied in West Africa and Bangladesh, *Danish Journal of Geography*, 103(1): 83-97.

Gray, W. M. and Jacobson, R. W. Jr., 1977. Diurnal variation of deep cumulus convection. *Mon. Wea. Rev.*, 105: 1171-1188.

Grecu, M. and E. N. Anagnostou, 2001. Overland Precipitation Estimation from Passive Microwave Observations. . *J. Appl. Meteor.,* 40: 1367-1380.

Grecu, M, 2001. Multi-sensor rainfall estimation: Hand out of course CE 320-02 *Hydrological Remote Sensing*.

Grecu, M. and E.N. Anagnostou, 2000. Variational Based Retrieval of Hydrometeor Profiles from Satellite Active and Passive Microwave Observations, *Journal of Geophysical Research-Atmosphere.*

Grecu, M. and E.N. Anagnostou, 2002. Use of passive microwave observations in a radar rainfall-profiling algorithm, *Journal of Applied Meteorology*, 41 (7): 702-715.

Grecu, M., E.N. Anagnostou and R.F. Adler, 2000. Assessment of the Use of Lighting Information in Satellite Infrared rainfall Estimation, *American Meteorological Society*, pp. 211-221.

Grody, N.C., 1991. Classification of snow cover and precipitation using the Special Sensor Microwave Imager, *J. Geophys. Res.*, 96(D4): 7423-7435.

Grody, N. C., 1984. Precipitation monitoring over land from satellite by microwave radiometry. Present at the Intertional Geoscience and Remote Sensing Symposium (IGARSS'84), Strasbourg, France, ESA SP-215. pp. 417-423.

Gruber, A. (1973). Estimating rainfall in regions of active convection. *J.Appl.Meteorol.*, 12: 110-118.

Guard, C., W.F. Krajewski, P. A. Kucera, A. Kruger, and M. A. Lander, 2001. Two Specialized Rain Gauge Networks in Western Pacific for TRMM, submitted to *Journal of Atmospheric and Oceanic Technology*.

Guetter, A.K. K.P. Georgakakos and A. A. Tsonis, 1996. Hydrologic applications of satellite data: 2. Flow simulation and soil water estimates. *J Geophys. Res.* 101(D21): 26,527-26,538.

Gunnel Cederlö f. Research Fellow, Development Studies, University of Uppsala, Box 514, 751 20 Uppsala, Sweden.

Habib, E., W.F. Krajewski, and A. Kruger, 2001. "Sampling Errors of Tipping-Bucket Rain Gauge Measurements", *ASCE Journal of Hydrologic Engineering*, pp. 159-166, March/April.

Haddad, Z.S., E. Im, S.L. Durden and S. Hensley, 1996. Stochastic filtering of rain profiles using radar, surface-referenced radar, or combined radar-radiometer measurements. *Journal of Applied Meteorology*, 35: 229-242.

Haddad, Z.S., E.A. Smith, C.D. Kummerow, T. Iguchi, M.R. Farrar, S.L. Durden, M. Alves and W.S. Olsen, 1997. The TRMM «day-1» radar/radiometer combined rain-profiling algorithm. *J. Meteor. Soc. Japan*, 75: 799-809.

Hamada, J. I., Yamanaka, M. D., Matsumoto, J., Fukao, S., Winarso, P. A., and Sribimawati, T., 2002. Spatial and temporal variations of the rainy season over Indonesia and their link to ENSO. *J. Meteor. Soc. Japan*, 80(2): 285-310.

Harlar, G. C., Sud, A. M. and Marathe, S. D., 1991. Diurnal variation of monsoon rainfall in central India, *Mausam*, 42: 37-40.

Harzallah, R. and R. Sadourny, 1997. Observed lead-lag relationship between the Indian summer monsoon and some meteorologiocal variables. *Climate Dynamic*, 13: 635-648.

Heerden, J.V. and J. J. Taljaard, 1998. *Africa and surrounding waters*. In: D. J. Karoly and D. G Vincent (Ed.), Meteorology of the Southern Hemisphere, *Amer. Meteor. Society*, pp. 141-174.

Herb, Wiebe. Prepared for Thematic Review IV.4: Assessment of Flood Control and Management Options (Bangladesh – The Evolution of Planning for Flood Control), Northwest Hydraulic Consultants, Canada.

Hong, Y., C. D. Kummerow and W. S. Olson, 1999. Separation of convective and stratiform precipitation using microwave brightness temperature. *J. Appl. Meteor.,* 38: 1195-1213.

Horvath, A. and R. Davies. 2001. Simultaneous retrieval of cloud motion and height from polar-orbiter multiangle measurements. *Geophysical Research Letters*, 28: 2915-2918.

Hossain, F., Dinku T, Anagnostou E, Agarwal N., 2003. Assessment of neural network schemes to classify cloud data. *Journal of Environmental Systems,* 29(2): 151-172.

Hossain, F., E.N. Anagnostou, M. Borga and T. Dinku, 2002. Hydrologic model sensitivity to parameter and radar rainfall estimation uncertainty. *Hydrol. Proc.* (SUBMITTED).

Hou, A. Y., S. Q. Zhang and A. M. da Silva, 2000b. Improving Global Data Set Using TMI Rainfall and Columnar Moisture observations. *J. Climate*, 13: 4180-4195.

Houze, R. A. Jr., 1993. Cloud Dynamics. Academic Press, Inc. New York, pp. 341-348.

Houze, R.A. Jr., 1997. Stratiform precipitation in regions of convection: A meteorological paradox? *Bull. Amer.Meteorol.Soc.*, 78: 2179-2196.

Huffman, G.J., R.F. Adler, M.M. Morrissey, D.T. Bolvin, S. Curtis, R. Joyce, B. McGavock and J. Susskind, 2001. Global Precipitation at One-Degree Daily Resolution from Multisatellite Observations. *J. Hydrometeor.*, 2: 36-50.

Huffman, G.J., Adler, R.F., Arkin, P., Chang, A., Ferraro, R., Gruber, A., Janowiak, J., McNab, A., Rudolph, B., Schneider, U., 1997. The Global Precipitation Climatology Project (GPCP) combined precipitation dataset. *Bulletin of the American Meteorological Society*, 78: 5-20.

Huffman, G.J., Adler, R.F., Rudolf, B., Schneider, U., Keehn, PR., 1995. Global precipitation estimates based on a technique for combining satellite-based estimates, rain gauge analysis, and NWP model precipitation information. *Journal of Climate*, 8: 1284–1295.

Huffman, G.J., R.F. Adler, P. Arkin, A. Chang, R., Ferraro, A. Gruber, J. Janowiak, A. McNab, B. Rudolf and U. Schneider, 1997. The Global Precipitation Climatology Project (GPCP) combined precipitation data set. *Bull. Am. Meteorol. Soc.*, 78: 5-20.

Husain, M.A. and N. Sultana, 1996. Rainfall distribution over Bangladesh stations during the monsoon months in the absence of depressions and cyclonic storms, *Mausam*, 47: 339-348.

IFCDR, 1997. Application of Remote Sensing Technology to Rainfall Estimation, Final Report of Japan Bangladesh Joint Study Project on Floods, Topic 1.

Iguchi T, Kozu T, Meneghini R, Awaka J, Okamoto K., 2000b. Rain profiling algorithm for the TRMM precipitation radar. *Journal of Applied Meteorology*, 39: 2038–2052.

Iguchi, T., Meneghini, R., Awaka, J., Kozu, T., Okamoto, K., 2000a. Rain profiling algorithm for TRMM precipitation radar data. *Advances in Space Research,* 25(5): 973–976.

Inoue, T., 1987a. A cloud type classification with NOAA 7 split-window measurements. *J.Geophys.Res.*, 92: 3991-4000.

Inoue, T., 1987b. An instantaneous delineation of convective rainfall area using split window data of NOAA-7 AVHRR. *J.Meteorol.Soc.Japan*, 65: 469-481.

Inoue, T., 1997. Detection of rain-bearing convective systems using cloud information derived from split window. *Proc. The 1997 Meteorological Satellite Data Users' Conf.*, EUMETSAT, pp. 173-182.

Islam, M.N. and C.M. Wahid, 2003. "Adaptation of a technique to estimate rainfall from satellite data in Bangladesh," *Journal of Atmosphere*, 2: 79-86.

Islam, M.N, Islam, A.K.M.S. and H. Uyeda, 2003. "Application of GMS-5 data in estimation of rainfall distribution," *Mausam*, 54(2): 521-528.

Islam, M.N, Islam, A.K.M.S, T. Hayashi, T. Terao and H. Uyeda, 2002. "Application of a method to estimate rainfall in Bangladesh using GMS-5 data," *Journal of Natural Disaster Science*, 24(2): 83-89.

Islam M.N., H. Uyeda and K. Kikuchi, 1999. Modification of Convective Stratiform Technique for Tropical Regions. Bang. *J. Sci. Res.*, 17(1): 17-24.

Islam, M.N. and C.M. Wahid, 1999. On the development of a technique to estimate surface rain using satellite data over Bangladesh. *Bang. J.Sci. Res*., 17(2): 181-188.

Islam, M.N. and S. Shafee, 1998. Prediction models for drought and different meteorological variables in Bangladesh. *Dhaka Univ. J. Sci*., 46(2): 327-334.

Islam, M.N., H. Uyeda and K. Kikuchi, 1997. Characteristics of clouds and cloud clusters obtained by radar and satellite data during the TOGA-COARE IOP. J. Fac. Sci. Hokkaido Univ. Japan, Ser. Vll *(Geophysics)*, 10(2): 189-223.

Islam, M.N., H. Uyeda, O. Kikuchi and K. Kikuchi, 1998. Convective and Stratiform Components of Tropical Cloud Clusters in Determining Radar Adjusted Satellite Rainfall during the TOGA-COARE IOP. J. Fac. Sci. Hokkaido Univ. Japan, Ser. Vll *(Geophysics)*, 11(1): 265-300.

Islam, M.N., Islam, A.K.M.S., Hayashi, T., Terao, T. and Uyeda, H., 2003. Application of a method to estimate rainfall in Bangladesh. *J. Nat. Dis. Sci.*, Japan, 24(2): 83-89.

Islam, M.N., T. Hayashi, T. Terao, J. Matsumoto, K. Kikuchi and H. Uyeda, 2002. Rainwater from the Tropical Mesoscale Convective Systems-A Case Study. Proceedings in the Int. Conf. On the Mesoscale Convective System and Heave Rainfall/Snowfall in East Asia, 29-31 Oct., Tokyo, Japan, pp. 71-76.

Islam, M.N., T. Terao, T. Hayashi, J. Matsumoto and T. Oka, 2001. Estimation of monsoon rain and the use of BMD radar data. Proceedings of the 3rd International Symposium on Asian Monsoon (ISAM3), Okinawa, Japan, December 2001, pp. 298-303.

Islam, M.N., Uyeda, H. and Kikuchi, K., 1997. Characteristics of clouds and cloud clusters obtained by radar and satellite data during the TOGA-COARE IOP. J. Fac. Sci. Hokkaido Univ. Japan, Ser. Vll *(Geophysics)*, 10(2): 189-223.

Islam, M.N., Uyeda, H., Kikuchi, O. and Kikuchi, K., 1998. Convective and Stratiform Components of Tropical Cloud Clusters in Determining Radar Adjusted Satellite Rainfall during the TOGA-COARE IOP. J. Fac. Sci. Hokkaido Univ. Japan, Ser. Vll *(Geophysics)*, 11(1): 265-300.

Islam, M.N., A.K.M Saiful *et al.*, 2002. Application of a Method to Estimate Rainfall in Bangladesh Using GMS-5 Data. *Journal of Natural Disaster Science*, 24(2): 83-89.

Janowiak, J.E., Arkin, P.A. and Morrissey, M., 1994. An examination of the diurnal cycle in oceanic tropical rainfall using satellite and in situ data. *Mon. Wea. Rev.*, 122: 2296-2311.

Jeffrey, R. McCollum and Rulph R. Ferraro, 2003. Next generation of NOAA/NESDIS, TMI, SSM/I and AMSR-E microwave land rainfall algorithms, *Journal of Geophysical Research*, 108(0): X1-X17.

Jobard, I. and M. Desbois, 1994. Satellite estimation of the tropical precipitation using the Meteosat and SSM/I data, *Atmospheric Research*, 34: 285-298.

Jobard, I. and M.Desbois, 1992. A method combining infrared and microwave satellite radiances for the estimation of the tropical rain. Proc. 6th Conf. Satellite Meteorology and Oceanography, AMS, pp. 264-267.

Jobard, I, 2001. Status of Satellite Retrieval of Rainfall at different Scales using Multi-source Data, MEGHA-TROPIQUES 2nd Scientific Workshop, France.

Johnson, R.H and R.A. Houze, 1987. *Precipitating systems of the Asian monsoon*. In: C.-P. Cahng and T.N. Kirshnamurti (Ed.), Monsoon Meteorology, Oxford University Press, pp. 298-353.

Karmakar, S. and A. Khatun, 1996. A statistical study on the highest 24 hours monsoon rainfall.

Karmaker, S. and A. Khatun, 1995. Variability and probabilistic estimates of rainfall extremes in Bangladesh during the southwest monsoon season. *Mausam*, 46: 47-56.

Keehn, P. R. and I.M.Hakkarinen, 1993. Estimation of monthly rainfall over Japan and surrounding waters from a combination of low-orbit microwave and geosynchronous IR data. *J. Appl. Meteorol.*, 32: 335-356.

Kidd, C, McGregor, G. 2007. Observation and characterization of rainfall over Hawaii and surrounding region from the Tropical Rainfall Measuring Mission. *International Journal of Climatology* Wiley InterScience, 27(4): 541–553.

Kidd, C., 1998. On rainfall retrieval using polarization-corrected temperatures. *Int.J. Remote Sensing*, 19: 981-996.

Kidd, C., D. Kniveton and E.C. Barrett, 1998. The advantages and disadvantages of statistically derived-empirically calibrated passive microwave algorithms for rainfall estimation. *J. Atmos. Sci.*, 55: 1576-1582.

Kidder S.Q. and T.H. Vonder Haar, 1995. Satellite Meteorology: An Introduction. Academic Press, p. 340.

King, P.W.S., Hogg, W.D. and Arkin, P.A. 1995. The role of visible data in improving satellite rainrate estimates. *J.Appl.Meteorol.*, 34: 1608-1621.

Kodama, Y-M, Ohta, A, Katsumata, M, Mori, S, Satoh, S, Ueda, H., 2005. Seasonal transition of predominant precipitation type and lightning activity over tropical monsoon areas derived from TRMM observations. *Geophysical Research Letters*, 32.

Krajewski, W.F. and J.A. Smith, 2001. Radar hydrology: Rainfall Estimation, *Advances in Water Resources.*

Krajewski, W.F., E.N. Anagnostou and G.J. Ciach, 1996. Effects of the radar observation process on inferred rainfall statistics, *Journal of Geophysical Research-Atmosphere*, 101(D21): 26493-26502.

Krajewski, W.F., G.J. Ciach and E. Habib, 2001. An analysis of small scale rainfall variability in different climatological regimes, *Hydrologic Science Journal*.

Kummerow, C. and Coauthors, 2000. The Status of the Tropical Rainfall Measuring Mission (TRMM) after Two Years in Orbit. *J. Appl. Meteor.*, 39: 1965-1982.

Kummerow, C. and L. Giglio, 1994. A passive microwave technique for estimating rainfall and vertical structure information from space, part I: Algorithm description. *J. Appl. Meteor.*, 33: 3-18.

Kummerow, C. and L. Giglio, 1994. A passive microwave technique for estimating rainfall and vertical structure information from space, part II: Application to SSM/I Data, *J. Appl. Meteor.*, 33: 19-34.

Kummerow, C., Y. Hong, W.S. Olson, S. Yang, R.F. Adler, J. McCollum, R. Ferraro, G. Petty, D. –B. Shin and T.T. Wilheit, 2001. The Evolution of the Goddard Profiling Algorithm(GPROF) for Rainfall Estimation from Passive Microwave Sensors. *J. Appl. Meteor.,* 40: 1801-1819.

Kummerow, C., Barnes, W., Kozu, T., Shiue, J. and Simpson, J., 1998. The Tropical Rainfall Measuring Mission (TRMM) sensor package. *J. Atmos. Oceanic Technol.*, 15: 809–817.

Kummerow, C., J. Simpson, O. Thiele, W. Barnes, A.T.C. Chang, E. Stocker, R.F. Adler, A. Hou, R. Kakar, F. Wentz, P. Ashcroft, T. Kozu, Y. Hong, K. Okamoto, T. Iguchi, H. Kuroiwa, E. Im, Z. Haddad, G. Huffman, B. Ferrier, W. S. Olson, E. Zipser, E. A. Smith, T. T. Wilheit, G. North, T. Krishnamurti, K. Nakamura, 2000. The Status of the Tropical Rainfall Measuring Mission (TRMM) after Two Years in Orbit. *J. Appl. Meteor.,* 39: 1965-1982.

Kummerow, C., Simpson, J., Thiele, O., Barnes, W., Chang, A.T.C., Stocker, E., Adler, R.A., Hou, A., Kakar, R., Wentz, F., Ashcroft, P., Kozu, T., Hong, Y., Okamoto, K., Iguchi, T., Kuroiwa, H., Haddad, E. Im, Z., Huffman, G., Ferrier, B., Olson, W. S., Zipser, E., Smith, E. A., Wilheit, T. T.,

North, G., Krishnamurti, T. and Nakamura, K., 2000. The Status of the Tropical Rainfall Measuring Mission (TRMM) after Two Years in Orbit. *J. Appl. Meteor.*, 39: 1965-1982.

Kummerow, C., W.S. Olson and L. Giglio, 1996. A simplified scheme for obtaining precipitation and vertical hydrometeor profiles from passive microwave sensors. *IEEE Transactions on Geoscience and Remote Sensing:* 34: 1213-1232.

Kurino, T., 1997a. A satellite infrared technique for estimating "deep/shallow" convective and stratiform precipitation. *Adv.Space Res*., 19: 511-514.

Kurino, T., 1997b. A rainfall estimation with the GMS-5 infrared spli-window and water vapour measurements. *Meteorol.Center Tech.Note*, Japan Meteorol. Agency, 33: 91-101.

Kurino, T., 1997. A satellite infrared technique for estimating "deep/shallow" convective and stratiform precipitation. *Adv.Space Res.*, 19: 511-514.

La. Barbara, P, Lanza L. G and Stagi L., 2002. Tipping bucket mechanical errors and their influence on rainfall statistics and extremes, *Water Science and Technology*, 45(2): 1-9.

Laing, A.G., J.M. Fritsch and A.J. Negri, 1994. Estimation of rainfall from mesoscale convective systems in Africa using geostationary infrared and passive microwave data. Proc. 7th Conf. Satellite Meteorology and Oceanography, AMS, 40-42.

Lang. T.J. and Barros, A.P, 2002. An Investigation of the Onsets of the 1999 and 2000 monsoons in Central Nepal, *Monthly Weather Review*, 130: 1299-1316.

Laurent H., I. Jobard and A. Toma, 1998. Validation of satellite and ground-based estimates of precipitation over the Sahel. *Atmospheric Research*, 47-48: 651-670.

Lebel, T., J.D. Taupin and M. Greard, 1995. Rainfall Monitoring: The EPSAT-Niger setup and its use for HAPEX-Sahel. Hydrologie et Meteorologie de Meso-Echelle dans HAPEX-Sahel: Dispositif de Mesures au Sol et Premiers Resultats, T. Lebel, Ed. OR-STOM, pp. 31-68.

Lensky, I.M. and Rosenfeld, D. 1997. Estimation of precipitation area and rain intensity based on the microphysical properties retrieved from NOAA AVHRR data. *J.Appl.Meteorol*., 36: 234-242.

Levizzani, V. *et al.*, 2003. Use of the MSG SERIRI Channels In A Combined SSM/I, TTRMM and Geostationary IR Method for Rapid Updates of Rainfall.

Levizzani, 2000. Combining SSM/I, TRMM and Infrared Geostationary Satellite Data in a Near-Realtime Fashion for Rapid Precipitation Updates: Advantages and Limitations.

Levizzani, V., 1998. Intense rainfall monitoring from geostationary satellites. Prepr. 9*th* Conf. Satellite Meteorology and Oceanography, *AMS*, pp. 327-330.

Levizzani, V., Porcù, F. and Prodi, F., 1990. Operational rainfall estimation using METEOSAT infrared imagery: An application in Italy's Arno river basin–Its potential and drawbacks. *ESA J*., 14: 313-323.

Levizzani, V., Porcù, F., Marzano, F.S., Mugnai, A., Smith, E.A. and Prodi, F., 1996. Investigating a SSM/I microwave algorithm to calibrate METEOSAT infrared instantaneous rainrate estimates. *Meteorol. Appl*., 3: 5-17.

Li, C. and M. Yanai, 1996. The onset and international variability of the Asian summer monsoon in relation to land-sea thermal contrast. *J. Climate,* 9: 358-375.

Liu, X. and M. Yanai, 2001. Relationship between the Indian monsoon rainfall and the tropospheric temperature over the Eurasian continent. *Q. J. R. Meteor. Soc*., 127: 909-937.

Lovejoy, S. and Austin, G.L., 1979. The delineation of rain areas from visible and IR satellite data from GATE and mid-latitudes. *Atmos.-Ocean*, 17: 77-92.

Machado, L.A.T., Duvel, J.–P. and Debois, M., 1993. Diurnal variations and modulation by easterly waves of the size distribution of convective cloud clusters over western Africa and the Atlantic Ocean. *Mon. Wea. Rev.*, 121: 37-49.

Machado, L., Rossow, W., Guedes, R. and Walker, A., 1998. Lifecycle variations of mesoscale convective systems over the Americans. *Mon. Wea. Rev.*, 126: 1630-1654.

Mapes, B.E. and Houze, R.A. Jr., 1993. Cloud clusters and super clusters over the oceanic warm pool. *Mon. Wea. Rev.*, 121: 1394-1415.

Mapes, B.E., T.T. Warner, M. Xu, and A.J. Negri, 2003. Diurnal; patterns of rainfall in Northwestern South America. Part I: Observations and context. *Mon. Wea. Rev*., 131: 799-812.

Mapes, B.E., Warner, T.T., Xu, M., 2003b. Diurnal; patterns pf rainfall in Northwestern South America. Part III: Diurnal gravity waves and nocturnal convection offshore. *Mon. Wea. Rev.*, 131: 830-844.

Mapes, B.E., Warner, T.T., Xu, M., Negri, A.J., 2003a. Diurnal; patterns pf rainfall in Northwestern South America. Part I: Observations and context. *Mon. Wea. Rev.*, 131: 799-812.

Marrocu, M., A.Pompei, G. Dalu, G.L. Liberti and A.J.Negri, 1993. Precipitation estimation over Sardinia from satellite infrared data. *Int.J.Remote Sensing*, 14: 115-134.

Martin D.W., B. Goodman, T.J. Schmit and E.C. Cutrim, 1990. Estimates of daily rainfall over the Amazon Basin. *J. Geophysics Res.*, 95(D10): 17043-17050.

Martin. C. Todd, Chris Kidd, Dominic Kniveton and Tim J. Bellerby, 2001. A combined Satellite Infrared and Passive Microwave Technique for Estimation of Small-Scale Rainfall, *American Meteorological Society*, 18: 742-755.

Mathon, V., H. Laurent and T. Lebel, 2002. Mesoscale Convective System Rainfall in the Sahel, *J. Appl. Meteor*., 41(11): 1081-1092.

Matsumoto, J.M.R., Rahman, T. Hayashi and N. Monji, 1996. Rainfall distribution over Indian subcontinent during the 1987 and 1988 severe floods in Bangladesh, *Bulletin Dept. of Geography, University of Tokyo, Japan*, 28: 25-44.

Matsumoto, J., 1988. Synoptic features of heavy monsoon rainfall in 1987 related to the severe flood in Bangladesh. *Bulletin Dept. of Geography, University of Tokyo*, *Japan*, 20: 43-56.

McAnelly, R.L. and Cotton, W.R., 1989. The precipitation life cycle of mesoscale convective complexes over the central United States. *Mon. Wea. Rev.*, 117: 784–808.

McGarry, M.M. and Reed, R.J., 1978. Diurnal variations in convective activity and precipitation during phases II and III of GATE. *Mon. Wea. Rev.*, 106: 101-113.

Meisner, B.N and P.A. Arkin, 1987. Spatial and annual variations in the diurnal cycle of large-scale tropical convective cloudiness and precipitation. *Mon. Wea. Rev*., 115: 2009-2032.

Menzel, W.P. and Purdom, J.F.W., 1994. Introducing GOES-I: the first of new generation of Geostationary Operational Environmental Satellites. *Bull.Amer.Meteorol.Soc*., 75: 757-781.

Miller, S.W., P.A. Arkin, R. Joyce, 2000. A combined microwave/infrared rain rate algorithm*. J. Rem. Sens*.

Mitchell, K. and Co-authors, 1999. GCIP Land Data Assimilation System (LDAS) project now underway. *GEWEX News*, 9(4): 3-6.

Mitchell, K. and Co-authors, 2000. Recent GCIP-sponsored advancements in coupled land-surface modeling and data assimilation in the NCEP Eta mesoscale model. Preprints, 15th AMS Conf. on Hydrology, Long Beach, CA, Paper P1.22.

Mooley, D.A. and J. Shukla, 1987. Variability and forecasting of the summer rainfall in India, Reviews in Monsoon Meteorology, Edited by C. P. Chang and T. N. Krishnamurti, pp. 26-59, Oxford University Press, New York.

Morales, C. and E.N. Anagnostou, 2003. Extending the Capabilities of High-Frequency Rainfall Estimation from Geostationary-Based Satellite Infrared via a Network of Long-Range Lightning Observations, *Journal of Hydrometeorology.*

Mugnai, A. and E.A. Smith, 1988. Radiative transfer to space through a precipitating cloud at multiple microwave frequencies. Part I: Model description. *J. Appl. Meteor.*, 27: 1055-1073.

Mugnai, A., Smith, E.A. and Tripoli, G.J. 1993. Foundations for statistical-physical precipitation retrieval from passive microwave satellite measurements. Part II: Emission-source and generalized weighting-function properties of a time-dependent cloud-radiation model. *J.Appl.Meteorol*., 32: 17-39.

Murakami, M., 1976. Analysis of summer monsoon fluctuations over India, *Journal of Meteorological Society of Japan*, 54: 175-181.

Negri, A.J, Nelkin, EJ, Adler, R.F, Huffman G.J., Kummerow, C., 1995. Evaluation of Passive Microwave Precipitation Algorithms in Wintertime Mid Latitude Situation, Journal of Atmospheric Ocean Technology, 12, 20-32.

Negri, A.J. and Adler, R.F., 1987. Infrared and visible satellite rain estimation, Part II: A cloud definition approach. J. Cli. Appl. Met., 26: 1565-1576.

Negri, A.J., R.F. Alder and P.J. Wentzel, 1984. Rain estimation from satellites: An examination of the Griffith- Woodley technique. *J. Climate Appl. Meteor.,* 23: 102-116.

Negri, A.J. and R.F. Adler, 1981. Relationship of satellite-based thunderstorm intensity to radar-estimated rainfall. *J. Appl. Meteor*., 20: 288-300.

Negri, Andrew J., Robert F. Adler, Eric J. Nelkin, George J. Huffman, 1994. Regional Rainfall Climatologies Derived from Special Sensor Microwave Imager (SSM/I) Data. *Bulletin of the American Meteorological Society*: 75(7): 1165–1182.

Nesbitt, S.W. and Zipser, E.J., 2003. The diurnal cycle of rainfall and convective intensity according to three years of TRMM measurements. *J. Climate*, 16: 1456-1475.

Nguyen, V.T.V, Nguyen, T.D. and Ashkar F., 2002. Regional Frequency Analysis of Extreme Rainfalls, *Water Science and Technology*, 45(2): 75-81.

North America, 2001. Chapter 15 of: Intergovernmental Panel on Climate Change (IPCC). Climate Change 2001: Impacts, Adaptation and Vulnerability. Cambridge University Press.

O'Sullivan, F., Wash, C.H., Stewart, M. and Motell, C.E., 1990. Rain estimation from infrared and visible GOES satellite data. *J.Appl.Meteorol*., 29: 209-223.

Ohsawa, T., H. Ueda, T. Hayashi, A. Watanabe and J. Matsumoto, 2001. Diurnal variations of convective activity and rainfall in tropical Asia. *J. Meteor. Soc. Japan,* 79: 333-352.

Ohsawa, T., Hayashi, T., Hayasti, T. Oka and Y. Mitsuta, Y., 1997a. Characteristics of mosoon rainfall over Bangladesh in 1995, Ann. Disaster Prevention Research Institute, Kyoto University, no. 40, B-1.

Ohsawa, T., Hayashi, T., Mitsuta, Y. and Matsumoto, J., 2000. Intraseasonal variation of monsoon activities associated with the rainfall over Bangladesh during 1995 summer monsoon season, *J. Geophys. Res.*, 105; 29445-29459.

Oki, T. and Musiake, K., 1994. Seasonal change of the diurnal cycle of precipitation over Japan and Malaysia. *J. Appl. Meteor.*, 33: 1445–1463.

Ose, T., 1998. Seasonal change of Asian summer monsoon circulation and its heat source. *Journal of the Meteorological Society of Japan*, 76: 1045–1063.

Pal, P.K, Neeraj, Agarwal and C.M. Kishtawal, 2001. Vertical Structure of Rainfall from TRMM PR Data for Assimilation in GCM, MEGHA-TROPIQUES 2nd Scientific Workshop, France.

Pant, G. B. and K.R. Kumar, 1997. Climate of South Asia, 320 pp, John Wiley, New York.

Petersen, W.A. and S.A. Rutledge, 1998. On the relationships between cloud-to-ground lightning and convective rainfall, *J. Geophys. Res. Atmos*., 103(D12): 14025-14040.

Petty, G.W., 1995. The status of satellite-based rainfall estimation over land. *Remote Sens.Environ*., 51: 125-137.

Petty, G.W. and Krajewski W.F., 1996. Satellite Estimation of Precipitation over Land, Hydrological Science Journal, IAHS, 41, p 435.

Poccard, I, Janicot, S and Camberlin, P., 2000. Comparison of rainfall structures between NCEP/NCAR reanalysis and observed data over tropical Africa, *Climate Dynamics*, 16: 897-915.

Porcù, F., F. Prodi, S. Franceschetti and S. Pasetti, 1997. Short term climatology of cloud systems leading to flood events in Europe (1991-1996). Proc. 1997 Meteorological Satellite Data Users' Conf., EUMETSAT, pp. 461-466.

Prabhakara C, R. Iacovazzi, R Oki and J. A. Weinman, 1999. A Microwave Radiometer Rain Retreival Method Applicable to Land Areas. *Journal of the Meteorological Society of Japan*, 77(4): 859-871.

Prabhakara C, R. Iacovazzi, R Oki, J.A. Weinman and G. Dalu, 2000. A TRMM Microwave Radiometer Rain Estimation Method with Convective and Stratiform Discrimination, *Journal of the Meteorological Society of Japan*, 78(3): 241-258.

Prabhakara, C., R. Meneghini, D.A. Short, J.A. Weinman, R. Iacovazzi, R. Oki and M. Cadeddu, 1998. A TRMM Microwave radiometer rain retrieval method based on fractional rain area. Journal of the Meteorological Society of Japan: 76: 765-781.

Prasad, B., 1974. Diurnal variation of rainfall in Brahmaputra valley. *Ind. J. Met. Geophysics,* 25(2): 245-250.

Quadir, D.A., Mehrun, Nessa, Hafizur, Rahman and A.M. Choudhury, 1999. On the Relationship of Rainfall and Satellite-based Cloud Top Temperature, *Journal of Remote Sensing and Environment*, vol. 3.

Quamrul, Huda, A.Q.M., 1998. Flood Control and Management for Improvement of Urban Environment, Proceedings of the Workshop on Regional Cooperation in Flood Control and Management for Improvement of Urban Environment in Asia and the the Pacific. Phase – I. October, 1998, ESCAP, Bangkok, Thailand.

Rahman, M. R., 1997. Environmental and Socio-economic aspects of flood in Bangladesh, in Proceedings of International Symposium on natural Disaster Prevention and Mitigation, Disaster Prevention Research Institute, Kyoto University, pp. 427-432.

Ramage, C.S., 1971. Mnosoon meteorology, Academic Press, New York, p 296.

Rao, A.V.R.K. and V.R. Rao, 1993. Diurnal variation of cloudiness during southwest monsoon season using INSAT-1B radiance data, *Mausam*, 44 (3).

Rao, Y.P., 1976. Southwest monsoon, *Synoptic Meteorology, Meteorological Monogr*., India Meteorological Department, 1, p. 367.

Reed, R.J. and Jaffe, J.D., 1981. Diurnal variation of summer convection over West Africa and the tropical eastern Atlantic during 1974 and 1978. *Mon. Wea. Rev.*, 109: 2527-2534.

Reudenbach, C, G. Heinemann, E. Heuel, J. Bendix and M. Winiger, 2001. Investigation of summertime convective rainfall in Western Europe based on a synergy of remote sensing and numerical models, *Meteorological Atmospheric Physics*, 76: 23-41.

Riehl, H. and A.L. Miller, 1978. Differences between morning and evening temperatures of cloud tops over tropical continents and oceans. *Quart. J. Roy. Meteor. Soc*., 104: 757-764.

Robinson, J.M. and R.A.Scofield, 1994. Using satellite imagery to analyze the devastating flash floods in the western region between December 1992 and February 1993. Proc. 7th Conf.Satellite Meteorology and Oceanography, *AMS*, pp. 417-420.

Rosenfeld, D., E. Amitai and D.B. Wolff, 1995. Improved accuracy of radar WPMM estimated rainfall upon application of objective classification criteria. *J. Appl. Meteor.,* 34: 212-223.

Rudolf and F. Rubel, Regional Validation of Satellite Based Global Precipitation Estimates.

Saleh, A.M.F, S.M.U. Ahmed, M. Miah, R. Rahman, M. Salehin and M. S. Mondal, 1998. Performance Evaluation of FCD/FCDI projects during 1998 flood, report, 113 pp, IFCDR, Bangladesh University of Engineering and Technology, Dhaka.

Satyamurty, P. and C.A. Nobre, 1998. Amazon. . In: D. J. Karoly and D. G Vincent (Ed.), Meteorology of the Southern Hemisphere, *Amer. Meteor. Society*, pp. 141-174.

Savage, R.C., E.A. Smith and A. Mugnai, 1994. Concepts for a geostationary microwave imaging sounder (GeoMIS). Proc. 7*th* Conf.Satellite Meteorology and Oceanography, *AMS*, pp. 516-519.

Sawinigan Lavalin Inc. and Northwest Hydraulic Consultants, 1993. Surface Water Resources of Northeast Region Report, Northeastern Regional Water Resources Management Project, Canadian International Dev. Agency.

Schmetz, J., Tjemkes, S.A., Gube, M. and van de Berg, L., 1997. Monitoring deep convection and convective overshooting with METEOSAT. *Adv. Space Res*., 19: 433-441.

Schmetz, J., Woick, H., Tjemkes, S.A. and Rattenborg, M., 1998. From METEOSAT to METEOSAT Second Generation (MSG). *Prepr. 9th Conf. Satellite Meteorology and Oceanography*, *AMS*, pp. 335-338.

Scofield, R. A, 1987. The NESDIS operational convective precipitation technique. *Mon. Wea. Rev*., 115(8): 1773-1792.

Scofield, R. A. and V. J. Oliver, 1980. Some improvements to the Scofield/Oliver technique. Proceedings of the Second Conference on Flash Floods. Atlanta, *Amer. Meteor. Soc.*, pp. 115-122.

Scofield, R.A. and V.J. Oliver, 1977. A scheme for estimating convective rainfall from satellite imagery. NOAA Tech. Memo. NESS 86, U.S. Dept. Commerce, Washington, DC, USA, 47 p.

Sevruk, B., 1982. Methods of correction for systematic error in point precipitation measurement for operational use, Operational Hydrology Report No 21, WMO Rep. No. 589, p. 91.

Shepherd J.M, E.A. Smith, W.J. Adams, 2002. Global Precipitation Measurement - Report 7 Bridging from TRMM to GPM to 3-Hourly Precipitation Estimates, GSFC, NASA.

Sherwood, S. C. and Wahrlich, R., 1999. Observed evolution of tropical deep convective events and their environment. *Mon. Wea. Rev.*, 127: 1777–1795.

Shih, S.F., 1989. Potential application of satellite data for rainfall estimation, Remote Sensing and Large Scale Global Processes, IAHS 3rd International Assembly, IAHS Publ. No. 186.

Short, D.A. and J.M. Wallace, 1980. Satellite-inferred morning-to evening cloudiness changes. *Mon. Wea. Rev*., 108: 1160-1169.

Silva, D.P.L., Bonatti, J.P. and Kousky, V.E., 1987. Diurnally forced tropical tropospheric circulation over South America. *Mon. Wea. Rev.*, 115: 1465–1478.

Simpson, J., Adler, R.F., North G.R., 1988. A proposed tropical rainfall measuring mission (TRMM) satellite. *Bulletin of the American Meteorological Society*, 69: 278–295.

Simpson, J. and Theon, J.S., 1991. The Tropical Rainfall Measuring Mission (TRMM) and Its Role in Studies of Climate Variations, present at the 1991 international Geoscience and Remote Sensing Symposium (IGARSS'91), Espoo, Finland, June 3-6, 1991.

Singh, O.P., 2001. Casue-effect relationships between sea surface temperature, precipitation and sea level along the Bangladesh coast, *Theoritecal Applied Climatology*, 68: 233-243.

Smith, E.A. and others, 1998. Results of the WetNet PIP-2 Project. *J. Appl. Meteor*., 55: 1483-1536.

Smith, E.A., Mugnai, A., Cooper, H.J., Tripoli, G.J. and Xiang, X., 1992. Foundations for statistical-physical precipitation retrieval from passive microwave satellite measurements. Part I: Brightness-temperature properties of a time-dependent cloud-radiation model. *J. Appl. Meteorol*., 31: 506-531.

Sorooshian, S., X. Gao, K. Hsu, R.A. Maddox, Y. Hong, H.V. Gupta, B. Imam, 2002. Diurnal Variability of Tropical Rainfall Retrieved from Combined GOES and TRMM Satellite Information. *Journal of Climate*: 15(9): 983–1001.

Spencer, R.W., Goodman, H.M. and Wood, R.E., 1988. Precipitation retrieval over land and ocean with the SSM/i, Part 1: Identification and characteristics of the scattering signal. *J. Atmos. Oceanic* Tech. 2, pp. 254-263.

Spencer, R.W., Goodman, H.M. and Hood, R.E., 1989. Precipitation retrieval over land and ocean with SSM/I. Part I: Identification and characteristics of the scattering signal. *J.Atmos.Ocean.Technol*., 6: 254-273.

Stein, S.E, Scott, D.R; 1994. Optimization and Testing of Mass Spectral Search Algorithms for Compound Identification*; J. Amer. Soc.* Mass. Spec., 5: 859-866.

Steiner, M. and R.A. Houze Jr., 1995. Sensitivity of the estimated monthly convective rain fraction to the choice of Z-R relation. *J. Appl. Meteor.,* 36: 452-462.

Steiner, M., J.A. Smith, S.J. Burges, C.V. Alonso and R.W. Darden, 1999. Effect of bias adjustment and rain gauge data quality control on radar rainfall estimation. *Water Resour. Res.*, 35: 2487-2503.

Steven A. Listemaa, 1997. A Modified Convective-Stratiform Partitioning Algorithm.

Tappia, A., J.A. Smith and M. Dixon, 1998. Estimation of convective rainfall from lightning observations, *J. Appl. Meteor*., 37: 1497-1509.

Terao, T, Islam, MN, Murata, F, Hayashi, T., 2006. Meso-scale characteristics of cloud systems over the Bengal plain in the pre- and mature summer monsoon seasons. In *Proceedings of the International Conference on Mesoscale Processes in Atmosphere, Ocean and Environmental Systems*, Delhi, India, 14–17 Feb. 2006, P-II 33.

Teruo Ohsawa, Hiromasa Ueda, Taiichi Hayashi, 2001. *Journal of the Meteorological Society of Japan*, 79(1B): 333-352.

Thorne, V., P. Coakeley, D. Grimes and G. Dugdale, 2001. Comparison of TAMSAT and CPC rainfall estimates with raingauges, for southern Africa. *Int. J. Remote Sensing*, 22(10): 1951-1974.

Tjemkes, S.A., L.van de Berg and J.Schmetz, 1997. Warm water vapour pixels over high clouds as observed by METEOSAT. *Beitr.Phys.Atmosph.*, 70: 15-21.

Todd, M.C., C. Kidd, D. Kniveton and T.J. Bellery, 2001. A combined satellite infrared and passive microwave techniques for estimation of small-scale rainfall. *J. Atmos. Oceanic Technol*., 18: 743-755.

Todd, M.C., Barrett, E.C., Beaumont, M.J. and Green, J.L., 1995. Satellite identification of rain days over the upper Nile river basin using an optimum infrared rain/no-rain threshold temperature model. *J. Appl.Meteorol.*, 34: 2600-2611.

Todd, M.C., E.C. Barrett, M.J. Beaumont and T.J. Bellerby, 1999. Estimation of daily rainfall over the upper Nile river basin using a continuously calibrated satellite infrared technique. *Meteor.* Appl.,6: 201-210.

Tokay, Ali, David A. Short, 1996. Evidence from Tropical Raindrop Spectra of the Origin of Rain from Stratiform versus Convective Clouds. *Journal of Applied Meteorology*. 35(3): 355–371.

TRMM report, 2002. Rain as seen from space, Edited by “Rain as seen from space” production committee, published by Japan Advanced Plan Co., Inc. First edition, 31 May 2002.

Tsintikidas, D., Anagnostou, E. N., Haferman, J.L., Krajewski, W.F. and Smith T.F., 1997. A Neural Network Approach to Estimating Rainfall from Spaceborne Microwave Data, *IEEE Trans. Geoscience Remote Sensing,* 35(5): 1997.

Tsonis, A.A., 1987. Determining rainfall intensity and type from GOES imagery in the midlatitudes. *Remote Sens.Environ.*, 21: 29-36.

Tsonis, A.A. and Isaac, G.A., 1985. On a new approach for instantaneous rain area delineation in the midlatitudes using GOES data. *J.Clim.Appl.Meteorol.*, 24: 1208-1218.

Turk, F.J., J. Hawkins, E.A. Smith, F.S. Marzano, A. Mugnai and V. Levizzani, 2000. Combining SSM/I, TRMM and Infrared Geostationary Satellite Data in a Near-real Time Fashion for Rapid Precipitation Updates: advantages and limitations. Proc.The 2000 EUMETSAT Meteorological Satellite data User's conference, Bologna, Italy, 29 May – 2 June 2000.

Turk, F.J., Marzano, F.S. and Smith, E.A., 1998a. Combining geostationary and SSM/I data for rapid rain rate estimation and accumulation. Prepr. 9th Conf.Satellite Meteorology and Oceanography, *AMS*, 462-465.

Turk, F.J., Marzano, F.S., Smith, E.A. and Mugnai, A., 1998b. Using coincident SSM/I and infrared satellite data for rapid updates of rainfall. Proc. IGARSS'98-Sensing and Managing the Environment Symposium, Proc. CD-ROM, IEEE, ISBN 0-7803-4406-5.

Uijlenhoet, R., J.A. Smith, M. Steiner, 2003. The microphysical structure of extreme precipitation as inferred from ground-based raindrop spectra. *Journal of the Atmospheric Science,* 60(10): 1220-1238.

Vicente, G.A., R.A. Scofield, W.P. Menzel, 1998. The operational GOES infrared rainfall estimation technique. *Bull. Amer. Meteor. Soc.*, 79: 1883-1898.

Vicente, G.A., 1996. Algorithm for rainfall rate estimation using a combination of GOES-8 11.0 and 3.9 micron measurements. Prepr. 8th Conf. Satellite Meteorology and Oceanography, *AMS*, pp. 274-278.

Vicente, G.A. and Anderson, J.R., 1994. A new rain retrieval technique that combines geosynchronous IR and MW polar orbit data for hourly rainfall estimates. Prepr. 7th Conf. Satellite Meteorology and Oceanography, *AMS*, pp. 34-37.

Wahid, C. M and Islam, M.N, 1999. "Patterns of rainfall in the northern part of Bangladesh," *Bang. J. Sci. Res*., 17(1): 115-120.

Wahid C.M, Nazrul Islam, 2000. Use of Satellite data to estimate rainfall over Bangladesh, Bangladesh *Journal of Science and Technology*, 2(1): 141-145.

Wahid, C.M, Nazrul Islam, Rezaur Rahman, 2000. Calculation of Rainfall from satellite data in and around Bangladesh, *Mausam*, 51: 359-364.

Wahid, C.M., R. Rahman and M.N. Islam, 1999. Single cell and multiple cell clouds analyzed with satellite data in and around Bangladesh. *Mausam*, 50(2): 177-180.

Wallace, J.M., 1975. Diurnal variations in precipitation and thunderstorm frequency over the conterminous United States. *Mon. Wea. Rev.*, 103: 406–419.

Wann-Jin Chen and Ching-Chung Li, 2002. An Infrared Rainfall Algorithm for the MCSs Prevailing over the South China Sea in the Mei-Yu Season, *TAO*, 13(1): 65-90.

Warner, T.T., B.E. Mapes, M. Xu, 2003. Diurnal patterns of rainfall in Northwestern South America. Part II: Model Simulations. *Mon. Wea. Rev*., 131: 813-829.

Webster, P.J. and R. Lukas, 1992. TOGA COARE: The Coupled Ocean-Atmosphere Response Experiment. *Bull. Amer. Meteor. Soc*., 73: 1377-1416.

Webster, P. and coauthors, 2002. The JASMINE pilot study. *Bull. Amer. Meteor. Soc.,* 83: 1603-1630.

Weller, R.A. and S.P. Anderson, 1996. Surface meteorology and air-sea fluxes in the western equatorial Pacific warm pool during the Coupled Ocean-Atmosphere Response Experiment. *J. Climate*, 9: 1959-1990.

Weng, F., R.R. Ferraro and C. Grody, 1994. Global precipitation estimations using Defense Meteorological Satellite Program F10 and F11 special sensor microwave imager data. *J. Geophys. Res.*, 99(D70): 14,493-14,502.

Weng, F., B. Yan and N. Grody, 2001. A microwave land emissivity model. *J. Geophys. Res.,* 106: 20,115-20,123.

Wilheit, T.T., 1986. Some Comments on Passive Microwave Measurement of Rain. *Bull. Amer. Meteor. Soc.*, 67(10): 1226-1232.

Wilheit, T.T., A.T.C. Chang and L.S. Chiu, 1991. Retrieval of monthly rainfall indices from microwave radiometric measurements using probability distribution functions. *J. Atmos. Oceanic. Technol.,* 8: 118-136.

Wilheit, T.T., Adler, R.F., Avery, S., Barrett, E., Bauer, P., Berg, W., Chang, A., Ferriday, J., Grody, N., Goodman, S., Kidd, C., Kniveton, D., Kummerow, C., Mugnai, A., Olson, W., Petty, G., Shibata, A., Smith, E.A. and Spencer, R., 1994. Algorithms for the retrieval of rainfall from passive microwave measurements. *Rem.Sens.Rev*., 11: 163-194.

Willmontt, C.J., S.M. Robeson, J.J. Feddema, 1994. Estimating continental and terrestrial precipitation average from rain-gauge networks. *Int. J. Climatology*, 14: 403-414.

Woick, H., Schmetz, J. and Tjemkes, S.A., 1997. An introduction to METEOSAT Second Generation imagery and products. Proc. The 1997 EUMETSAT Meteorological Satellite Data Users' Meeting, 395-400.

Woodley, W.L., A.R. Olsen, A. Herndon and V. Wiggert, 1975. Comparison of gauge and radar methods of convective rain measurements. *J. Applied Meteor.* 14: 909-928.

World Climate Research Programme (1986). Global large-scale precipitation data sets for the WCRP. WCP, 111, WMO/TD no. 94.

Wylie, D.P., 1979. An application of a geostationary satellite rain estimation technique to an extratropical area. *J.Appl.Meteorol.*, 18: 1640-1648.

Xu, L., S. Sorooshian, X. Gao and H. V. Gupta, 1999. A cloud-patch technique for identification and removal of no-rain clouds from satellite infrared imagery. *J. Appl. Meteor.*, 38: 1170-1181.

Xu, L., X. Gao and S. Sorooshian, 2001. A microwave threshold technique to improve the GOES precipitation index. *J. Appl. Meteor.*, 38: 369-579.

Xu, L., X. Gao, S. Sorooshian, P.A. Arkin, B. Imam., 1999. A microwave infrared threshold technique to improve the GOES Precipitation Index. *J. Appl. Meteor*., 38: 569-579.

Yang, D., B. Goodson and S. Ishida, 1998. Adjustment of daily precipitation data at 10 climate stations in Alaska: Application of World Meteorological Organization inter comparison results. *Water Resources Research*, 34: 241-256.

Yang, G.Y. and Slingo, J., 2001. The diurnal cycle in the tropics. *Mon. Wea. Rev.*, 129: 784-801.

Ye Hong, Christian D. Kummerow, W.S. Olson, 1999. Separation of Convective and Stratiform Precipitation Using MW Brightness Temperature, *Journal of Applied Meteorology*, 38: 1195-1213.

Yunfei Fu and Guosheng Liu, 2001. The variability of tropical precipitation profiles and its impacts on Microwave brightness temperatures as infrared from TRMM data, *Journal of Applied Meteorology*, 40: 2130-2143.

Zalina, M.D., Desa. M.N.M, Nguyen V.T.V. and Kassim, A.H.M, 2002. Selecting a propability distribution for extreme rainfall series in Malaysia, *Water Scienece and Technology*, 45(2): 63-68.

Zuidema, P., 2003. Convective clouds over the Bay of Bengal. *Mon. Wea. Rev.,* 131: 780-798.

GLOSSARY

Active Sensor: A sensor designed to transmit and receive radiation, not necessarily of the same spectral band, e.g. radar.

Passive Sensor: A sensor designed only to receive radiation up welling from the scene below.

Attenuation: A decrease in the amount of radiation received by a sensor due to absorption or scattering by atmp. constituents so that the scene imaged may appear cooler than it really is.

Backscatter: Radiation scattered back towards source. Decreasing size parameter increases backscatter.

Scattering: Also called thermal emission. Occurs when outgoing radiation from thermalization of a particle is released at different wavelengths and directions than the incoming radiation.

Brightness Temperature: Applicable to long wavelengths (microwave and longer). The effective temperature producing irradiance $B\lambda$ at wavelength.

Emissivity: The property of a medium to emit radiation when irradiated, calculated from the absorptivity*irradiance.

Geostationary Orbit: A geosynchronous orbit in which the satellite has the same angular velocity as the Earth, an altitude on the order of 104 km, near zero eccentricity, and zero inclination angle. Satellite can take continuous images of the scene below with little or no perceived movement.

Goddard Profiling Algorithm GPROF: A physical precipitation retrieval that uses a numerical model (cloud-resolving), adjusting the parameters of that model so that the radiation up welling from model clouds matches observed radiation. The resulting vertical profile of hydrometeors producing the desired radiation is then used to calculate instantaneous rain rates.

Goddard Scattering Algorithm GSCAT: A statistical precipitation retrieval, a linear equation relating the horizontally polarized 85 GHz brightness temperature to instantaneous rainfall rate in mm/hr.

GOES Precipitation Index GPI: A statistical precipitation retrieval, a linear equation relating the fraction of cold cloud cover < 235 K (-38 C), an average precipitation rate (3 mm/hr), and the observation interval to rainfall in that interval.

Mesoscale Convective System: A large organized convective weather system comprised of a number of individual thunderstorms. It normally persists for several hours and may be rounded or linear in shape. This term is often used to describe a cluster of thunderstorms that does not meet the criteria of a mesoscale convective complex (MCC).

Monsoon: The seasonal shift of winds created by the great annual temperatures variation that occurs over large land areas in contrast with associated ocean surfaces. The monsoon is associated primarily with the moisture and copious rains that arrive with the southwest flow across southern India.

Radiative Transfer Theory states that the T_B measured by a space-borne radiometer is the linear sum of individual contributions from the atmosphere and surface

- Surface emission
- Upwelling atmosphere emission
- Downwelling atmosphere emission that is reflected from surface

ENSO is a coupled ocean-atmosphere phenomenon centered in and over the tropical Pacific and refers to large-scale anomalies in a number of oceanic and atmospheric variables such as sea surface temperature (SST), sea level pressure (SLP), and rainfall. El Niño and La Niña episodes are the opposite extremes of the ENSO phenomenon. A typical El Niño (La Niña) event starts in late summer-early fall, reaches its peak sometime between December and February and decays by late spring-early summer. However, no two events are exactly the same as each event has its own distinct characteristics (e.g., distribution of SST in the tropical Pacific, onset, amplitude, duration, and climatic impacts). There are several standard oceanic and atmospheric indices for monitoring

ENSO. The most commonly used atmospheric index is the Southern Oscillation index (SOI). SOI is a measure of large-scale anomalies in the sea level pressure between the western and eastern tropical Pacific.

Southern Oscillation Index (SOI) is calculated from the monthly or seasonal fluctuations in the air pressure difference between Tahiti and Darwin. Sustained negative values of the SOI often indicate El Niño episodes. These negative values are usually accompanied by sustained warming of the central and eastern tropical Pacific Ocean, a decrease in the strength of the Pacific Trade Winds, and a reduction in rainfall over eastern and northern Australia. The most recent strong El Niño was in 1997/98. Positive values of the SOI are associated with stronger Pacific trade winds and warmer sea temperatures to the north of Australia, popularly known as a La Niña episode. Waters in the central and eastern tropical Pacific Ocean become cooler during this time. Together these give an increased probability that eastern and northern Australia will be wetter than normal. The most recent strong La Niña was in 1988/89; a moderate La Niña event occurred in 1998/99, which weakened back to neutral conditions before reforming for a shorter period in 1999/2000. This last event finished in Autumn 2000.

Thermal sensors directly measure the emitted thermal energy of the Earth's surface. Surface temperature changes are the result of the balance of radiant, latent, sensible and ground heat fluxes. Analyses of remotely sensed thermal data can be used to develop maps of the environmental conditions of the Earth's surface. In general, thermal sensors are used to measure variations in temperature across the landscape. One infers information about the properties of the landscape that affect temperature change. Examples of the use of thermal data are to estimate evaporation, soil moisture, drainage patterns, ground water seepage zones, canopy temperatures, and thermal plumes from thermoelectric power plants or industrial sources.

Microwave sensors can directly measure the dielectric properties of the Earth's surface. Any changes in these properties directly affect the reflectivity or emissivity measured by microwave systems. The dielectric property of the Earth's surface layer is in turn strongly dependent on the moisture content. Measurements in the microwave region of the electromagnetic spectrum can be related to the moisture content of the soil surface layers. Similar relationships exist for snow. The physical relationships between moisture, dielectric properties and microwave response, together with the ability of microwave sensors to penetrate cloud cover, make microwave sensors a useful

all-weather sensor to measure the moisture of the Earth's surface. Meanwhile, active microwave systems (radar) send out an energy pulse and measure the reflected pulse and the Earth's naturally emitted microwave radiation. Active microwave and passive microwave systems have been flown on aircraft and satellites. Examples of the use of microwave data are to estimate soil moisture, vegetation type, snow water equivalent, condition of snow pack, frozen soil and sea ice.

APPENDIX – A

Description of GIS Data in Bangladesh

Description of Data Layers	Data Group	Data Type	Remarks
Digital elevation model of Bangladesh at 300m resolution	Base Data	Topography	DTM - GRID Format
District boundaries (64) from AEZ - 1991 Population Census	Base Data	District	By NWRD - Including 1991 population
Detail River System in Bangladesh captured by FAP19 and NWRD	Base Data	River	From SPOT89 image and LANDSAT97 image
Major River System in Bangladesh captured by FAP19 and NWRD	Base Data	River	From SPOT89 image and LANDSAT97 image
Padma, Ganges, Jamuna, Meghna rivers etc		River	Whole Bangladesh
Road network upto to feeder road type A	Base Data	Road	Generated by RHD map and updated by NWRD
Spot elevation points of whole Bangladesh	Base Data	Topography	BWDB Topo, Irrig. Maps & SoB Topo maps - FAP19
Perennial water bodies of Bangladesh	Base Data	Waterbodies	By NWRD from SPOT89, LANDSAT97 and IRS image
Tornado affected areas - From a map of natural hazard mapping.	Environment	Natural Disaster	Published by Ministry of Relief Disaster Mang Bureau
Flood and river bank erosion map - From a map of natural hazard mapping	Environment	Natural Disaster	Published by Ministry of Relief Disaster Mang Bureau
Forest area of Bangladesh identified by SPARRSO in 1984	Forest	Forest Land	Published by Ministry of Relief Disaster Mang Bureau
Location of 33 climatic stations maintained by BMD	Meteorological	Climate	
Location of 12 evaporation stations maintained by BMD	Meteorological	Evaporation	
Location of 47 evaporation stations maintained by BWDB	Meteorological	Evaporation	
Location of 304 rainfall stations maintained by BWDB	Meteorological	Rainfall	
Agro ecological regions and subregions	Soil and Agriculture	Agro Echological Zone	Generated from AEZ mapping by FAP19 - Attribute??
Physiographic units of Bangladesh	Soil and Agriculture	Agro Echological Zone	Captured from AEZ mapping by FAP19/NWRD
Crop suitability classification of Bangladesh	Soil and Agriculture	Crop Suitability	Generated from AEZ mapping
Soil association map	Soil and Agriculture	Soil Association	Generated from AEZ mapping
Location of 129 nontidal discharge stations	Surface Water	Discharge	Maintained by BWDB
Location of 16 tidal discharge stations	Surface Water	Discharge	Maintained by BWDB
Location of 176 tidal waterlevel stations	Surface Water	Water Level	Maintained by BWDB
Location of 260 nontidal waterlevel stations	Surface Water	Water Level	Maintained by BWDB

APPENDIX - B

Rainfall Data Collected from Different Agencies in Bangladesh

1. BUET- (Main source – BMD)

No. of Stations : 32 data available (but total stations 35 under BMD)

Data Period : 2000/01/01 to 2000/12/31 (Frequency: 3 hr.)

Time and Data Units : UTC and in mm

2. BMD (Chart_Data)

No. of Station : 33 (Frequency: ½ hr.)

Period : 1999-2001 (not continuously for all stations and for all months)

Time and Data Units : BST and in mm

3. BMD (Source – India)

No. of Station : 32 (Frequency: Daily)

Period : 1998/6/01-1999/10/31 (For all stations)

1999/11/1-2000/11/30 and 2000/12/1-2000/12/30 (7 stations)

1998/6/1-98/11/30 and 1999/4/1-1999/10/31 (8 stations)

1998/6/1-1998/11/30 and 1999/4/1-1999/10/31 (10 stations)

1998/6/1-98/11/30 and 1999/4/1-1999/10/31 (7 stations)

4. BWDB (Source : Surface Hydrology)

No. of station : 218 (that also included above FFWC – 44 stations)

Frequency : Daily and data are in mm and time in BST

Period : 1998, 31/3/99-1/11/2001

5. IFCDR (Source : Prof. JUC)

No. of station : 02

Frequency : 05 mins and 0.2 mm rainfall by each tip

Periods : 30/5/00 – 15/10/00

Time and data format : BST and in mm

6. IFCDR (Source : Prof. Bala)

No of station : 08 (1998), 09 (1999), 10 (2000), 10 (2001)

Frequency : Hourly and Daily and 05 mins (BST and in mm)

Periods : 7/3/1998, 99, 00 & 01 – 24/10/1998, 99, 00 & 01

APPENDIX - C

PR-TMI Calibration/Validation

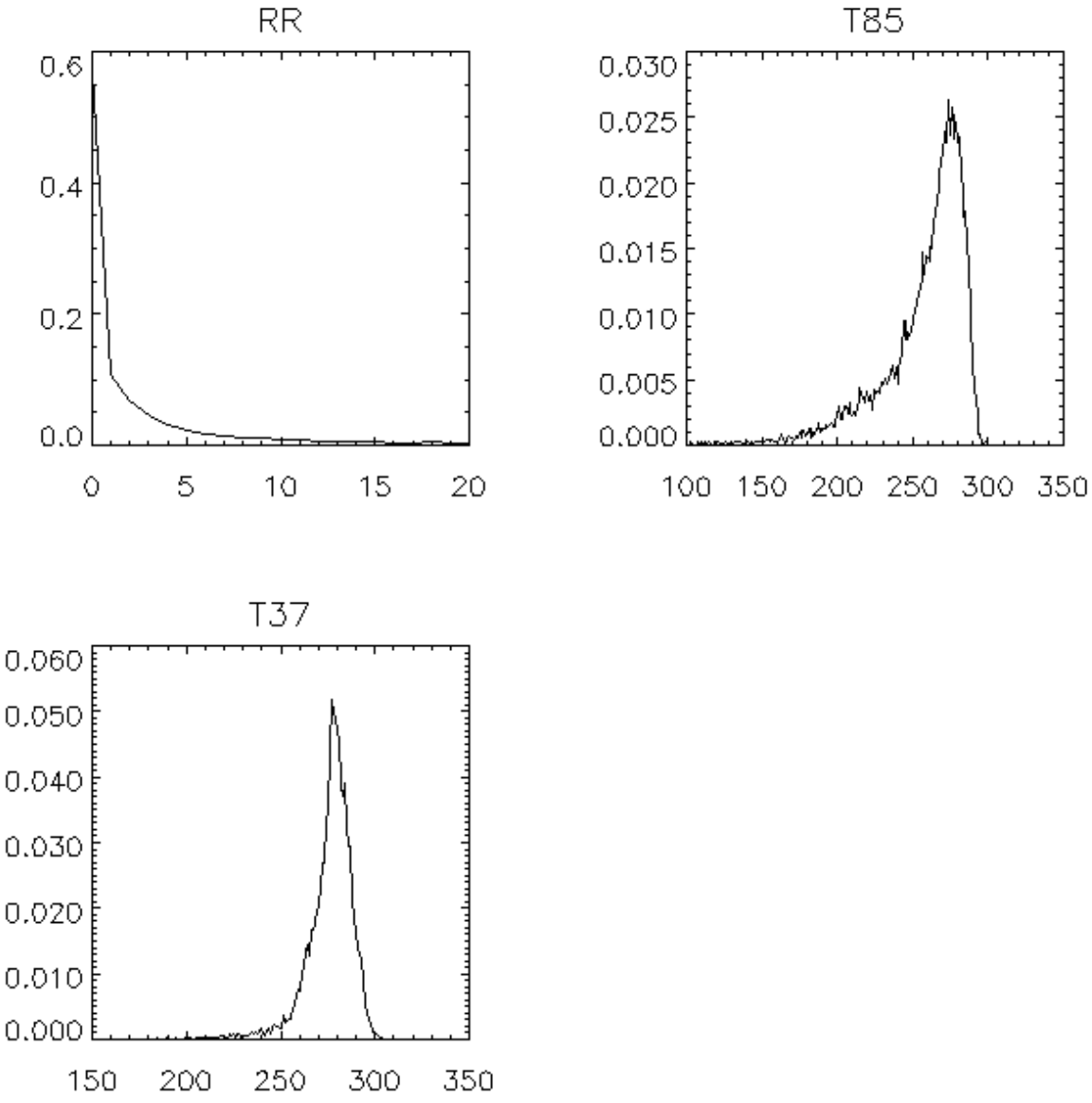

TRMM PR Rain Rate (2A25) and TMI Brightness Temparatures (1B11) of 85 and 37 GHz.
Passive MW Channels (RR-TT Histogram1)

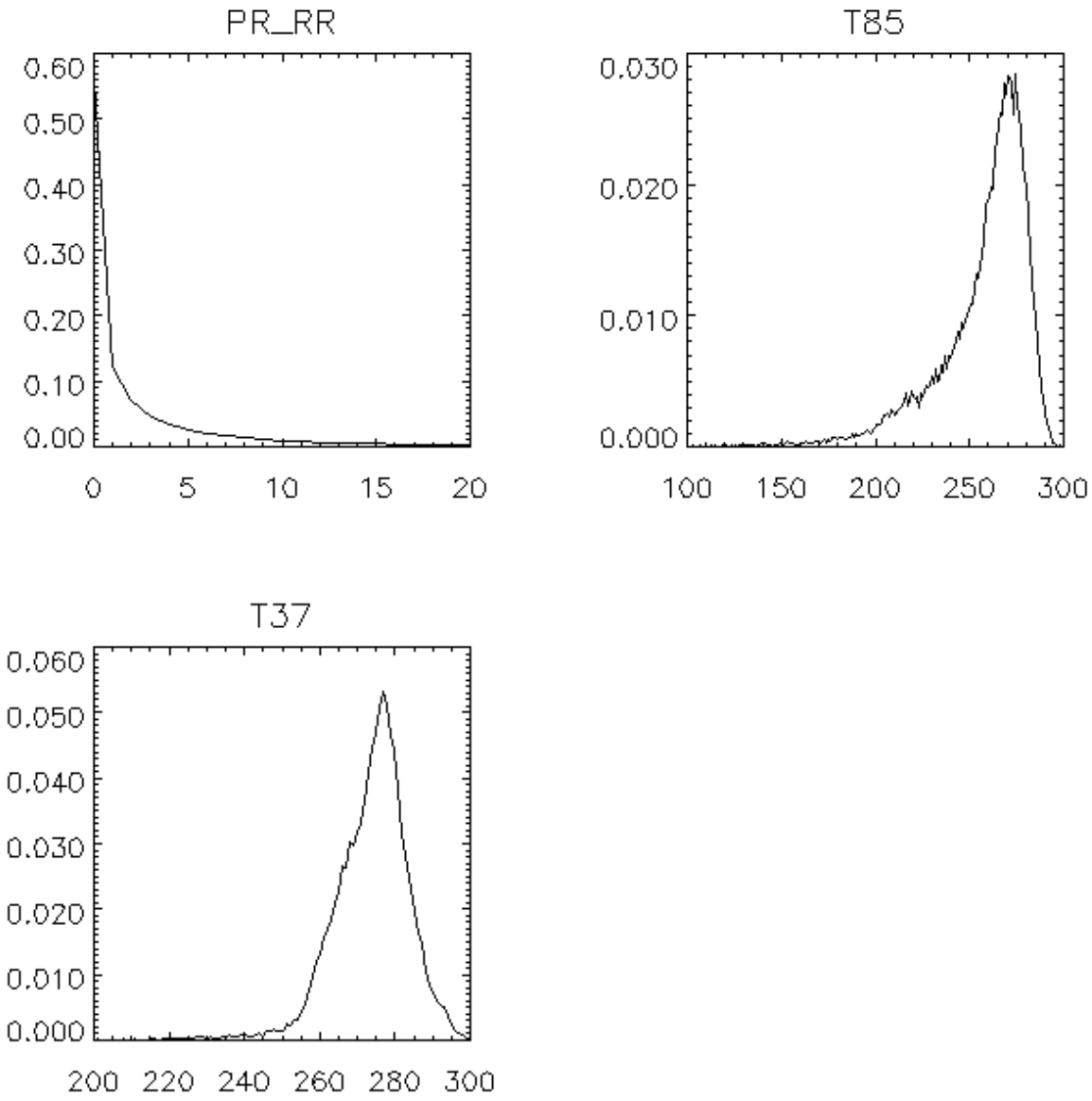

TRMM PR Rain Rate (2A25) and TMI Brightness Temparatures (1B11) of 85 and 37 GHz. Passive MW Channels (RR-TT Histogram2)

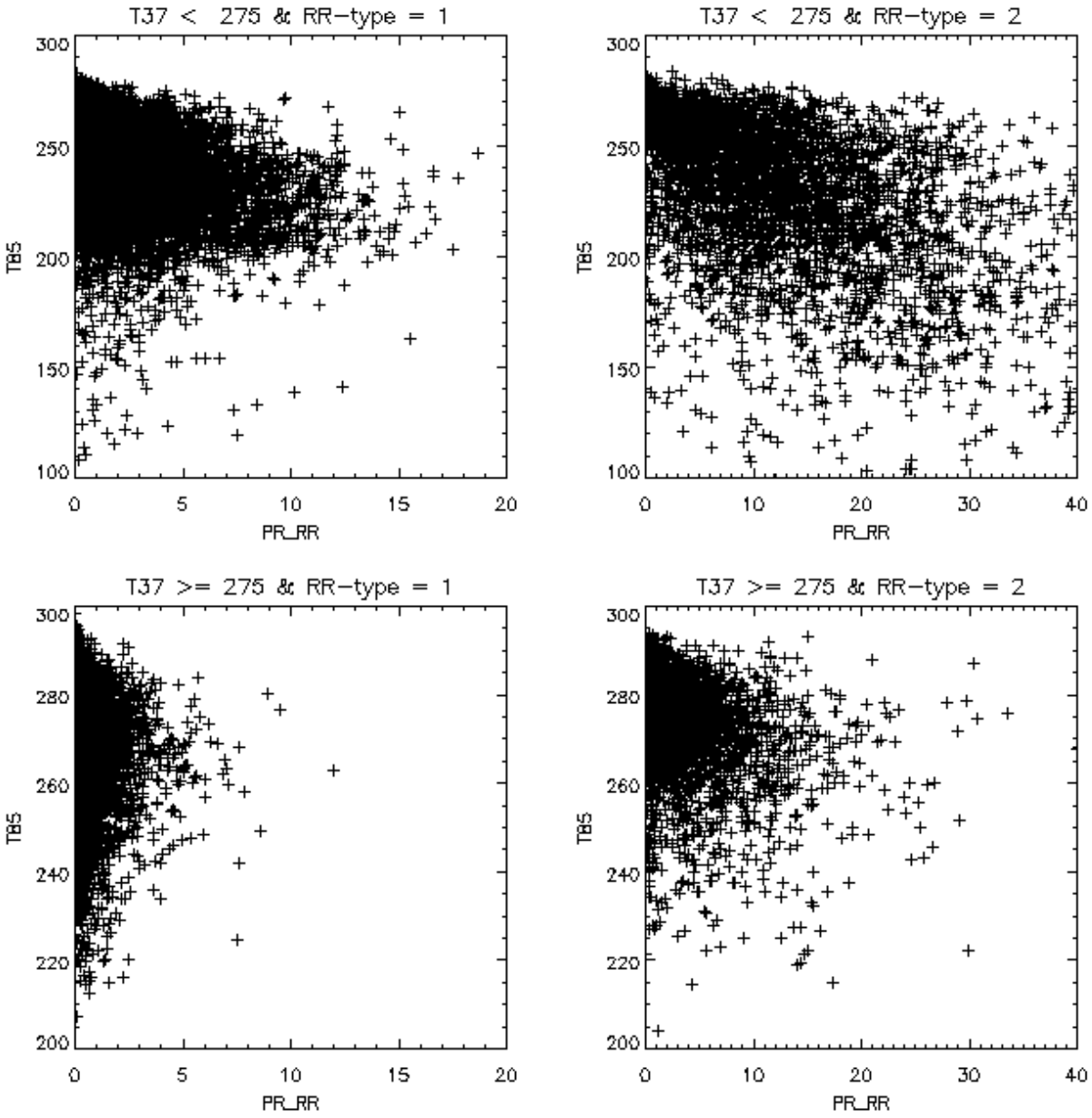

PR-RR and TMI T85 Scatterplot

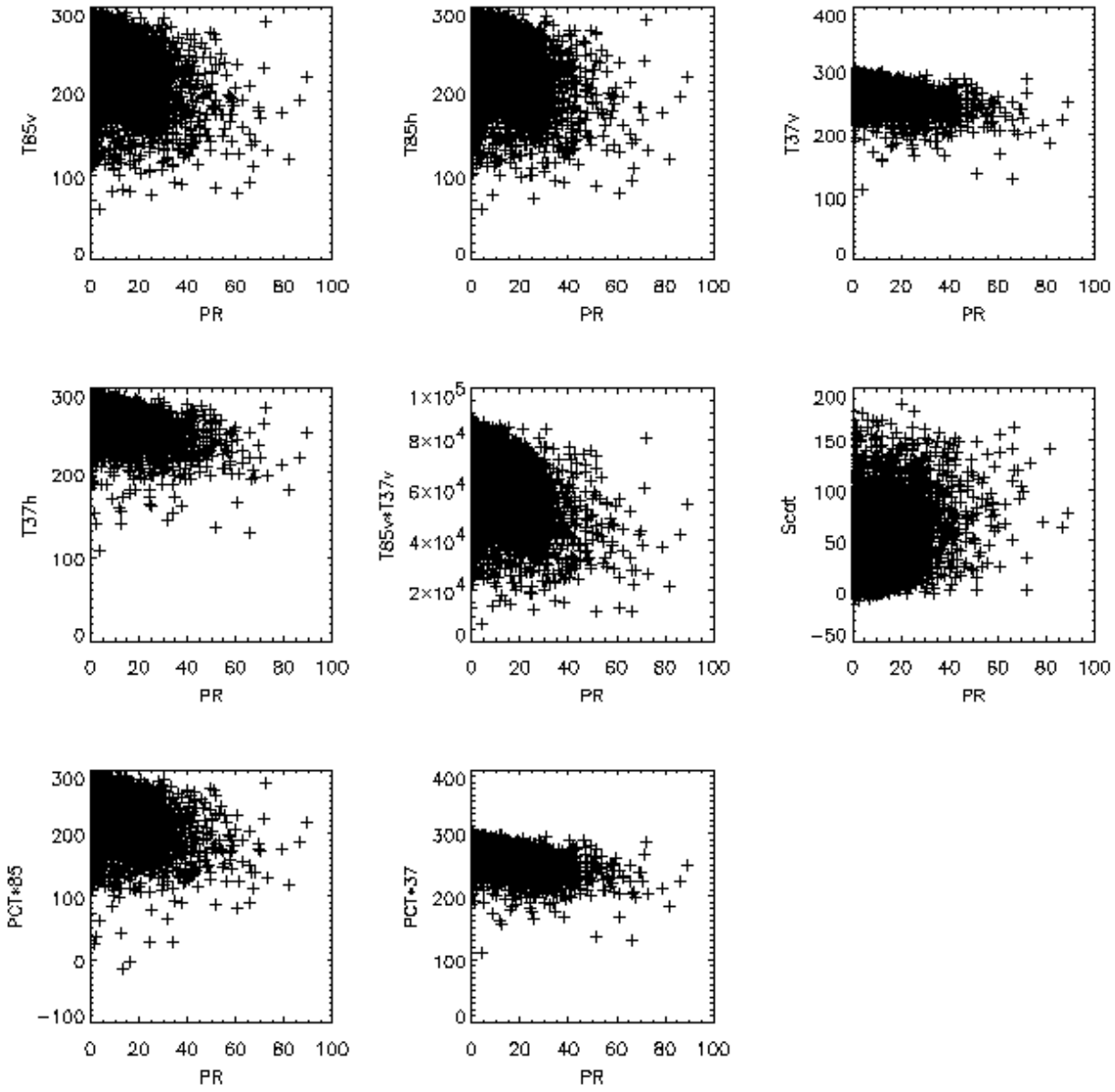

Predictor1

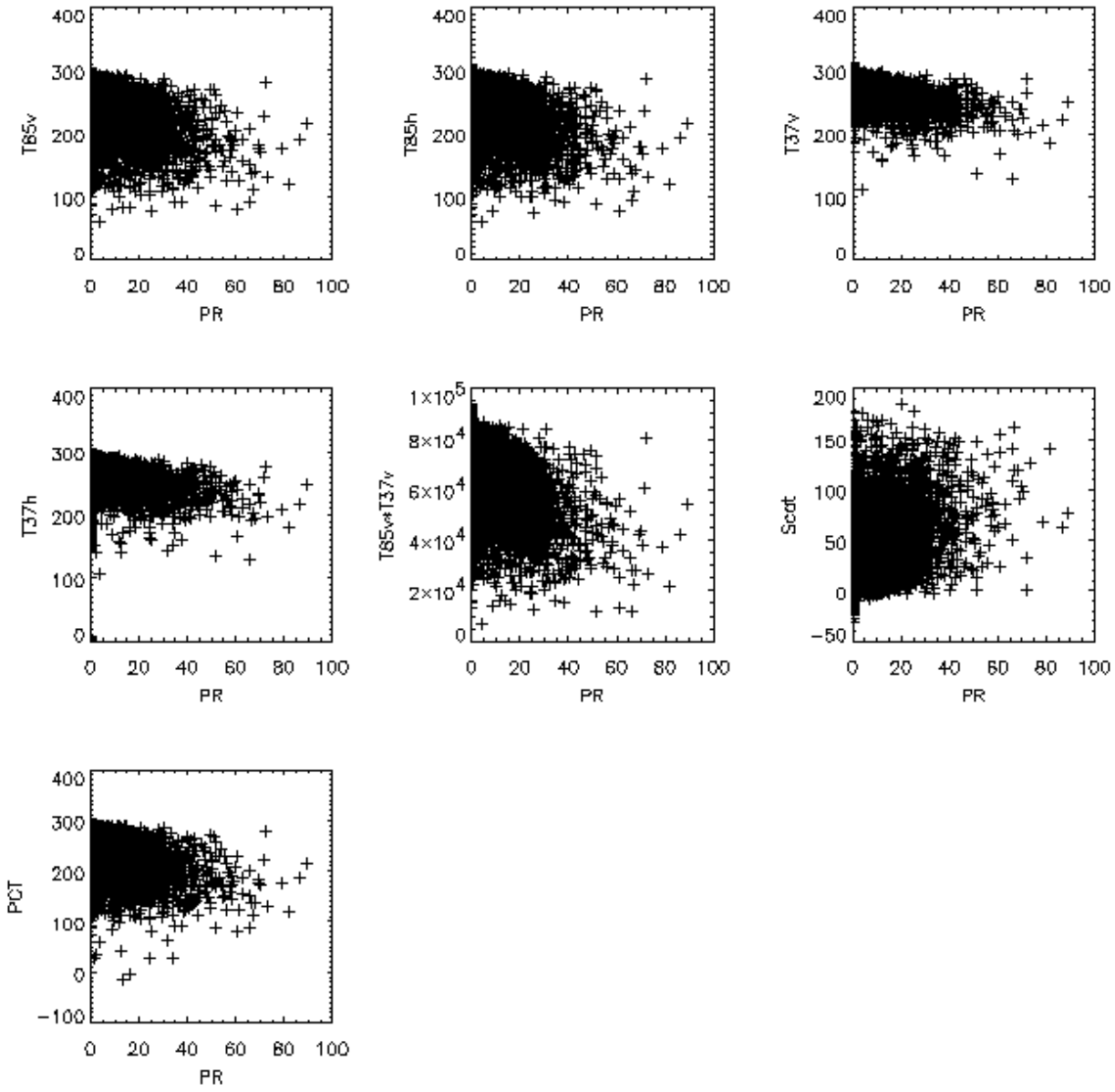

Predictor2

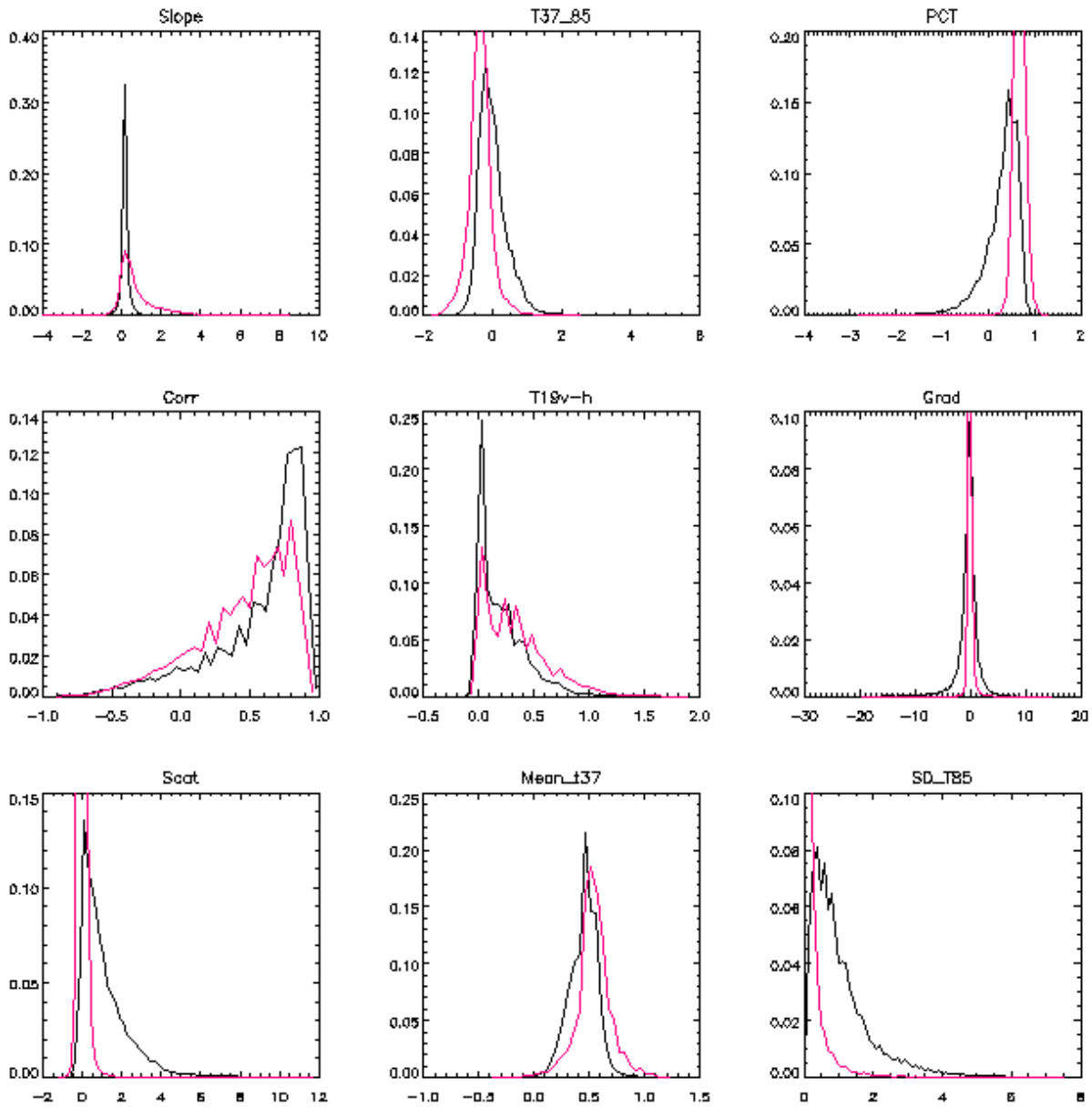

RNR-Features (Rain/No Rain Features over GBM)

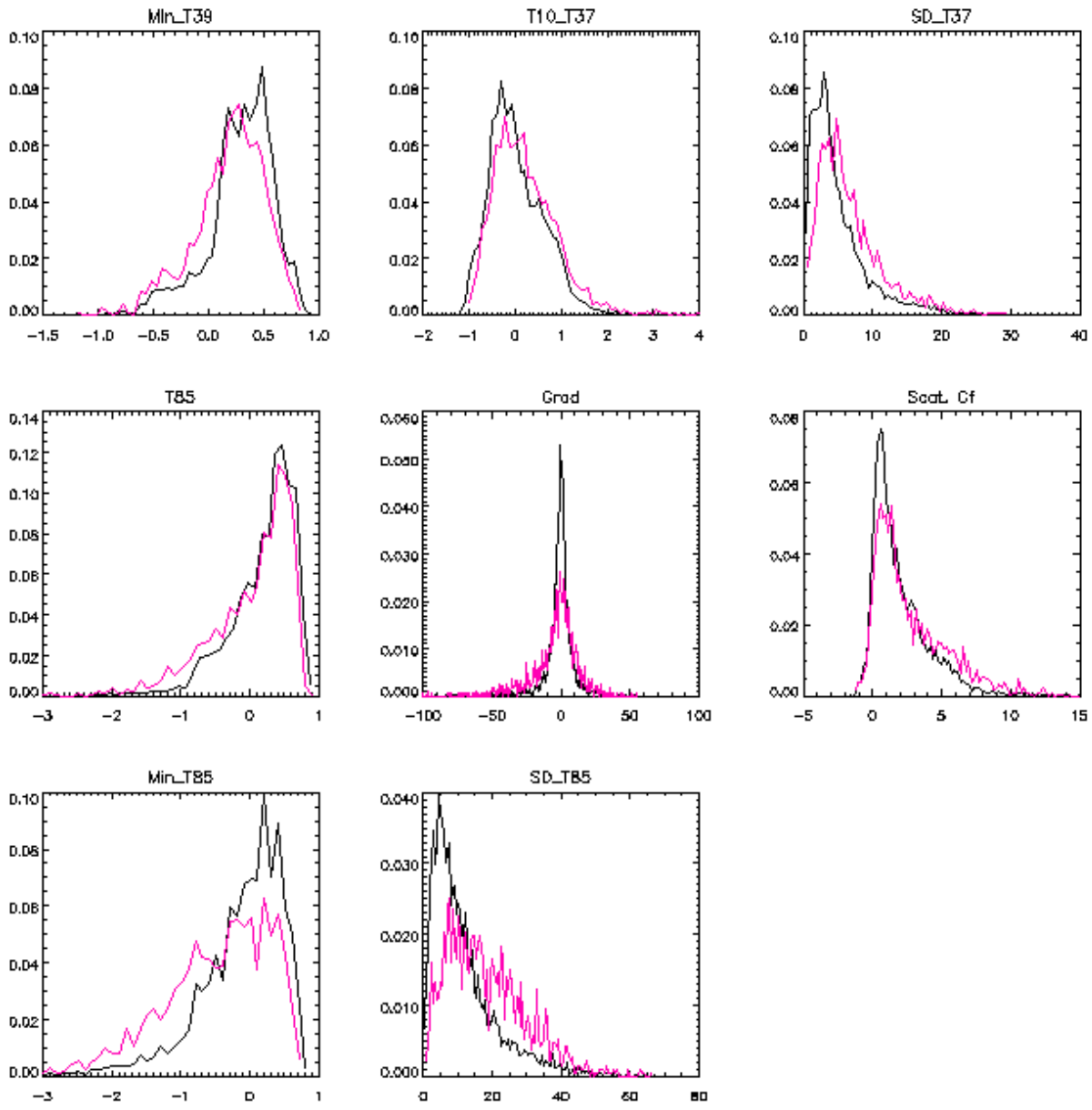

Convective and Stratiform Features (CS Features)

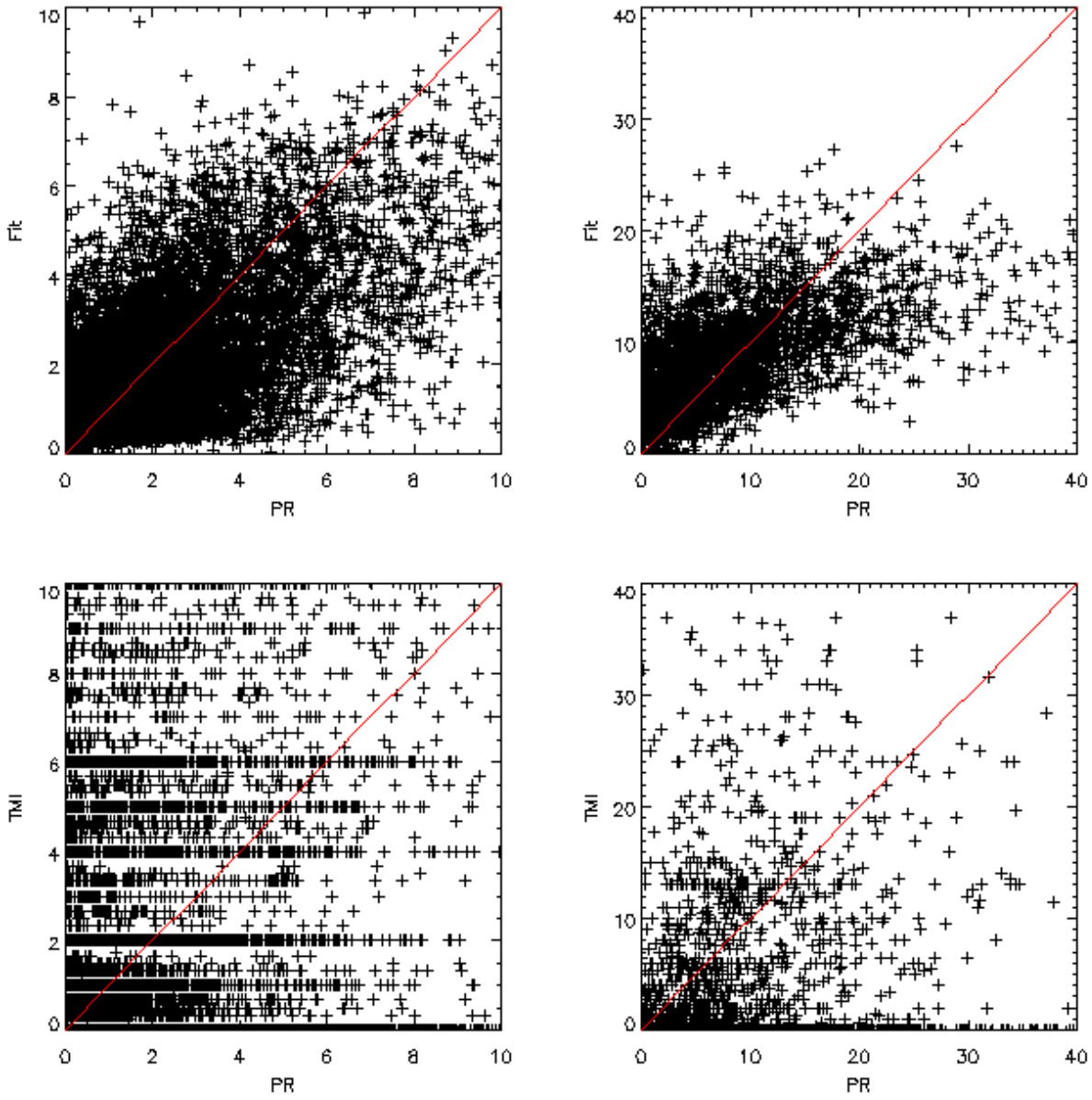

Validation_GBM

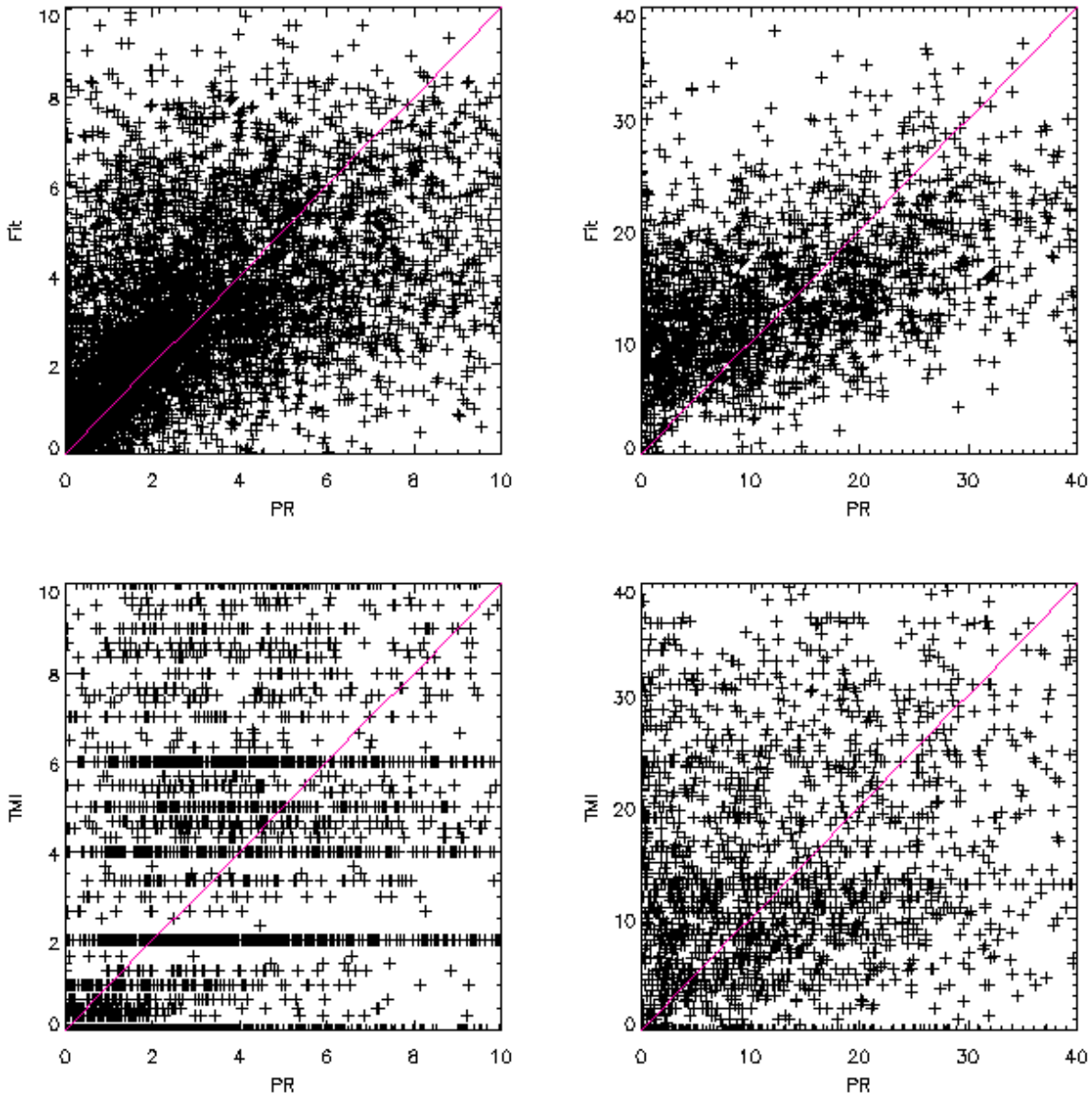

TRMM Calibration (Validation) using Probability Matching

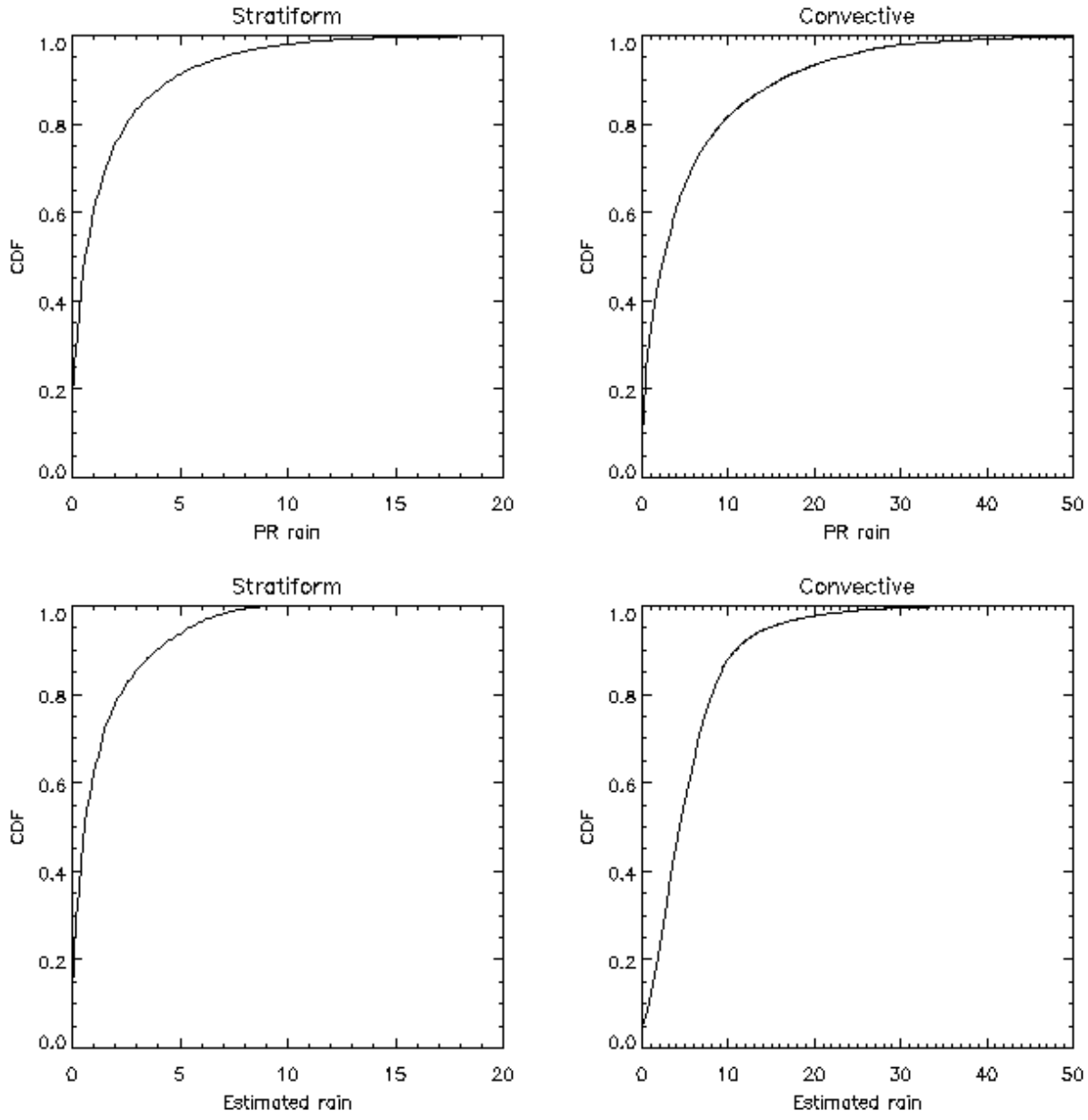

Cumulative Distribution Function of Estimated rain rate (RR-CDF)

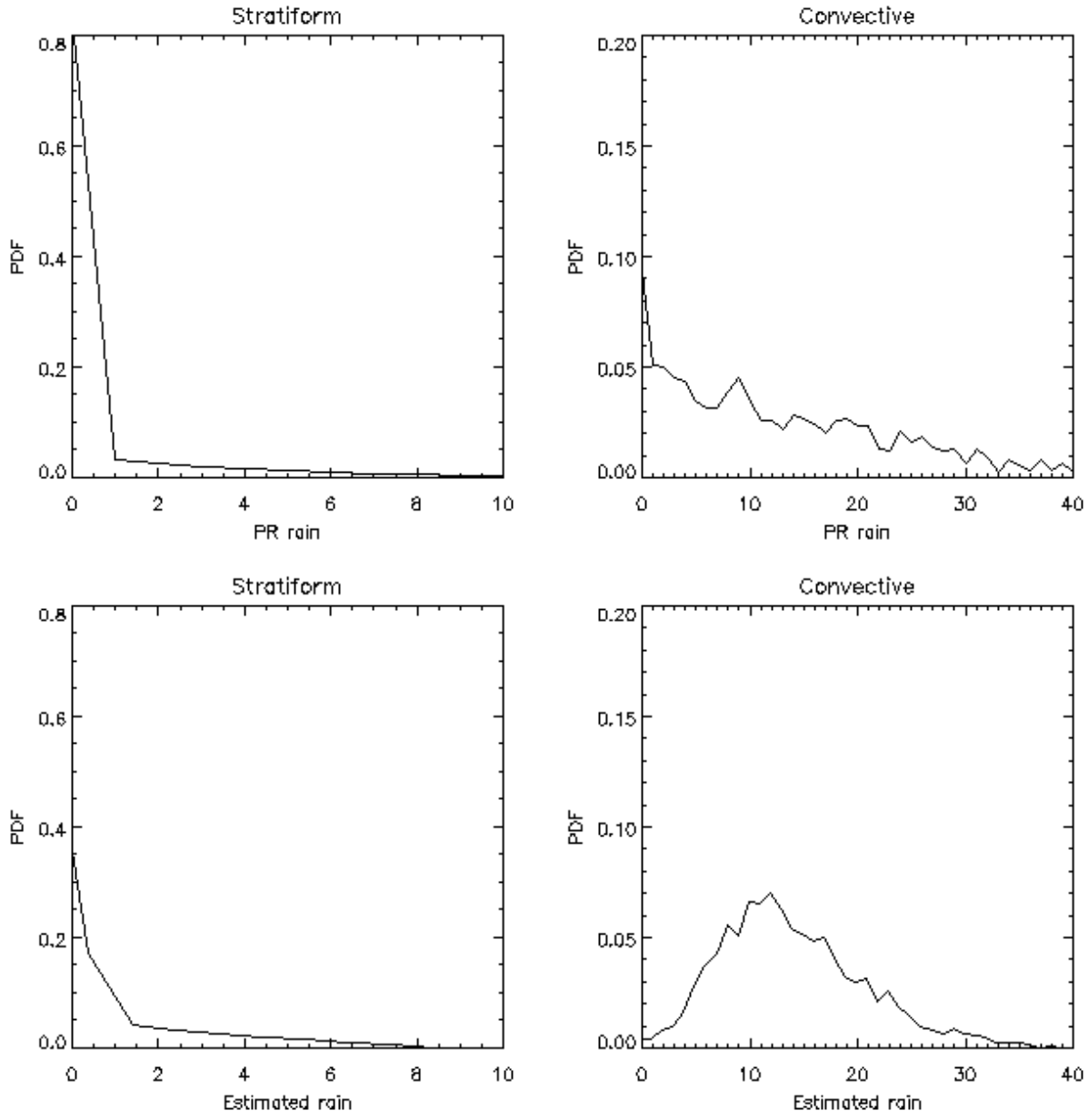

Probability Density Function of Estimated rain rate (RR-PDF)

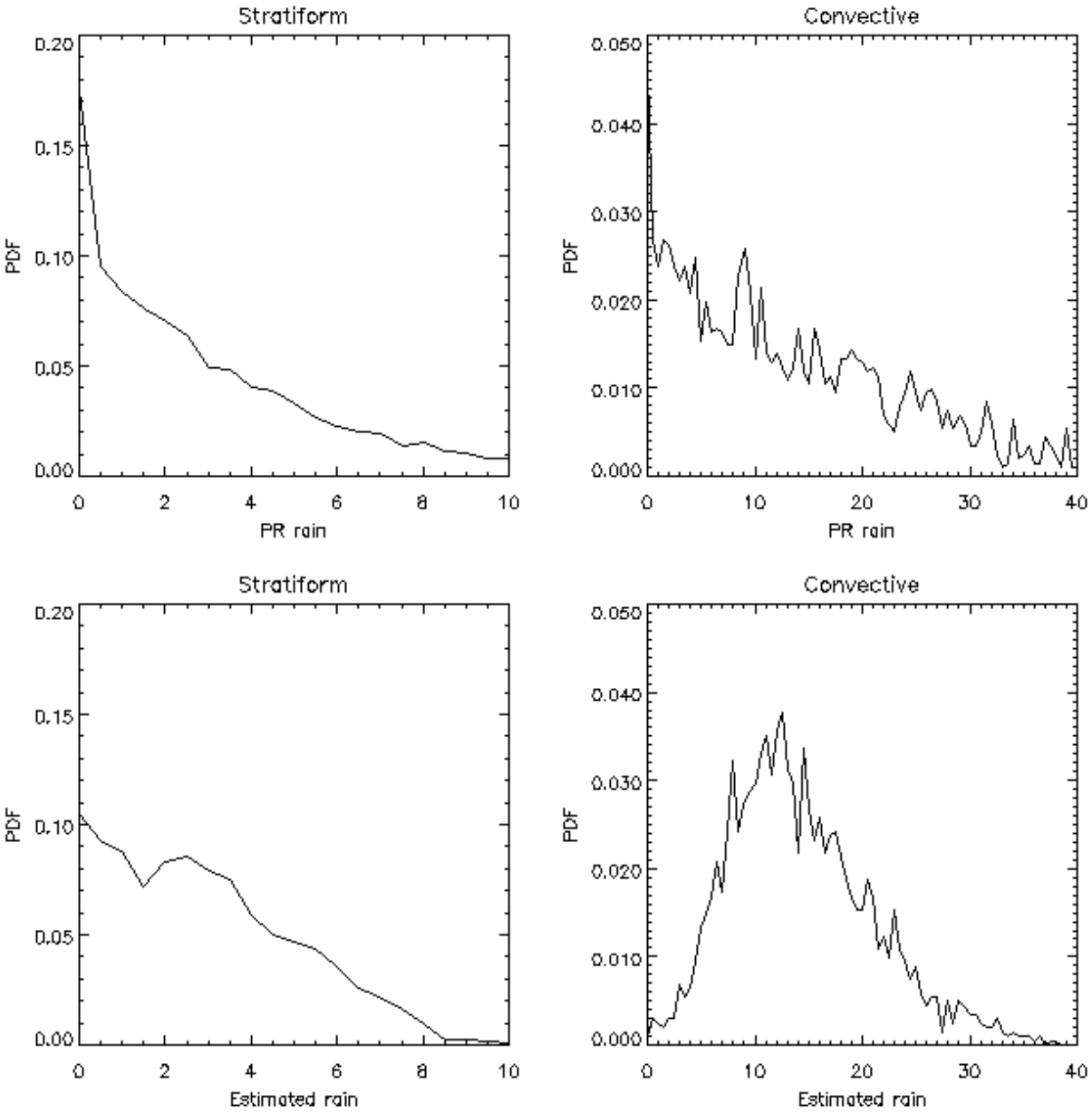

Probability Density Function of Estimated rain rate (RR-PDF)

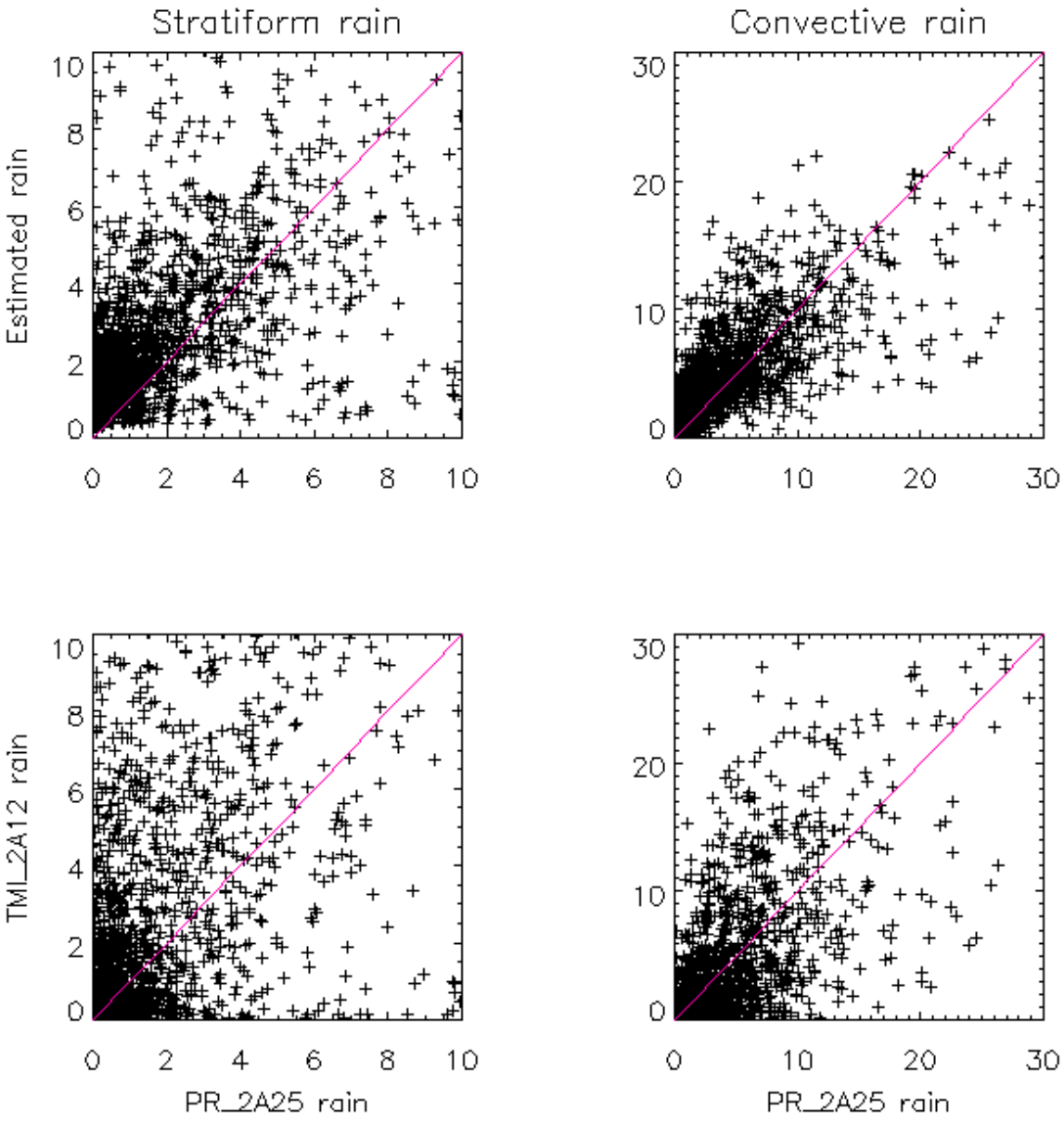

PR-TMI Validation